PROJECT ADMINISTRATION DATA SHEET

[X] ORIGINAL [ ] REVISION NO. _____

Project No. E-16-801 T5124-0A0 GTRC/~~GIT~~ DATE 6 /16 / 86

Project Director: Dr. L.N. Sankar School/~~GIT~~ Aerospace Engineering

Sponsor: National Aeronautics & Space Administration, Lewis Research Center

Type Agreement: Grant No. 3-730

Award Period: From 6/1/86 To ~~10/31/86~~ 4/30/88 (Performance) 10/31/86 (Reports)

Sponsor Amount:	This Change	Total to Date
Estimated:	$	$
Funded:	$ 3,300	$ 3,300

Cost Sharing Amount: $ _____ Cost Sharing No: _____

Title: Numerical Investigations of Stall Flutter Phenomena

ADMINISTRATIVE DATA OCA Contact E. Faith Gleason

1) Sponsor Technical Contact:

K. Kaza (216) 433-6038
Structure Dynamics Branch
NASA Lewis Research Center
Mail Stop 5230
21000 Brookpark Road
Cleveland, OH 44135

2) Sponsor Admin/Contractual Matters:

Boyd M. Bane
Grants Officer
NASA Lewis Research Center
Mail Stop 500-302
21000 Brookpark Road
Cleveland, OH 44135

Defense Priority Rating: N/A Military Security Classification: N/A

(or) Company/Industrial Proprietary: _____

RESTRICTIONS

See Attached _____ Supplemental Information Sheet for Additional Requirements.

Travel: Foreign travel must have prior approval – Contact OCA in each case. Domestic travel requires sponsor approval where total will exceed greater of $500 or 125% of approved proposal budget category.

Equipment: Title vests with GIT, requires prior written consent from Grants Officer if over $1,000.

COMMENTS:

COPIES TO:

SPONSOR'S I. D. NO. 02.105.000.86.004

Project Director
Research Administrative Network
Research Property Management
Accounting
Procurement/GTRI Supply Services
Research Security Services
Reports Coordinator (OCA)
Research Communications (2)
GTRC
Library
Project File
Other A. Jones/Legal

FORM OCA 65:285

GEORGIA INSTITUTE OF TECHNOLOGY
OFFICE OF CONTRACT ADMINISTRATION

NOTICE OF PROJECT CLOSEOUT

Closeout Notice Date 02/06/91

ject No. E-16-801 Center No. T5124-0A0

ject Director SANKAR N L School/Lab AERO ENGR

nsor NASA/LEWIS RESEARCH CTR, OH

tract/Grant No. NAG 3-730 Contract Entity GTRC

me Contract No.

le NUMERICAL SIMULATION OF UNSTEADY ROTATIONAL FLOW OVER PROPFAN CONFIGURATI

ective Completion Date 901130 (Performance) 901130 (Reports)

seout Actions Required:	Y/N	Date Submitted
Final Invoice or Copy of Final Invoice	Y	
Final Report of Inventions and/or Subcontracts	Y	
Government Property Inventory & Related Certificate	Y	
Classified Material Certificate	N	
Release and Assignment	N	
Other	N	

Comments

project Under Main Project No.

tinues Project No.

tribution Required:

Project Director	Y
Administrative Network Representative	Y
GTRI Accounting/Grants and Contracts	Y
Procurement/Supply Services	Y
Research Property Managment	Y
Research Security Services	N
Reports Coordinator (OCA)	Y
GTRC	Y
Project File	Y
Other	N
	N

: Final Patent Questionnaire sent to PDPI.

DISCLAIMER:

This document has been proofed and
its original formatting has been retained.

NUMERICAL SIMULATION OF UNSTEADY ROTATIONAL FLOW OVER PROPFAN CONFIGURATIONS

NASA GRANT No. NAG 3-730

SEMI-ANNUAL STATUS REPORT

for the period

June 1- November 30, 1986

Submitted to

NASA LEWIS RESEARCH CENTER
CLEVELAND, OHIO

Attn: Dr. K. R. V. Kaza
Technical Monitor

INTRODUCTION

The objective of this research effort is to develop efficient numerical techniques for the prediction of unsteady transonic flow past propfan configurations. A two-dimensional compressible Navier-Stokes solver, and a three-dimensional unsteady compressible Euler solver, developed at the Georgia Institute of Technology, are being modified to address this problem.

SUMMARY OF PROGRESS

During the reporting period, the 2-D compressible Navier-Stokes solver was modified as follows. A two-degree of freedom structural model was developed, and incorporated into the computer code. This modification allows the airfoil fluid dynamics and the structural dynamics equations to be simultaneously integrated in time. The airfoil undergoes oscillatory pitching, and plunging motion as a result of the aerodynamic forces acting on the structure. In return, the resultant change in the airfoil angle of attack, its angular velocity in pitch, and its plunging velocity alter the aerodynamic forces. The modifications incorporated allow this fluid-structure interaction to be studied in detail, for a user input set of structural parameters, airfoil shape, and mean flow Mach number and angle of attack.

The modified code was exercised by performing a number of transonic and subsonic flutter calculations, for small and large angle of attack conditions, for thick and thin airfoils, with and without viscous effects considerations. Some preliminary computations for the stall flutter of airfoils were also carried out. These calculations have been documented in a paper to be presnted at the AIAA Dynamics Specialists Conference in May 1987.

PLANNED EFFORT FOR THE PERIOD DEC. 1, 1986- JUNE 1, 1987

During the period Dec. 1, 1986 - June 1, 1987, the 2-D Navier-Stokes solver will be tested further by a number of calculations in the high transonic Mach number regime. An attempt will be made to predict the transonic dip phenomenon which is characterized by an abrupt drop in the flutter speed as Mach number is increased.

A three-dimensional Euler solver developed by the principal investigator for rotary wing applications will be modified to handle propfan problems. A O-H grid topology will be used, and an algebraic grid generator which can handle arbitrarily shaped propfan blades will be developed.

NUMERICAL SIMULATION OF UNSTEADY ROTATIONAL FLOW OVER PROPFAN CONFIGURATIONS

NASA GRANT No. NAG 3-730

SEMI-ANNUAL STATUS REPORT

for the period

December 1, 1986 - May 31, 1987

Submitted to

NASA LEWIS RESEARCH CENTER
CLEVELAND, OHIO

Attn: Dr. K. R. V. Kaza
Technical Monitor

Prepared by:

L. N. Sankar
Associate Professor

Rakesh Srivastava
Graduate Research Assistant

School of Aerospace Engineering
Georgia Institute of Technology
Atlanta, GA 30332

INTRODUCTION

The objective of this research is to develop efficient numerical techniques for the prediction of unsteady transonic flow past propfan configurations. A two-dimensional compressible Navier-Stokes solver, and a three-dimensional unsteady Euler solver, both developed at the Georgia Institute of Technology, are being modified to address this problem.

SUMMARY OF PROGRESS

During the previous reporting period (June 1- November 30, 1986) the 2-D compressible Navier-Stokes solver had been modified for numerical simulation of stall flutter and transonic flutter phenomena. During the current reporting period, a number of calculations were made using this solver to predict the transonic flutter speed of a NACA 0012 airfoil as a function of the freestream Mach number. The airfoil was allowed to pitch and plunge, and the structural stiffness and damping parameters were the same as those used by other investigators who have studied this problem. In Figure 1, the flutter speed is plotted as a function of Mach number. It is seen that the present approach predicts the dip in the flutter speed that occurs in the Mach number range $0.80 < M < 0.9$. The present theory however tends to underpredict the aerodynamic damping in the Mach number range $0.75 < M < 0.8$ compared to other techniques. Effort is now underway for determining the cause of this behavior. First, a denser grid is used in the vicinity of the airfoil to determine the effect of grid spacing on the predicted flutter speeds. Second, a second order time marching scheme is being implemented in place of the first order time marching scheme presently in place.

Stall flutter calculations are also being carried out for a number of propfan airfoil shapes.

The 3-D Euler solver at Georgia Tech was modifed to solve the unsteady transonic flow past isolated propfan blades. An algebraically generated H-O grid system, as well as a H-H grid system are being investigated. In Figure 2, a sample H-O body-fitted grid around a typical blade-nacelle combination is shown.

PLANNED RESEARCH EFFORT FOR THE PERIOD JUNE 1- NOV 30, 1987

During the next reporting period, 3-D Euler calculations will be carried out for the blade nacelle combination shown in figure 2, for a set of flow conditions chosen in cooperation with researchers at NASA Lewis. Comparisons of the computed surface pressures and loads will be made with experiments, and other numerical solutions.

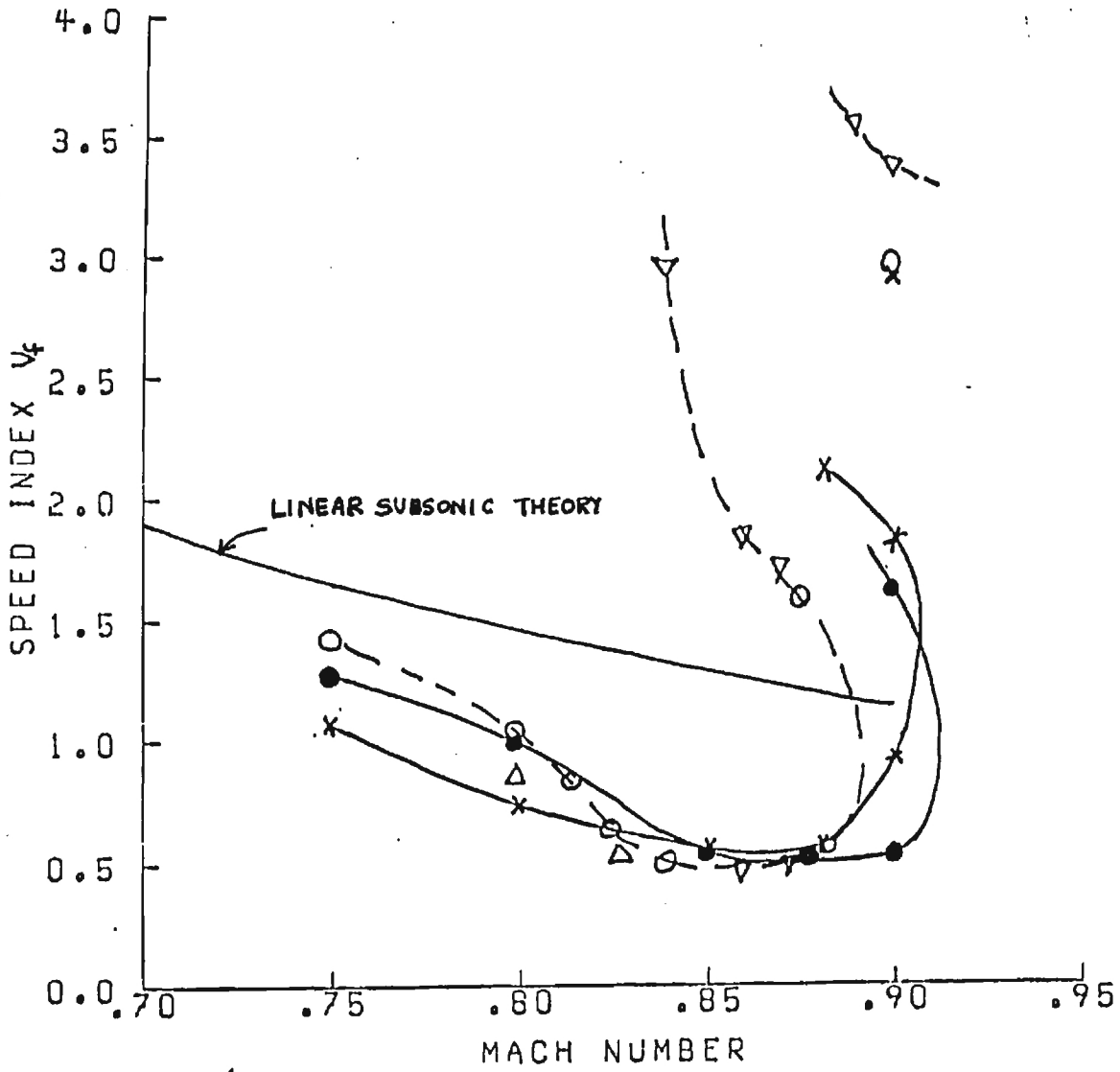

FIG 1 CALCULATED FLUTTER BOUNDARIES

× PRESENT CODE
○ HYTRAN2
● BENEDIKSON'S CODE
▽ OPTRAN2
△ LTRAN2

Grid in Y–Z Plane

At Trailing Edge of Wing

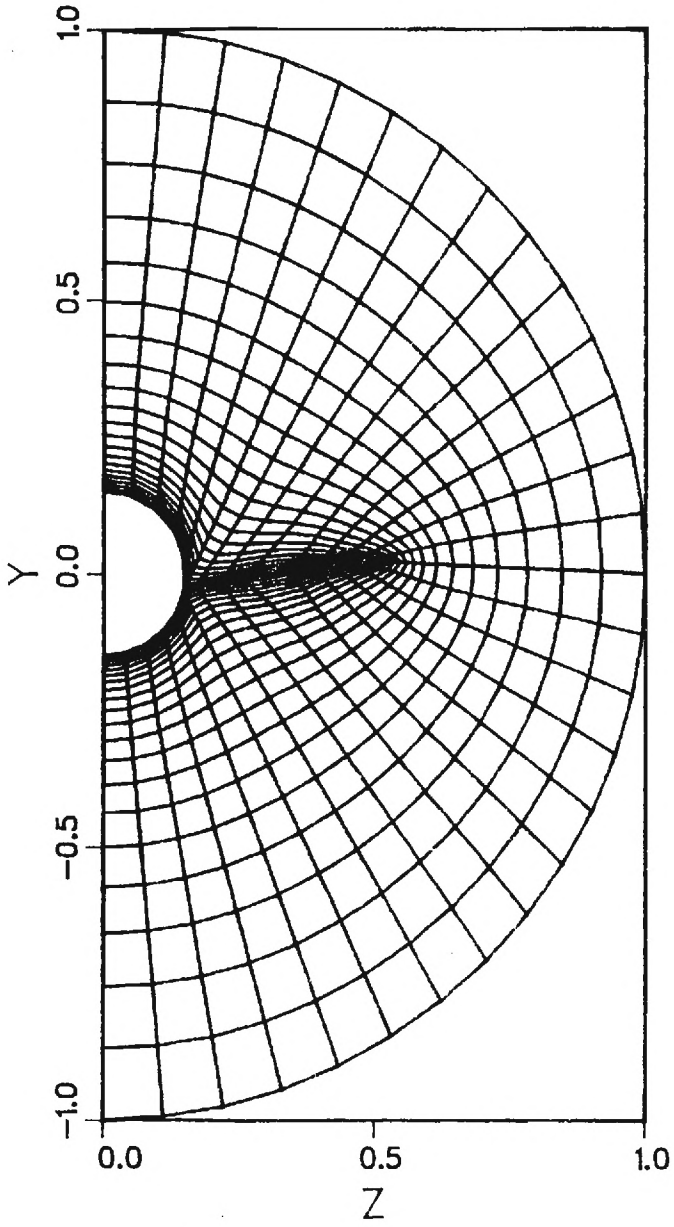

Grid in Y–Z Plane

AT LEADING EDGE OF WING

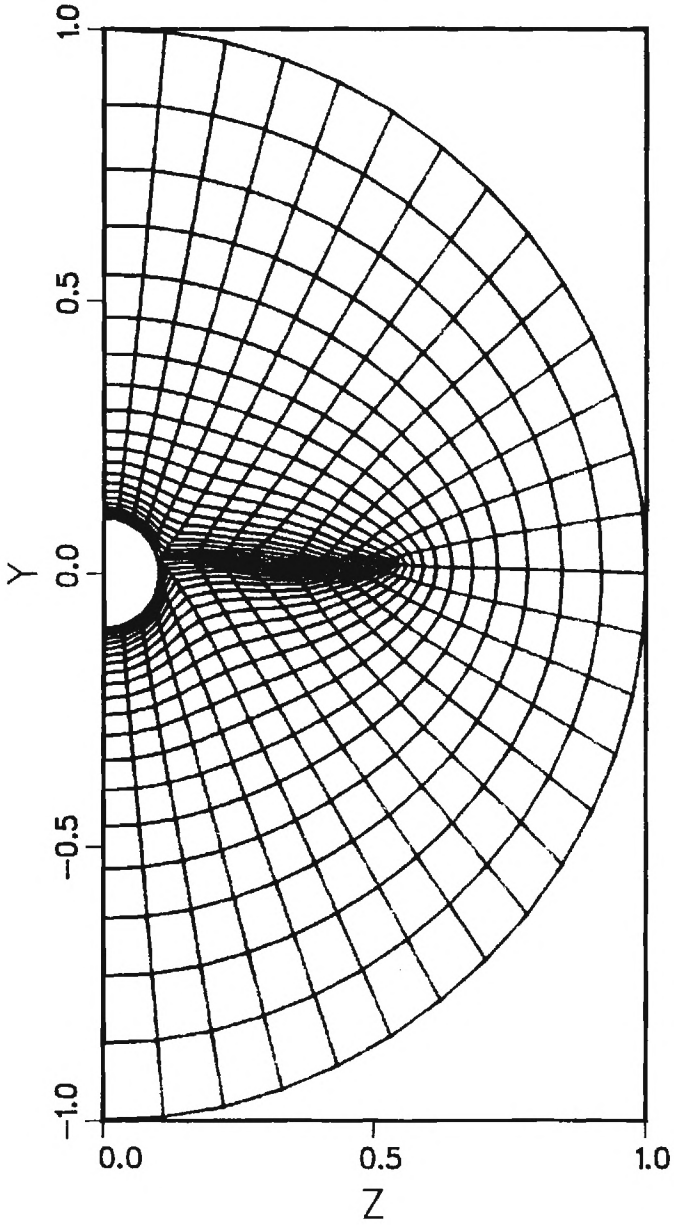

Grid in Y–Z Plane

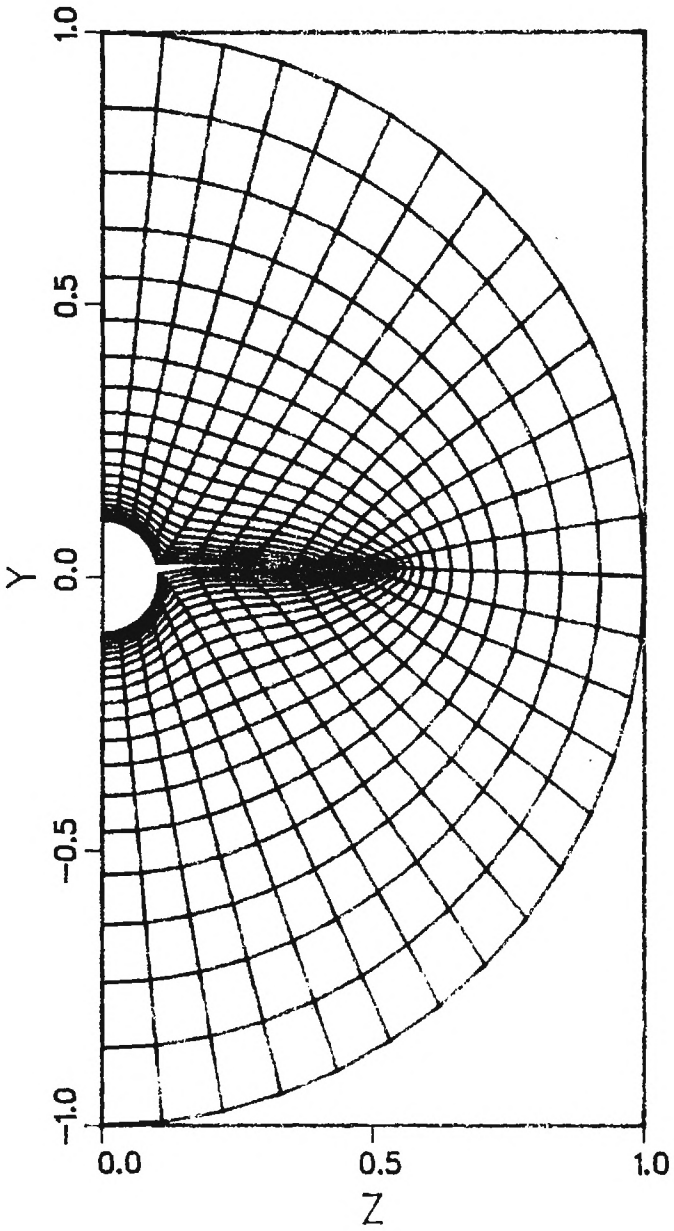

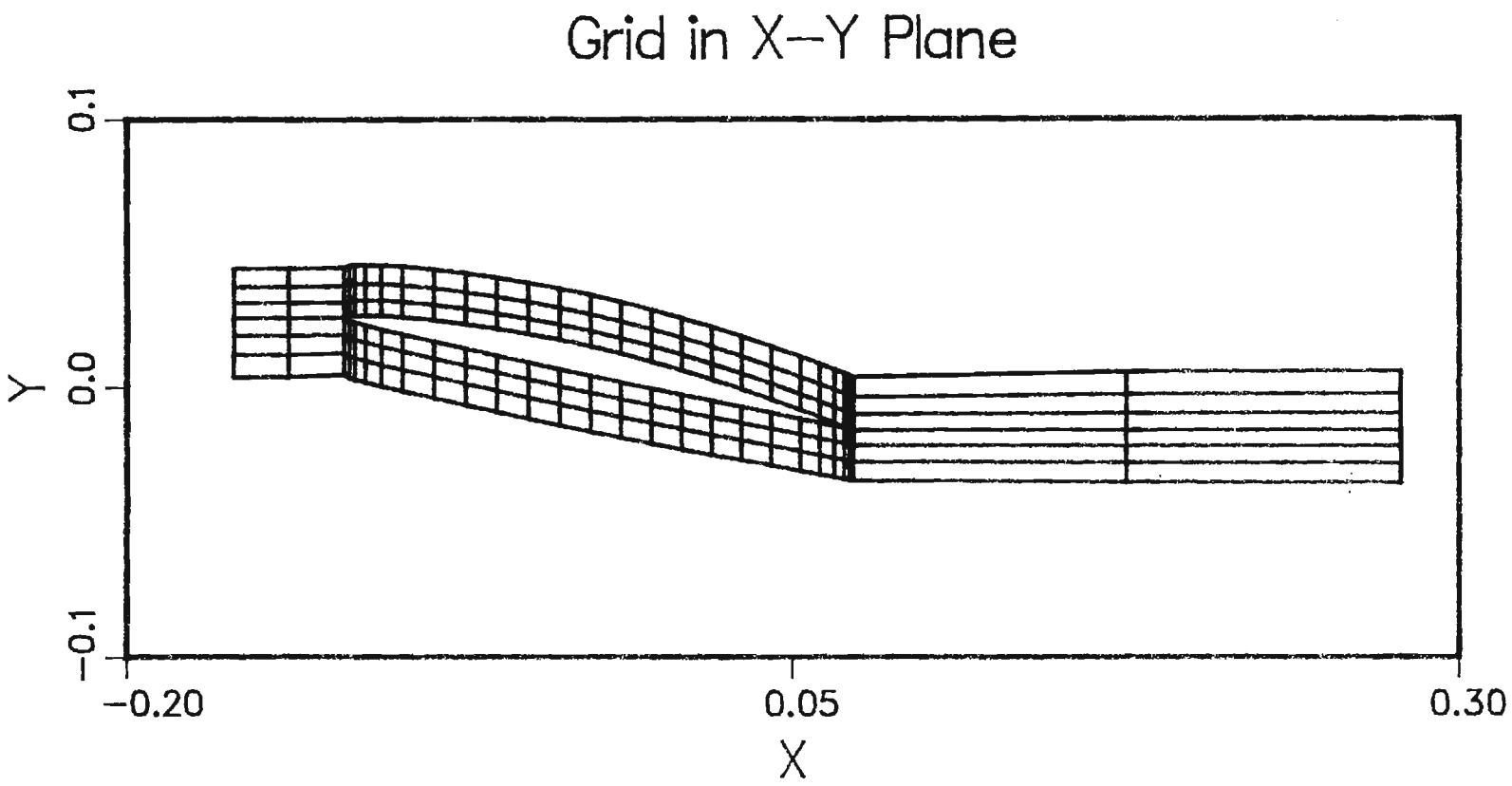
Grid in X–Y Plane
0.1
0.0
−0.1
Y
−0.20
0.05
0.30
X

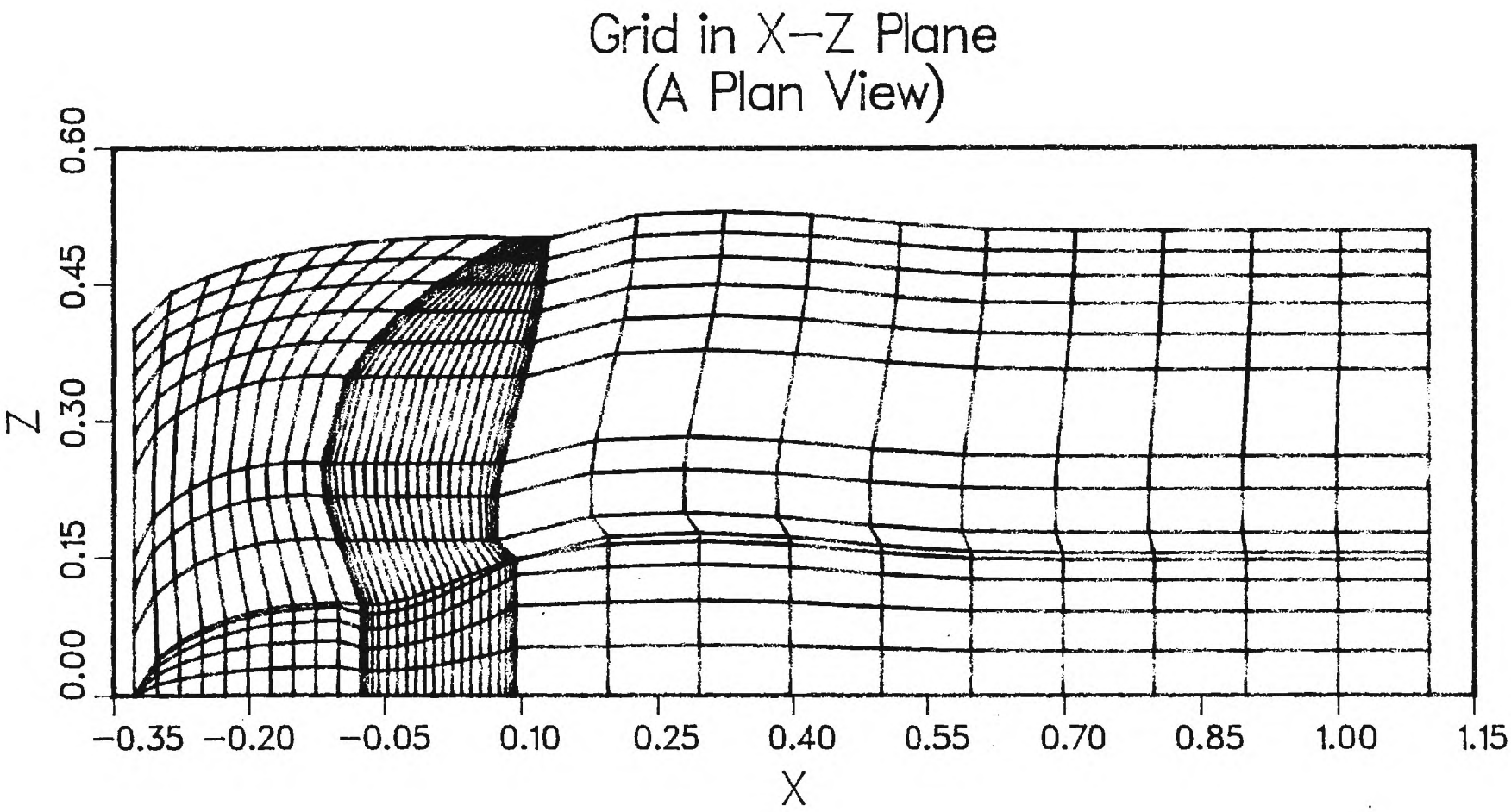
Grid in X–Z Plane
(A Plan View)
Z
0.00
0.15
0.30
0.45
0.60
−0.35
−0.20
−0.05
0.10
0.25
0.40
0.55
0.70
0.85
1.00
1.15
X

NUMERICAL SIMULATION OF UNSTEADY ROTATIONAL FLOW OVER PROPFAN CONFIGURATION

NASA GRANT No. NAG 3-730

SEMI-ANNUAL STATUS REPORT

for the period

December 1, 1987 - April 30, 1988

submitted to

NASA LEWIS RESEARCH CENTER

CLEVELAND, OHIO

Attn: Dr. K. R. V. Kaza

Technical Monitor

Prepared by:

L. N. Sankar
Associate Professor

Rakesh Srivastava
Graduate Research Assistant

School of Aerospace Engineering
Georgia Institute of Technology
Atlanta, Georgia 30332

INTRODUCTION

The objective of this research is to develop efficient numerical techniques for the prediction of unsteady transonic flow past propfan configurations. A two-dimensional compressible Navier-Stokes solver, and a three dimensional unsteady, compressible Euler solver, both developed at the Georgia Institute of Technology, are being modified to address this problem.

SUMMARY OF PROGRESS

2-D Transonic Flutter Studies

During the previous reporting period (December 1, 1987 to April 30, 1988) the compressible Navier-Stokes code was successfuly applied to the problem of transonic flutter dip for airfoils of various shapes and thickness. The effect of viscosity was also studied. It was found that the thickness had more effect on the dip than the shape. Reducing the thickness, as expected, shifts the dip to higher Mach numbers, as the occurrence of shock is delayed. Also the recovery of the dip decreases with thickness. It was further found that angle of attack, viscosity and initial conditions had little effect on the minima of the dip, however they had noticeable effect away from the dip. These results along with other results and conclusions were presented at the 29^{th} SDM conference in Williamsburg, Virginia, Ref. 1. However, some problems were encountered for very thin airfoils at mean angles of attack.

3-D Propfan Simulation

During a previous reporting period December 1, 1986 to May 31, 1987 a H-O grid had been generated. Use of this grid in the Euler solver led to some problems when applied to propfan blade geometry, because the grid wrapped around the blade tip. To alleviate this difficulty another H-O body fitted grid has been developed

and is in the process of being applied to the three-dimensional Euler solver. A few sample grids are plotted in figure-1 for one blade of the ten bladed SR-7 propfan configuration.

In the meantime the Euler solver was applied to an isolated propfan blade using an existing C grid within the code, similar to that in the two-dimensional solver. Due to the nature of the C-grid, it was not possible to model the nacelle. Some preliminary calculations were carried out for a tip Mach number of 0.8 and an advance ratio ($J = V/nD$) of 3.06. This set of flow conditions was chosen in co-operation with researchers at NASA Lewis.

In the present computer code the flow field around a propfan blade can be modelled in three different ways:

- The grid along with the blade can be moved with time to simulate the advancing of the blade in the free stream direction
- The grid may be held stationary with respect to the blade, but the blade sees a forward velocity along with the rotational velocity
- An effective aerodynamic twist, equivalent to an effective angle of attack, may be specified as a function of radial distance to an untwisted rotating blade. The effective angle of attack is based on the advance ratio, rotational speed and geometric twist.

The large geometric twist of the planform results in a highly skewed grid. This caused numerical problems for the first and second methods. Hence the third option was used to compute the pressure distribution over the blade. The computed pressure distributions are compared with the experimental results available in figure-2.

A fairly good pressure distribution correlation is found for the upper surface, in the outboard region. In the inboard region the prediction compares only qualitatively. This is because of handling an isolated blade without the nacelle and also because the cascade effects are more significant inboard. Also the lower surface

prediction is very poorly correlated. It is felt that the flow might have artificially seperated in the Euler solver, due to the lack of viscous effects. This is being investigated. In the experimental results for the inboard stations, on the upper surface, there seems to be a vortex sitting near the leading edge. This vortex is understandably not predicted by Euler solver as the leading edge vortex and tip vortices are primarily due to viscosity. It may be noted that predictions based on other existing solvers (full potential and Euler) also perform poorly on the pressure side (Ref. 2).

PLANNED REASERCH FOR THE PERIOD MAY 1 - NOV 30 1988

During the next reporting period, the new H-O grid will be implemented in the three-dimensional Euler solver. This will enable us to handle the effect of nacelle geometry and cascade effects. The cascade effects will be modelled by incorporating the periodic boundary condition on the outer boundaries.

REFERENCES

1. Reddy, T. S. R., Srivastava, R., and Kaza, K. R. V., "The Effects of Rotational Flow, Viscosity, Thickness, and Shape on Transonic Flutter Dip Phenomena", AIAA Paper 88-2348, April 1988.

2. Huff, D. L., Private Communications.

Figure-1a Grid in X-Z Plane

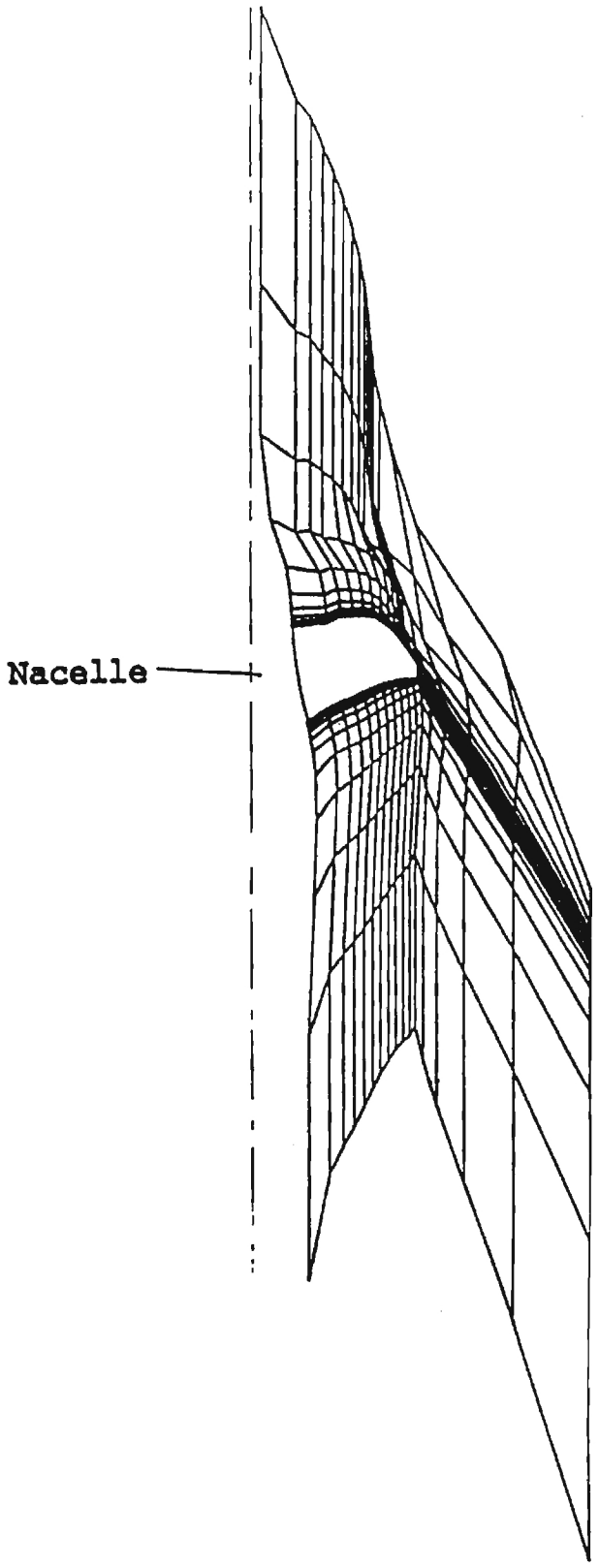

Figure-1b Grid in X-Y Plane

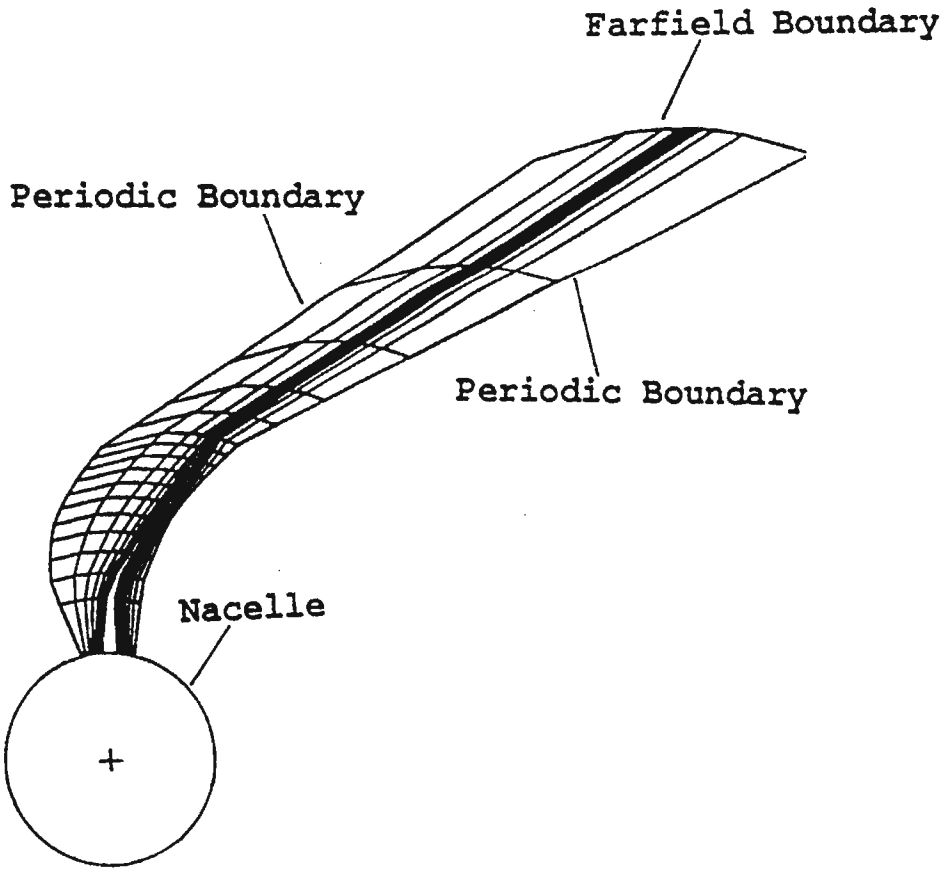

Figure-1c Grid in Y-Z Plane

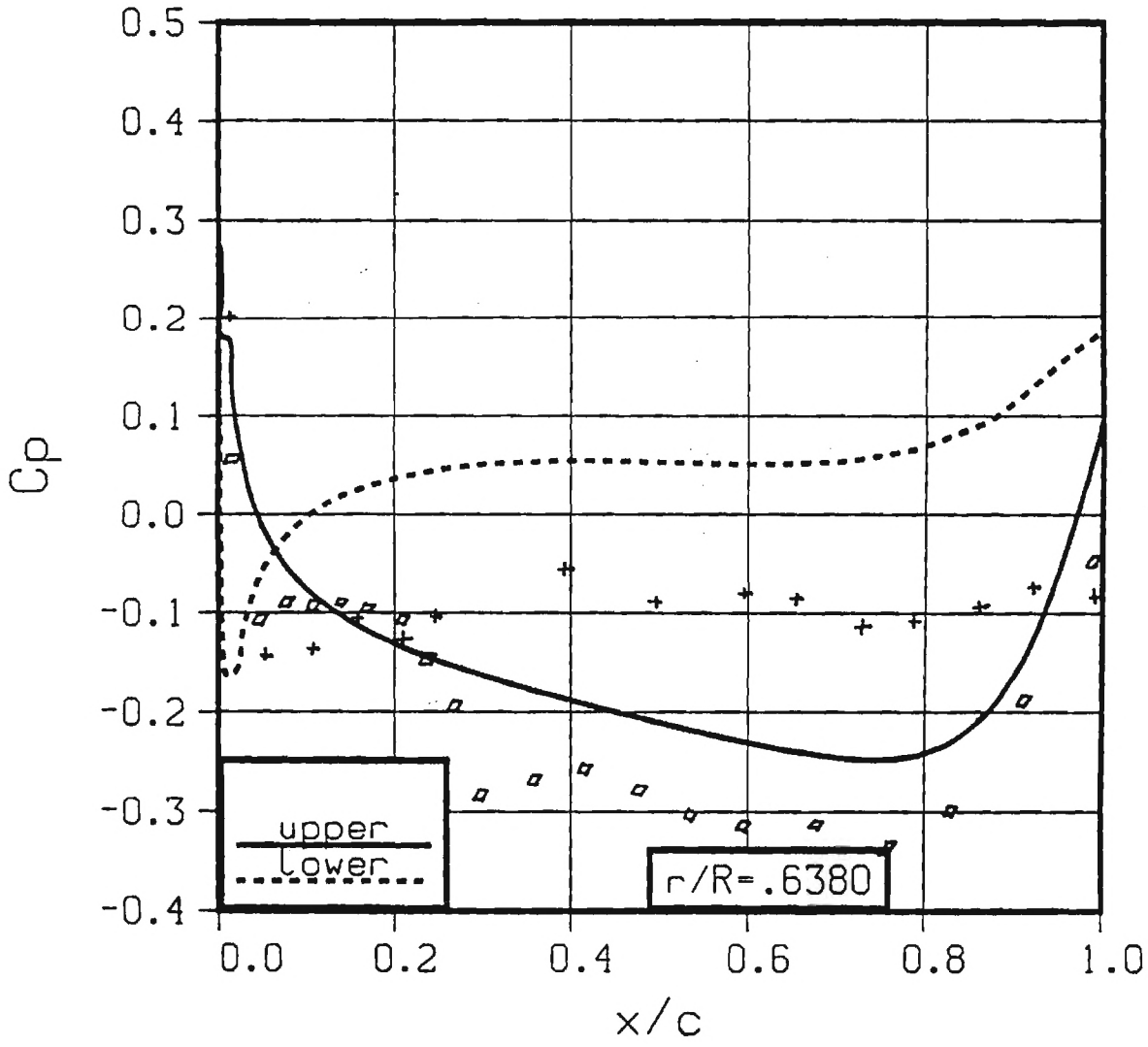

Figure-2a Pressure Distribution Comparison at 63% Radial Station

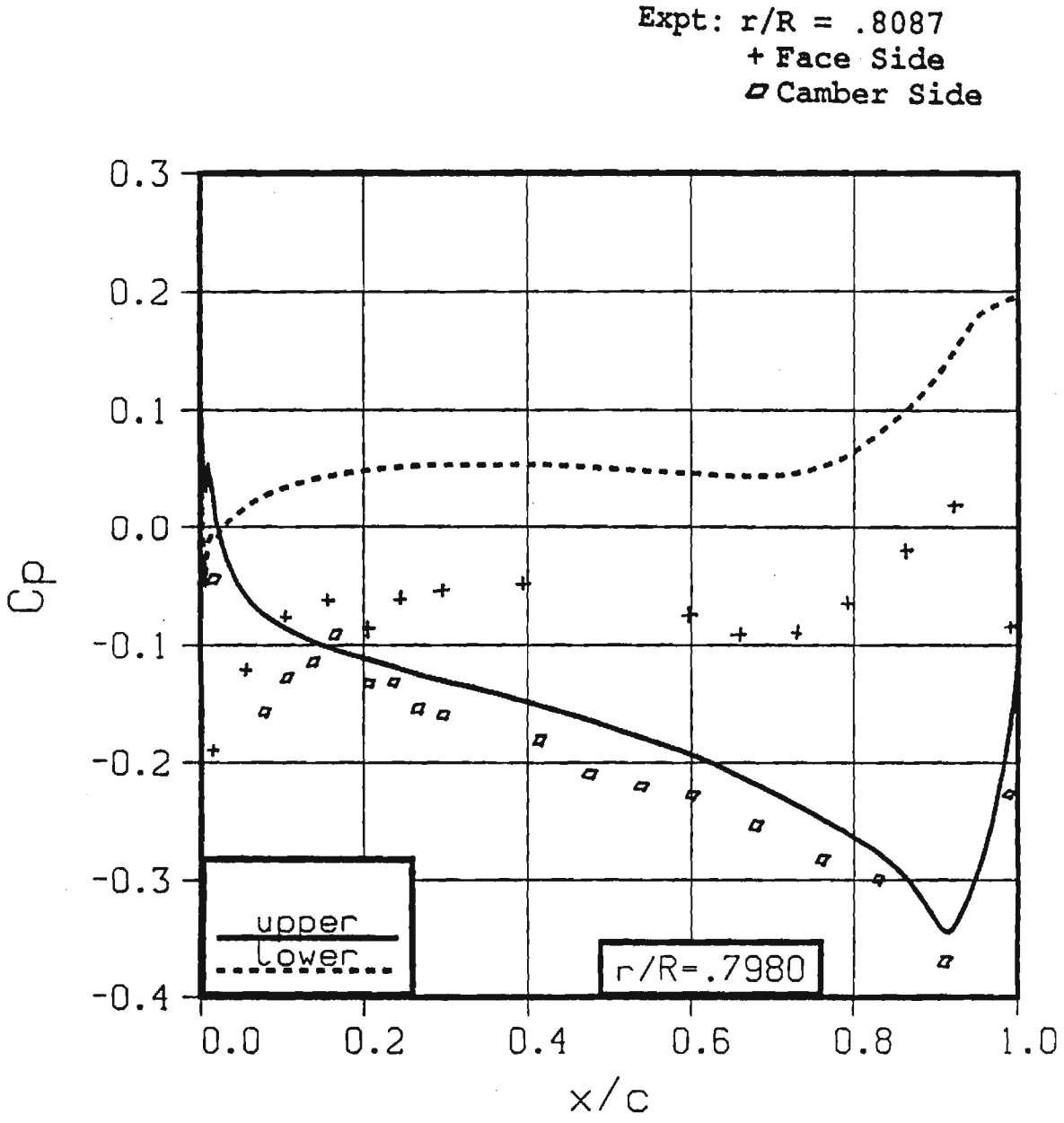

Figure-2b Pressure Distribution Comparison at 80% Radial Station

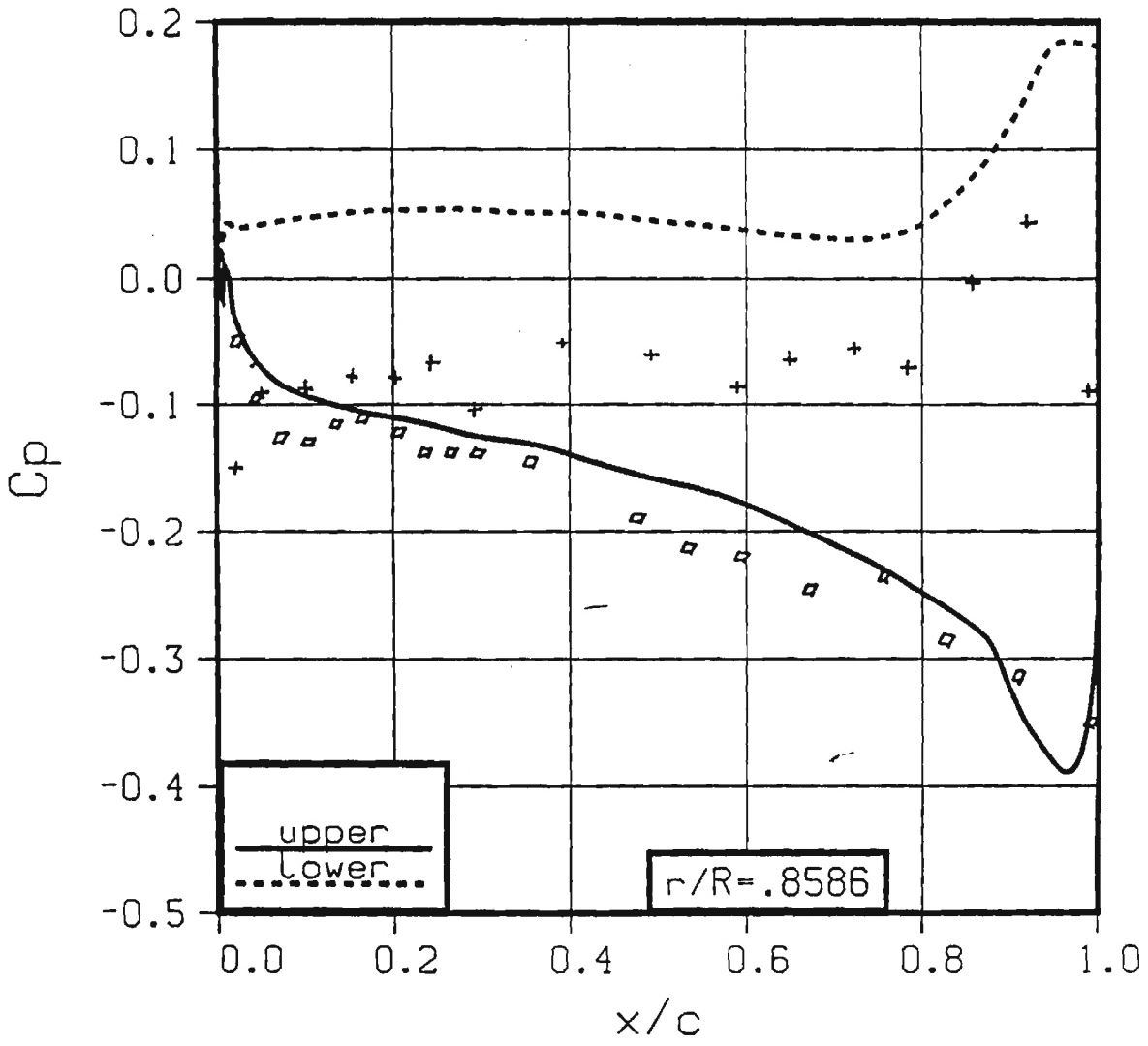

Figure-2c Pressure Distribution Comparison at 86% Radial Station

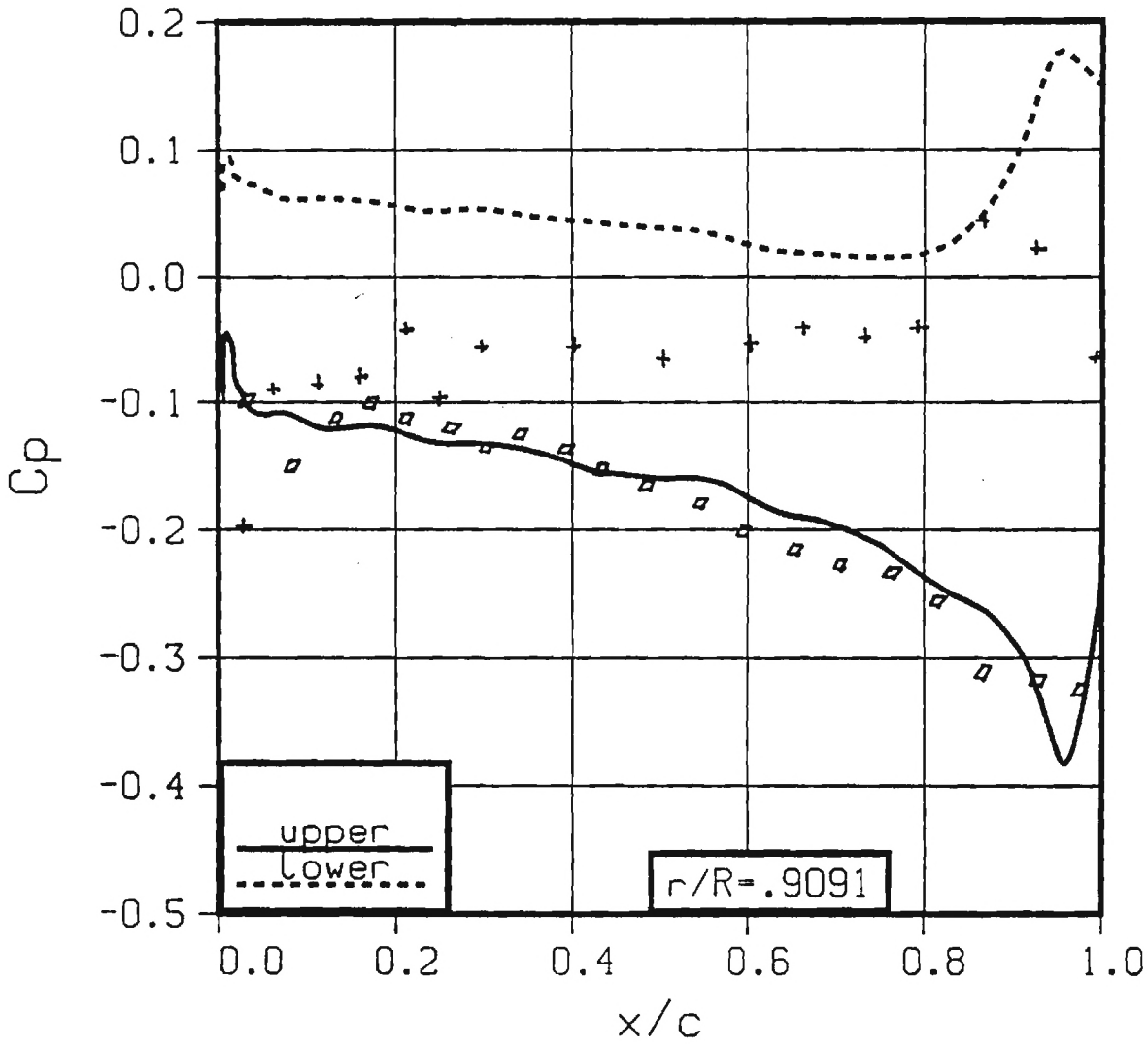

Figure-2d Pressure Distribution Comparison at 91% Radial Station

E-16-801

SIMULATION OF UNSTEADY ROTATIONAL FLOW OVER PROPFAN CONFIGURATION

NASA GRANT No. NAG 3-730

SEMI-ANNUAL STATUS REPORT

for the period

May 1, 1988 - November 30, 1988

submitted to

NASA LEWIS RESEARCH CENTER

CLEVELAND, OHIO

Attn: Mr. G. L. Stefko

Project Monitor

Prepared by:

L. N. Sankar
Associate Professor

Rakesh Srivastava
Graduate Research Assistant

School of Aerospace Engineering
Georgia Institute of Technology
Atlanta, Georgia 30332

INTRODUCTION

The objective of this research is to develop efficient techniques for the prediction of unsteady transonic flow past propfan configurations. A three dimensional unsteady compressible Euler solver, developed at Georgia Institute of Technology, is being modified to adress this problem. This solver can easily be upgraded to a Navier-Stokes solver and also, with small modifications, can be apllied to address the flutter problem for the propfans.

SUMMARY OF PROGRESS

A new algebraic, body fitted H-O grid has been developed and implemented in the Euler solver. This grid, shown in figure-1, is a body fitted grid for the nacelle-blade configuration. This permits to account for the effects of nacelle, and along with appropriate boundary conditions, allows to incorporate the effects of cascade. The grid generator is internal to the solver, this provides the flexibility of varrying the geometry with ease, for a parametric study. It takes less than 4 seconds to genarate a 50,000 point grid on the CRAY XMP at NASA Lewis. However the grid generator is in a modular form and can very easily be replaced by a better and more efficient generator. The Euler solver also has the provision to use a grid generated outside the solver.

In order to improve the prediction of pressure distribution in the viscinity of the shock, the artificial dissipation model was improved. The explicit dissipation terms were modified to incorporate a combination of second and fourth order dissipation terms, in the streamwise direction. The coefficients of the second and fourth order terms varry, based on the magnitude of the local pressure gradient. A purely fourth order dissipation gives good solution, except near the shock where wiggles appear. Whereas a purely second order dissipation, while removing the wiggles near the shock, smears the leading edge suction peak. This results in predicting incorrect loads. The present model supresses, the fourth order terms in the viscinity of a

shock, and the second order terms near the leading edge suction peak. This scheme was suggested by Jameson et al.[1].

The code was also modified to simulate the blade motion by grid motion. This allows to solve the flow field for the exact blade planform. Some prliminary calculations, using this method, were carried out for a 2-bladed rotor and an 8-bladed rotor. For the 2-bladed rotor, the free stream Mach number was 0.78 and the advance ratio ($J = V/nD$) was 3.06. The β at $0.75R$ was set at 53.6 deg. The flow field around an 8-bladed rotor was also solved for the same flow conditions as the 2-bladed rotor. The power coefficient obtained was compared with experiment. There is some uncertainity with respect to the β at $0.75R$ hence it was suggested that the power coefficient be matched with the experiment to arrive at the appropriate β [2]. This study is currently under progress. The pressure coefficients are plotted in figure-2 and compared with experiment, where available. The comparison, presently, is poor. This could be because of the uncertainity in the β setting angle. This is being investigated.

A trial run was also made with another grid to study the effect of grid. This grid has been developed at NASA Lewis by Bruce J. Clark. Qualitatively both the grids gave similar results. Because the grids had different spacing in the normal direction, they predicted different shock strengths. Comparisons with similar grids is under progress.

PLANNED RESEARCH for the PERIOD DEC 1 1988 - APR 30 1989

During the next reporting period the correlation of pressure coefficient with experiment will be improved and the code will be validated against the experiment. The code will also be applied to unsteady flow conditions where nacelle will be at an angle of attack with respect to the free stream. An attempt will also be made to incorporate user specified unsteady motion to the blade to study the forced response characteristic of the propfan. This can be later upgraded to provide a capablity to

investigate the aeroelastic behaviour of the propfans by simultaneously integrating the structure and fluid equation of motion.

REFERENCES

1. Jameson, A., Schmidt, W. and Turkel, E., "Numerical Solutions of the Euler Equations by Finite Volume Methods Using Runge-Kutta Time-Stepping Scehemes," AIAA Paper 81-259, 1981.

2. Huff, D. L., Private Communications.

8 NOV 88 18:11: 5

RID

I= 1 TO 60
J= 3 TO 3
K= 1 TO 25

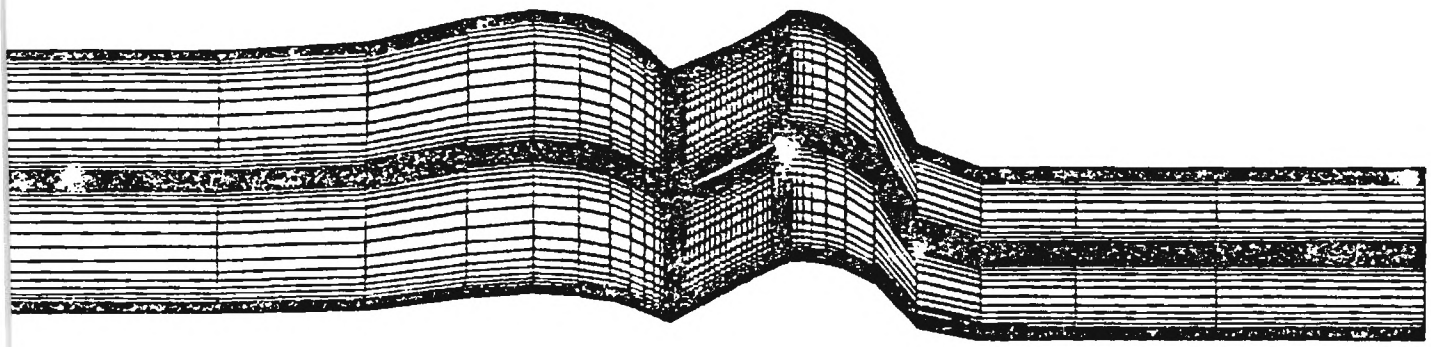

Figure-1a Grid in X-Z Plane

7 NOV 88 11:47:59

GRID

I= 1 TO 60
J= 1 TO 15
K= 1 TO 1

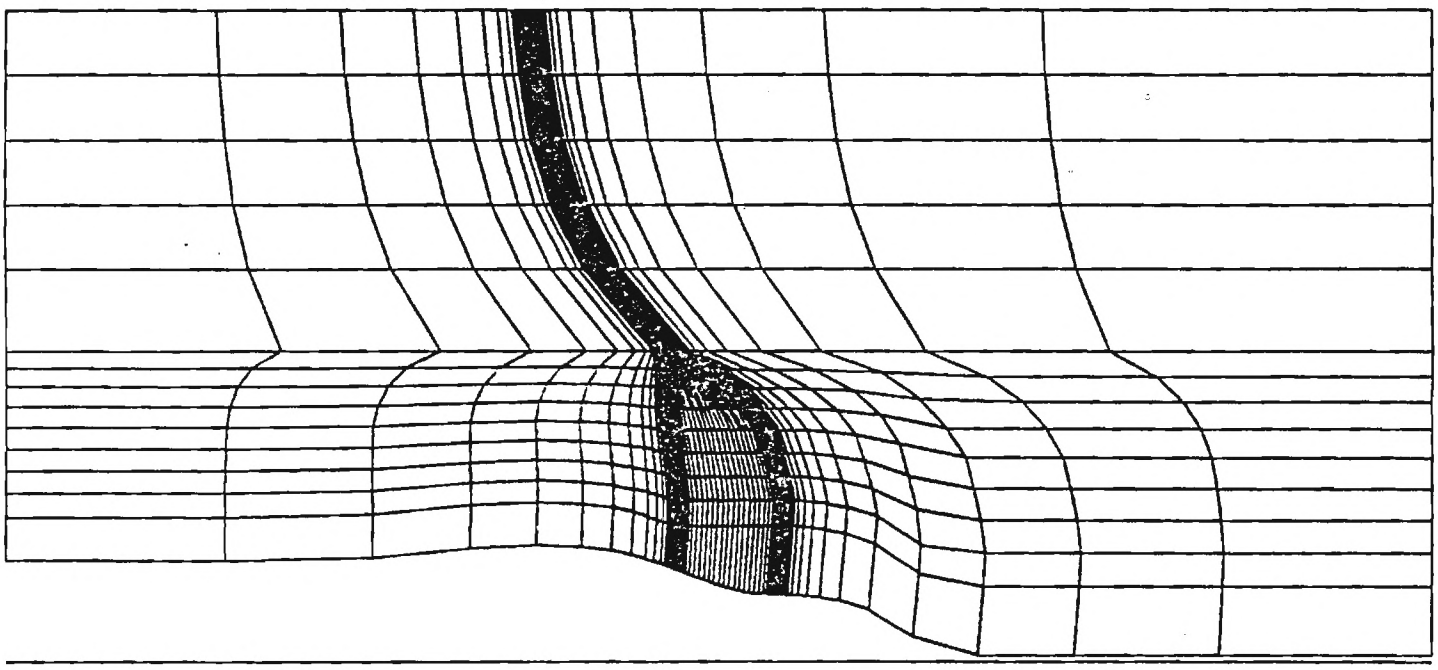

Figure-1c Grid in Y-Z Plane

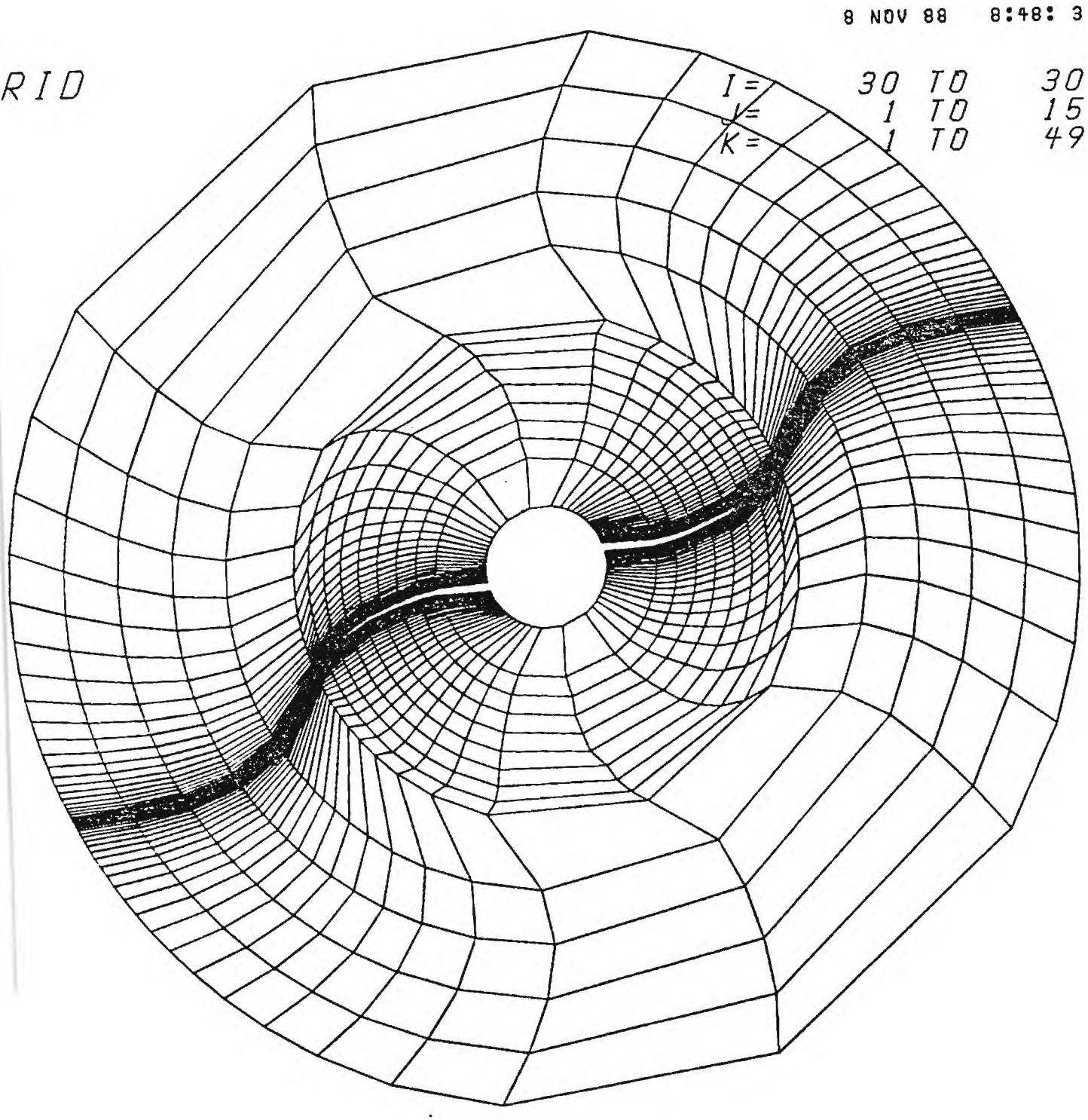

Figure-1b Grid in X-Y Plane

Figure 2a

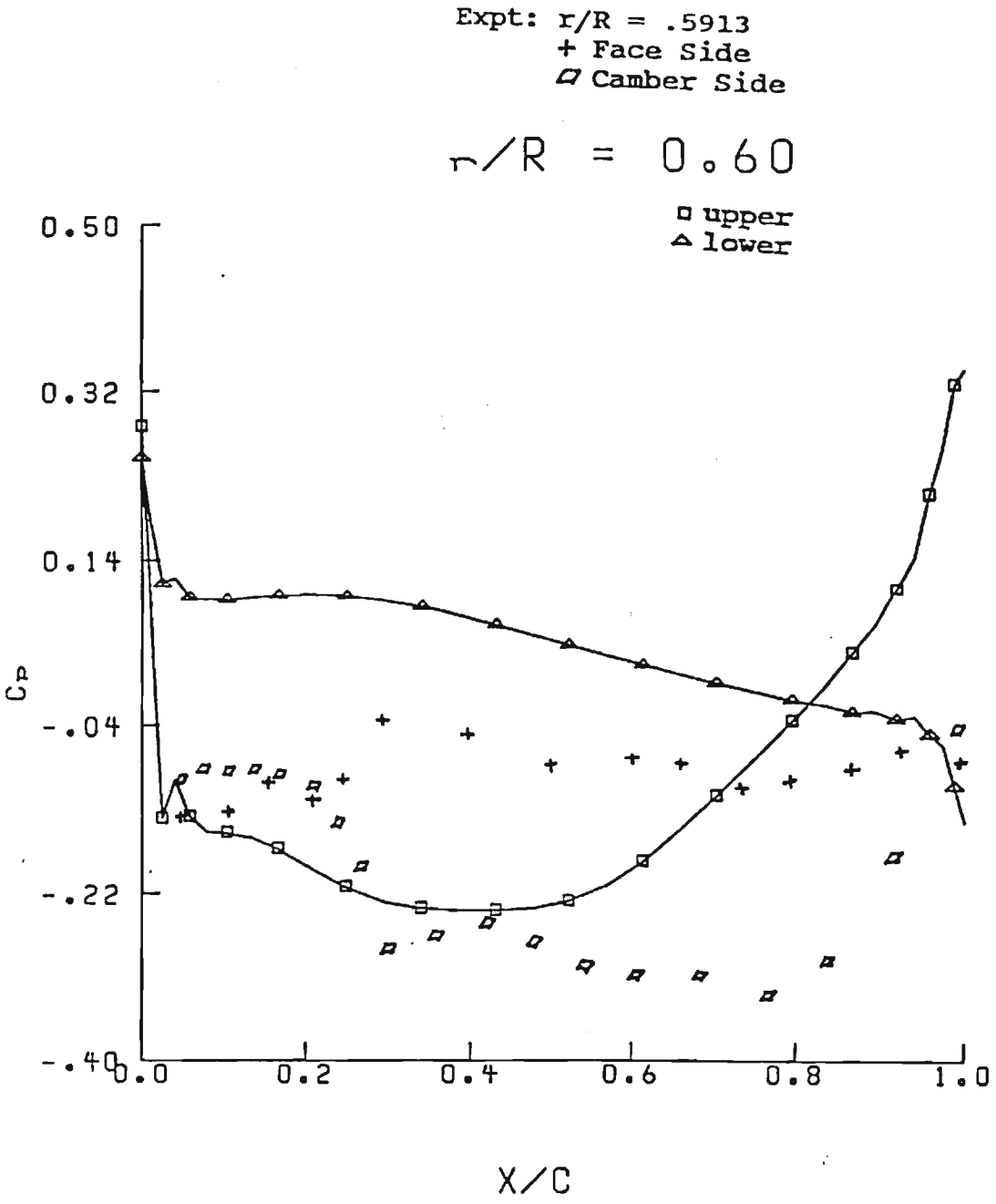

Cp PLOT FOR SR7L PROPFAN

M_∞=0.8, J=3.06, $\beta_{3/4}$=53.6, 2 *blades*

Figure 26

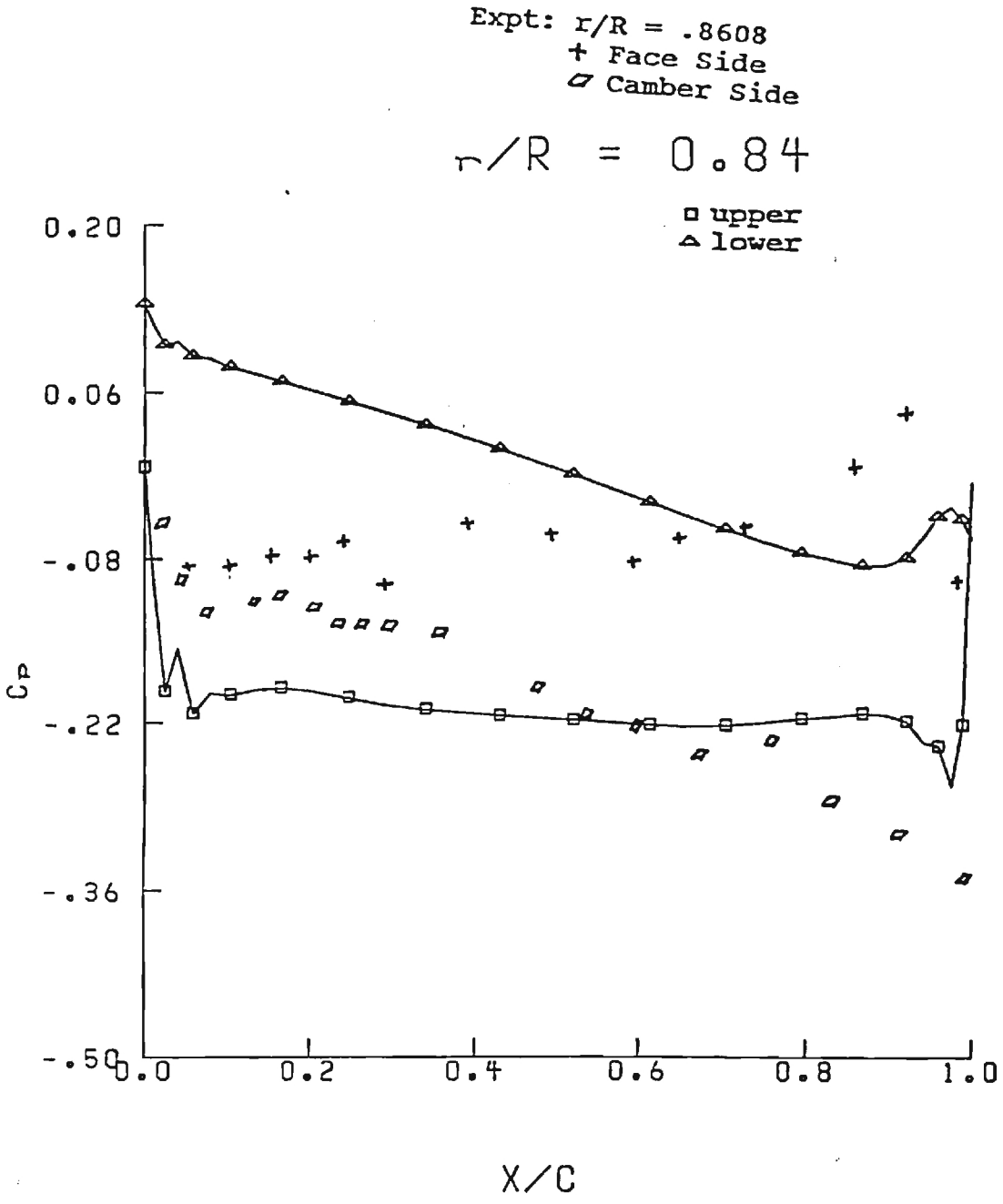

Cp PLOT FOR SR7L PROPFAN

M_∞=0.8, J=3.06, $\beta_{3/4}$=53.6, 2 *blades*

Figure 2C

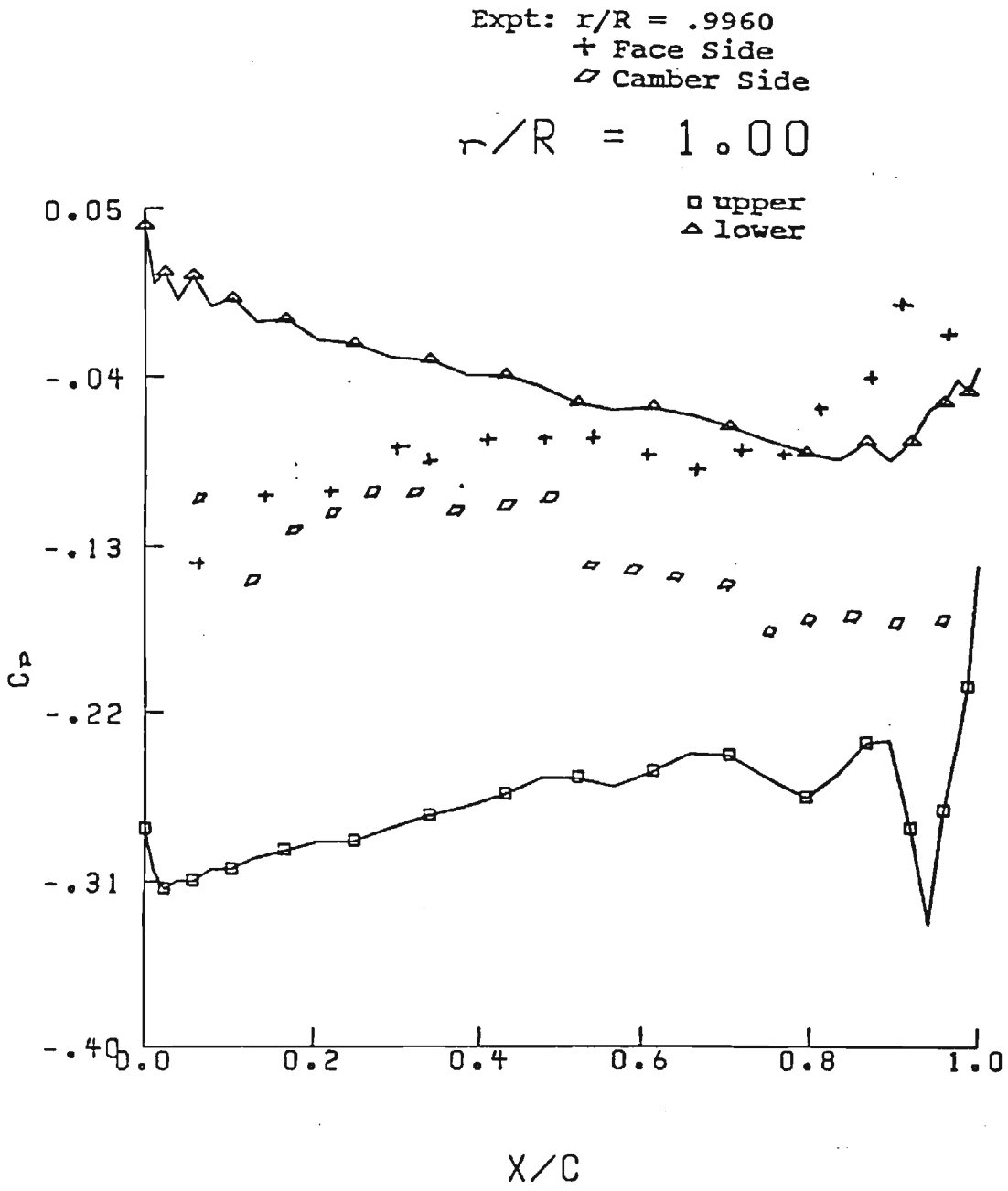

Cp PLOT FOR SR7L PROPFAN

M_∞=0.8, J=3.06, $\beta_{3/4}$=53.6, 2 *blades*

E-16-801

SIMULATION OF UNSTEADY ROTATIONAL FLOW OVER PROPFAN CONFIGURATION

NASA GRANT No. NAG 3-730

SEMI ANNUAL STATUS REPORT

for the period

December 1, 1988 - April 30, 1989

submitted to

NASA LEWIS RESEARCH CENTER

CLEVELAND, OHIO

Attn: Mr. G. L. Stefko

Project Monitor

Prepared by:

Rakesh Srivastava
Graduate Research Assistant

L. N. Sankar
Associate Professor

School of Aerospace Engineering
Georgia Institute of Technology
Atlanta, Georgia 30332

INTRODUCTION

The objective of this research is to develop efficient numerical techniques for the study of aeroelastic response of a propfan in an unsteady transonic flow. A three dimensional unsteady Euler solver, developed at Georgia Institute of Technology is being modified to address this problem.

SUMMARY OF PROGRESS

The Euler solver has been sufficiently modified to be able to efficiently solve unsteady transonic flow past the propfan. The capabilities of the solver can be summarized as follows :

Grid Generation:

A versatile grid generator has been developed to generate a curvilinear body fitted grid for propfan type geometry, having any number of blades and any planform shape. The grid is generated for one passage of the blade, between the upper surface of one blade and lower surface of the adjoining blade. This makes the solid blade surfaces as the zone boundary having inward surface normals. The nacelle is exactly modelled, except for the fact that a thin cylindrical extension is added upstream of the nose of the nacelle. This was necessary in order to avoid having zero metrics of transformation. The propfan code has been modified to accept the grid from the grid generator and analyze periodic flows, and propfans at angle of attack.

A zonal grid such as this is ideally suited for propfan calculations. If only symmetric flowfield is of interest, solution in only one zone or one blade passage is sufficient. If unsymmetric flow field is of interest, solution of all blades is required. Solving the whole propfan geometry would lead to prohibitive memory requirements. A zonal treatment allows the solution with a reasonable memory requirement. A version of our solver allows the flow field variables of the zones to be stored on solid state devices and brought into computer core one zone at a time to be advanced through time one time step at a time. The grid for other zones is generated simply by rotating the grid about the centerline of the nacelle.

A typical grid for an SR-3 blade is shown in figure (1). As can be seen, the grid topology is H-type in the streamwise plane and O-type in the azimuthal plane.

Boundary Conditions:

The boundary conditions have been suitably modified to handle the cascade effects. As stated earlier, there are two options for the boundary conditions. The first option assumes that the flow is symmetric, and hence the flow is periodic at the blade interface or zonal boundaries. The second approach considers the flow to be unsymmetric and allows angle of attack effects. Hence the boundary condition requires that the flow be continuous across the zonal fluid boundaries. In this approach, as mentioned earlier, the zones are independently advanced in time. The interior of the flow field is solved first. Then the fluid boundaries are updated explicitly by averaging the flow quantities across the boundary using the latest available information.

SR-3 Simulations:

The first approach has been applied to solve the flow field around an SR-3 8 bladed propfan for which both numerical and experimental results have been published. These results are shown in figure (2) for the variation of power coefficient with advance ratio. The power coefficients predicted by this code are in good agreement with other published results. The difference with experimental results could be attributed to several factors. It has been observed experimentally in reference (1), and in our calculations that the power coefficients are very sensitive to even small changes in 75% span twist angle setting. The difference with experiment, as seen in our calculations, can be caused by as small as 0.5 deg difference in setting angle, which is well within experimental tolerances. It could also be attributed to the fact that the blades being flexible, can deform in operation. This will change the shape, namely the twist, and hence the angle of attack at each airfoil section. Taking this deformation into account in a purely aerodynamic code is not possible. This can be taken care of by using the aerodynamic loads to obtain a new deformed shape by static structural analysis. Using this new shape, aerodynamic loads can be updated, and a new deformed shape can be obtained. This iteration can be carried out till convergence. This process should, hopefully, improve the correlation in power coefficients. Such a coupled aero-structural analysis will be attempted in cooperation with Dr. Reddy of NASA Lewis Research Center during the first authors visit to Lewis in summer 1989.

Figure (3) shows a comparison of swirl angles. The swirl angles predicted by the present code, are in poor agreement with other published results. Even though the error is large, approximately 100% in the inboard regions, it follows the trend similar to those predicted by other researchers. Also, the error in absolute terms can be considered small, only about 6 or 7 deg, which can be caused by interpolation required to calculate them. Furthermore due to the nature of the grid, the stretching in

the wake is large, hence interpolating quantities could lead to substantial errors. The source of the error is being investigated.

A few pressure coefficient plots for free stream Mach number of 0.8, advance ratio of 3.06 and beta setting angle of 60.5 deg have been attached.

SR-7 Simulations:

A sample case for a two bladed SR-7 propfan has been computed for a free stream Mach number of 0.775, advance ratio of 3.088 and beta setting angle of 54.6 deg. This has been done in order to compare the pressure coefficients with the available experimental values from the full scale wind tunnel tests at Modane, France. Some plots comparing the pressure coefficients have also been attached. The results plotted are very priliminary, as no attempts have been made to match the computed and measured power coefficients. The experimental results have a scatter of 2.6 deg in the beta setting angle over the span. Further runs are under progress to try to match the power coefficient in order to obtain more meaningful comparison.

The second boundary condition has also been implemented and the algorithm has been tested. However as it is computationaly demanding to solve flow field around a propfan for an unsymmetric flow, it was decided that the symmetric flow algorithm will be validated before extensive calculations for the unsymmetric case would be attempted.

Provision has already been made in the solver to allow treatment of surface motion. However the solver does not have the ability to solve the structural dynamics equations of motion. But the code can interact with a structural solver, passing the current aerodynamic loads to it and receiving deformed shapes from it. This allows the code to be independent of the sophistication of the structural modelling and hence can be coupled with any structural solver to permit aeroelastic calculations.

PROPOSED RESEARCH DURING THE PERIOD MAY 1 - OCTOBER 31, 1989

During this period the aerodynamic code will be coupled with a structural solver to carry out aeroelastic calculations. Also the work to modify the code for solving supersonic flow through fans will be initiated. Further validations, of the obtained results, with experimental results, where available, will be done.

REFERENCES

1. Rohrbach, C., Metzger, F. B., Black, D. M., and Ladden, R. M., "Evaluation of Wind Tunnel Performance Testing of an Advanced 45 deg Swept Eight-Bladed Propeller at Mach Numbers from 0.45 to 0.85," NASA CR-3505, 1982.

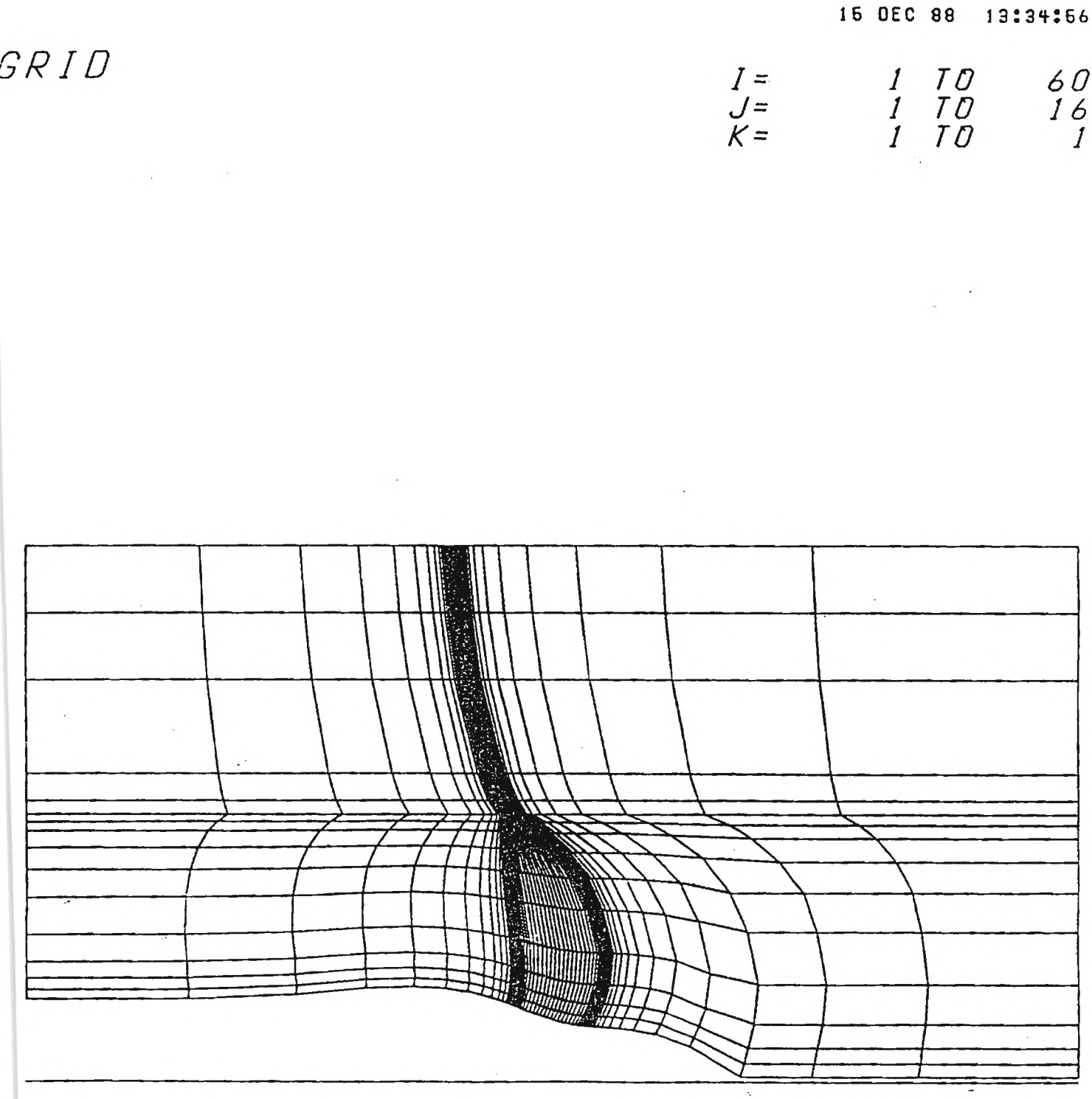

Figure-1a H-grid in Streamwise Plane

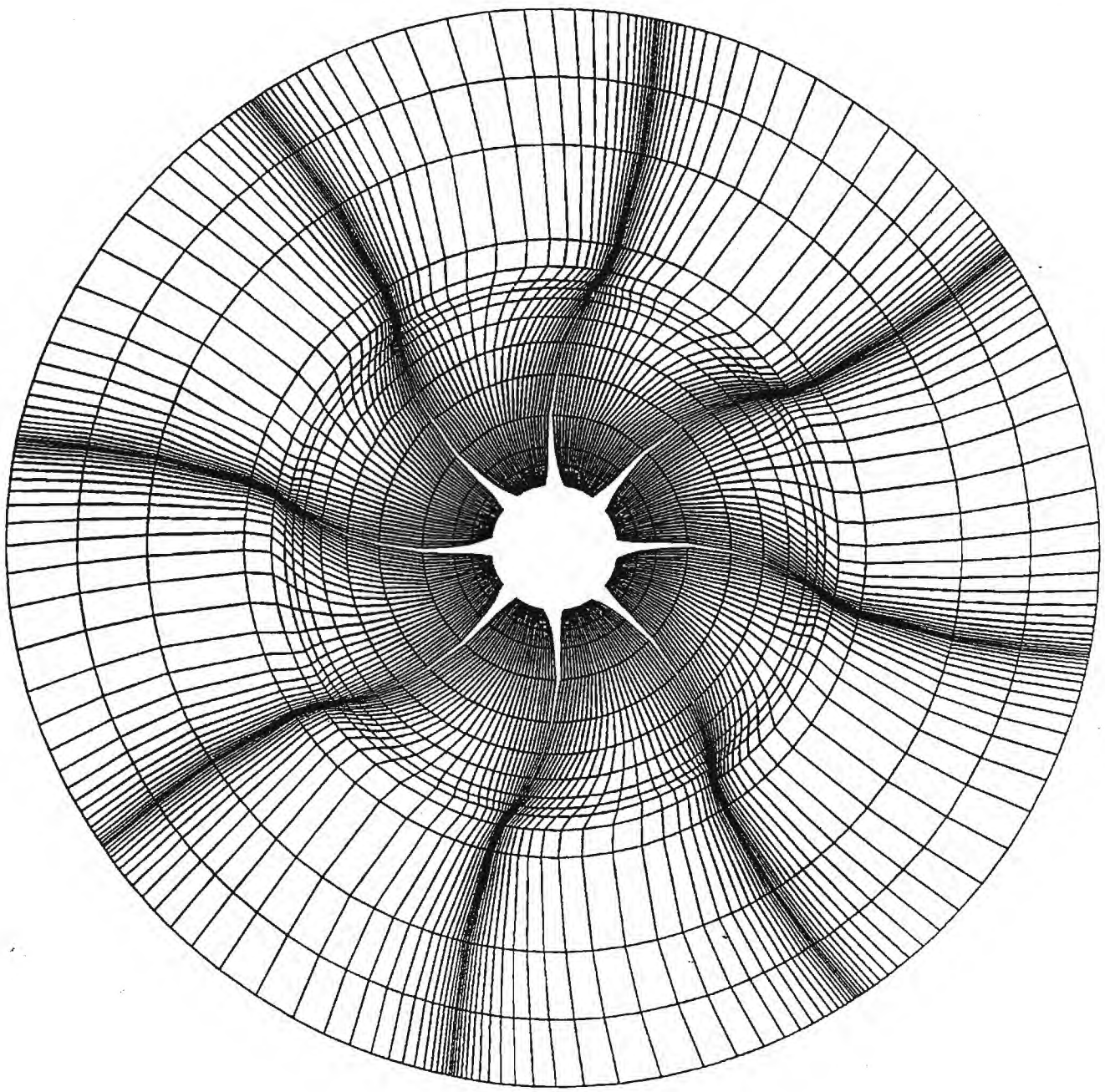

Figure-1b O-grid in Azimuthal Plane

Power Coefficient vs. Advance Ratio
8 Bladed SR-3 Propfan

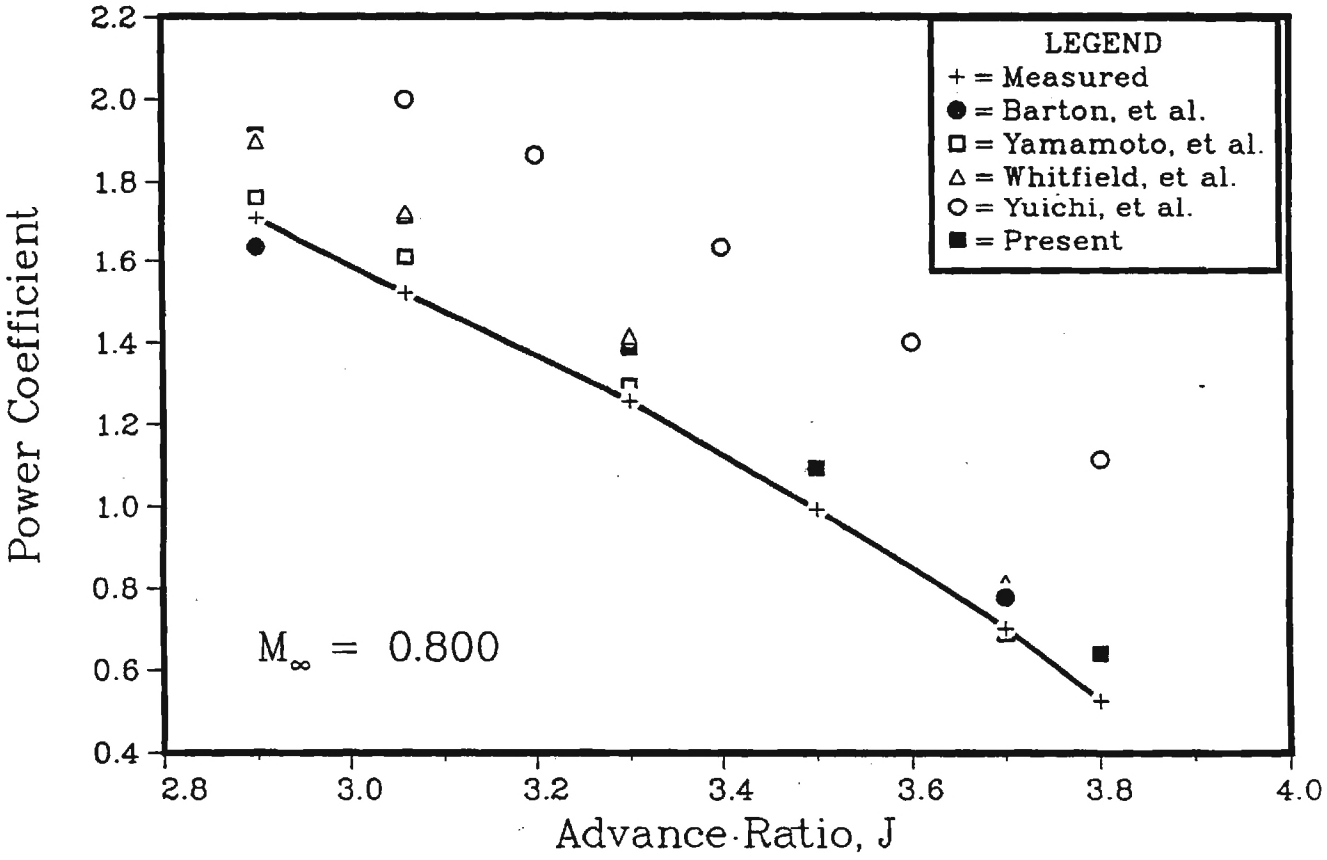

Figure 2a

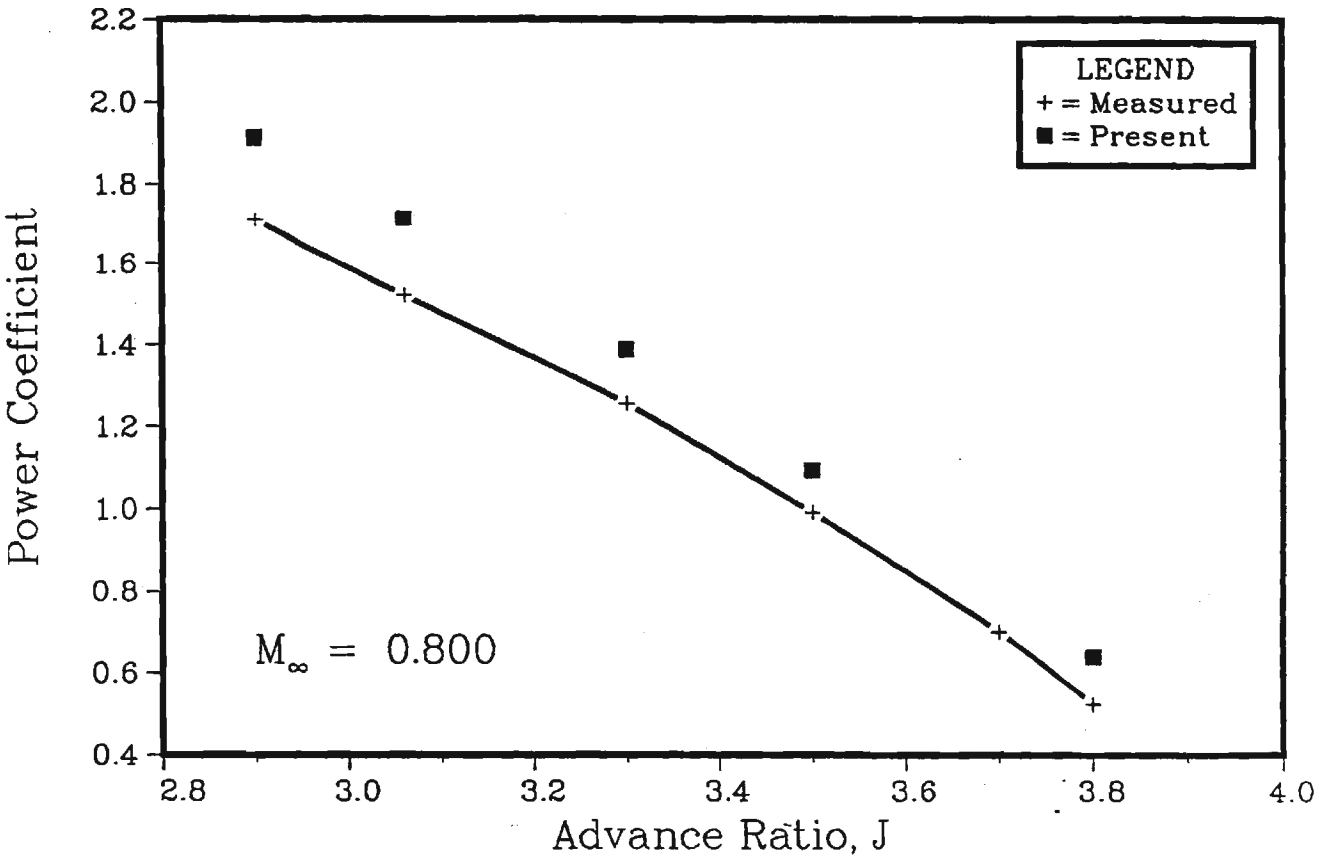
Power Coefficient vs. Advance Ratio
8-Bladed SR-3 Propfan
Power Coefficient
2.2
2.0
1.8
1.6
1.4
1.2
1.0
0.8
0.6
0.4
2.8
3.0
3.2
3.4
3.6
3.8
4.0
Advance Ratio, J
LEGEND
+ = Measured
■ = Present
M_∞ = 0.800

Figure 2b

Swirl Angles

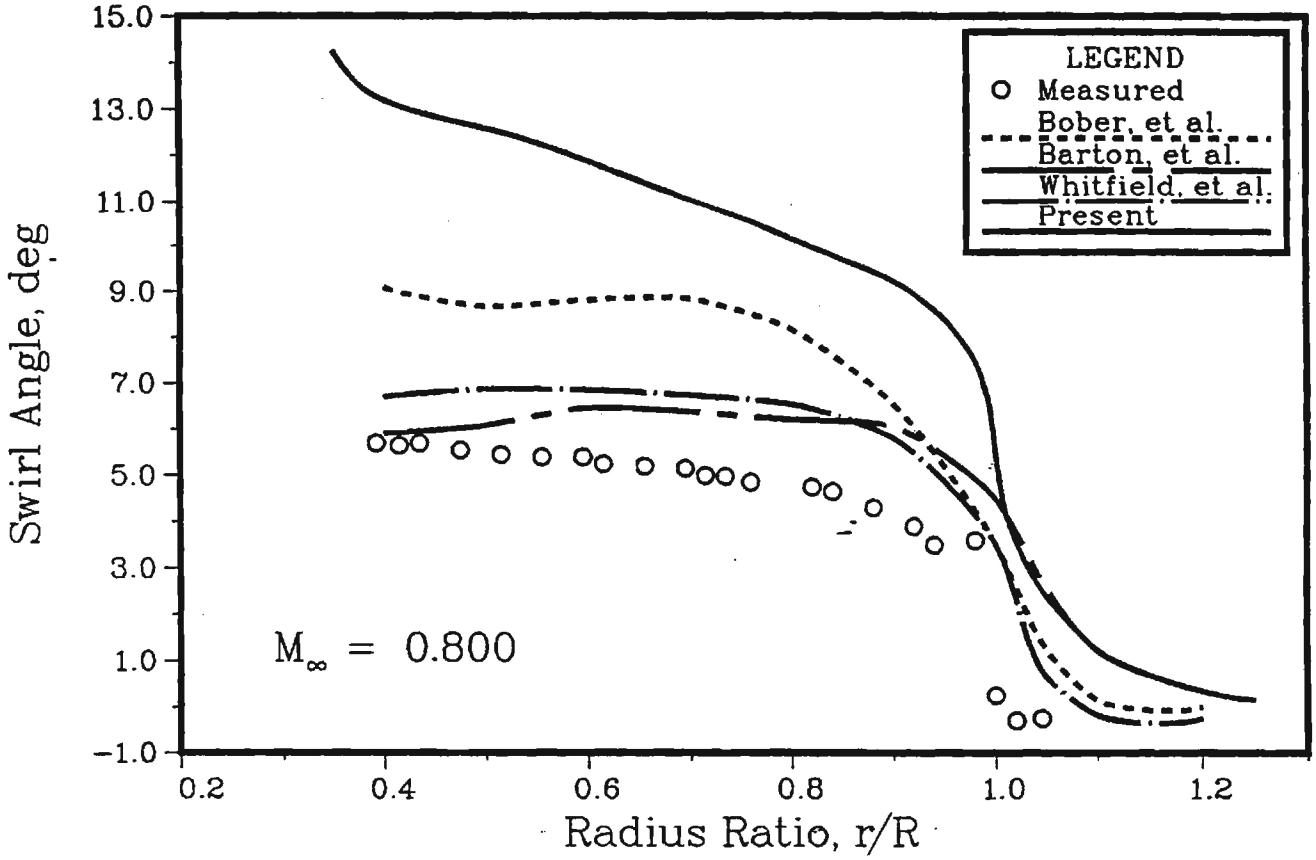

Figure 3

SR-3 8-Bladed Propfan

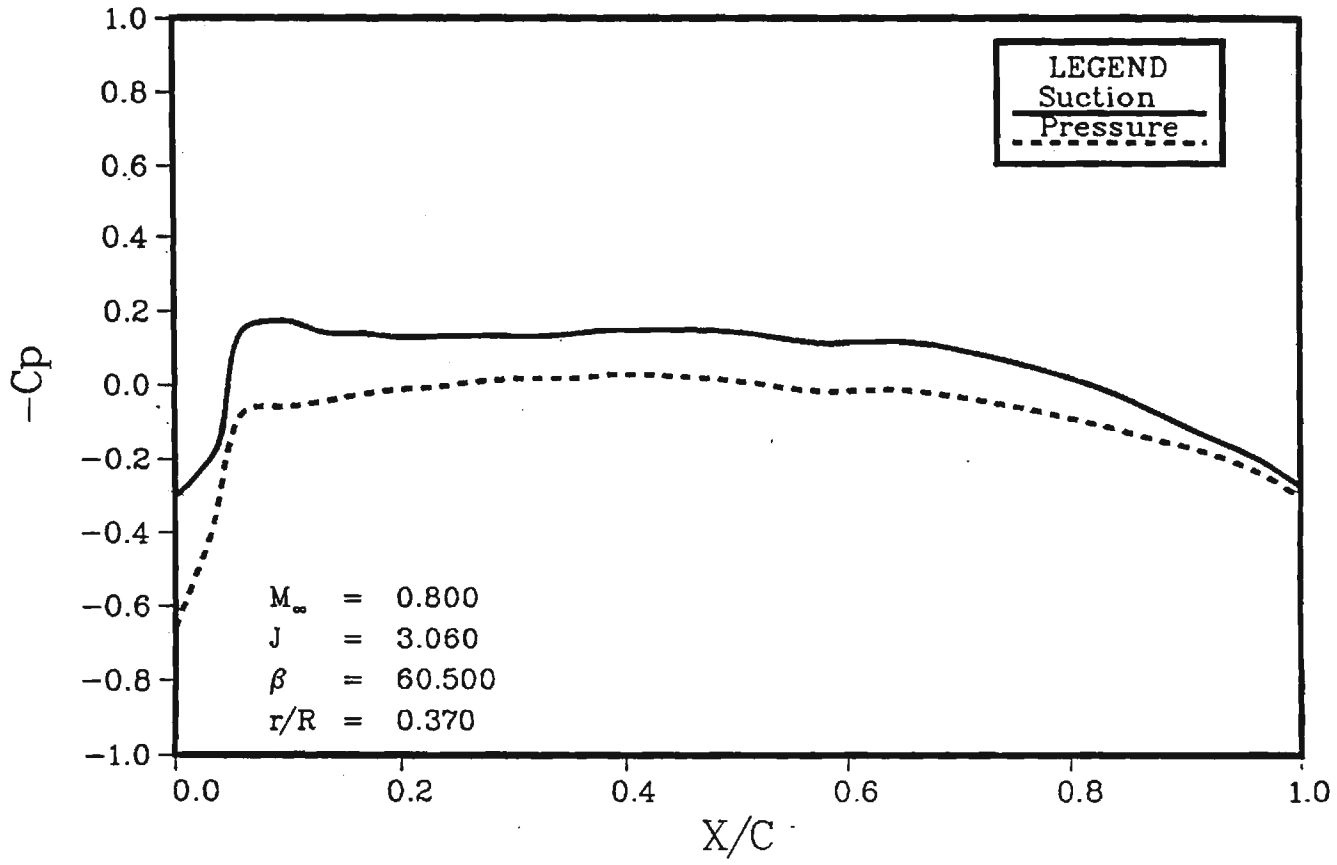

SR-3 8-Bladed Propfan

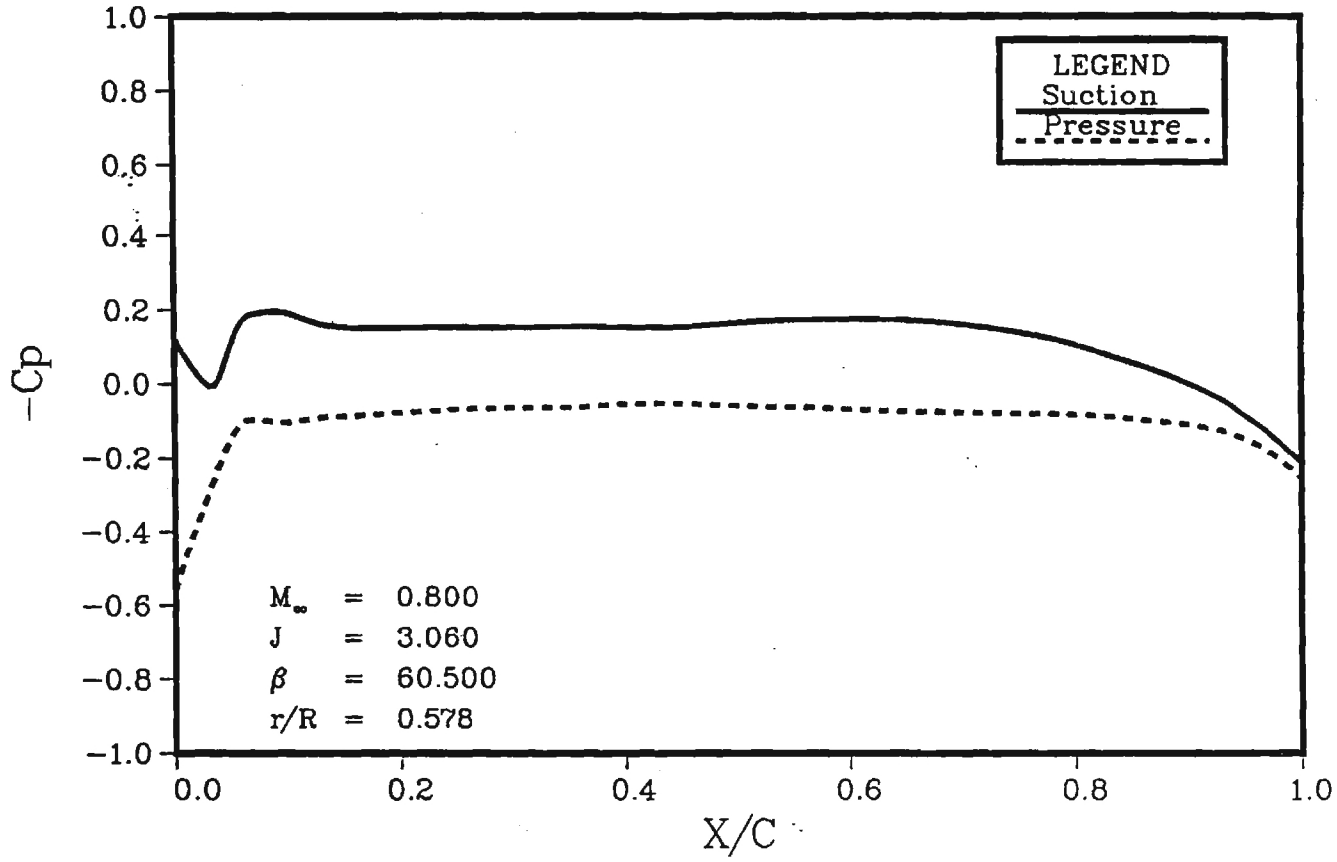

SR-3 8-Bladed Propfan

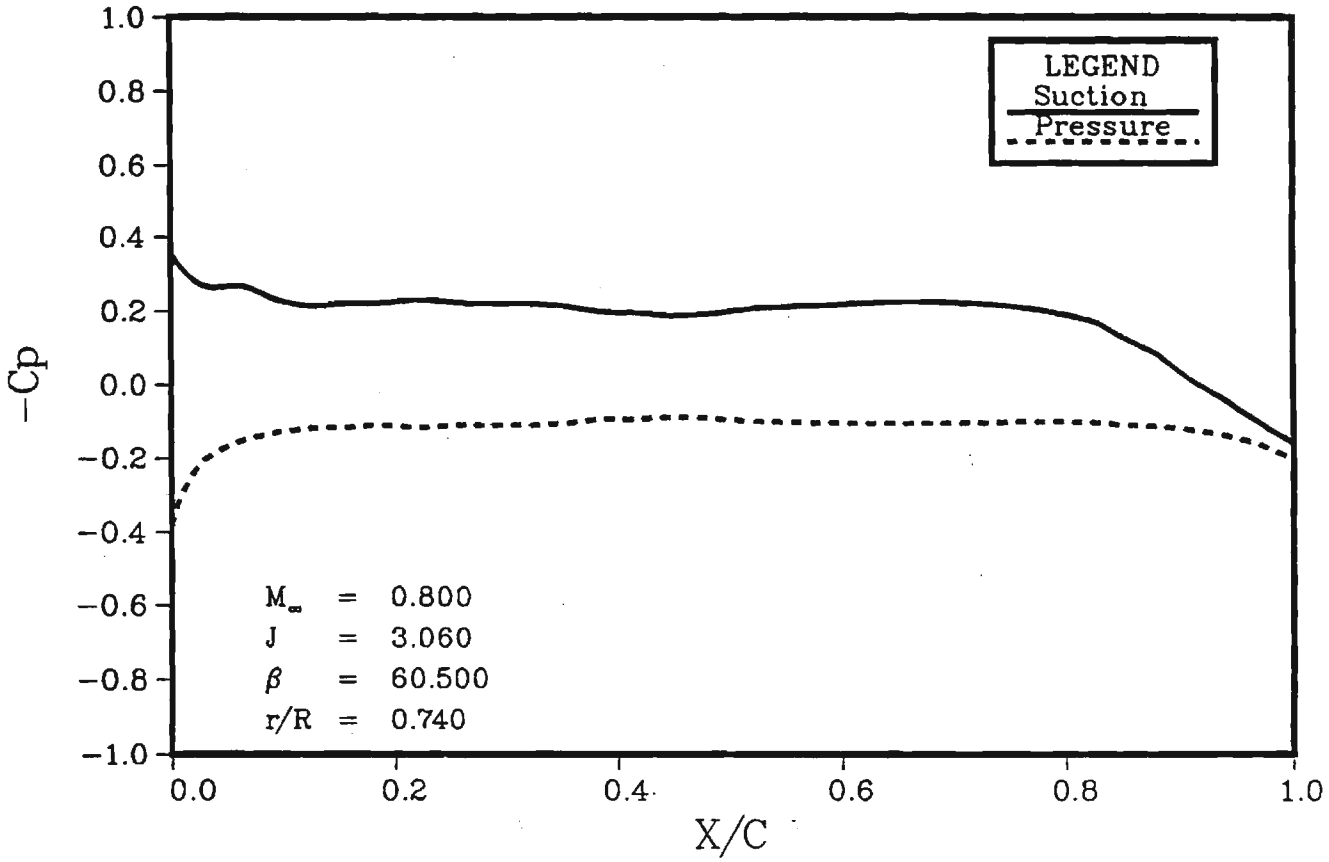

SR-3 8-Bladed Propfan

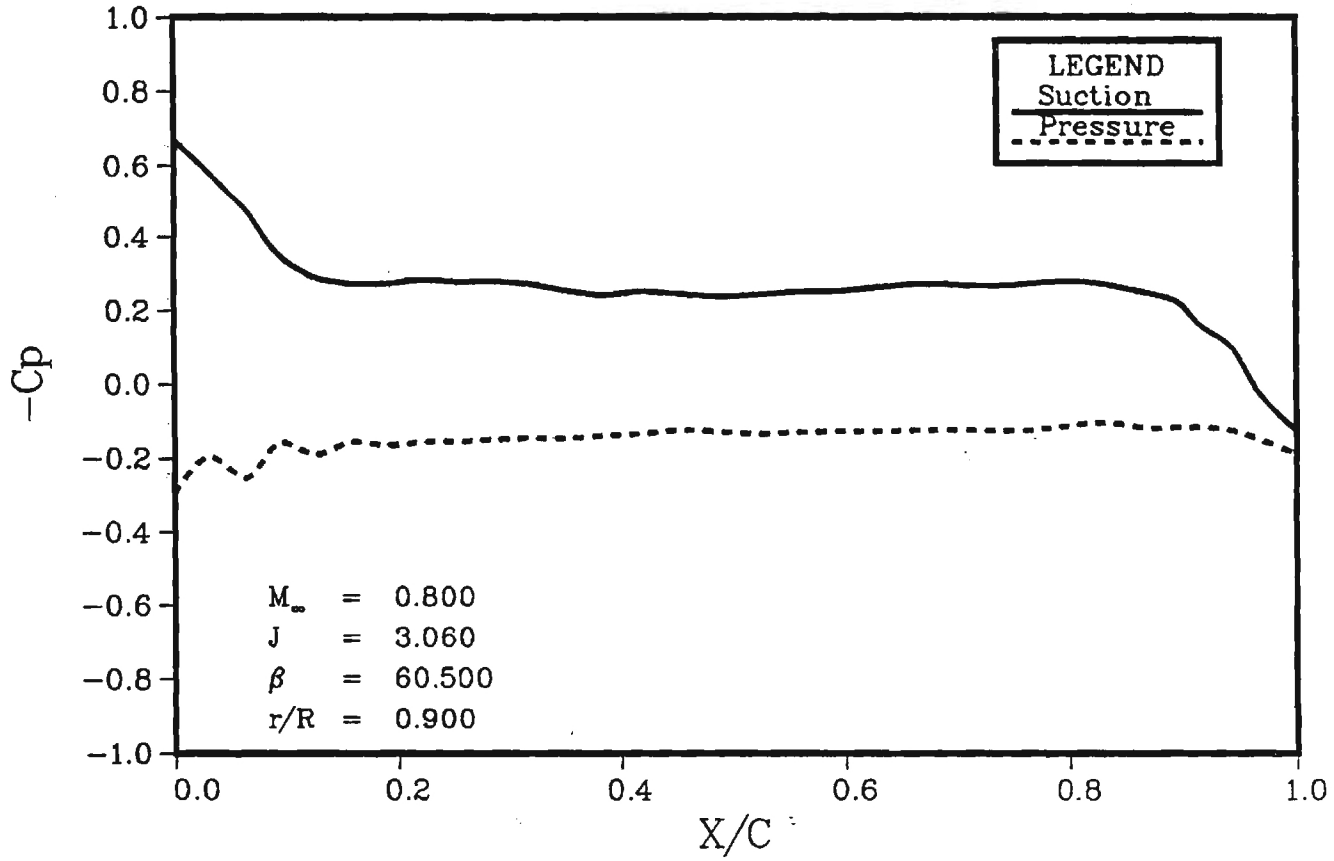

SR-3 8-Bladed Propfan

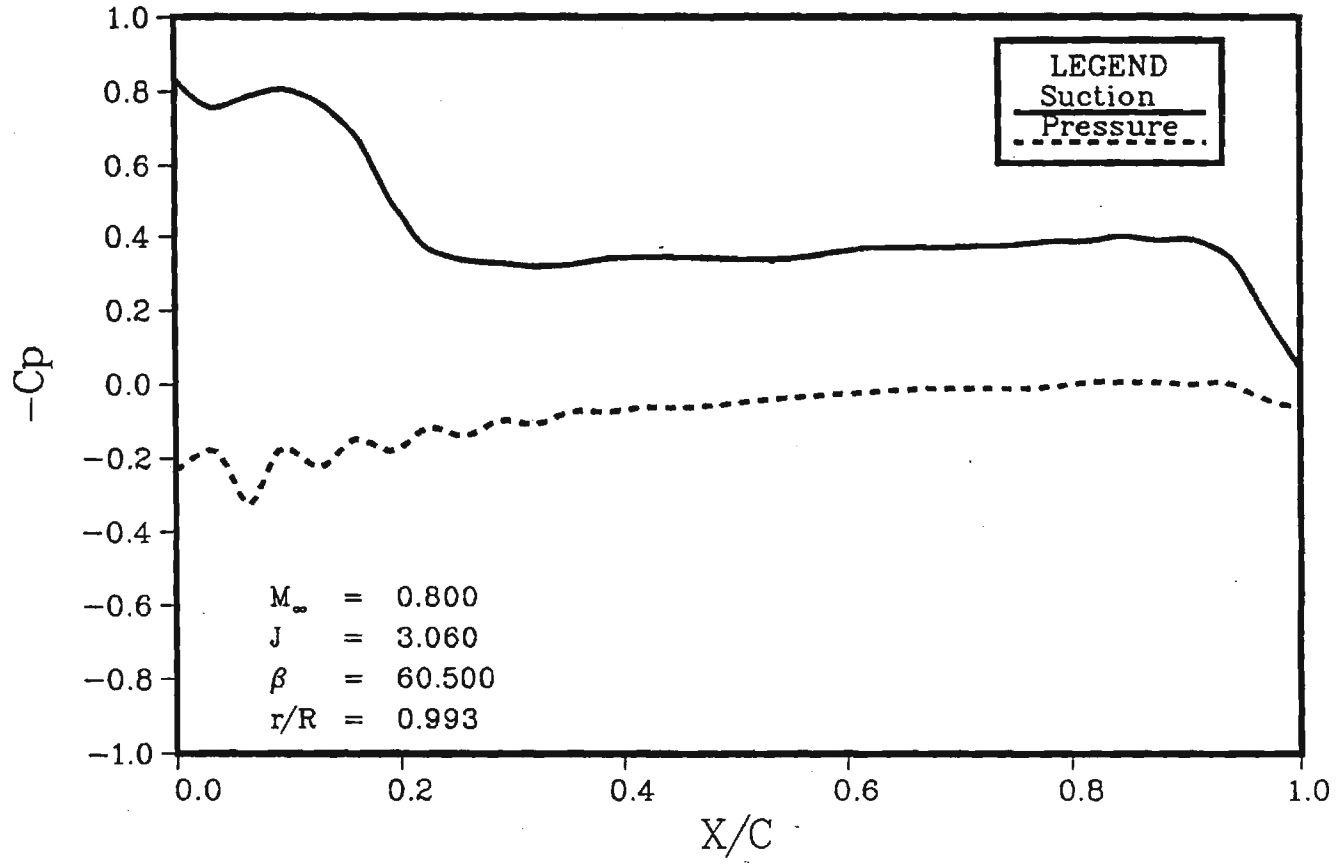

SR-7 2-Bladed Propfan

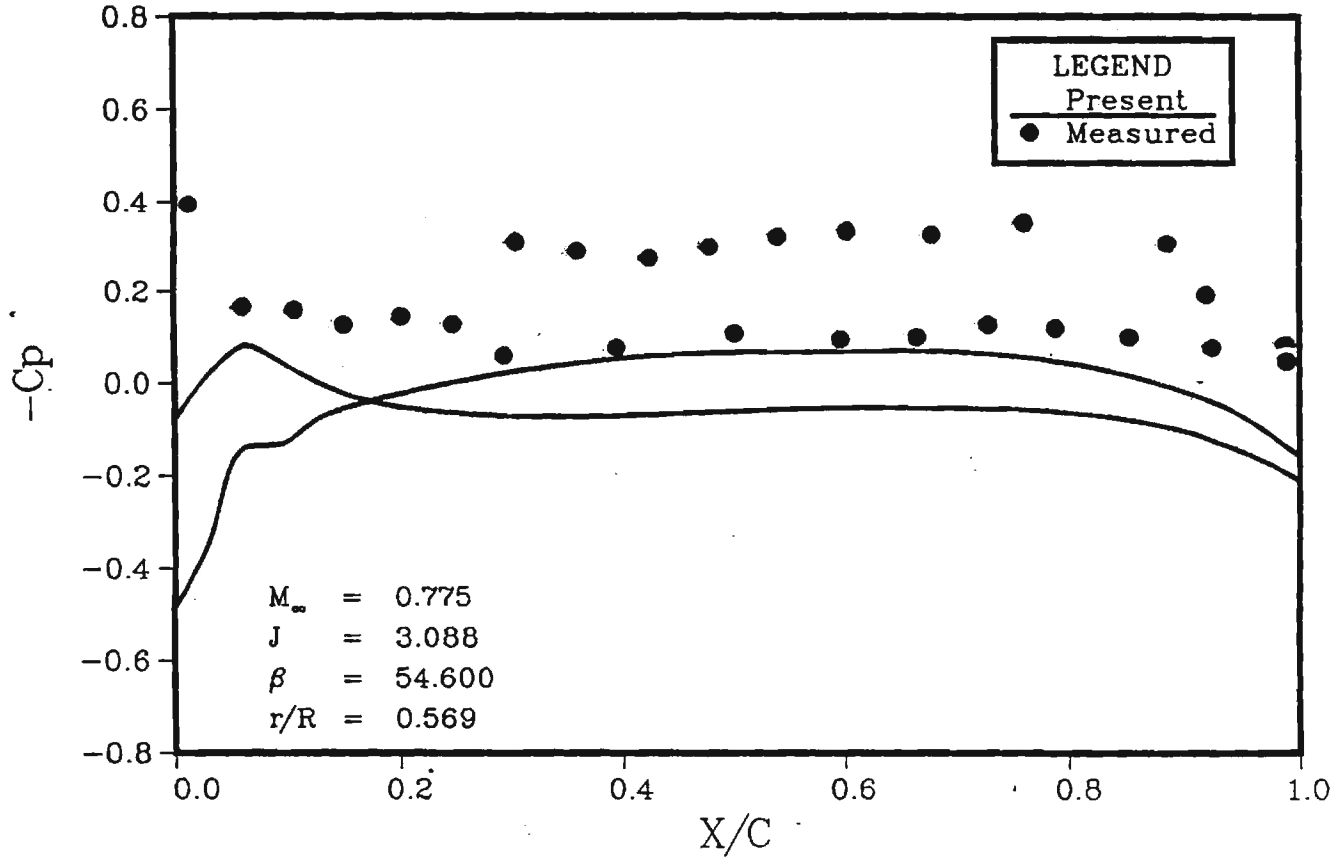

SR-7 2-Bladed Propfan

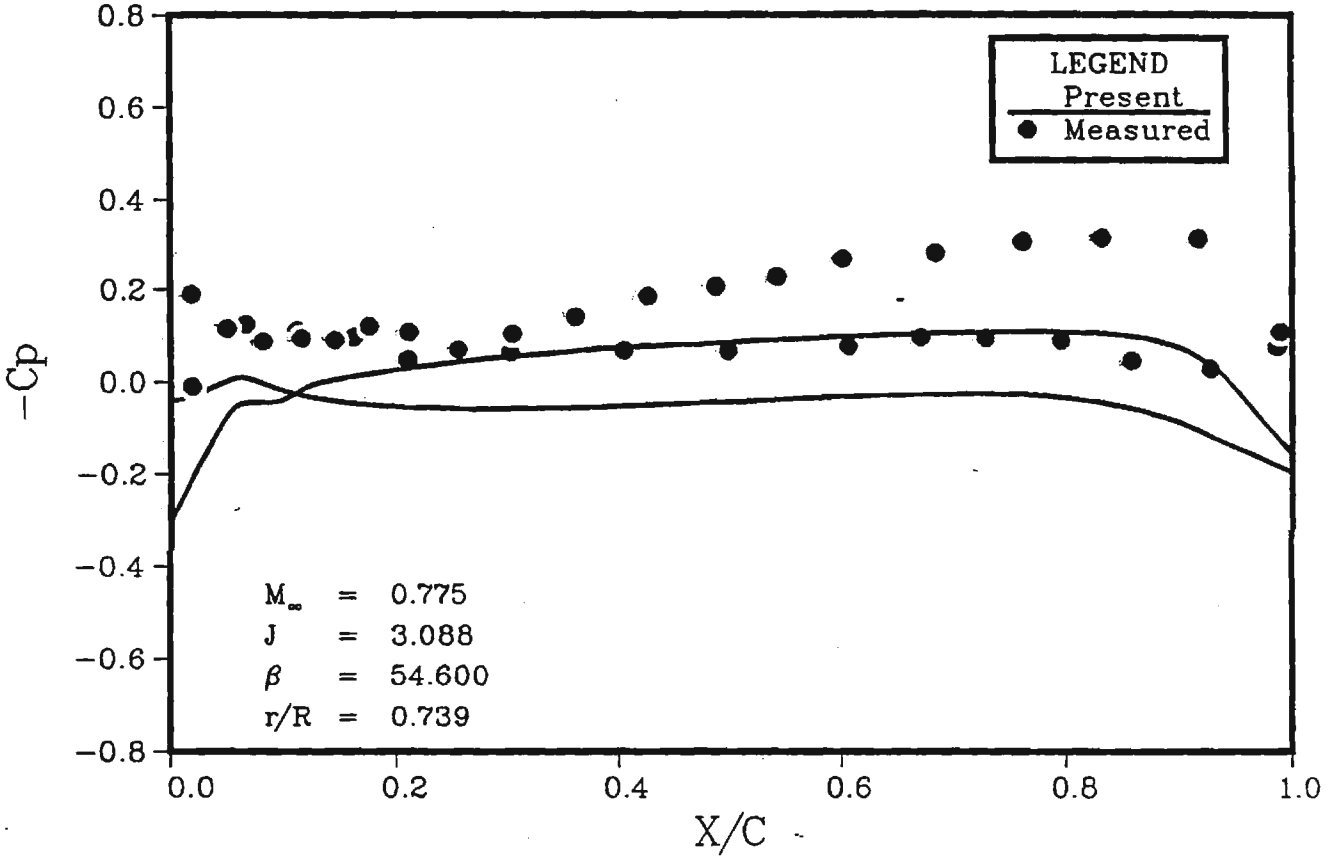

SR-7 2-Bladed Propfan

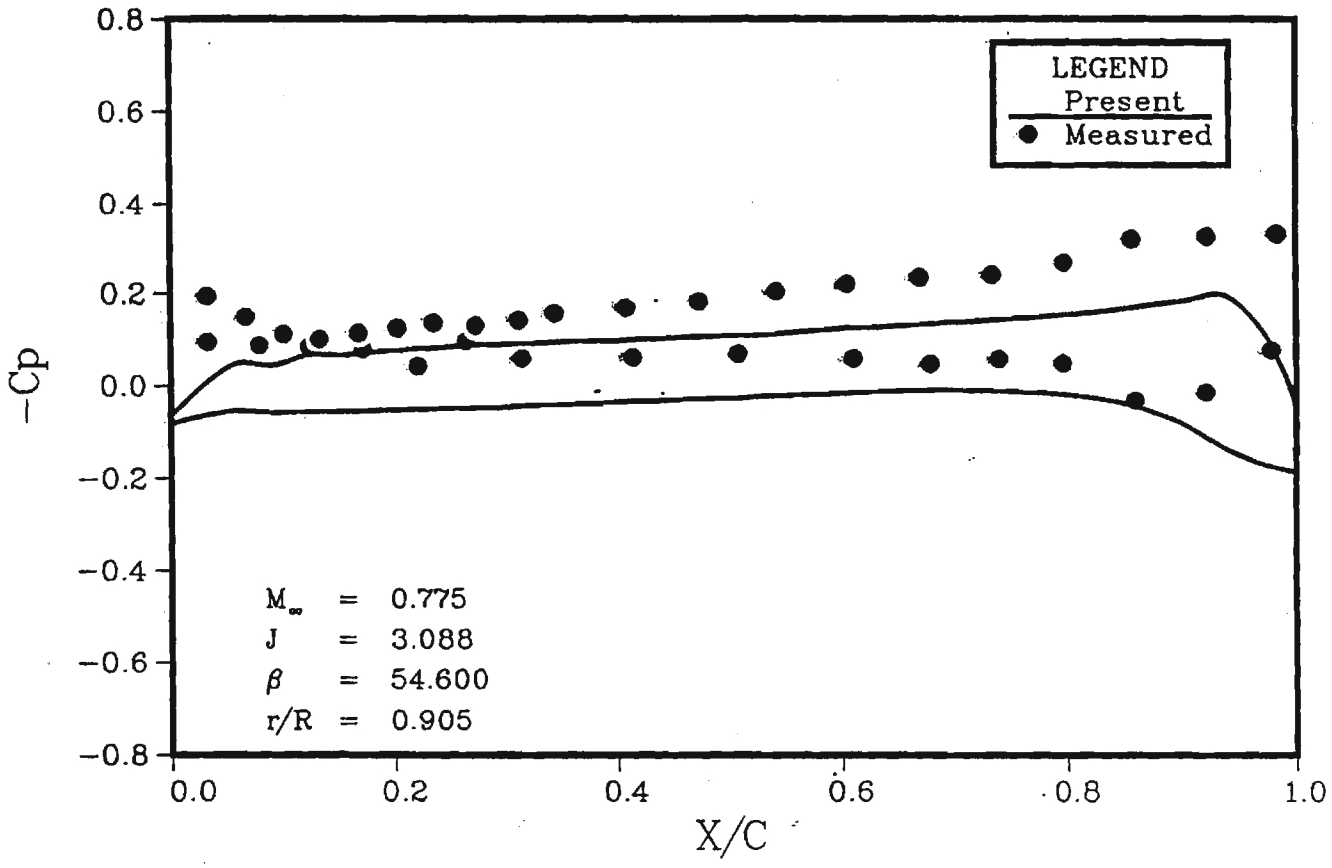

SR-7 2-Bladed Propfan

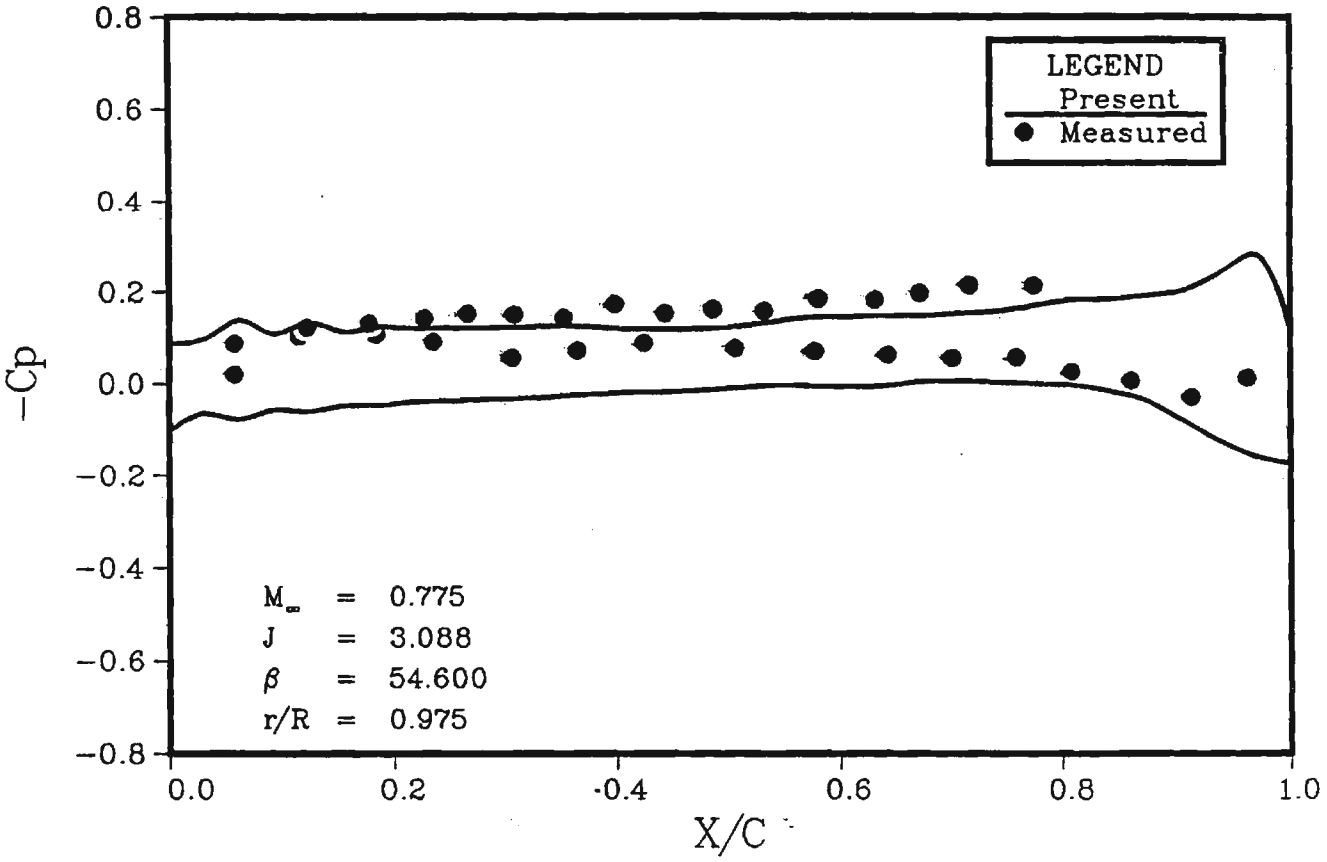

E-16-801

NUMERICAL SIMULATION OF UNSTEADY ROTATIONAL FLOW OVER PROPFAN CONFIGURATIONS

NASA GRANT No. NAG-3-730

SEMI-ANNUAL STATUS REPORT

For the Period

May 1, 1989 - November 30, 1989

Submitted to

NASA LEWIS RESEARCH CENTER
CLEVELAND, OHIO

Attn: George Stefko
Chief, Structural Dynamics Branch

Prepared By

R. Srivastava
Graduate Research Assistant

L. N. Sankar
Associate Professor

School of Aerospace Engineering
Georgia Institute of Technology
Atlanta, GA 30332

November 1989

INTRODUCTION

The objective of this research is to develop efficient numerical techniques for the study of aeroelastic response of a propfan in an unsteady transonic flow. A three dimensional unsteady Euler solver, developed at Georgia Institute of Technology is being modified to address this problem.

SUMMARY OF PROGRESS DURING MAY 1 - NOVEMBER 30, 1989

The Euler solver has been applied to solve flow field around propfan configurations. The results obtained have been compared against other numerical results as well as measured data. The performance prediction of the solver compares well with measured data. The solver was also used to study the effect of blade flexibility on the performance. the airloads obtained from the solver were used to obtain blade deflection using NASTRAN. The deflection calculations were carried out by Dr. T. S. R. Reddy of NASA Lewis Research Center.

A heavily loaded blade was used to perform the study of blade flexibility on performance. Under aerodynamic loading the blade deflection resulted in large changes in power and thrust. Based on this study, it was concluded that for future aeroelastic calculations, blade flexibility should be properly accounted for.

A paper, discussing this study and its results, will be presented in the forthcoming AIAA 28th Aerospace Sciences Meeting and Exhibit at Reno, Nevada from January 8 to 11, 1990. A NASA TM is also under review. A copy of the text of the paper is enclosed.

PLANNED RESEARCH DURING THE PERIOD DECEMBER 1, 1989-APRIL 30,1990

During this period the aerodynamic solver will be modified to solve counter rotating propfan calculations. A few test cases will be chosen in consultation with NASA Lewis Research Center personnel to calibrate the counter-rotating propeller code.

APPENDIX

Application of an Efficient Hybrid Scheme for Aeroelastic Analysis of Advanced Propellers

by

R. Srivastava* and N. L. Sankar**
Georgia Institute of Technology
Atlanta, GA

and

T. S. R. Reddy† and D. L. Huff††
NASA Lewis Research Center
Cleveland, OH

* Graduate Student, Member AIAA and AHS
** Associate Professor, Member AIAA and AHS
† Resident Research Associate, Member AIAA and AHS
†† Research Engineer, Member AIAA

Application of an Efficient Hybrid Scheme for Aeroelastic Analysis of Advanced Propellers

Abstract

An efficient three dimensional hybrid scheme is applied for solving Euler equations to analyze advanced propellers. The scheme treats the spanwise direction semi explicitly and the other two directions implicitly, without affecting the accuracy, as compared to a fully implicit scheme. This leads to a reduction in computer time and memory requirement.

The calculated power coefficients for two advanced propellers, SR3 and SR7L, and various advance ratios showed good correlation with experiment. Spanwise distribution of elemental power coefficient and steady pressure coefficient differences also showed good agreement with experiment. A study of the effect of structural felxibility on the performance of the advanced propellers showed that structural deformation due to centrifugal and aero loading should be included for better correlation.

Introduction

It has been known for some time now that the best propulsive efficiency is offered by propellers. However the efficiency drops off very rapidly as the cruise Mach number increases beyond 0.5, as high tip Mach numbers lead to high compressibility losses (due to wave drag). Currently an effort is underway to improve the propulsive efficiency of commercial and military aircraft. Newly designed high speed advanced propellers, also known as propfans, show a very high propulsive efficiency at cruise speeds upto Mach 0.8 [1].

The propfans are designed to delay the compressibility losses, thus extending the high efficiency of a propeller to relatively higher cruise Mach numbers. This is accomplished by sweeping the blade backwards and using thinner airfoils, on

improved on this method by using the curved lifting line concept to account for the sweep. In this approach the vortex wake is represented by a finite number of vortex filaments in place of the continuous sheet of vorticity as used in Goldstein's approach. The analysis has been further extended in reference [5] by placing the vortex filaments along the stream surfaces so that they conform to the shape of the axisymmetric nacelle.

Hanson [6] and Williams [7] applied the Kernel function approach to a propfan blade. They numerically solve a linear integral equation for upwash angle due to the blade pressure distribution by discretizing the load representation. The friction drag is obtained from the two- dimensional airfoil tables as a function of lift coefficient for the appropriate section camber, thickness and a Mach number adjusted for sweep and three-dimensional effects. The induced drag is obtained by determining the kinetic energy-per-unit-length of the far wake. The methods mentioned so far are based on linearized analyses. However, as the advanced propeller operates at or near transonic tip Mach number, flow nonlinearties may become important.

Jou [8] has applied the finite volume approach of Jameson [9] for the analysis of propfans using full potential equation. The formulation was not able to provide converged solutions for free stream Mach numbers greater than 0.6. It was concluded that strong rotational flow effects were present near the leading edge, which could not be modelled by the potential equation. In addition the potential flow equations at times, lead to non-unique solutions.

Chausee [10] and Whitfield *et al.* [11] have applied the unsteady, three dimensional Euler equations to the propfan geometry. Matsuo *et al.* [12] have recently solved the full Navier - Stokes equations around a propfan. Some of these methods have been reviewed in reference [13], with regards to performance prediction.

All the analyses mentioned so far, with the exception of Whitfield *et al.* [11] have been for axisymmetric flows. For a propfan in flight configuration, the flow is not axisymmetric. Even for cruise conditions the nacelle is at an angle of attack

explicitly requires only two costly inversions of block tridiagonal matrix, as opposed to three inversions for a fully implicit scheme, per time step. It also reduces the memory requirement as only two time levels of information needs to be stored at any given time, one of which needs to be only two dimensional. The use of such a hybrid scheme leading to reduction in computer time and memory requirement, makes the scheme more efficient.

The specific objectives of the present paper are 1) to apply an efficient hybrid scheme to analyze advanced propellers, 2) to calculate steady performance, 3) to include structural deformation, due to centrifugal and steady aero loading in the analysis, 4) to study the effects of structural flexibility on the performance of advanced propellers. The governing equations and the numerical solution method are described first followed by results and discussion. The methods developed here are expected to be helpful for future aeroelastic research.

Formulation

Aerodynamic Model:

The Euler equations, in conservation form, in Cartesian coordinate system can be written as:

$$(\hat{\mathbf{q}})_t + (\hat{\mathbf{E}})_x + (\hat{\mathbf{F}})_y + (\hat{\mathbf{G}})_z = 0 \tag{1}$$

where $\hat{\mathbf{q}}$ is the vector containing conserved flow properties. $\hat{\mathbf{E}}, \hat{\mathbf{F}}$ and $\hat{\mathbf{G}}$ are the nonlinear flux vectors which are functions of the vector $\hat{\mathbf{q}}$. The subscripts denote the partial derivative of the vector. In the above equation

$$\begin{aligned} \xi &= \xi(x,y,z,t) \\ \eta &= \eta(x,y,z,t) \\ \zeta &= \zeta(x,y,z,t) \\ \tau &= t \end{aligned} \tag{4}$$

These coordinates are non orthogonal and completely general. The equation (1) can be rewritten as:

$$\mathbf{q}_\tau + \mathbf{E}_\xi + \mathbf{F}_\eta + \mathbf{G}_\zeta = 0 \tag{5}$$

where

$$\mathbf{q} = J^{-1}\begin{pmatrix} \rho \\ \rho u \\ \rho v \\ \rho w \\ e \end{pmatrix} \qquad \mathbf{E} = J^{-1}\begin{pmatrix} \rho U \\ \rho u U + \xi_x p \\ \rho v U + \xi_y p \\ \rho w U + \xi_z p \\ (e+p)U - \xi_t p \end{pmatrix}$$

$$\mathbf{F} = J^{-1}\begin{pmatrix} \rho V \\ \rho u V + \eta_x p \\ \rho v V + \eta_y p \\ \rho w V + \eta_z p \\ (e+p)V - \eta_t p \end{pmatrix} \qquad \mathbf{G} = J^{-1}\begin{pmatrix} \rho W \\ \rho u W + \zeta_x p \\ \rho v W + \zeta_y p \\ \rho w W + \zeta_z p \\ (e+p)W - \zeta_t p \end{pmatrix} \tag{6}$$

U, V, and W are the contravariant velocities, and J is the jacobian and ξ_x, η_x, ζ_x etc. are the metrics of transformation.

Initial and Boundary Conditions

A large number of problems can be described by the same set of governing

inflow boundary, all quantities are fixed to that of the free stream,as disturbances cannot travel upstream in a supersonic flow. At the subsonic outflow boundary, four characteristics should escape, thus the four quantities $\rho, \rho u, \rho v, \rho w$ are extrapolated from inside while the pressure is fixed to that of the free stream. For supersonic outflow, all characteristics should escape, hence all quantities are extrapolated from inside the flow domain.

The block interface boundary :

It is neither efficient nor practical to solve all the blades at the same time, hence, one blade passage is handled at a time. This introduces additional boundaries for computation. Across these boundaries all the variables must be continuous, except on solid boundaries and boundaries downstream of the blade. The boundary condition, for these boundaries, depends on the type of flow being solved. An axisymmetric flow would require periodicity on the fluid interface boundaries. Periodicity will require that the two boundaries have same fluid properties. As shown in figure (1a), the fluid properties at the boundaries K=1 and K=KMAX are updated as the average of fluid properties at K=2 and K=KMAX-1 for a symmetric flow field.

For an unsymmetric flow, the periodicity on these boundaries does not exist. Therefore, in order to obtain the solution for such a case, the whole propfan should be solved. This is done by advancing the solution of each block one time step, one block at a time. In this case again the boundaries are updated explicitly, after the interior points have been updated.This is done by averaging the flow variables from the nodes on each side of the boundary from the adjoining blocks. Referring to figure (1b), (the subscripts refer to the corresponding block) the quantities at boundary K=KMAX of block N (which is also the boundary K=1 for block N+1) would be the average of flow quantities at K=KMAX-1 of block N and K=2 of block

marching direction is reversed after every sweep, in order to remove any dependency on the marching direction. Equation (10) can then be rewritten as :

$$\mathbf{q}^{n+1} = \mathbf{q}^n - \Delta\tau \left(\mathbf{E}_\xi^{n+1} + \mathbf{F}_\eta^{n,n+1} + \mathbf{G}_\zeta^{n+1} \right) \tag{11}$$

Since the η marching direction is changed every iteration, the $\mathbf{F}_\eta^{n,n+1}$ alternates between

$$\frac{\mathbf{F}_{i,j+1,k}^{n} - \mathbf{F}_{i,j-1,k}^{n+1}}{2\Delta\eta}$$

during the odd time steps, and

$$\frac{\mathbf{F}_{i,j+1,k}^{n+1} - \mathbf{F}_{i,j-1,k}^{n}}{2\Delta\eta}$$

during the even time steps.

The above discretization leads to a set of algebraic equations for $\mathbf{q}$. These equations are costly to solve since the flux vectors $\mathbf{E}$ and $\mathbf{G}$ are highly nonlinear. The nonlinearity is removed by linearising the fluxes about the previous time step value, resulting in the following linear equation :

$$\left[I + \Delta\tau \left(\delta_\xi A^n + \delta_\zeta B^n \right) \right] \mathbf{q}^{n+1} = \left[I + \Delta\tau \left(\delta_\xi A^n + \delta_\zeta B^n \right) \right] \mathbf{q}^n + \mathbf{R}^{n,n+1} \tag{12}$$

where

$$\mathbf{R}^{n,n+1} = -\Delta\tau \left(\delta_\xi \mathbf{E}^n + \delta_\eta \mathbf{F}^{n,n+1} + \delta_\zeta \mathbf{G}^n \right) \tag{13}$$

and the operator notation $\delta_\xi(A\mathbf{q}) = [\delta_\xi A]\mathbf{q}$ and $\delta_\zeta(B\mathbf{q}) = [\delta_\zeta B]\mathbf{q}$ is used.

This Euler equation formulation can be very easily extended to solve the Navier-Stokes equations by simply adding the viscous terms to the right hand side. This does not alter the numerical formulation.

name 'Alternating Direction'. These inversions are performed at each spanwise station, marching along the spanwise direction. As mentioned earlier, the marching direction is reversed every iteration. Each element of the block tridiagonal matrix has 5×5 elements.

Artificial Dissipation:

The use of central difference, makes the scheme mildly unstable, and also introduces odd even decoupling. This is remedied by adding artificial dissipation. The implementation of artificial dissipation, in the present work is based on the formulation of Jameson et al. [16]. This scheme has a second order implicit dissipation and a blend of second/ fourth difference explicit dissipation terms. A scaling factor for both implicit and explicit dissipation is employed to control the amount of dissipation in the scheme. Adding the dissipation terms, equations (18) and (19) can be written as:

$$\left[I + \Delta\tau \left(\delta_\xi A^n + \epsilon_I D_{I_\xi}\right)\right] \Delta\mathbf{q}^{*n+1} = \mathbf{R}^{n,n+1} - \epsilon_E D_E \Delta\tau \quad (20)$$

$$\left[I + \Delta\tau \left(\delta_\zeta B^n + \epsilon_I D_{I_\zeta}\right)\right] \Delta\mathbf{q}^{n+1} = \Delta\mathbf{q}^{*n+1} \quad (21)$$

where D_{I_ξ} and D_{I_ζ} are second order implicit dissipation terms and D_E is the explicit dissipation term, given in reference [22]. ϵ_I and ϵ_E are user supplied constants, which depend on grid spacing. At the boundaries the fourth order differences are repalced by second order differences.

Aeroelastic Model:

As mentioned earlier, the propfan has thin, swept, and twisted blades. Since the blades are thin and flexible, deflections due to centrifugal and steady aero loads are large. Hence, the aeroelastic problem is inherently nonlinear, requiring geometric nonlinear theory of elasticity [17].

The blades have large sweep and twist, which couples blade bending and tor-

i.e., until the change in deflection from the $(i+1)^{th}$ iteration is equal to that from the i^{th} iteration.

Results and Discussion

The hybrid numerical scheme discussed in the previous section, was first applied to an isolated aircraft wing in reference [21] and to a helicopter rotor blade in reference [22]. Typical results showing blade loading, are reproduced in figures (3) and (4). As can be seen from both these figures, the hybrid scheme is able to predict flow phenomena of varying complexity with fairly good degree of accuracy.

The propfan blade has a much more complex shape than the aircraft wing or the helicopter blade. The high twist, large sweep, low aspect ratio, close proximity of other blades, presence of nacelle and thinner blades near the tip, make the flow field around it very complex. In the following, the flow solutions obtained for two advanced propellers, namely SR3 and SR7L, are presented. The calculations have been performed on a 'hot shape', obtained by including the deflections due to centrifugal loading in the undeflected blade shape ('cold shape').

A body fitted H-O grid was used for these calculations. A typical grid used in the calculation is shown in figure (5). The domain of calculation was taken to be the region between two blades with upper surface of one blade and lower surface of the adjoining blade as the boundaries of the domain. This region is referred to as blade passage. In general, in order to model the influence of adjacent blades (cascade effect) the entire propfan with all the blades (passages) are solved. However, for an axisymmetric flow field, considered here, all blade passages can be assumed to be identical, and only one blade passage is solved enforcing the conditions of symmetry.

SR3 Propfan

The hybrid scheme, described earlier, was used to solve the flow field around an 8-bladed SR3 propfan. The SR3 propfan was designed to operate at a free stream Mach number of 0.8, advance ratio of of 3.06, at an altitude of 30,000 feet.

an overprediction in the tip region results in an under prediction on the inboard region.

SR7L Propfan

The SR7L propfan has been designed for an operating free stream Mach number of 0.8, rotational speed of 1700 rpm, at an altitude of 35,000 feet. In this section calculations for a two bladed SR7L propfan are presented. The aerodynamic calculations are first performed on the 'hot shape'. The effect of blade flexibility is then included in the calculations.

In figure (8) the elemental pressure coefficient difference is compared with experiment for a 2-bladed SR7L propfan. The blade was operating at a free stream Mach number of 0.775 and advance ratio of 3.088. The 75% span setting angle was adjusted to match the power coefficient by a rigid body rotation of the blade about the pitch change axis. The pressure coefficient difference ΔC_p $(C_{p_l} - C_{p_u})$ is plotted and compared against experimental data [27] at various span locations. The comparison is good, except near the leading edge on the outboard stations.

The effect of blade flexibility on performance was studied next for the SR7L propfan blade. The effect of flexibility is included by the aeroelastic iteration process, described earlier and shown in figure (2).

It is important that the blade finite element model accurately reflects its structural characteristics, since the entire analysis process is centered around the stiffness matrix. The NASTRAN finite element model used in this study is based on the final blade design [24]. The SR7L blade has an aluminum spar, nickel sheath, and fiber glass shell with foam fill. The shell, adhesive, spar, and shell filler material were combined using the Composite Blade Structural Analysis (COBSTRAN) program to produce equivalent, monolithic shell elements [25]. The finite element model of the SR7L blade is shown in figure (9a). The model has 261 nodes and 449 triangular shell elements. Bar elements are used to model the shank. Multipoint constraint grid chords are used to define the shank/blade interface [26].

the final blade shape.

In figure (11) the thrust coefficient is plotted against the power coefficient for subsequent iterations. The setting angle used in the calculations has been obtained by rigid body rotation of the hot shape so as to match the power coefficient obtained by experiments. The experimental point is also plotted. The power coefficient obtained from the hot shape (marked 1), compares well with the experiment. However, the power coefficient changes considerably (marked 2 to 4), as the blade is allowed to deform under this load. It can be seen from figures (10) and (11), that the initial change in shape, lead to large change in power coefficient. For this particular case, under which the blades are loaded heavily almost 40% change in power coefficient is observed when the effect of aerodynamic loading is included in the blade shape. The subsequent changes are not as large. Hence, in order to obtain a better comparison with experimental power coefficient and load distribution on blade, the blade setting angle should be chosen such that the converged shape power coefficient is compared against the experimental data. This requires some trial and error in selecting the 'cold' or 'hot' shape from which the aeroelastic iteration should be started. Arriving at the final blade shape might be critical for vibration and flutter calculations, as well.

In figure(12) the relative change in twist angle over the span is plotted. This shows that the largest deflection occurs near the tip, with practically no deflection on the root sections. Also it should be noted that the variation in the blade twist is nonlinear and is largest near the tip. A rigid body rotation of the blade to account for the change in twist, would result in a linear variation along the span. This clearly shows that for better performance calculations, structural flexibility should be included in the analysis.

Figure (13) shows the in-plane deflection of the blade planform and figure (14) shows the out of plane deflection of the blade at constant chord. Again, the largest deflection is towards the tip, with practically no deflection towards the root. Figure

4. The effect of aero loads was to compensate for the untwisting due to centrifugal loads

Acknowledgements

The authors wish to acknowledge Dr. Richard August of Sverdrup Technology Inc., Cleveland, OH, for many helpful suggestions. This work has been carried out under NASA grant NAG3-730 from NASA Lewis Research Center in Cleveland, Ohio, Mr. George L. Stefko, grant monitor.

References

[1] Whitlow, J. B., Jr. and Sievers, G. K.," Fuel Savings Potential of the NASA ATP," NASA TM 83736, 1984.

[2] Mehmed, O. and Kaza, K. R. V., " Experimental Classical Flutter Results of a Composite Advanced Turboprop Model," NASA TM-88792

[3] Goldstein, S.," On the Vortex Theory of Screw Propellers," Royal Society Proceedings, Vol. 123, No. 792, Apr. 6, 1929, pp 440-465

[4] Sullivan, J. P.," The effect of Blade Sweep on Propeller Performance,"AIAA Paper 77-176, June 1977

[5] Egolf, T. A., Anderson, O. L., Edwards, D. E., and Landgrebe, A. J.," An Analysis for High Speed Propeller-Nacelle Aerodynamic Performance Prediction; Volume 1, Theory and Initial Application and Volume 2, User's Manual for the Computer Program," United Technologies Research Center, R79-912949-19, June 1979.

[6] Hanson, D. B.," Compressible Lifting Surface Theory for Propeller Performance Calculation," AIAA paper 82-0020.

[17] Kaza, K. R. V., et al.,"Analytical Flutter Investigation of a Composite Propfan Model," Journal of Aircraft, Vol. 26, No. 8, pp 772-780, August 1989.

[18] Subrahmanyan, K. B., Kaza, K. R. V., Brown, G. V., and Lawrence, C.," Nonlinear Bending-Torsional Vibration and Stability of Rotating, Pretwisted, Preconed Blades Including Coriolis Effects," NASA TM 87207, 1986.

[19] "The NASTRAN Theoretical Manual," NASA SP 221(06), 1981.

[20] August, R., and Kaza, K. R. V.," Vibration, Performance and Flutter Response Characteristics of a Large-Scale Propfan and its Aeroelastic Model," AIAA Paper 88-3155, 24^{th} Joint Propulsion Conference, Boston, Massachusetts, July 11-13, 1988.

[21] Ruo, S. Y., and Sankar, L. N., "Euler Calculations for Wing-Alone Configuration," *Journal of Aircraft*, Vol. 25, No. 5, pp 436-441, May 1988.

[22] Wake, B. E., and Sankar, L. N., "Solutions of the Navier-Stokes Equations for the Flow about a Rotor Blade," *Journal of the American Helicopter Society*, Vol. 34, No. 2, pp 13-23, April 1989.

[23] Rohrbach, C., Metzger, F. B., Black, D. M., and Ladden, R. M., "Evaluation of Wind Tunnel Performance Testings of an Advanced 45° Swept Eight-Bladed Propeller at Mach Numbers From 0.45 to 0.85," NASA CR-3505, 1982.

[24] Sullivan, W. E., Turnberg, J. E., and Violette, J. A.," Large Scale Advanced Propfan (LAP) Blade Design," NASA CR 174790.

[25] Aiello, R. A., and Chi, S.," Advanced Composite Turboprops: Modeling, Structural and Dynamic Analyses," ASME Paper 87-GT-78, 1987.

[26] Chou, S., "SR7L Turboprop Blade Finite Element Model," Sverdrup Topical Report, March 1986.

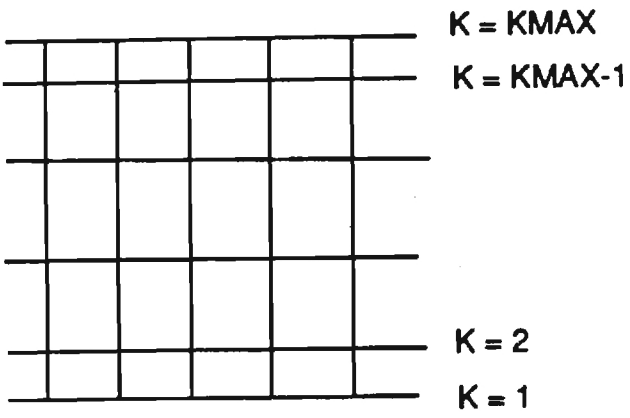

Figure-1a

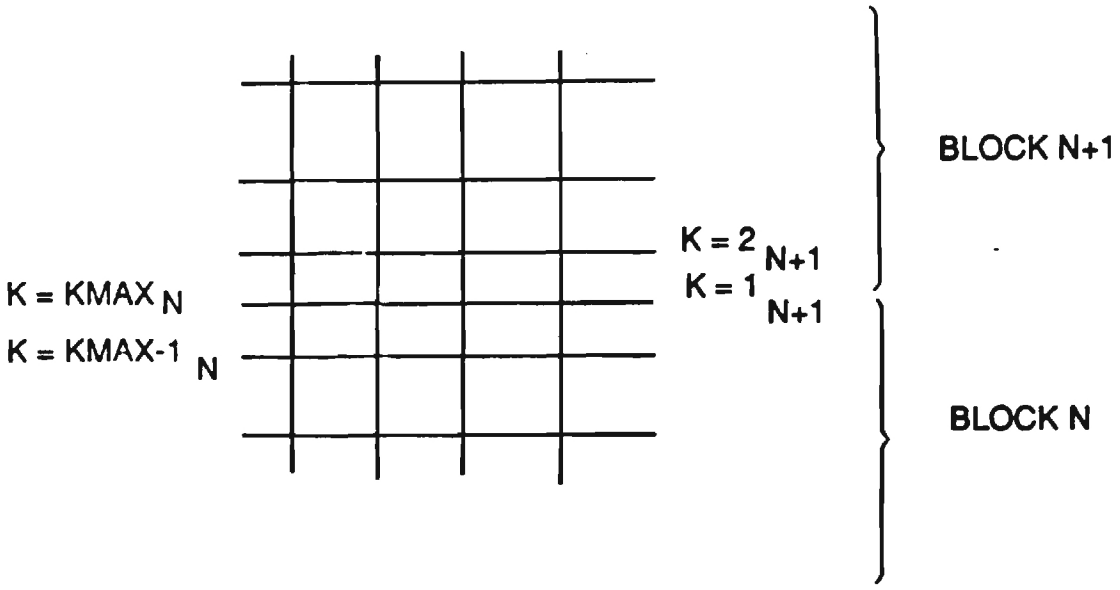

Figure-1b

Figure-1 Block-Interface Boundaries

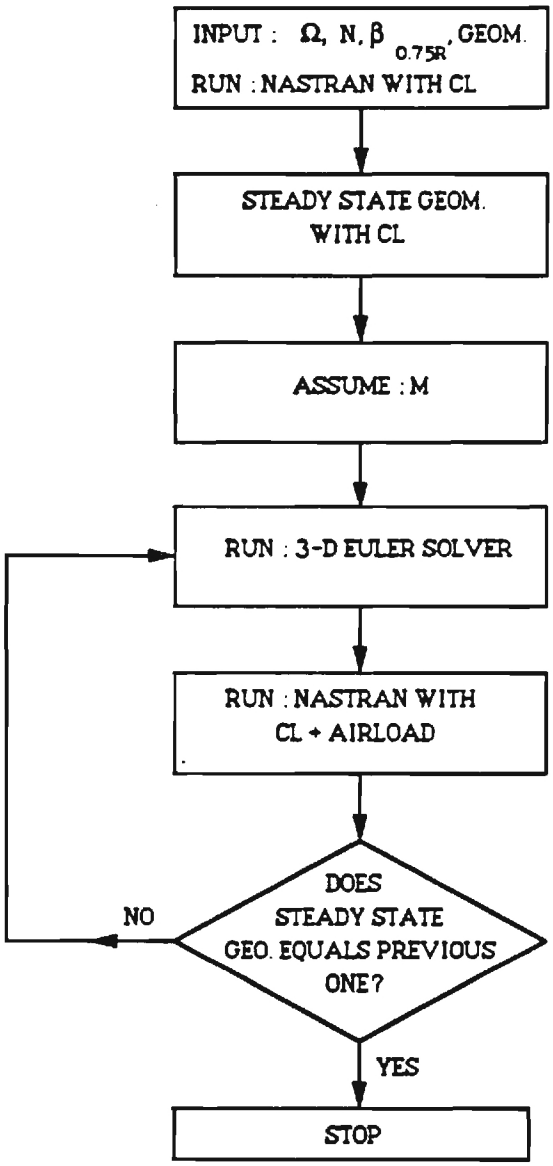

Figure-2 Flow Chart of the Aeroelastic Analysis

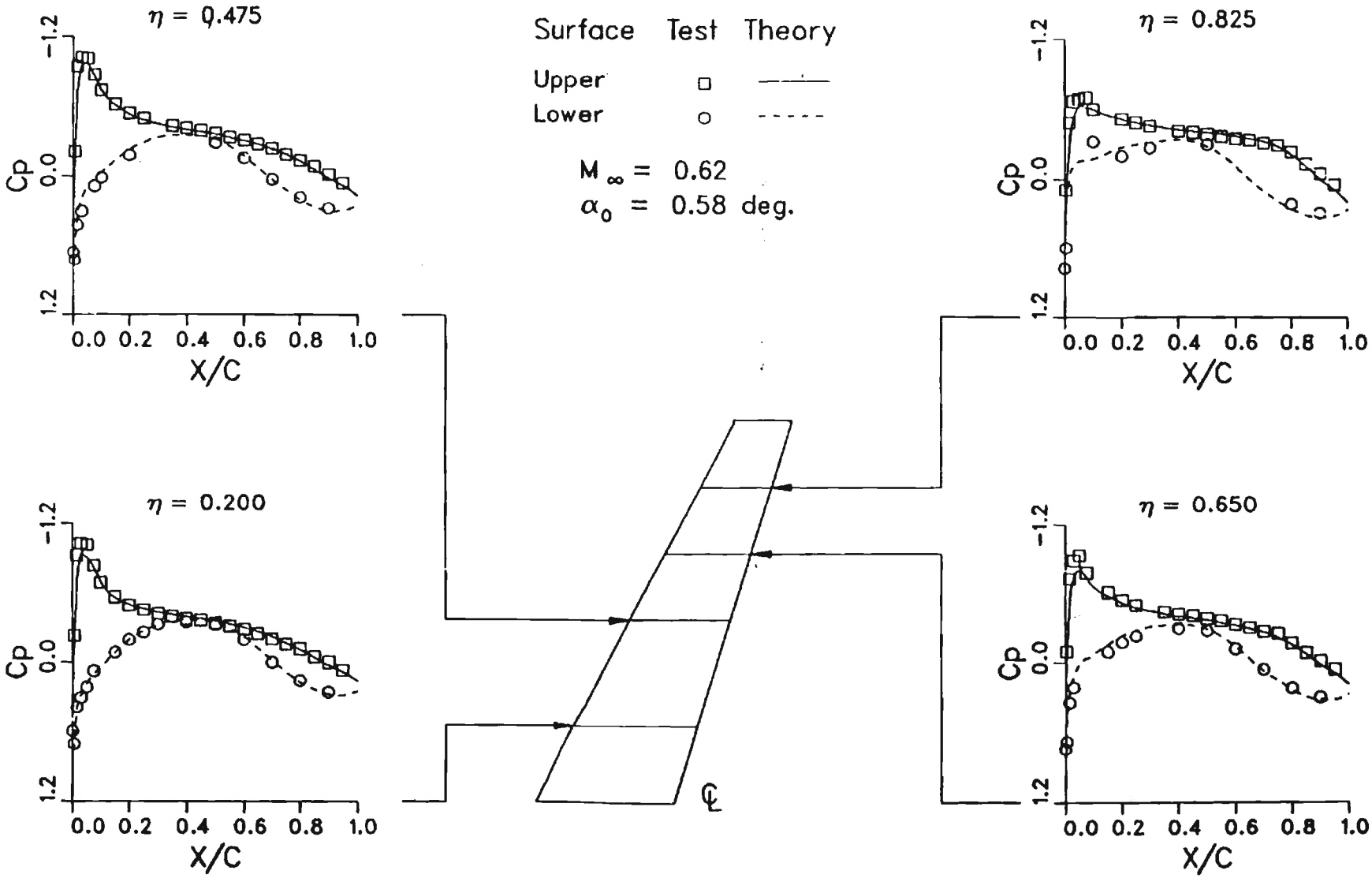

Figure-3 Euler Calculations for a Wing

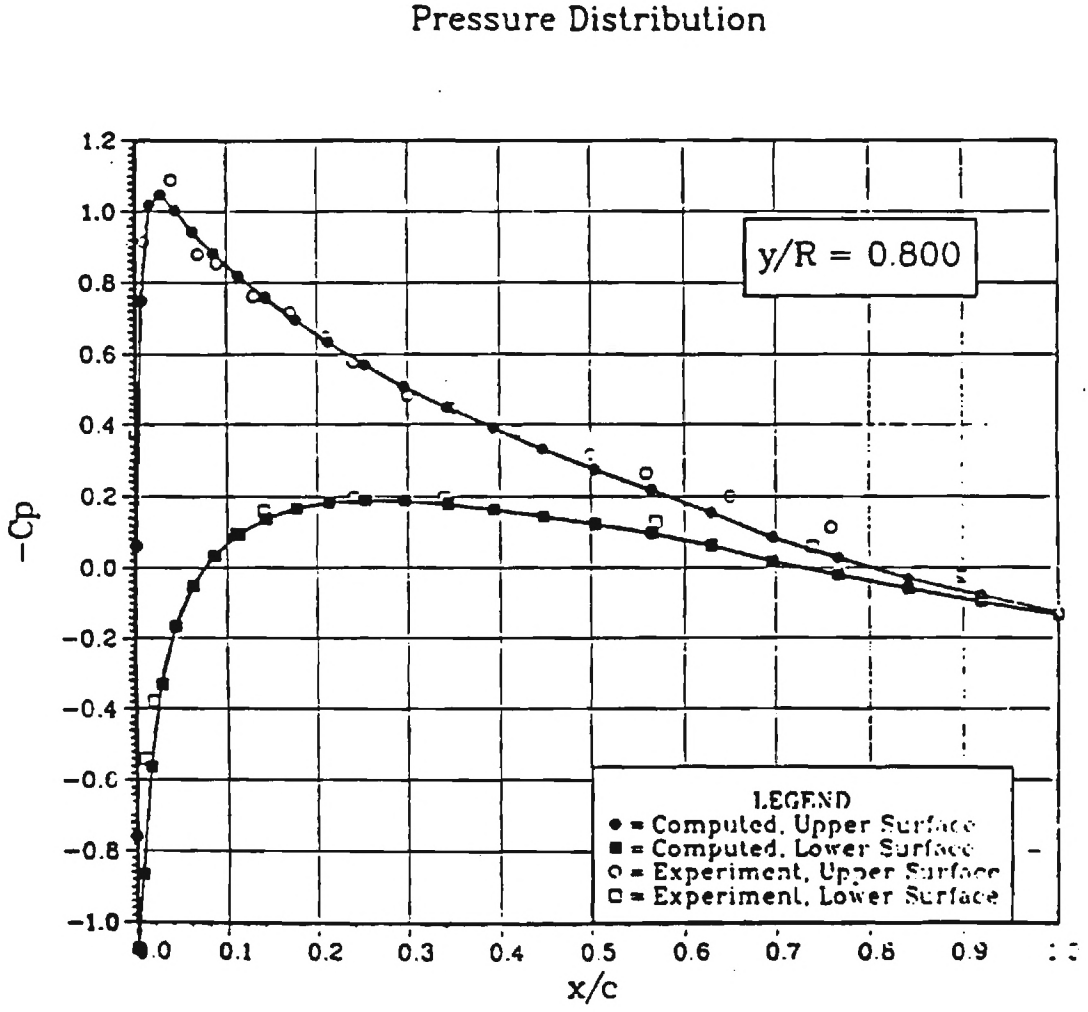

Figure-4a Pressure Coefficient for a NACA 0012 Rotor Blade in Hover

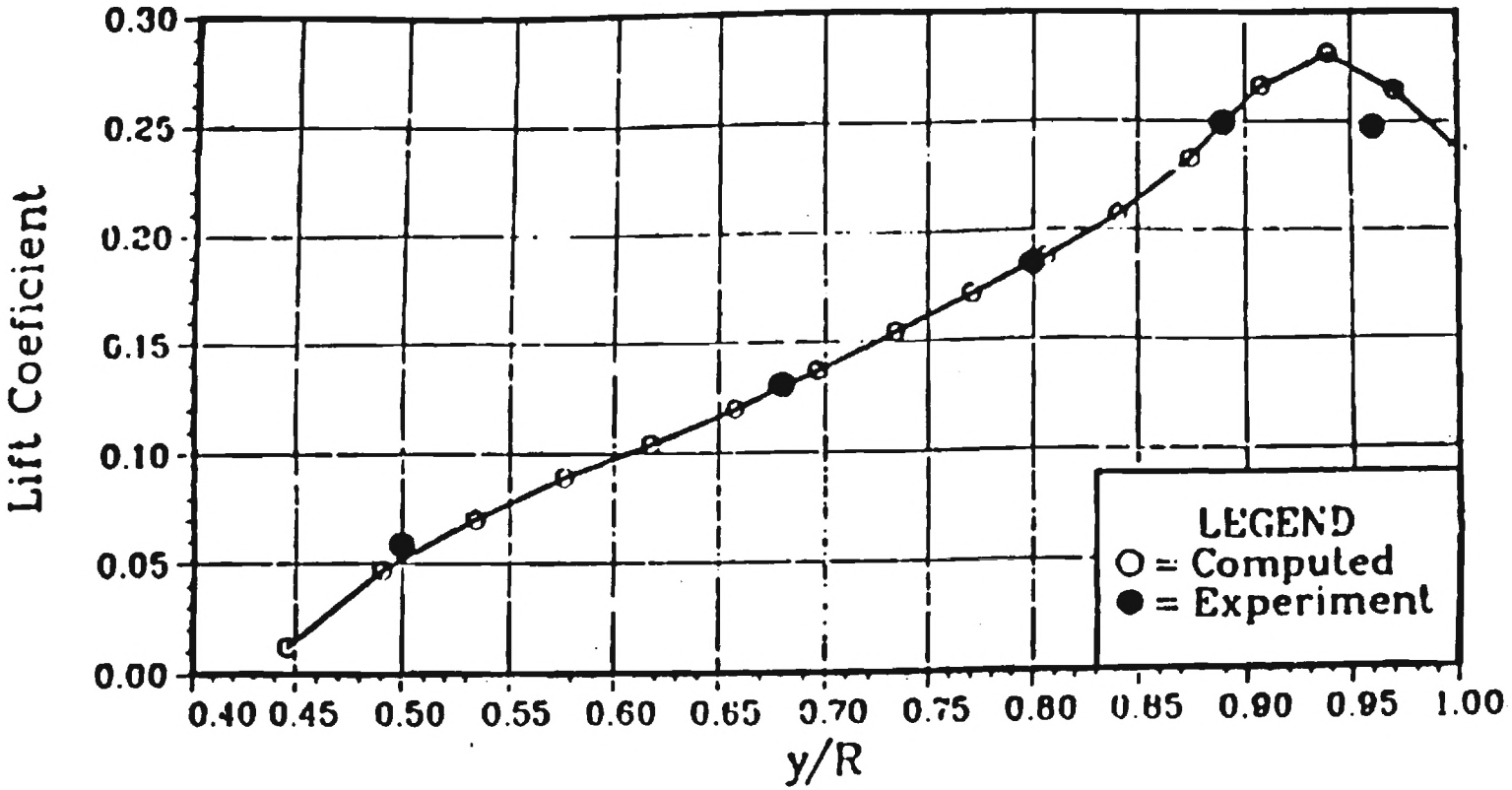

Figure-4b Lift Distribution for a NACA 0012 Rotor Blade in Hover

GRID

16 DEC 88 13:34:66

I= 1 TO 60
J= 1 TO 16
K= 1 TO 1

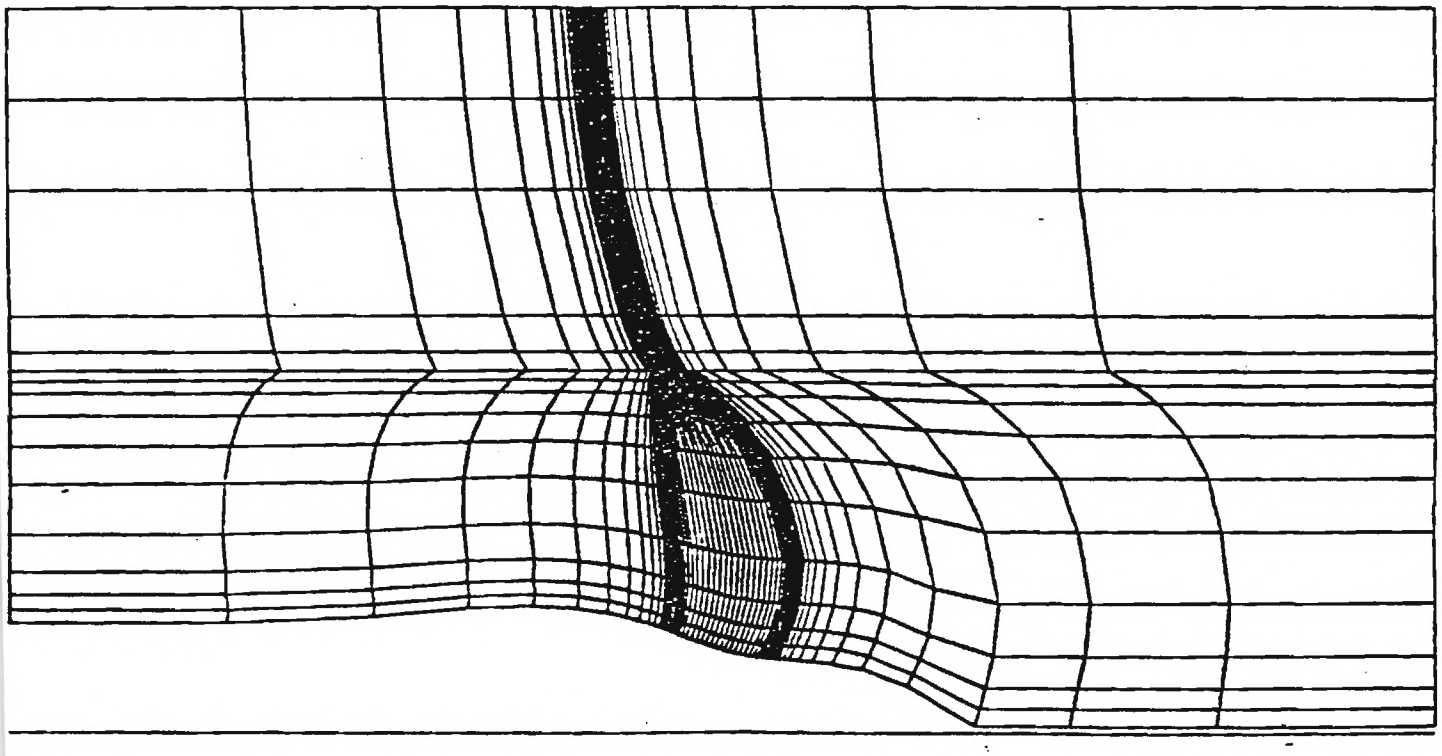

Figure-5a H-grid in Streamwise Plane

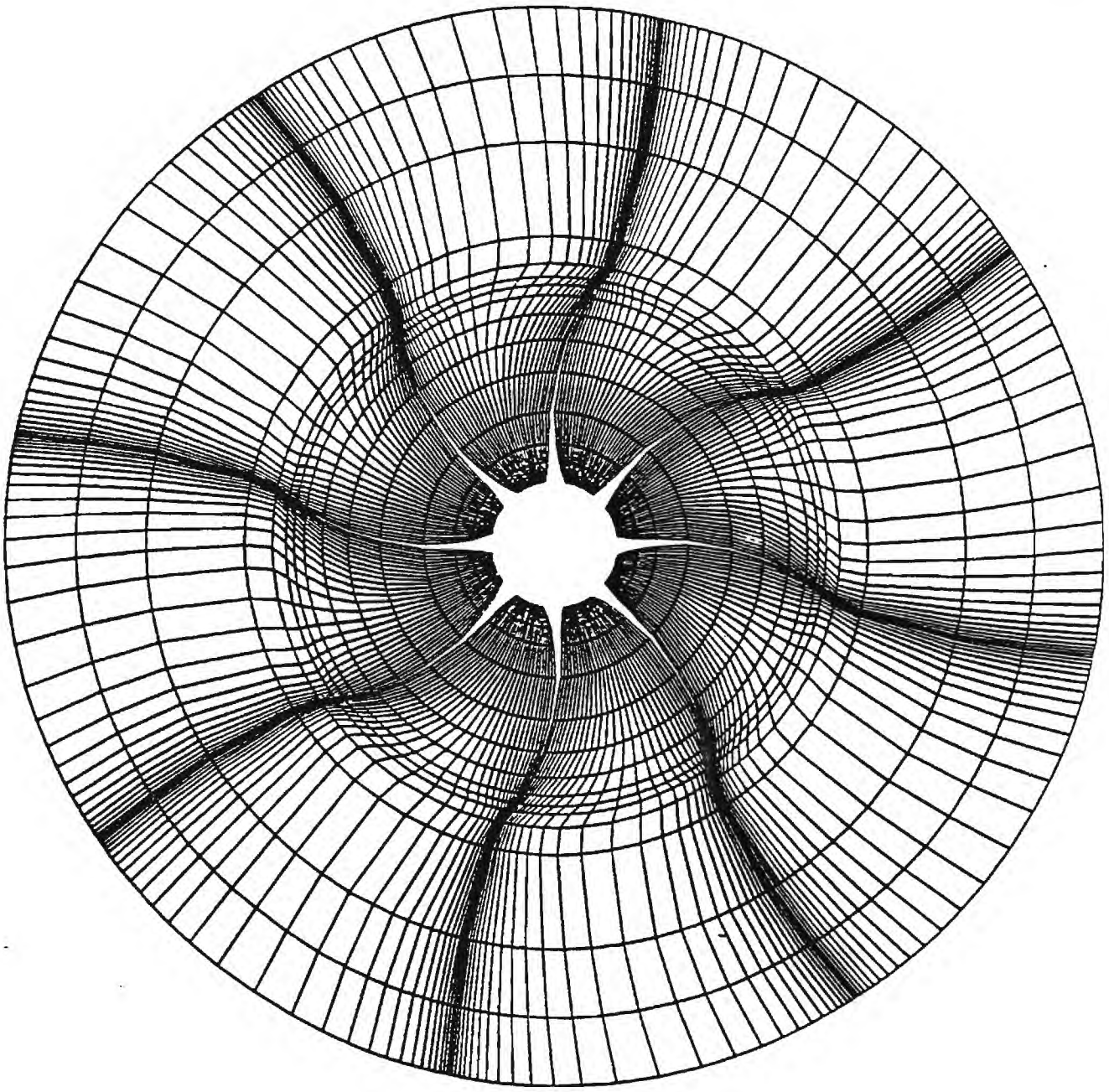

Figure-5b O-grid in Azimuthal Plane

Power Coefficient vs. Advance Ratio
8 Bladed SR-3 Propfan

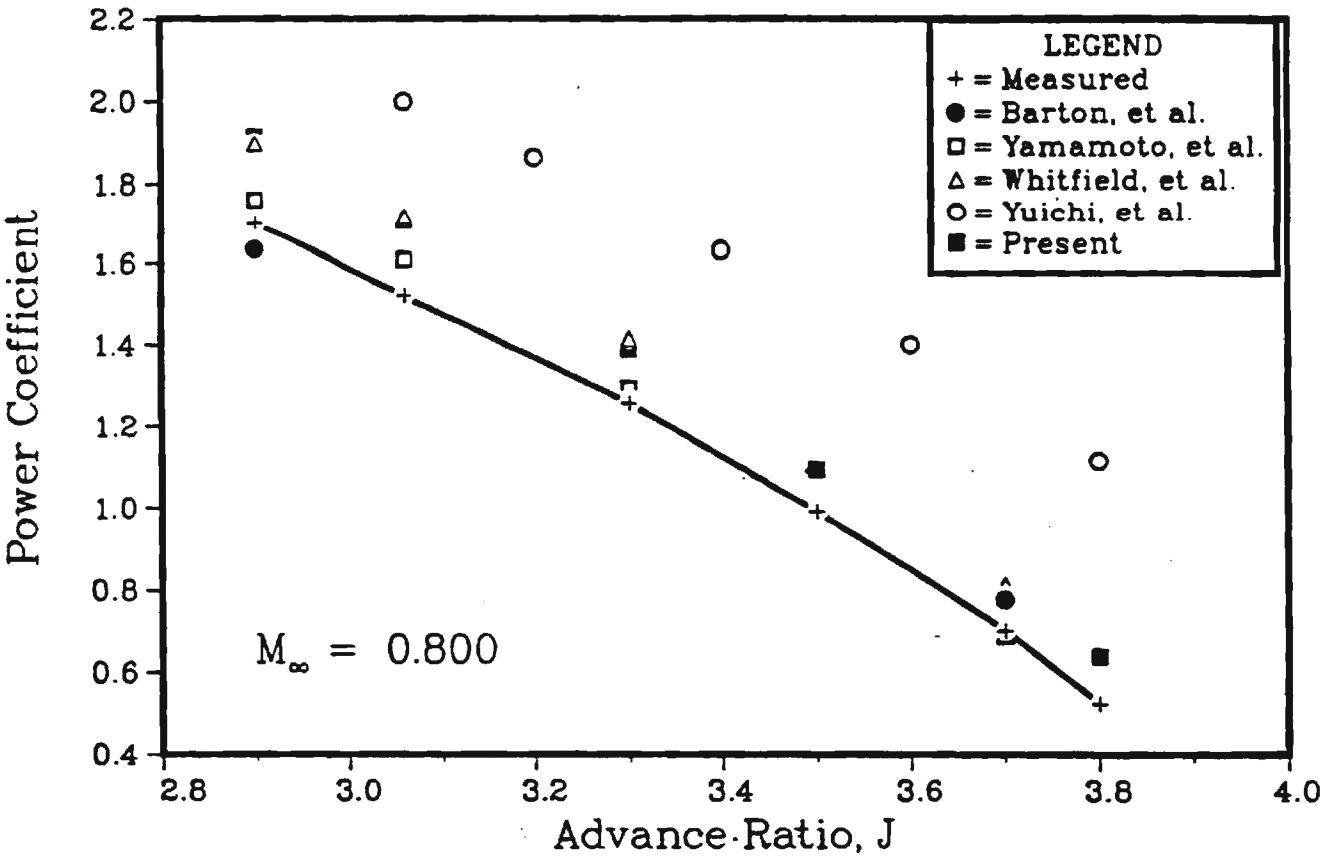

Figure-6a

Power Coefficient vs. Advance Ratio
8–Bladed SR–3 Propfan

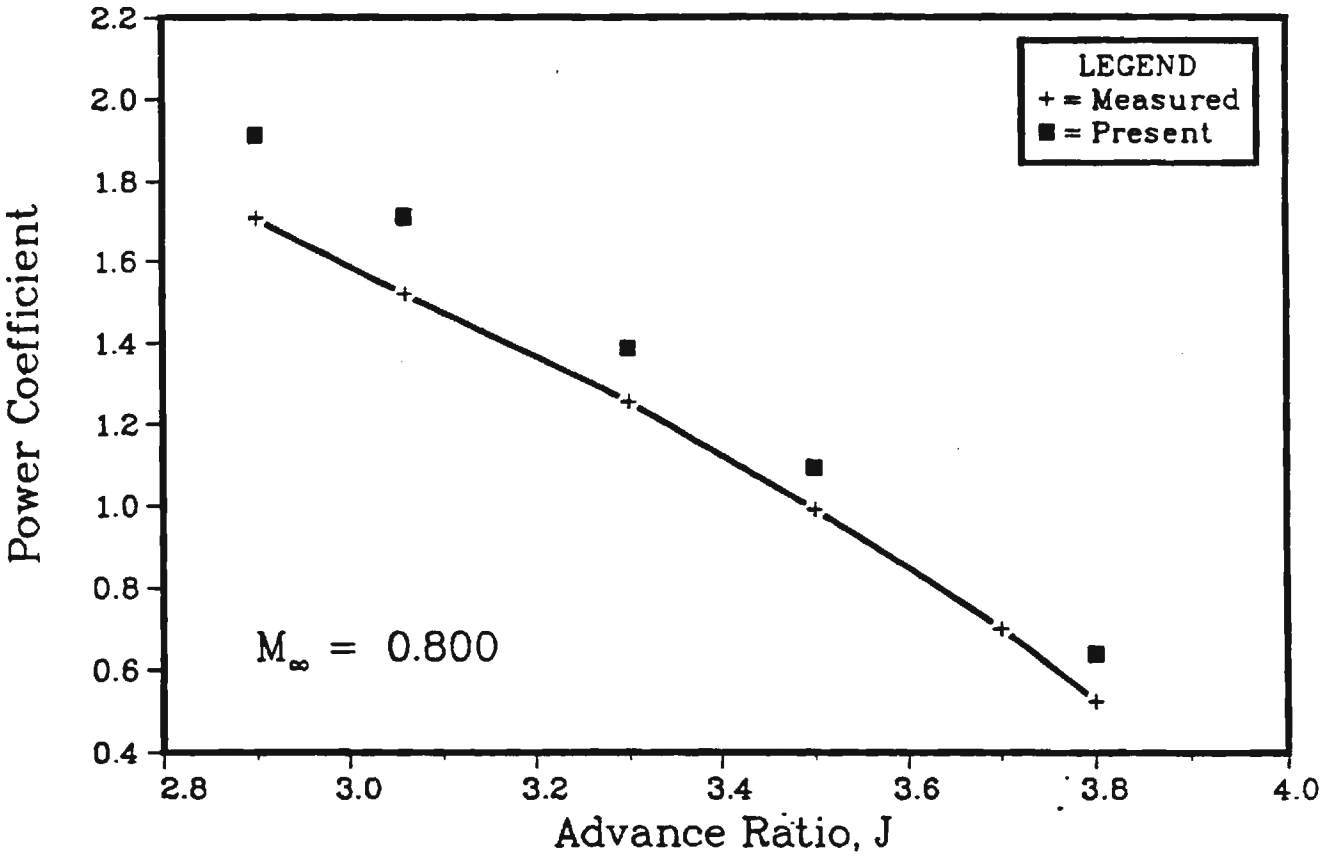

Figure-6b

SR-3 8-Bladed Propfan

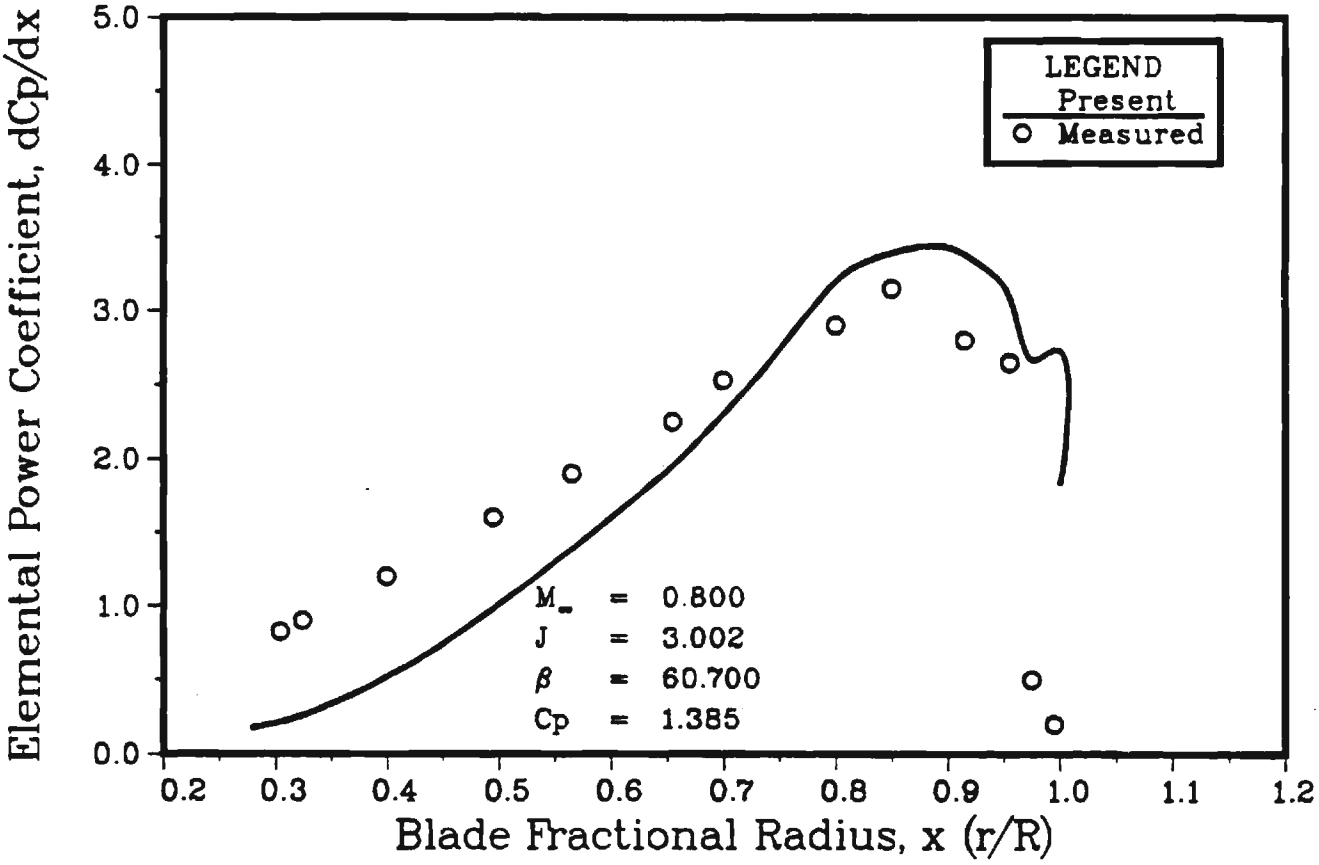

Figure-7

SR7L 2-Bladed Propfan

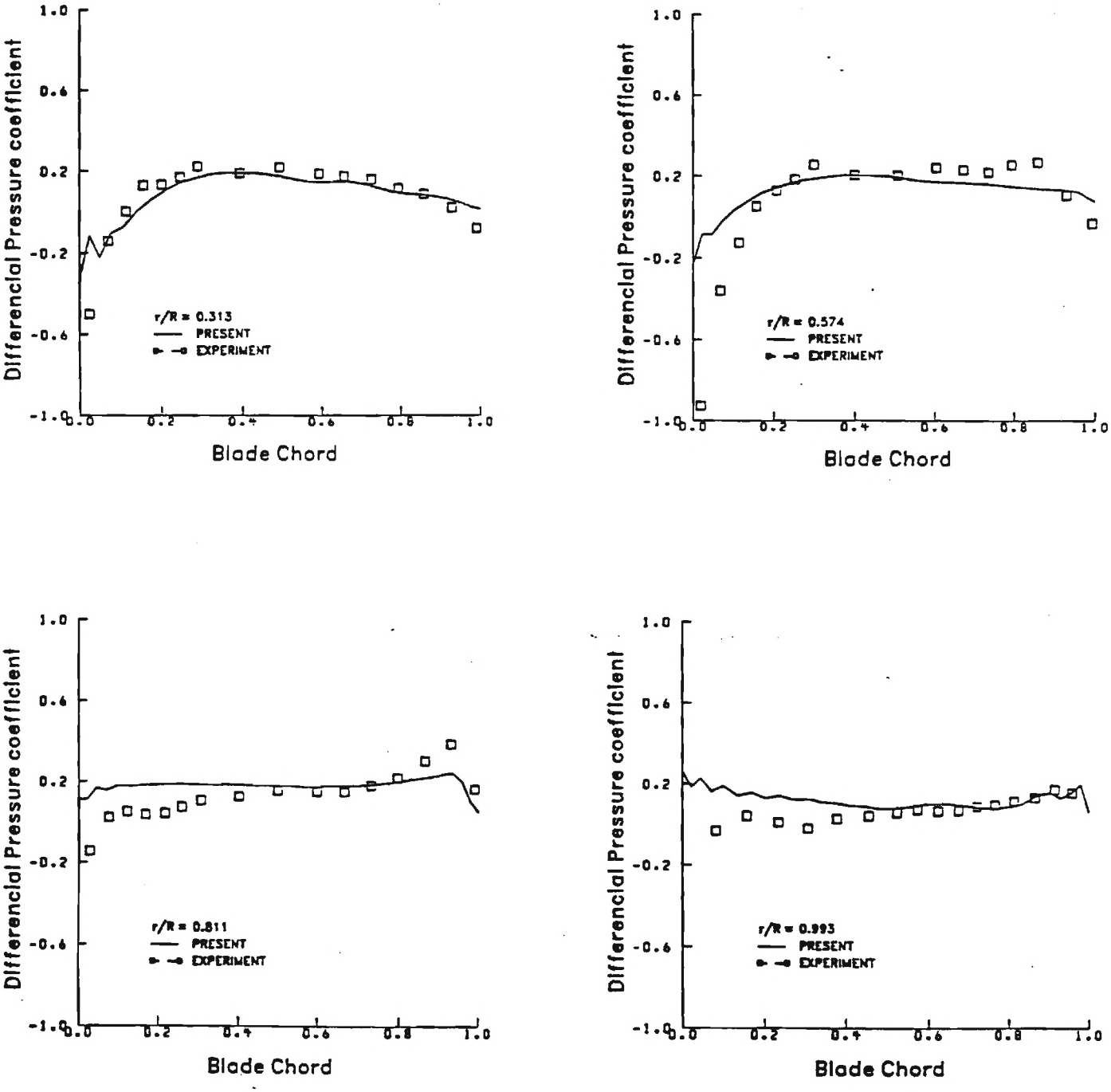

Figure-8 Differential Pressure Coefficient at Various Radial Locations
$M_\infty = 0.775$, $J = 3.088$, $\beta = 54.6$

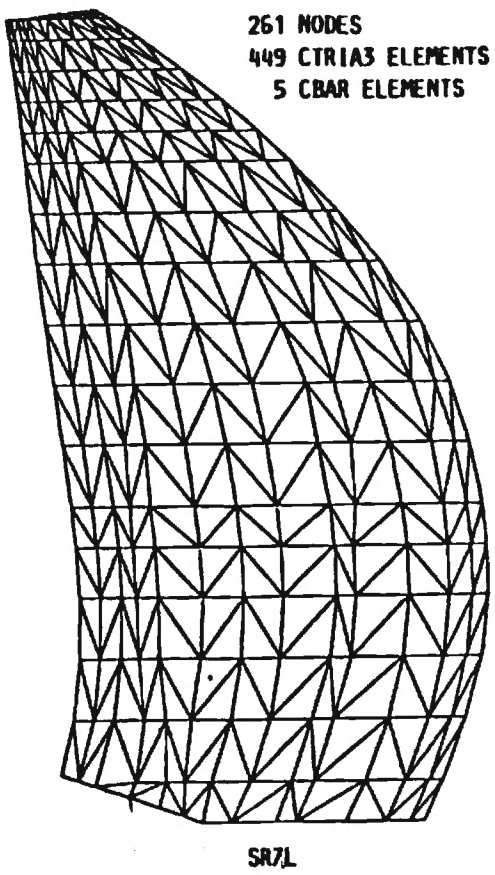

Figure-9a Propfan Blade Finite Element Model

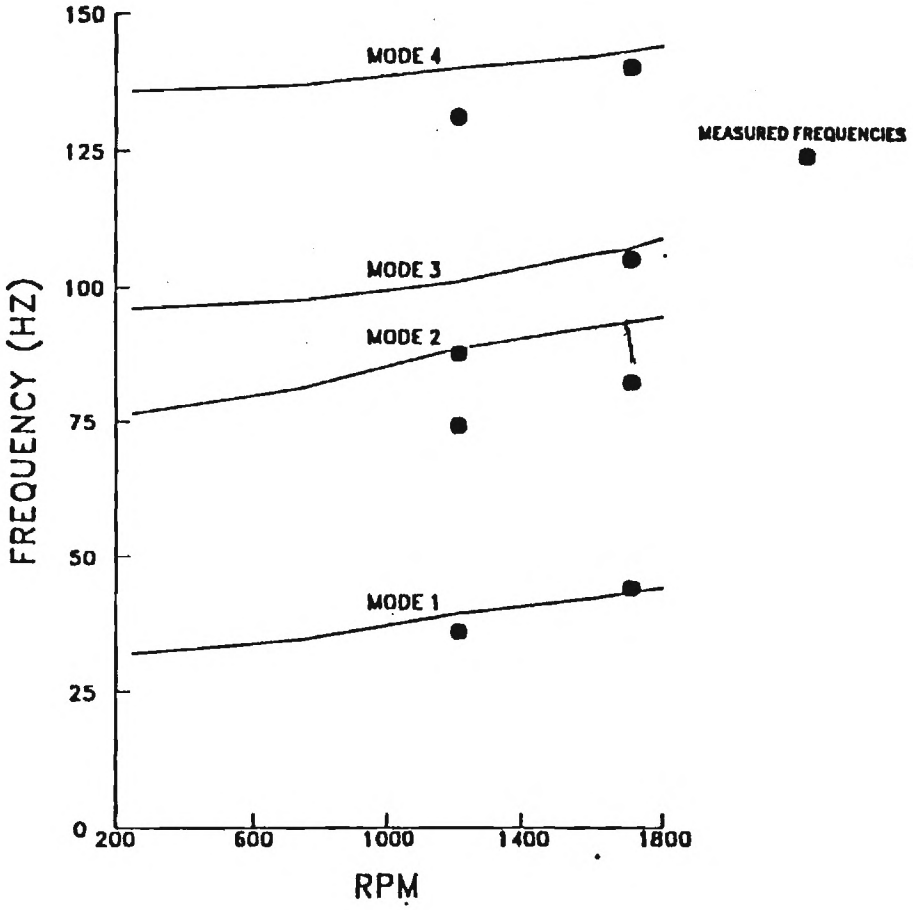

Figure-9b SR7L Frequencies - vs. - RPM

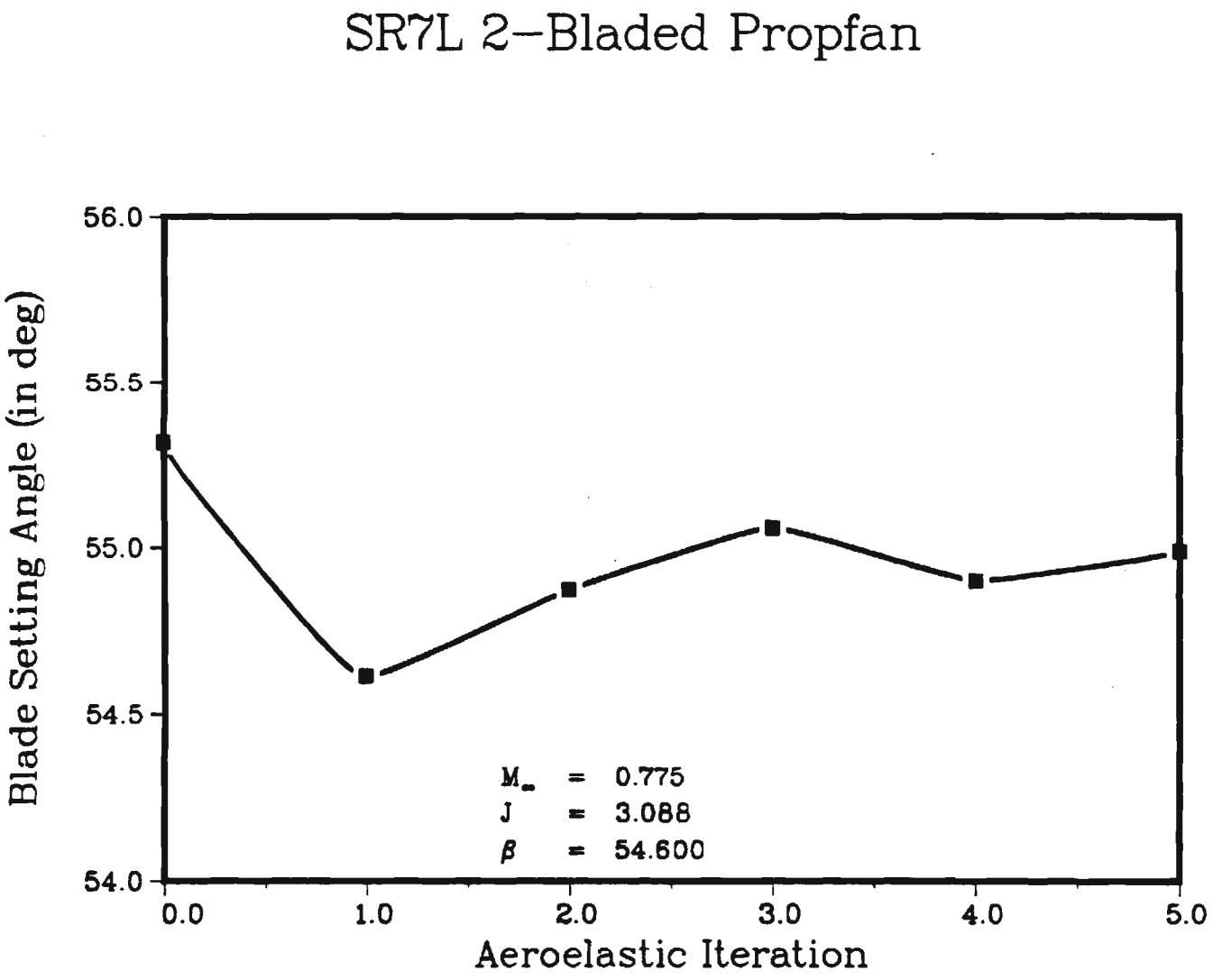

Figure-10 Blade Setting Angle at 75% Span versus Aeroelastic Iteration

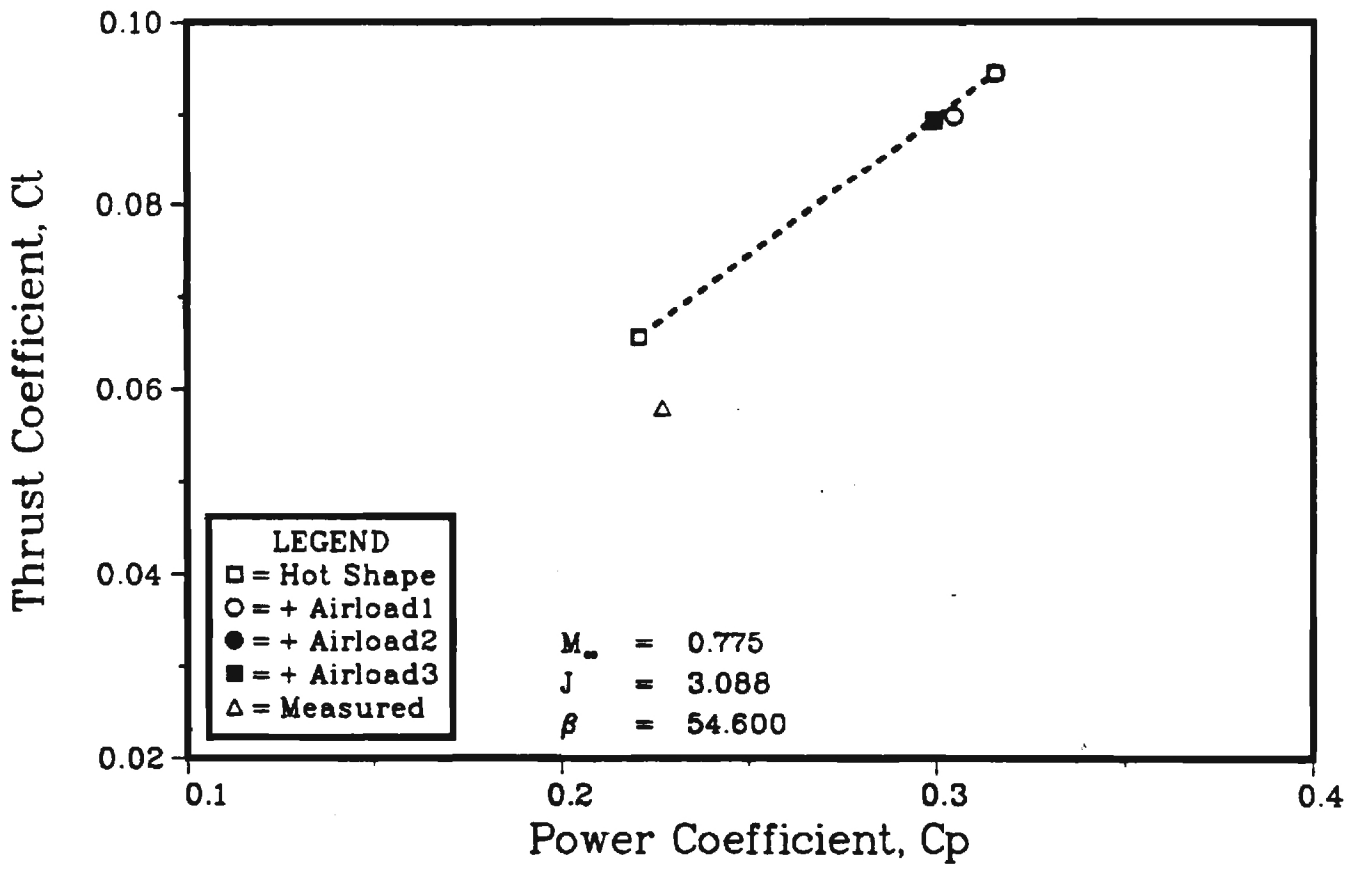

Figure-11 Calculated Thrust Coefficient versus Power Coefficient for Each Aeroelastic Iteration

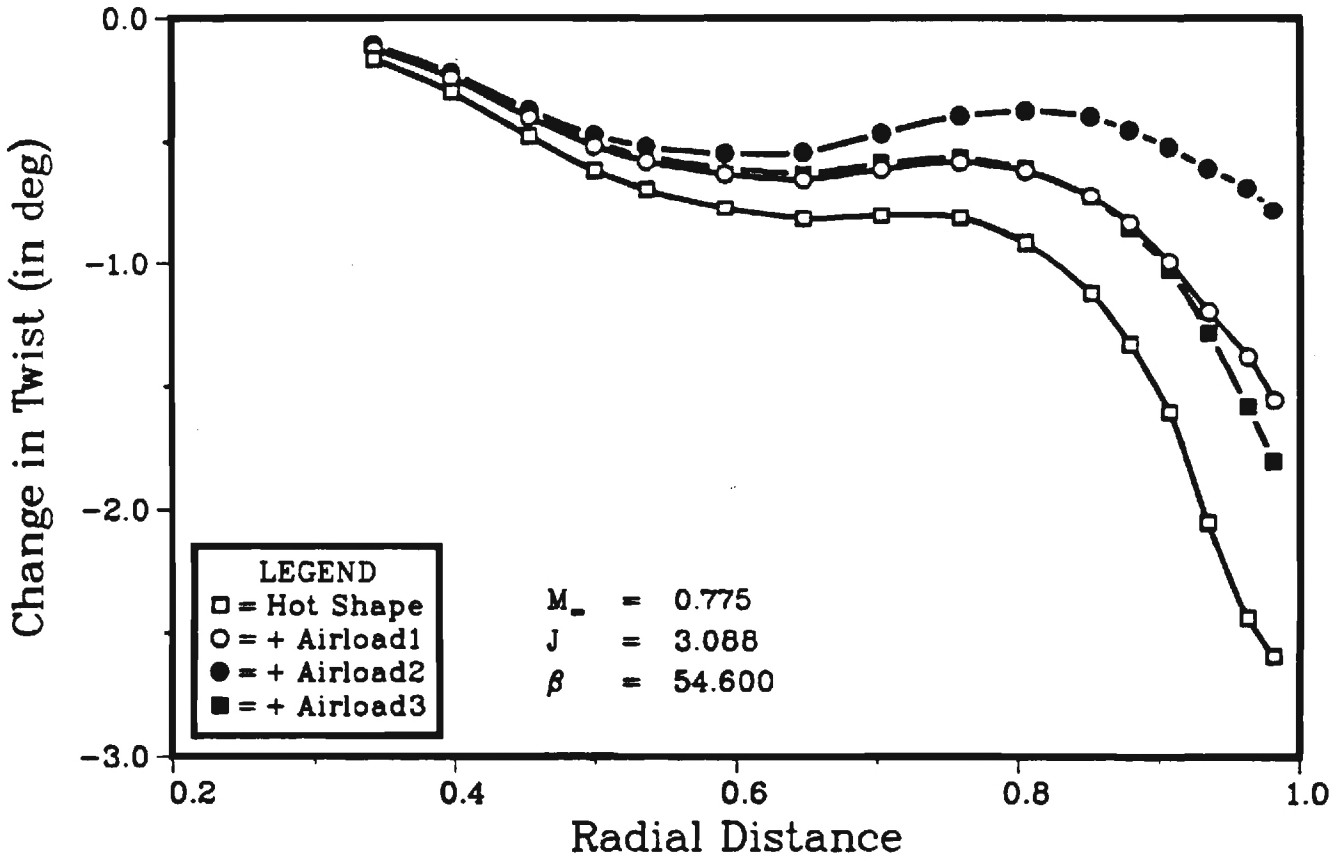

Figure-12 Change in Blade Setting Angle versus Blade Span
$M_\infty = 0.775$, $J = 3.088$

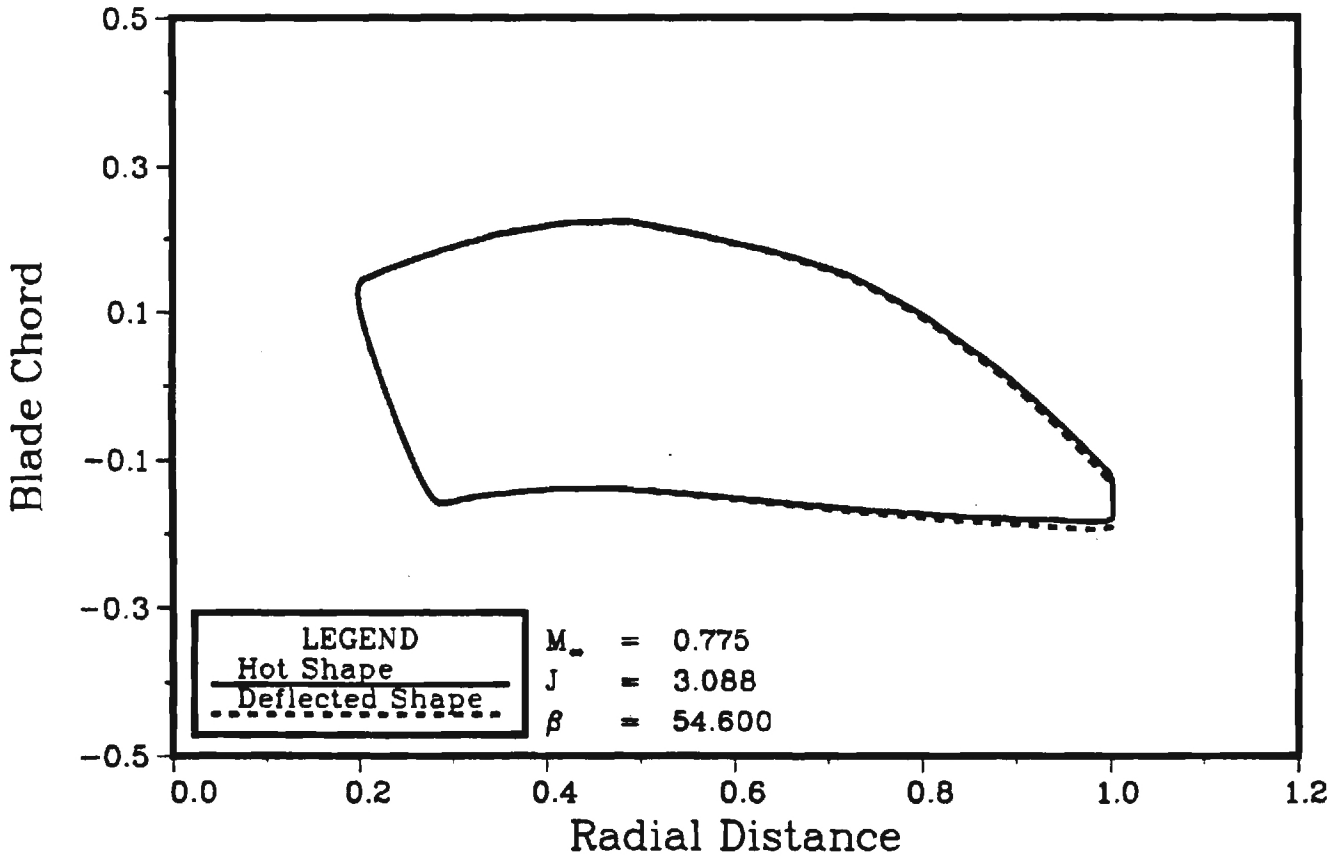

Figure-13 In Plane Deflection of Blade Planform
$M_\infty = 0.775$, $J = 3.088$, $\beta = 54.6$

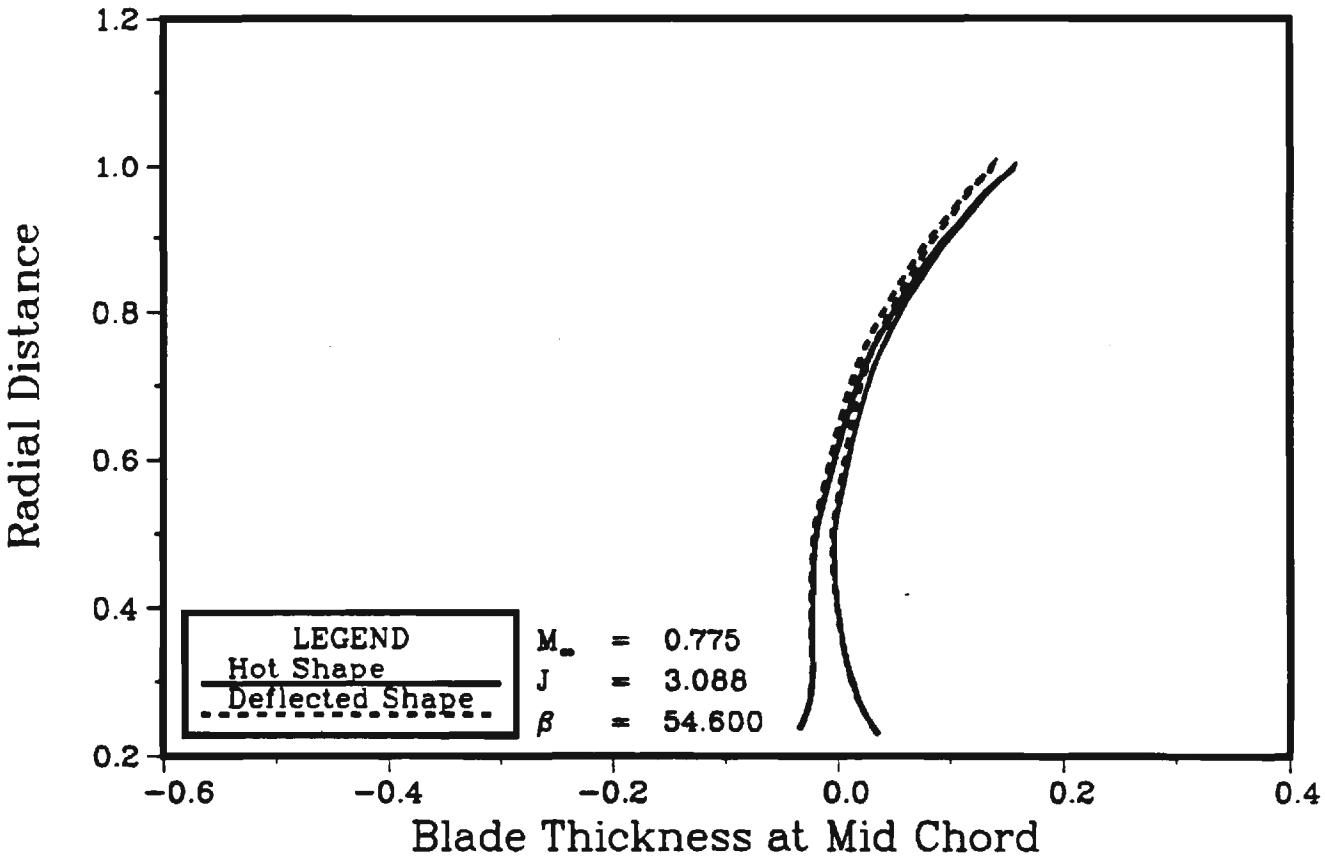

Figure-14 Out of Plane Deflection at Mid Chord
$M_\infty = 0.775$, $J = 3.088$, $\beta = 54.6$

E-16-801

SIMULATION OF UNSTEADY ROTATIONAL FLOW OVER PROPFAN CONFIGURATION

NASA GRANT No. NAG 3-730

SEMI ANNUAL STATUS REPORT

for the period

December 1, 1989 - May 30, 1990

submitted to

NASA LEWIS RESEARCH CENTER

CLEVELAND, OHIO

Attn: Mr. G. L. Stefko

Project Monitor

Prepared by:

Rakesh Srivastava
Graduate Research Assistant

L. N. Sankar
Associate Professor

School of Aerospace Engineering
Georgia Institute of Technology
Atlanta, Georgia 30332

INTRODUCTION

The objective of the present study is to develop numerical capabilities for predicting aerodynamic performance and aeroelastic response of single or counter rotation propfan in an unsteady transonic flow. A three dimensional Euler solver has been developed at Georgia Institute of Technology to address this problem.

SUMMARY OF PROGRESS

In the present reporting period the Euler solver, with the help of NASA Lewis personnel was coupled with the NASTRAN code in an open-loop fashion to predict the effects of structural deflections on propeller performance. A paper documenting these results was presented at the 28th Aerospace Sciences Meeting at Reno, Nevada.

In the previous reporting periods, it was noted that even though the performance quantities and the blade loading compared well with experimental data and other numerical results, there was a shift in individual surface pressures. Since the shift was same for both the surfaces, the blade loading and performance quantities compared well. This shift was traced to an error in calculating grid velocities. This error has been corrected, and now the individual surface pressures also compare well with experiment. These comparisons are presented in the Appendix.

The Euler solver was further modified to solve the flowfield around a counter rotating propfan. The first step involved in this modification was to generate a body fitted grid around the counter rotating propfan. For this purpose, the grid generator for the single rotation propfan was modified. The space between the trailing edge of the front blade row and the leading edge of the rear blade row was equally divided to define the solution domain associated with each blade row. The grid was then generated for each solution domain separately.

The solver was then modified to solve the Euler equations in each of the solution domains consecutively. Again, as in single rotation solver, the equations are solved in the interior of the each of the domains and the boundaries are explicitly updated. The additional blade row interface boundary is updated by averaging the flow solution from across the boundary after both the interior domains have been updated. This solver was used to solve the

flowfield around a GE F7/A7 counter rotating propfan operating at a free stream Mach number of 0.71 and an advance ratio of 2.8. The performance quantities obtained compared well with experimental data obtained in wind tunnel tests at NASA Lewis.

The results obtained during the present reporting period are discussed in detail in the Appendix. It is also an abstract sent for considerations for a paper at the forthcoming 29th Aerospace Sciences Meeting to be held at Reno, Nevada during January 7 to January 10, 1991.

WORK TO BE CARRIED OUT DURING NEXT REPORTING PERIOD

During the next six months (June 1 - November 30, 1990), the Euler solver will be thoroughly tested against the existing experimental data and numerical solutions. This will help in further calibrating the Euler solver for counter rotating propfan geometry.

Effort is also underway to improve the spatial accuracy of the current scheme from second order to fourth order. For this purpose, an operator-compact scheme, also known as Pade scheme will be investigated and implemented in the present solver. A parametric study will be carried out to determine if the increase in the spatial accuracy of the scheme will translate into fewer grid points and lesser CPU time.

A recent concept, to further increase the efficiency of the propfans, is to put a duct around it. A very preliminary analysis of this concept, has shown that a ducted single rotation ultra high by pass ratio propfan can provide similar power capabilities, using fewer parts and having a smaller fuel burn ratio than a modern high by pass ratio turbofan engine. The aerodynamic solver will be modified to incorporate the duct around the propfan geometry. Some preliminary calculations will be carried out to test the solver for this geometry. A useful by-product of this effort will be a version of the code that can handle unsteady viscous flow through multi-stage compressors.

APPENDIX

Proposed for Presentation at the AIAA
29th Aerospace Sciences Meeting
January 7-10, 1991, Reno, Nevada

An Efficient Hybrid Scheme for Analysis of Counter Rotating Propfans

by

R. Srivastava* and N. L. Sankar**
Department of Aerospace Engineering
Georgia Institute of Technology
Atlanta, GA

* Graduate Student, Member AIAA and AHS
** Associate Professor, Member AIAA and AHS

An Efficient Hybrid Scheme for Analysis of Counter Rotating Propfans

Introduction

The propfans are designed to delay the compressibility losses, thus extending the high efficiency of a propeller to relatively higher cruise Mach numbers. This is accomplished by sweeping the blade backwards and using thinner airfoils, on the outboard section of the blade. In addition low aspect ratio blades are used. This, combined with high tip Mach number, leads to high blade twist and high disk loading. The requirement of high disk loading further dictates a large number of blades per propeller, which must maintain structural integrity. However, as the blades are very highly loaded, loss in efficiency due to swirl becomes important. By recovering the swirl losses, the efficiency can be further increased by 4% - 5%. This can be done either by using stationary guide vanes, as done in turbomachinery, or another set of blades rotating in opposite direction. The latter configuration of counter rotating blades is currently under study by industry.

In order to be able to predict the performance and aeroelastic characteristics, an accurate prediction of blade loading is essential. These could be obtained through experimental or numerical techniques. At the design stage experimental techniques are very expensive. Therefore, a need definitely exists to support the development of potentially high propulsive efficiency propfans through numerical techniques. With numerical techniques it is easier and cheaper to obtain pressure distribution, and flow details can easily be obtained at any point in the flow field.

Several numerical techniques varying in complexity from simple Goldstein type strip analysis to analyses that solve the Euler and Navier - Stokes equations references [1 - 10], have been applied to single-rotation propfans. The only researchers to study the counter rotation propfans are Celestina et al.[11], and Whitfield et al.[9], using finite volume schemes. Celestina et al. have solved the steady Euler equations around the counter rotating configuration by casting the equations in blade fixed

coordinates, where the axisymmetric flow reduces to steady flow. However, this reduces the scheme to be applicable to only symmetric flow field.

Whitfield et al. have also solved the unsteady Euler equations around the counter rotating configuration using finite volume scheme. A finite volume scheme is memory intensive, which could become critical in handling unsteady flowfield for counter rotating propfans. Also, their scheme requires special handling of the row interface boundary to allow arbitrary time step.

Objectives

The primary objective of the present research is to develop a method to predict the aeroelastic characteristics of a counter rotating propfan. To facilitate it, the method to be described here, has the capability to incorporate blade static deformation, rigid blade dynamics, and dynamic elastic deformations. As a first step towards using this solver to such aeroelastic application, this solver has been used to compute the steady airloads and performance characteristics of GE F7/A7 unducted counter rotating propfan.

Formulation

Mathematical Formulation:

The Euler equations, in conservation form, in Cartesian coordinate system can be written as:

$$(\hat{\mathbf{q}})_t + (\hat{\mathbf{E}})_x + (\hat{\mathbf{F}})_y + (\hat{\mathbf{G}})_z = 0 \tag{1}$$

where $\hat{\mathbf{q}}$ is the vector containing conserved flow properties. $\hat{\mathbf{E}}, \hat{\mathbf{F}}$ and $\hat{\mathbf{G}}$ are the nonlinear flux vectors which are functions of the vector $\hat{\mathbf{q}}$. The subscripts denote the partial derivative of the vector. In the above equation

$$\hat{\mathbf{q}} = \begin{pmatrix} \rho \\ \rho u \\ \rho v \\ \rho w \\ e \end{pmatrix} \qquad \hat{\mathbf{E}} = \begin{pmatrix} \rho u \\ \rho u^2 + p \\ \rho uv \\ \rho uw \\ u(e+p) \end{pmatrix}$$

$$\hat{\mathbf{F}} = \begin{pmatrix} \rho v \\ \rho uv \\ \rho v^2 + p \\ \rho vw \\ v(e+p) \end{pmatrix} \qquad \hat{\mathbf{G}} = \begin{pmatrix} \rho w \\ \rho uw \\ \rho vw \\ \rho w^2 + p \\ w(e+p) \end{pmatrix} \tag{2}$$

where ρ is the fluid density, u, v, w are the inertial Cartesian components of the flow velocity, e is the total energy of the fluid per unit volume and p is the hydrodynamic pressure and may be expressed using the equation of state for perfect gas as:

$$p = (\gamma - 1)[e - \frac{1}{2}\rho(u^2 + v^2 + w^2)] \tag{3}$$

where γ is the ratio of specific heats. The advantage of using the conservation form is that it ensures the conservation of physical flux properties across discontinuities (e.g. shock) in the flow [12].

The following coordinate transformation :

$$\begin{aligned} \xi &= \xi(x, y, z, t) \\ \eta &= \eta(x, y, z, t) \end{aligned}$$

$$\begin{aligned} \zeta &= \zeta(x, y, z, t) \\ \tau &= t \end{aligned} \tag{4}$$

is used to recast the governing equation in (1) in a generalized coordinate system as

$$\mathbf{q}_\tau + \mathbf{E}_\xi + \mathbf{F}_\eta + \mathbf{G}_\zeta = 0 \tag{5}$$

where

$$\mathbf{q} = J^{-1} \begin{pmatrix} \rho \\ \rho u \\ \rho v \\ \rho w \\ e \end{pmatrix} \qquad \mathbf{E} = J^{-1} \begin{pmatrix} \rho U \\ \rho u U + \xi_x p \\ \rho v U + \xi_y p \\ \rho w U + \xi_z p \\ (e+p)U - \xi_t p \end{pmatrix} \tag{6}$$

$$\mathbf{F} = J^{-1} \begin{pmatrix} \rho V \\ \rho u V + \eta_x p \\ \rho v V + \eta_y p \\ \rho w V + \eta_z p \\ (e+p)V - \eta_t p \end{pmatrix} \qquad \mathbf{G} = J^{-1} \begin{pmatrix} \rho W \\ \rho u W + \zeta_x p \\ \rho v W + \zeta_y p \\ \rho w W + \zeta_z p \\ (e+p)W - \zeta_t p \end{pmatrix}$$

U, V, and W are the contravariant velocities, and J is the jacobian and ξ_x, η_x, ζ_x etc. are the metrics of transformation.

Initial and Boundary Conditions

The initial conditions may be critical to convergence of the numerical scheme. An intelligent guess of the initial conditions could help in achieving convergence faster. For these calculations the free stream conditions are used as the initial condition.

In the present analysis the flow variables at the boundaries are updated explicitly after the governing equations have been solved for the interior flow field. The boundary conditions are applied to the total velocities.

On the solid surfaces of blade and nacelle the no penetration condition is applied as:

$$\vec{V_b}.\vec{n} = 0 \tag{7}$$

Where $\vec{V_b}$ is the velocity vector at the surface and $\vec{n}$ is the unit vector normal to the surface. The tangential velocity components are extrapolated from interior of the domain.

For steady state calculations all disturbances from the solid surface must propagate to infinity. On the subsonic inflow boundary, one characteristic should be allowed to escape hence ρ is extrapolated and the remaining variables $\rho u, \rho v, \rho w$ and e are fixed at the free stream value. For a supersonic inflow boundary, all quantities are fixed to that of the free stream. At the subsonic outflow boundary, four characteristics should escape, thus the four quantities $\rho, \rho u, \rho v, \rho w$ are extrapolated from inside while the pressure is fixed to that of the free stream. For supersonic outflow, all characteristics should escape, hence all quantities are extrapolated from inside the flow domain.

It is neither efficient nor practical to solve all the blades at the same time, hence, one blade passage is handled at a time. This introduces additional boundaries for computation. Across these boundaries all the variables must be continuous, except on solid boundaries. The boundary condition, for these boundaries, depends on the type of flow being solved. An axisymmetric flow requires periodicity on the fluid interface boundaries. Periodicity is enforced by forcing the two boundaries to have the same fluid properties.

For an unsymmetric flow, the periodicity on these boundaries does not exist. Therefore, in order to obtain the solution for such a case, the whole propfan should be solved. In this case again the boundaries are updated explicitly, after the interior

points have been updated. This is done by averaging the flow variables from the nodes on each side of the boundary from the adjoining blocks.

To simplify the solution procedure the domain of counter rotating blade is divided into two sets of blocks associated with each blade. This creates an additional fluid boundary. Proper handling of this boundary is critical as it is through this boundary each row of blades feels the presence of the other. As the rest of the boundaries, this boundary is also updated explicitly after the interior of the computational domain has been updated. This boundary is updated as the average of the adjacent constant ξ plane. However as the two blocks are rotating in the opposite direction, the grid lines do not always align.

To carry out the averaging process the solution needs to be known for the 360° ring associated with each of the constant ξ planes. For an unsymmetric flow field this information is automatically available, as all the blades are required to be solved. For an axisymmetric flow field, where only one blade passage needs to be solved for each blade row, this information is obtained by imaging the block data to obtain flow properties for the 360° ring.

A schematic of the grid at the interface boundary for a constant η plane is shown in figure (1). The I=IMAX plane for the front blade row, and I=1 plane of the rear blade row form the interface boundary. The interface boundary of the rear blade row is updated first, one grid point at a time. In order to update the flow properties at the node B, the grid line AB is extended till it intersects the plane I=IMAX-1 of the front row at point C. The flow properties are then obtained at point C by interpolating from the flow properties of the IMAX-1 plane using a Lagrangian polynomial. The node B is then updated by taking the average of the values at node A and point C. This is repeated for all the nodes associated with I=1 plane of the rear row.

Again, for an axisymmetric flow field this is done for only one block and the solution is imaged. For an unsymmetric flow field, the process is repeated for all

the nodes for all the blade passages. The boundary I=IMAX of the front row is then updated by simply interpolating flow variables from the boundary I=1 of the rear row. The only restriction in this process, in order to minimize the error, is to require that the constant η planes from both the rows, at the interface boundary, are at the same radial distance.

Solution Procedure:

The governing equations in (5) are in fully conservative form. They are discretized using second order accurate central differencing for the spatial derivatives and a first order upwind differencing for the temporal derivative, to obtain a set of algebraic equation. A second order implicit dissipation and a blend of second / fourth difference explicit dissipation is used. In order to decrease the computational time, flux terms in two directions (ξ, ζ), are treated implicitly while the radial direction (η) flux terms are treated semi-explicitly. The η derivative is obtained using the latest available values of the flow variables, hence the η derivative alternates between

$$\frac{\mathbf{F}^{n}_{i,j+1,k} - \mathbf{F}^{n+1}_{i,j-1,k}}{2\Delta\eta}$$

during the odd time steps, and

$$\frac{\mathbf{F}^{n+1}_{i,j+1,k} - \mathbf{F}^{n}_{i,j-1,k}}{2\Delta\eta}$$

during the even time steps.

This method requires only two costly inversions of the block tridiagonal matrix, in the two implicit directions. It also reduces the memory requirement as only two time levels of information needs to be stored at any given time, one of which needs to be only two dimensional. Rizk and Chausee [13] first used this hybrid scheme with the Beam and Warming algorithm. Using this technique the solver marches

along the η direction, solving the equations one η plane at a time. The marching direction is reversed after every sweep, in order to remove any dependency on the marching direction.

The discretized form of the governing equations are approximately factorized to the following set of algebraic equations :

$$\left[I + \Delta\tau\left(\delta_\xi A^n + \epsilon_I D_{I_\xi}\right)\right]\Delta\mathbf{q}^{*n+1} = \mathbf{R}^{n,n+1} - \epsilon_E D_E \Delta\tau \tag{8}$$

$$\left[I + \Delta\tau\left(\delta_\zeta B^n + \epsilon_I D_{I_\zeta}\right)\right]\Delta\mathbf{q}^{n+1} = \Delta\mathbf{q}^{*n+1} \tag{9}$$

where

$$\mathbf{R}^{n,n+1} = -\Delta\tau\left(\delta_\xi \mathbf{E}^n + \delta_\eta \mathbf{F}^{n,n+1} + \delta_\zeta \mathbf{G}^n\right) \tag{10}$$

$$\Delta\mathbf{q}^{n+1} = \mathbf{q}^{n+1} - \mathbf{q}^n \tag{11}$$

D_{I_ξ} and D_{I_ζ} are second order implicit dissipation terms and D_E is the explicit dissipation term, given in reference [14]. ϵ_I and ϵ_E are user supplied constants, which depend on grid spacing. At the boundaries the fourth order differences are replaced by second order differences.

The factorized algebraic equations (9) and (10) are then solved using the Alternating Direction Implicit (ADI) scheme [15]. In solving the flow field using multi block grid technique, only one grid and its solution is kept in the core memory. Once the interior points are updated, the flow solution and the grid is written on solid state storage. The next block is then brought into the core memory to update the interior points. The interface boundary points, and the adjoining nodes used to update them are always kept in the core memory. As mentioned earlier, the row interface boundary is updated after all the interior points have been updated.

Results and Discussion

Previous Studies:

The hybrid numerical scheme discussed in the previous section, was first applied to a single rotation propfan in [15]. Typical results of variation of power coefficient with advance ratio and spanwise blade loading for an eight bladed SR-3 propfan are reproduced in figures (2) and (3). In figure (4) the pressure coefficient for a two bladed SR-7L propfan is compared with experimental data for different span location, for free stream Mach number of 0.5, and advance ratio of 3.067. The pressure coefficients compare well, except near the leading edge. For this flight condition, a leading edge vortex exists. Since the present scheme solves Euler equations, it is not possible to capture this leading edge vortex. As can be seen from these figures, the hybrid scheme successfully predicts the spanwise and chordwise loading, alongwith performance quantities for a single rotation propfan.

New Results:

Again, as in Ref. [15] a body fitted H-O grid was used for calculating the flow field around the counter rotating propfan. A typical grid used in the calculation is shown in figure (5). In general, in order to model the influence of adjacent blades (cascade effect) the entire propfan with all the blades (passages) need to be solved. However, for an axisymmetric flow field, with same number of blades in both the rows, considered here, all blade passages can be assumed to be identical. Hence only one blade passage, for each blade row, is solved enforcing the conditions of symmetry.

The scheme has been applied here to a GE F7/A7 counter rotating propfan operating at a free stream Mach number of 0.71. This propfan has 8 blades in each blade row. Both the blade rows operate at the same advance ratio. In figure (6) the power coefficients and in figure (7) the thrust coefficients are compared with experimental data. The blade setting angles have been adjusted to match the

power coefficient at the advance ratio of 3.0, but was not changed for other advance ratios. As can be seen, the total power and thrust coefficients are over predicted for lower advance ratio, whereas they compare well for higher advance ratios with experiment. The individual blade row power coefficients, exhibit the same trend, whereas the thrust coefficient is consistently over predicted for the front row. In figure (8), the variation of torque ratio, (aft rotor : front rotor), with advance ratio is compared. The comparison, in this case, is better for lower advance ratio.

From these figures, it can be seen that the prediction of the global performance quantities compare well with experimental data. At the lower advance ratios, the blades are heavily loaded. This causes the blade to deflect more during operation. Such deflections are not possible to account for, in a purely aerodynamic code. Also the Euler calculations tend to overpredict the shock strength, which will lead to higher wave drag. Furthermore the absence of viscous effects will not account for complex shock wave and boundary layer interaction and flow seperation. Any or all of the above factors could be contributing to the over prediction of the performance parameters.

In figures (9) and (10), the pressure and density are plotted at two constant η locations, on the nacelle and near mid span. The front rotor is rotating in a counter clockwise direction, and the aft rotor is rotating in the clockwise direction, as viewed from the front. The free stream is moving from left to right, with a relative Mach number of 0.71, and the advance ratio, for both the blade rows, is 2.8. The blade setting angles were obtained by matching the individual rotor power coefficients with experimental data. The pressure and the density plots shown in these figures, show that the treatment of the interface boundary as discussed earlier, does not introduce any significant error. In fact it is very difficult to locate the boundary from these figures. The interface boundary lies exactly halfway between the two blade rows. Furthermore, these figures also show that a strong shock exists on the suction surface of the front blade, at approximately 60% of the chord. This

shock does not extend from blade to blade, and its strength reduces, away from the centerbody. The shock also moves downstream along the chord, and is almost at the trailing edge, near the mid span location. The aft blade does not have a strong shock, however it does have a larger stagnation region, as compared to the front blade. This is to be expected, as the energy of the fluid increases as it passes through the front blade row. These figures also show that the solver successfully captures the physics of the flow field around the counter rotating propfan.

In the full paper, one other flight condition (free stream Mach number of 0.660) will be studied and the solutions obtained will be compared with experimental data. If possible this solver will be coupled to a structural analysis code (as done in reference [15]) to study the effect of structural deformations on performance.

Computer Requirements:

All of the above computations were performed on the CRAY XMP24 computer available at NASA Lewis Research Center. For a grid size of 58 x 22 x 15, used for each block, the total memory and CPU time per time step required were 1.3 MW and 1.7 sec. respectively.

Acknowledgements

This work has been carried out under NASA grant NAG3-730 from NASA Lewis Research Center in Cleveland, Ohio. Mr. George L. Stefko is the grant monitor.

References

[1] Goldstein, S.," On the Vortex Theory of Screw Propellers," Royal Society Proceedings, Vol. 123, No. 792, Apr. 6, 1929, pp 440-465

[2] Sullivan, J. P.," The effect of Blade Sweep on Propeller Performance,"AIAA Paper 77-176, June 1977

[3] Egolf, T. A., Anderson, O. L., Edwards, D. E., and Landgrebe, A. J.," An Analysis for High Speed Propeller-Nacelle Aerodynamic Performance Prediction; Volume 1, Theory and Initial Application and Volume 2, User's Manual for the Computer Program," United Technologies Research Center, R79-912949-19, June 1979.

[4] Hanson, D. B.," Compressible Lifting Surface Theory for Propeller Performance Calculation," AIAA paper 82-0020.

[5] Williams, M. H., and Hwang, C.," Three Dimensional Unsteady Aerodynamics and Aeroelastic Response of Advanced Turboprops," AIAA Paper 86-0846.

[6] Jou, W. H.," Finite Volume Calculation of the Three - Dimensional Flow Around a Propeller," AIAA Paper 82-0957.

[7] Jameson, A., and Caughy, D. A., " A Finite Volume Method for Transonic Potential Flow Calculations," Proceedings Third AIAA Computational Fluid Dynamics Conference, Albuquerque, 1977.

[8] Chausee, D. S.," Computation of Three-Dimensional Flow Through Prop Fans," Nielsen Engineering and Research Inc., NEAR TR-199, June 1979.

[9] Whitfeild, D. L., Swafford, T. W., Janus, J. M., Mulac, R. A., Belk, D. M., "Three-Dimensional Unsteady Euler Solutions for Propfans and Counter-Rotating Propfans in Transonic Flow," AIAA Paper 87-1197, June 1987.

[10] Matsuo, Y., Arakawa, C., Saito, S., and Kobayashi, H., "Navier-Stokes Computations for Flowfield of an Advanced Turboprop," AIAA Paper 88-3094.

[11] Celestina, M. L., Mullac, R. A., Adamczyk, J. J., "A Numerical Simulation of the Inviscid Flow Through A Counter-Rotating Propeller", NASA TM-87200.

[12] Lax, P. D., "Weak Solutions of Nonlinear Hyperbolic Equations and their Numerical Computation," *Communications in Pure and Applied Mathematics*, Vol. 7, pp. 159-193.

[13] Rizk, Y. M. and Chaussee, D. S., "Three-Dimensional Viscous-Flow Computations Using a Directionally Hybrid Implicit-Explicit Procedure," AIAA paper 83-1910, 1983.

[14] Wake, B. E., and Sankar, L. N., "Solutions of the Navier-Stokes Equations for the Flow about a Rotor Blade," *Journal of the American Helicopter Society*, Vol. 34, No. 2, pp 13-23, April 1989.

[15] Srivastava, R., Sankar, N. L., Reddy, T. S. R., Huff, D. L., "Application of an Efficient Hybrid Scheme for Aeroelastic Analysis of Advanced Propellers", AIAA Paper 90-0028, January 1990.

[16] Bushnell, P.," Measurement of the Steady Surface Pressure Distribution on a Single Rotation Large Scale Advanced Numbers from 0.03 to 0.78," NASA CR 182124, July 1988.

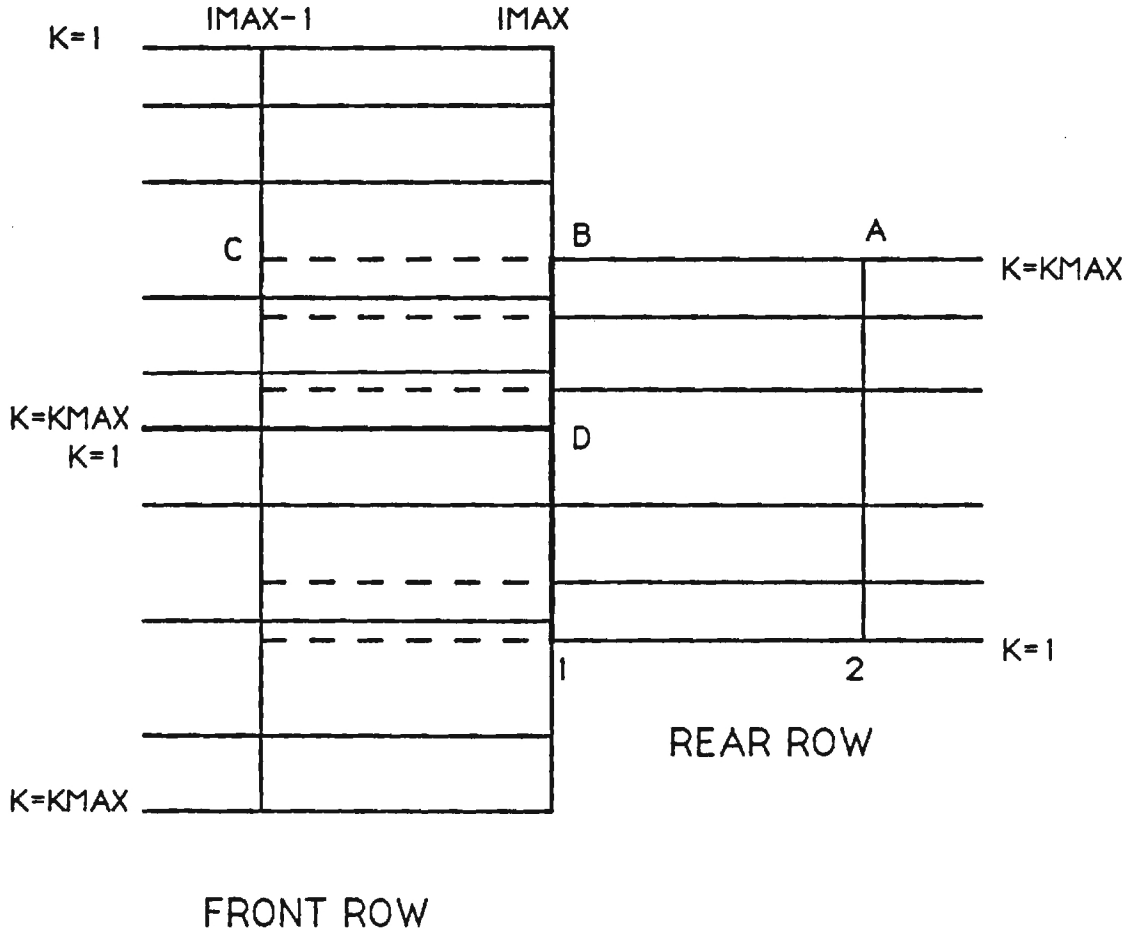

Figure-1 Schematic Grid at Interface Boundary

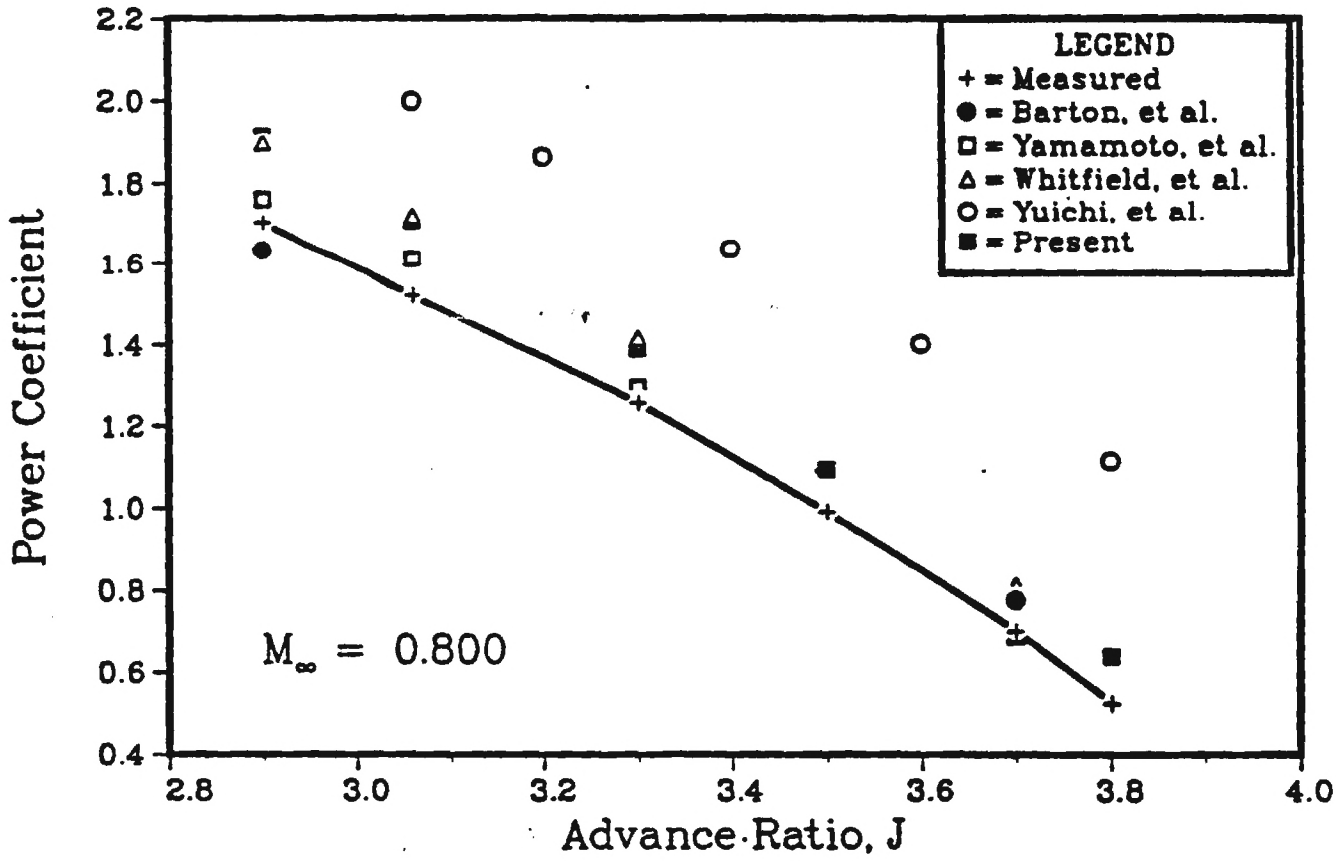

Figure-2 Power Coefficient vs. Advance Ratio

SR-3 8-Bladed Propfan

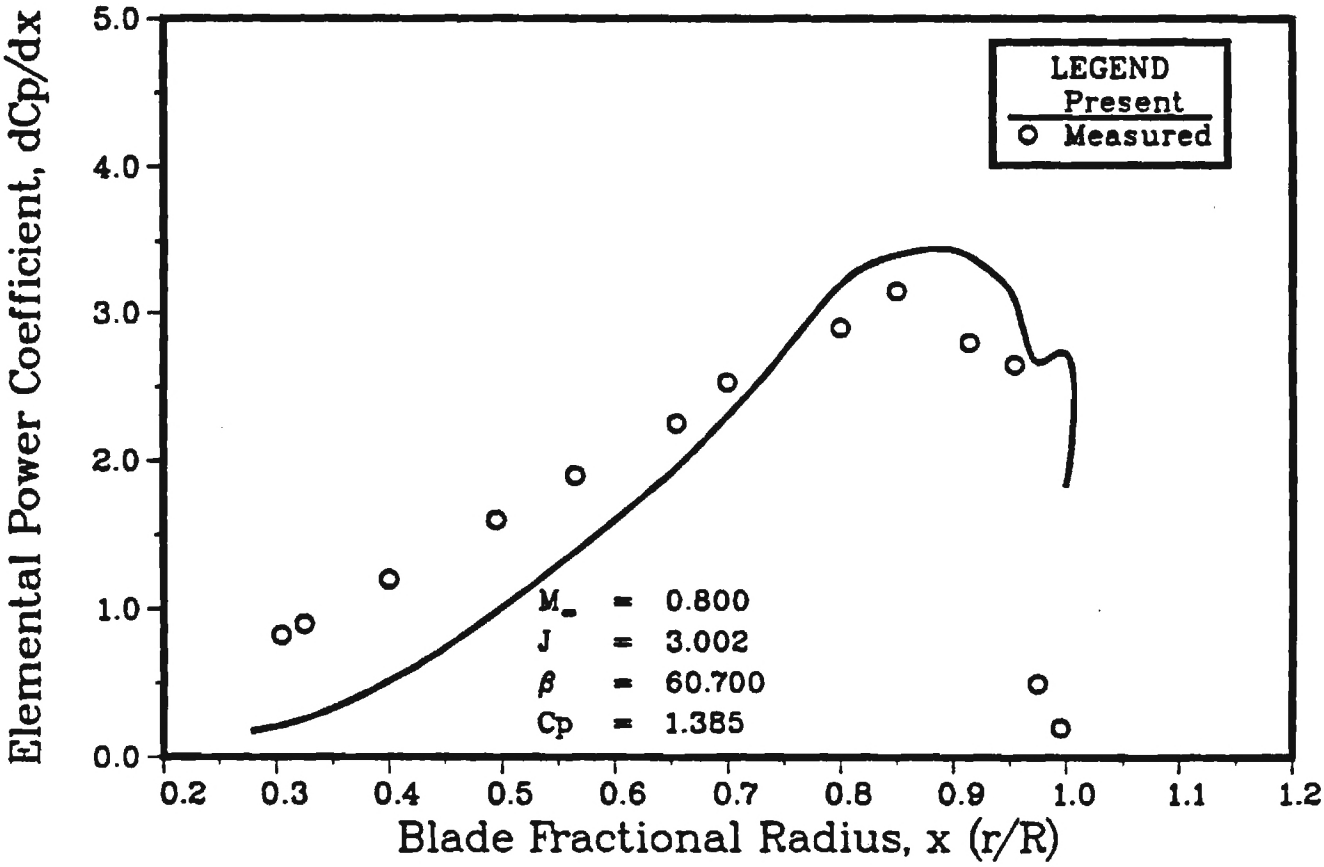

Figure-3 Elemental Power Coefficient vs. Radius

SR-7 2-Bladed Propfan

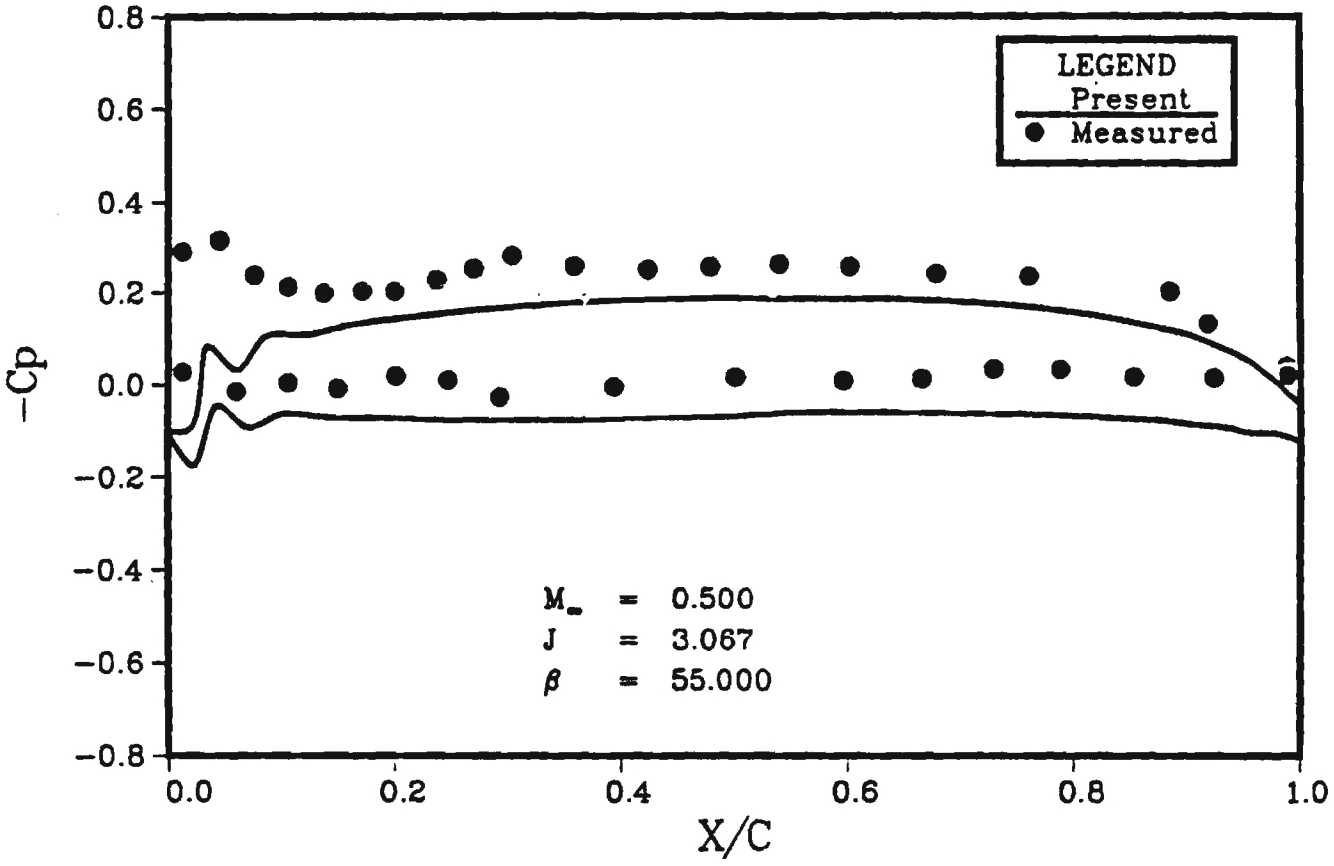

Figure-4a Pressure Coefficient Near Root

SR-7 2-Bladed Propfan

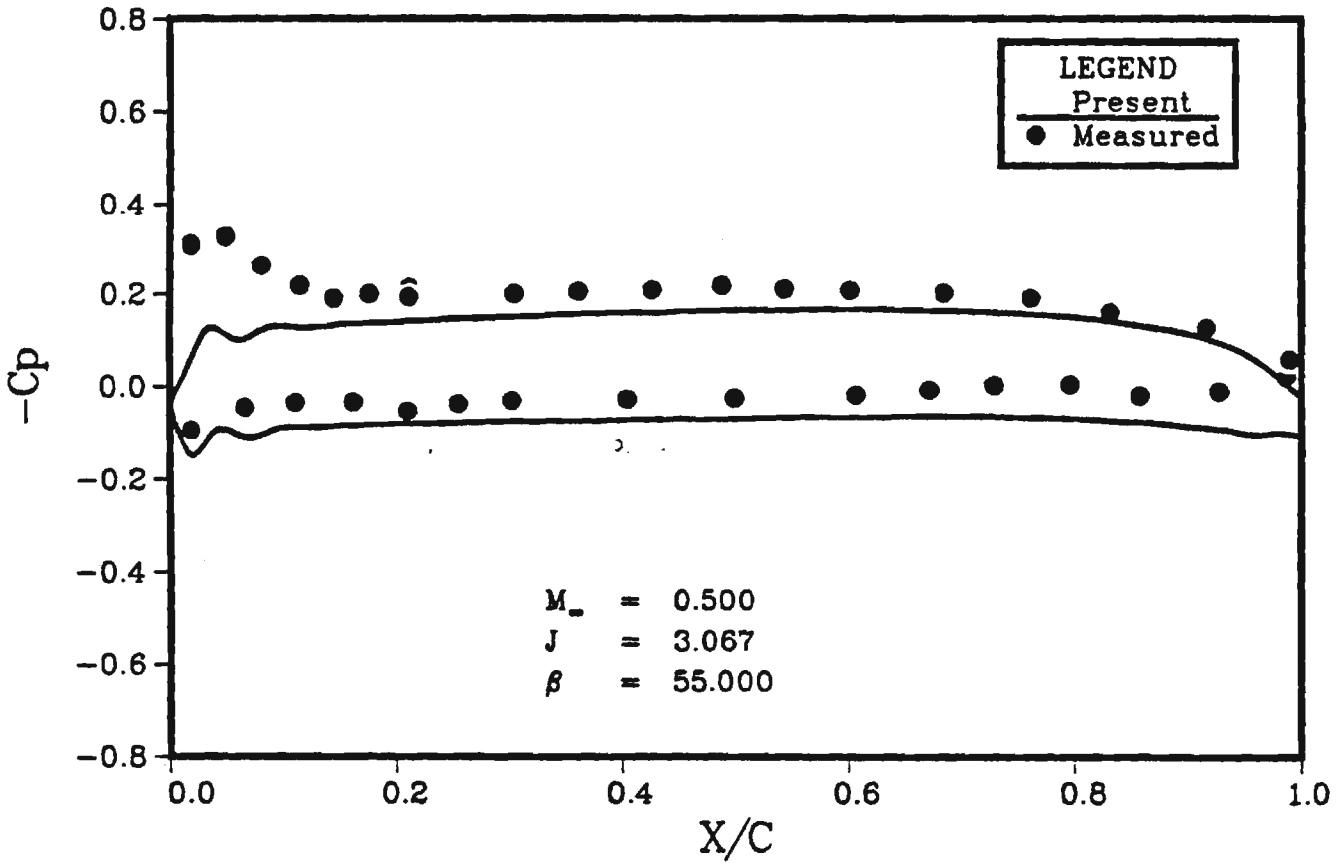

Figure-4b Pressure Coefficient Near Mid Span

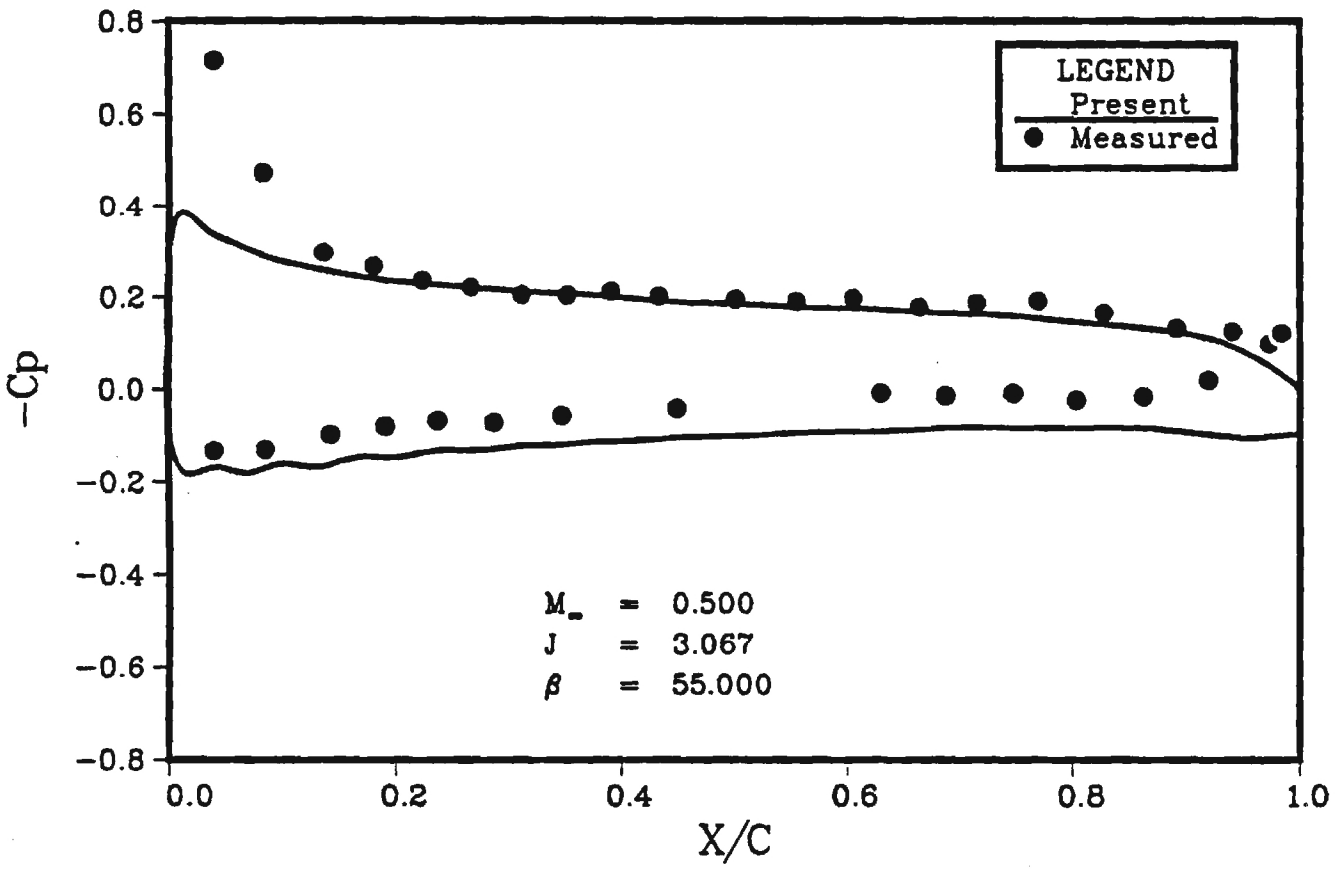

Figure-4c Pressure Coefficient Near Tip

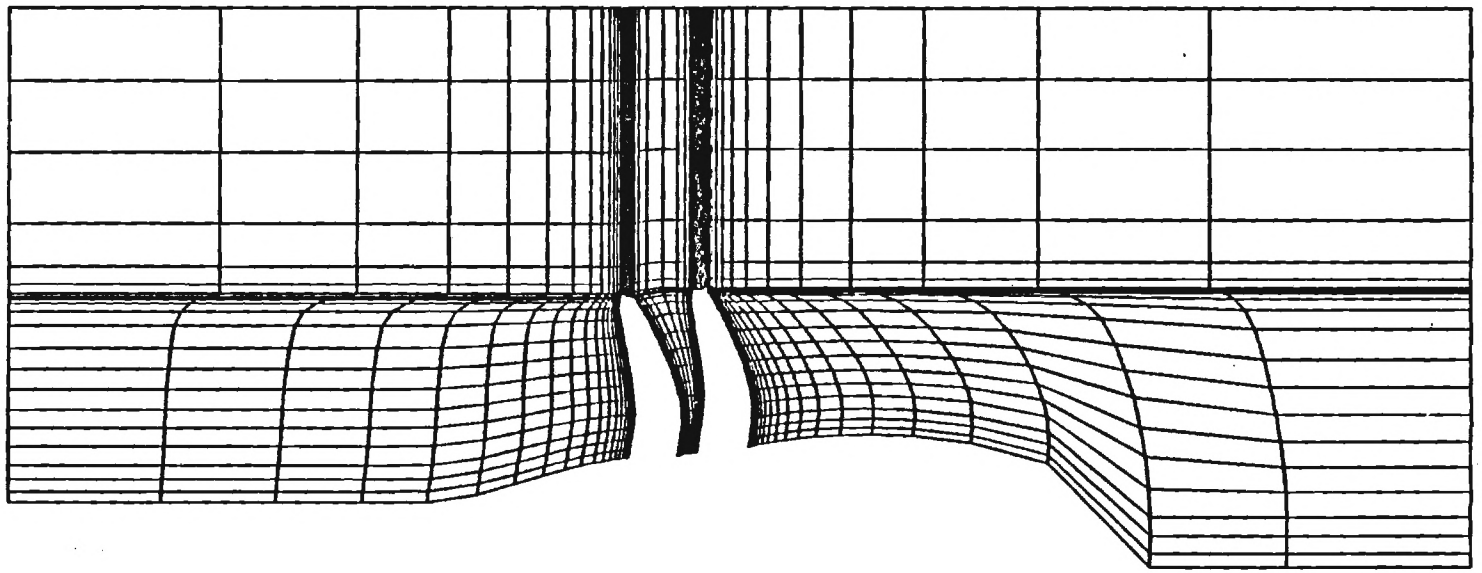

Figure-5a H - Grid in Streamwise Plane

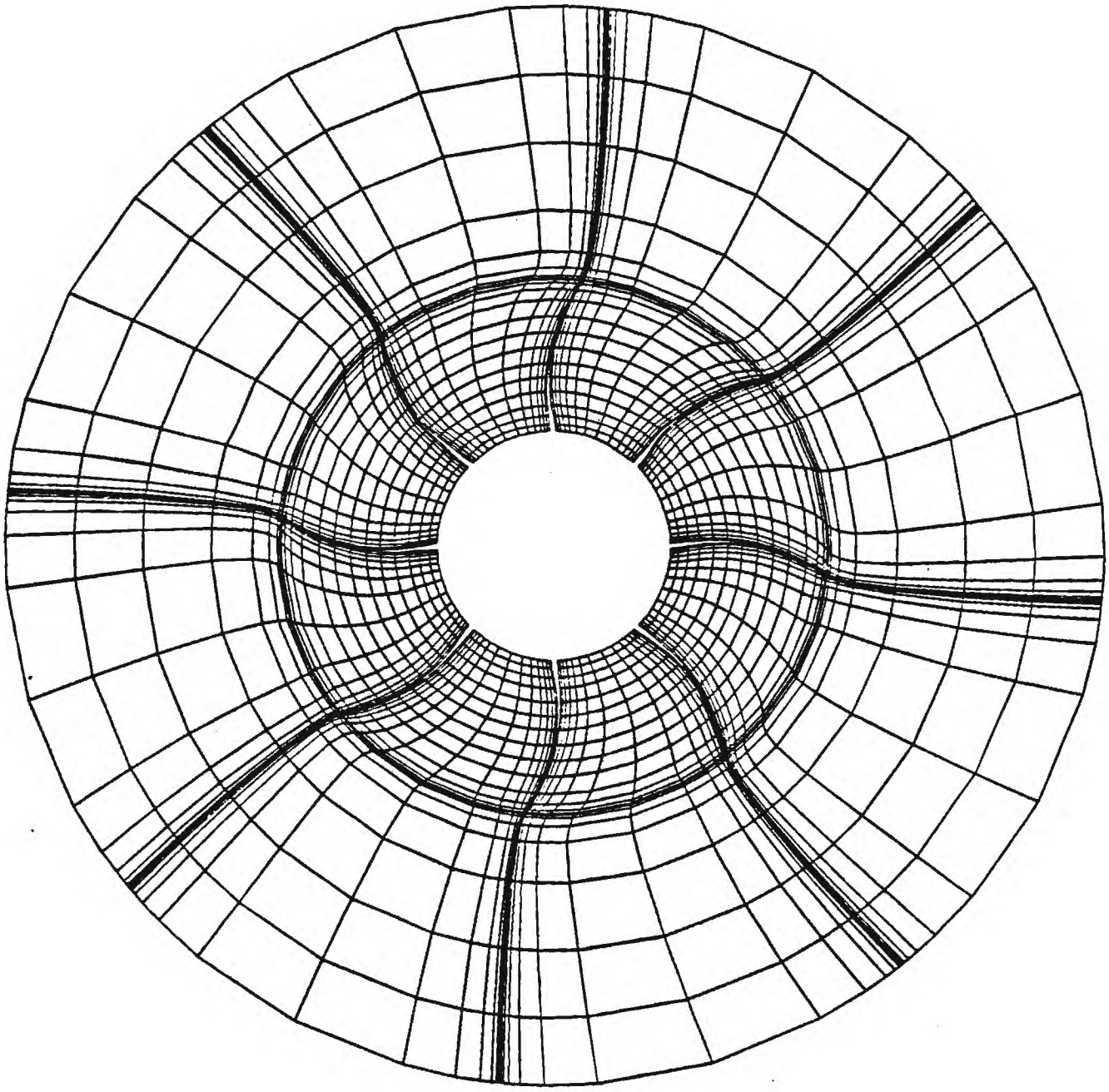

Figure-5b O - Grid in Azimuthal Plane

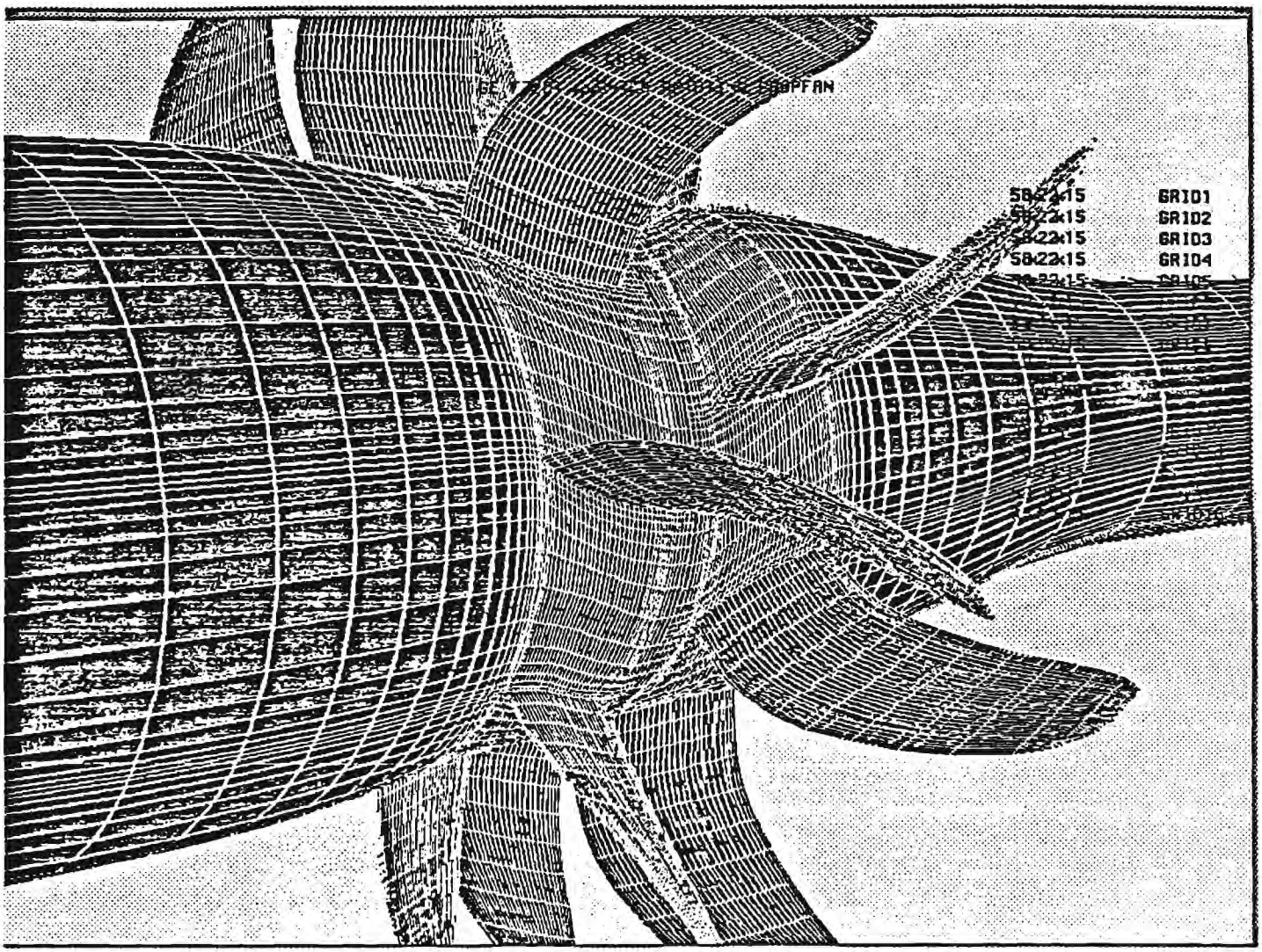

Figure-5c Wire Frame Grid in the Vicinity of Blades

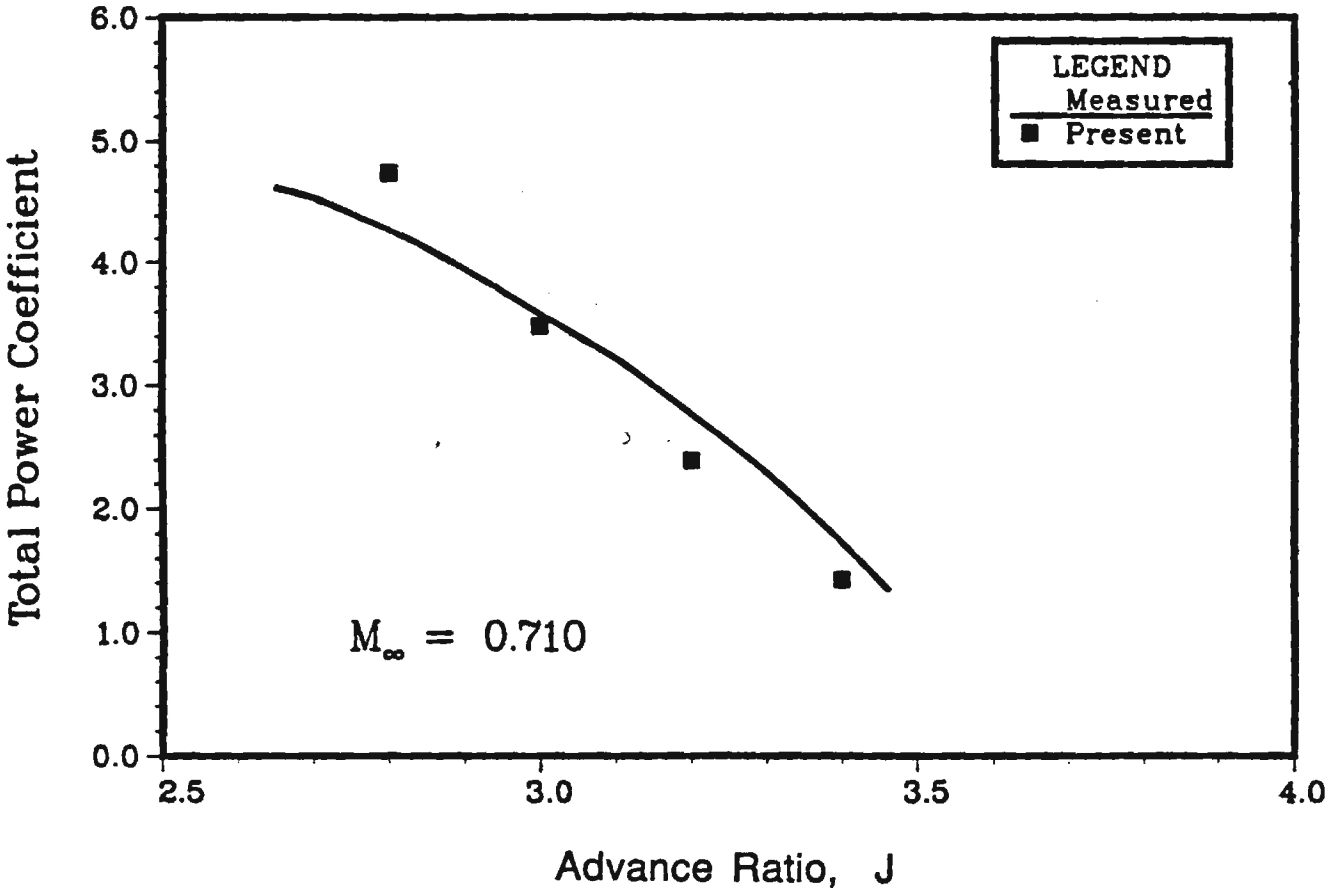

Figure-6a Total Power Coefficient vs. Advance Ratio

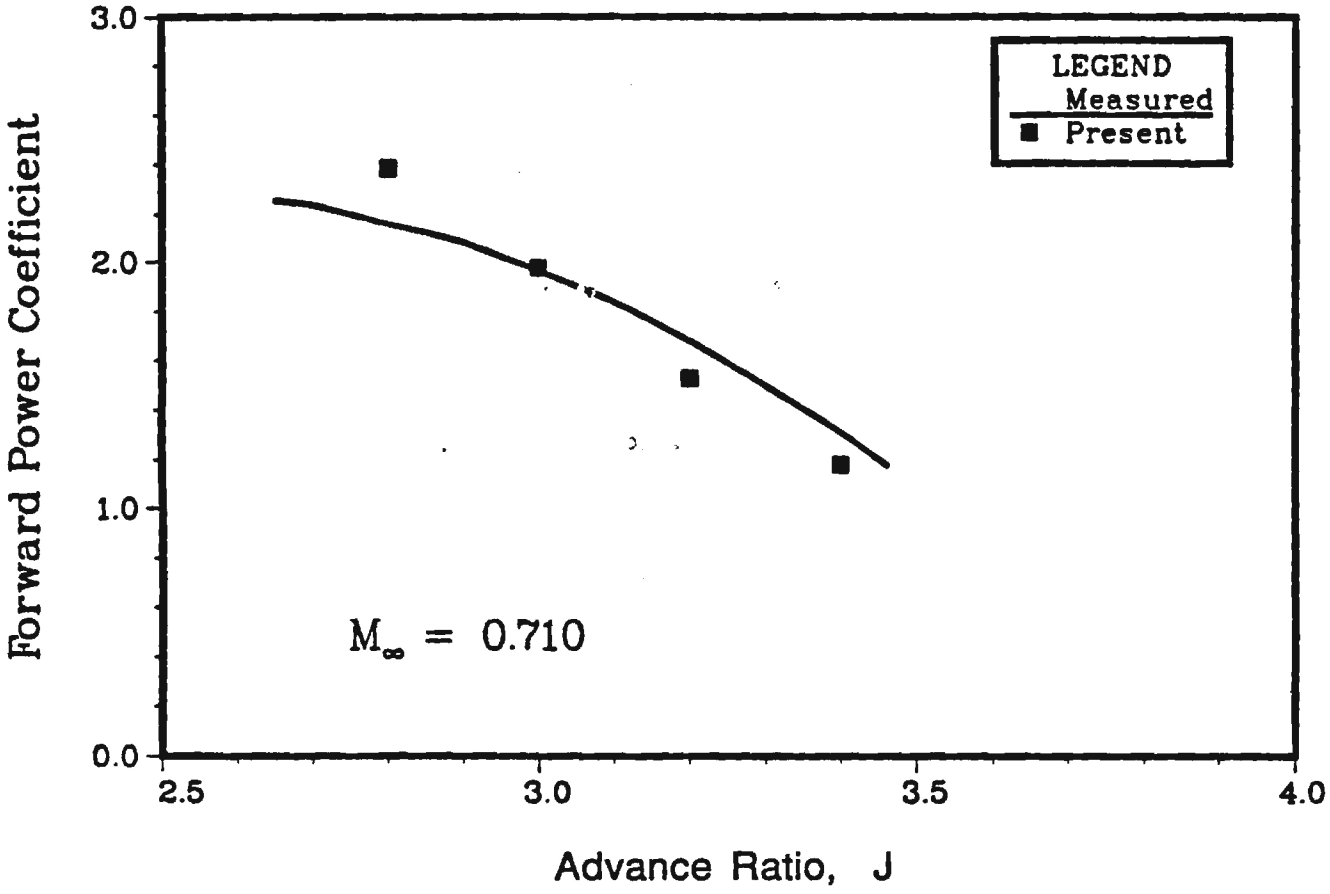

Figure-6b Forward Rotor Power Coefficient vs. Advance Ratio

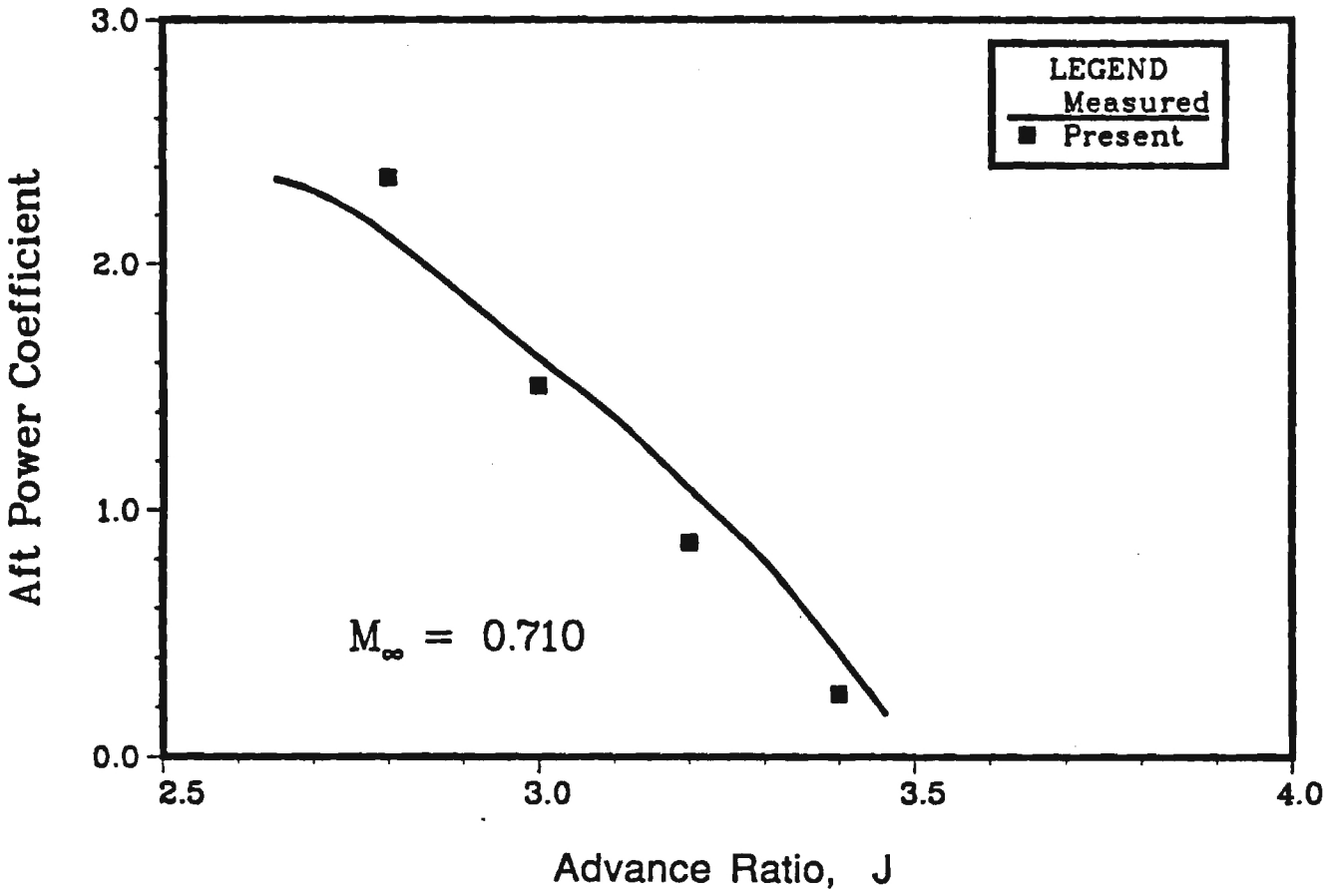

Figure-6c Aft Rotor Power Coefficient vs. Advance Ratio

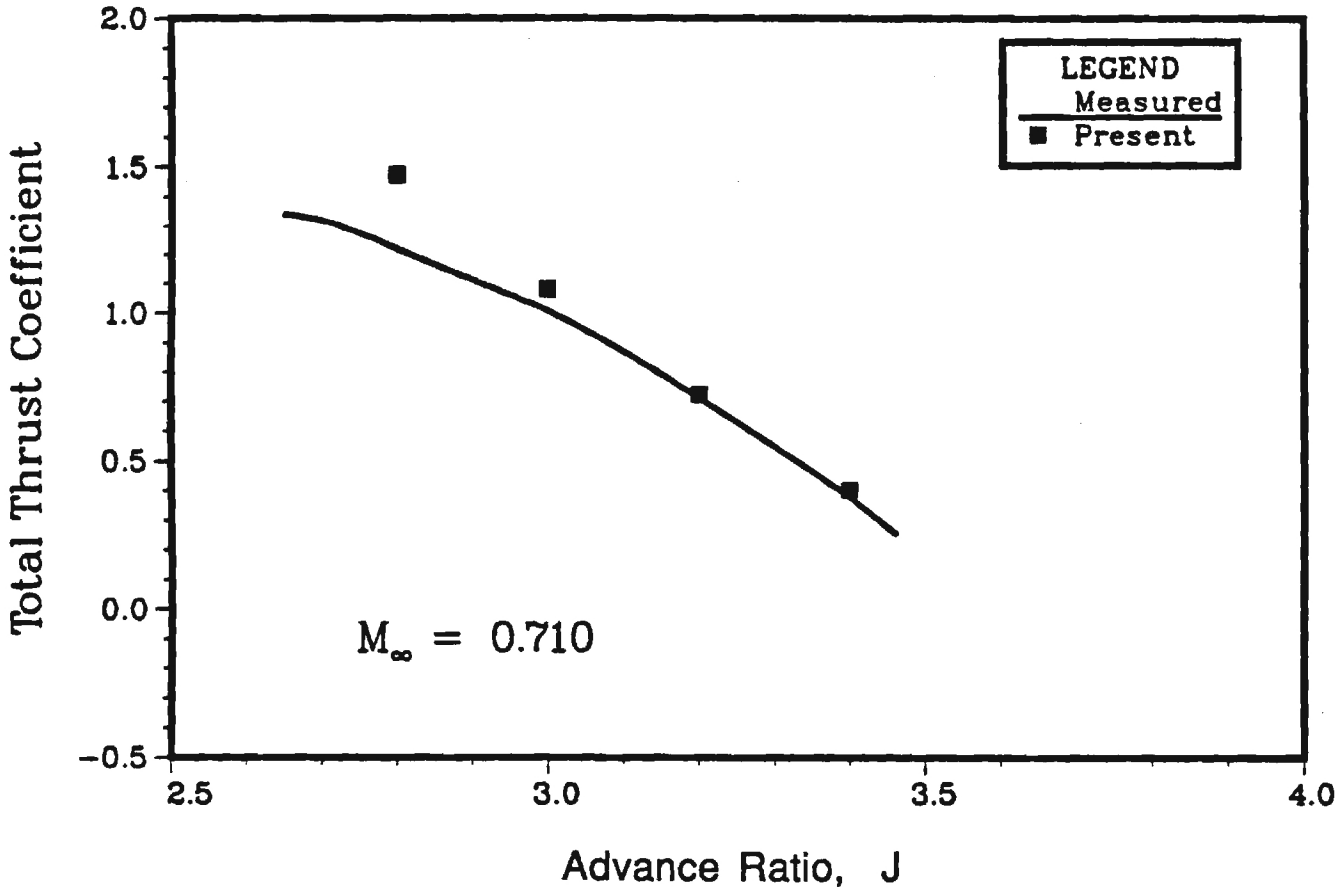

Figure-7a Total Thrust Coefficient vs. Advance Ratio

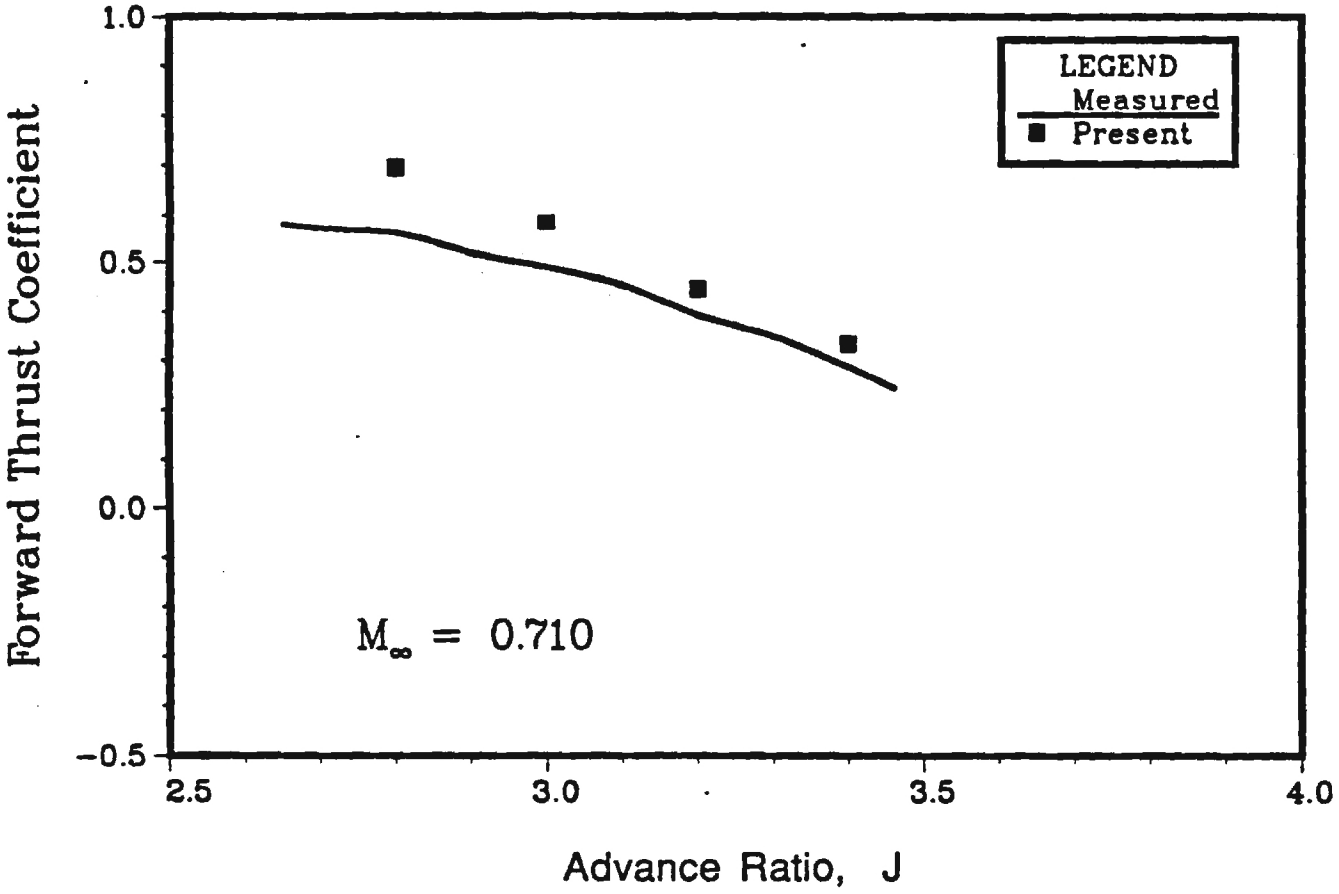

Figure-7b Forward Thrust Power Coefficient vs. Advance Ratio

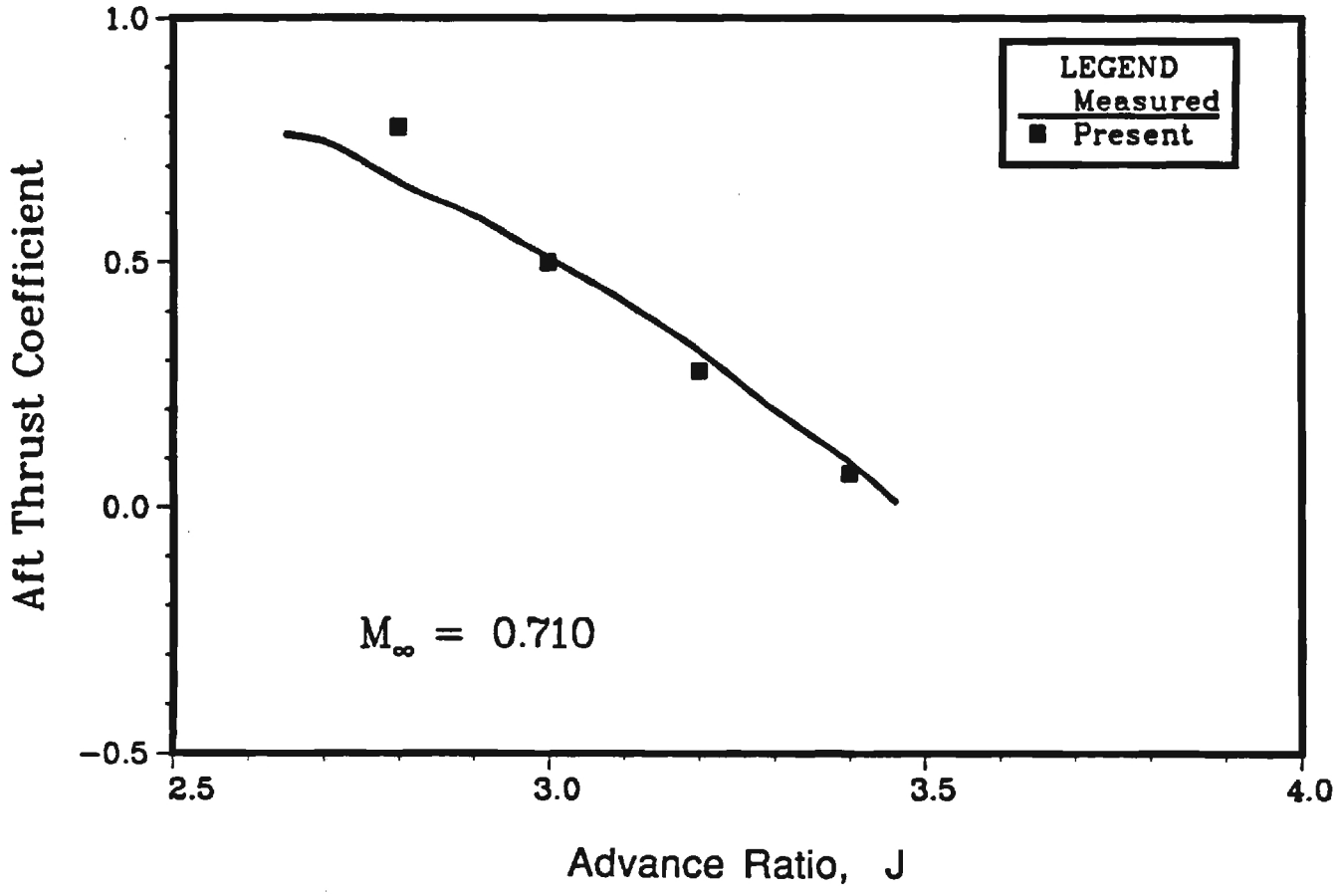

Figure-7c Aft Rotor Thrust Coefficient vs. Advance Ratio

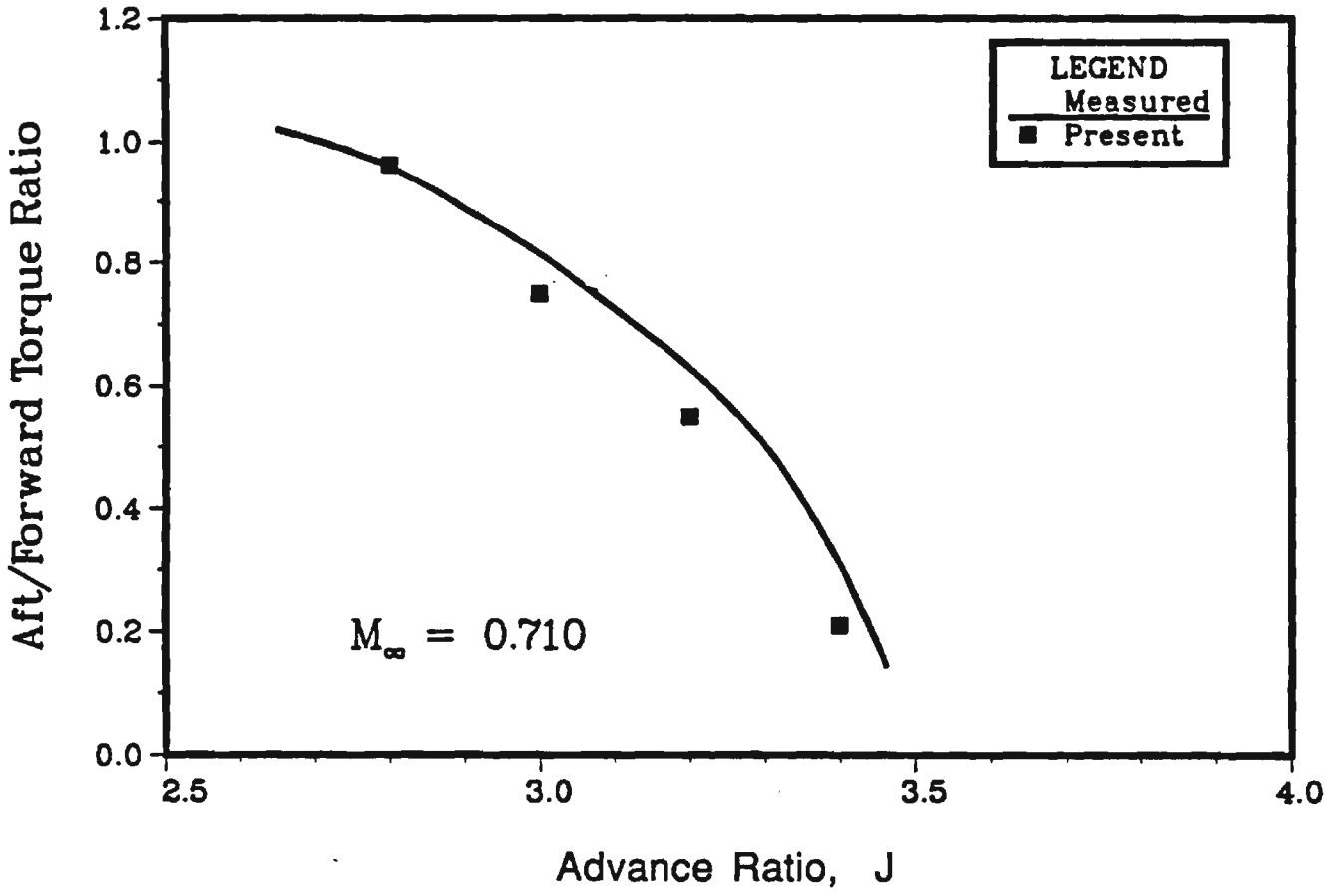

Figure-8 Aft/Forward Torque Ratio vs. Advance Ratio

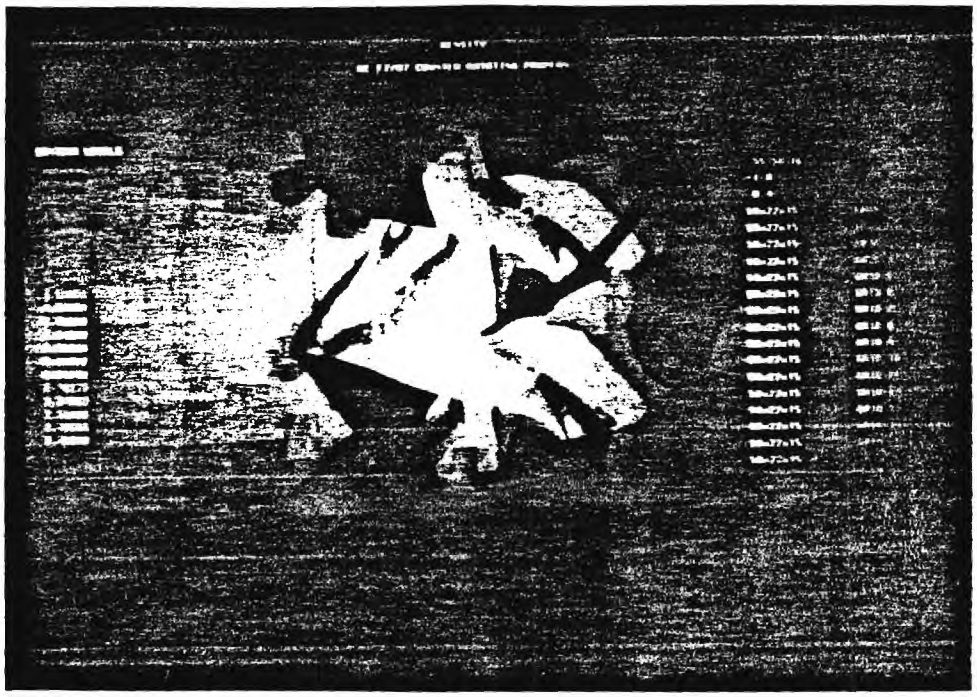

Figure-9a Density Contours on the Nacelle

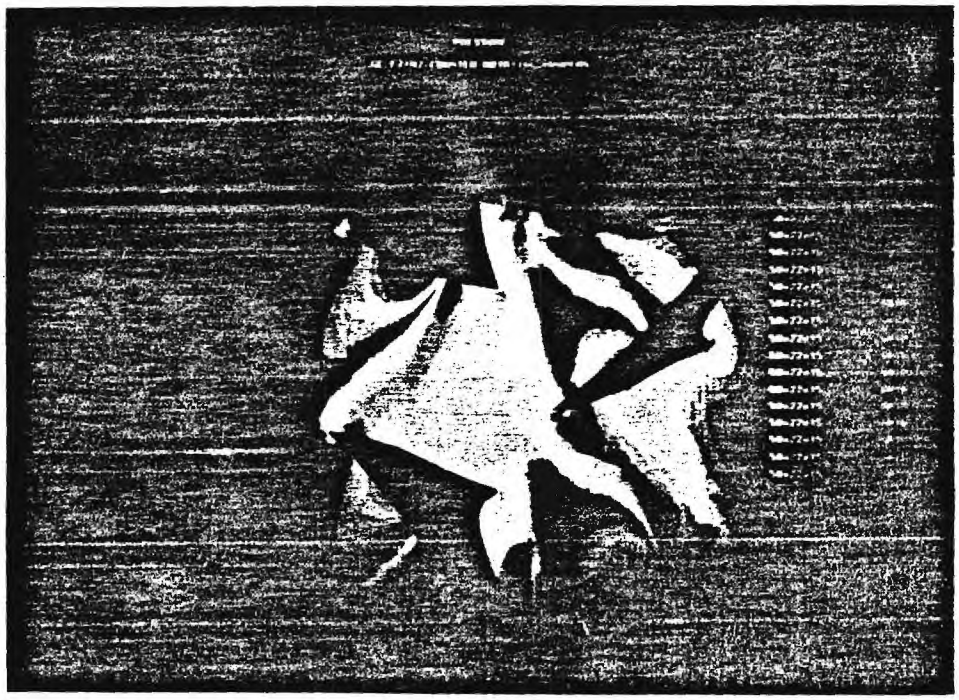

Figure-9b Pressure Contours on the Nacelle

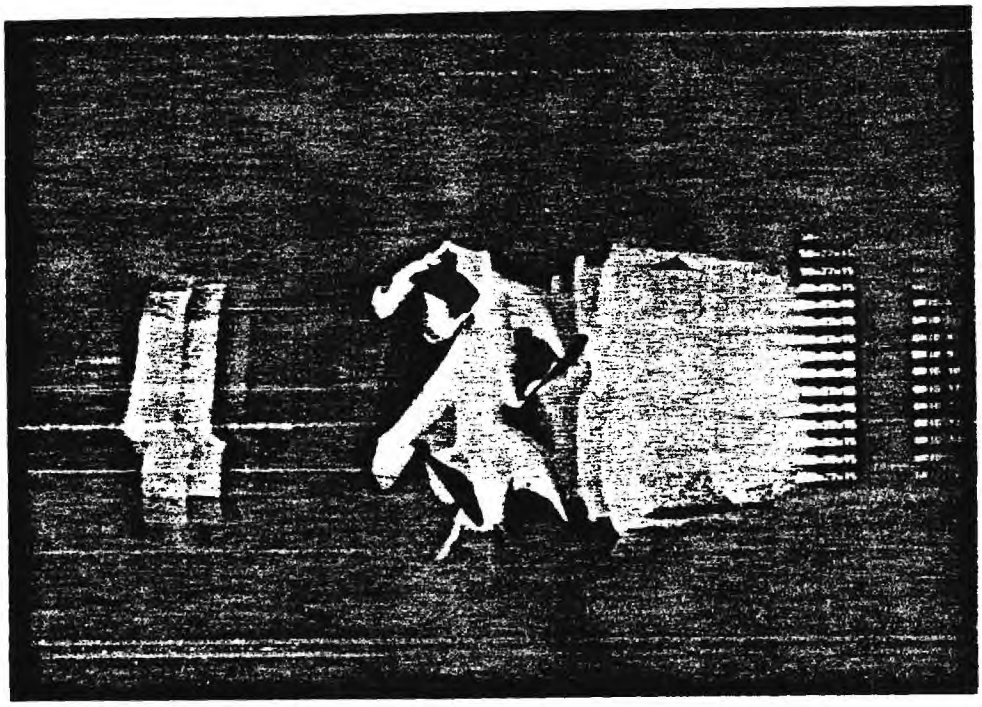

Figure-10a Density Contours at Constant η Plane near Mid Span

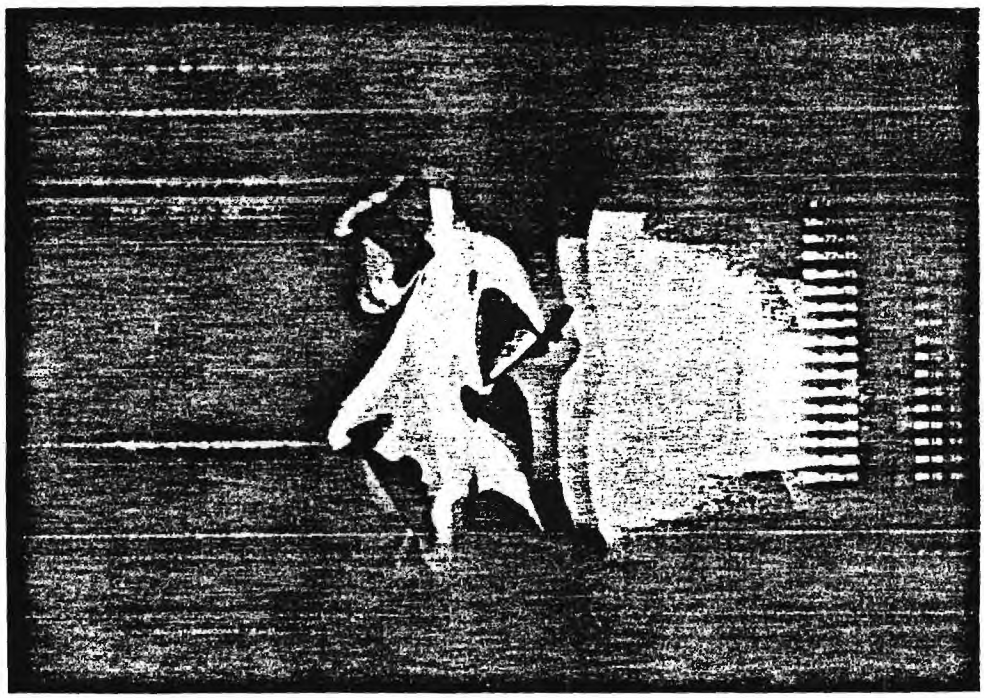

Figure-10b Pressure Contours at Constant η Plane near Mid Span

E-16-801

GEORGIA TECH RESEARCH CORPORATION

GEORGIA INSTITUTE OF TECHNOLOGY
ATLANTA, GEORGIA 30332-0420

Telex: 542507 GTRCOCAATL
Fax: (404) 894-3120

Phone: (404) 894-4817

Refer to: RDF/02.105.011.88.003

25 September 1987

NASA Lewis Research Center
Operations and Industry Assistance Office
Mail Stop 500-306
21000 Brookpark Road
Cleveland, OH 44135

Attention: Mr. Boyd M. Bane
Grants Officer

Subject: Research Proposal Entitled, "Numerical Study of Effects of Sweep on Viscous Flow Over Wings"

Dear Mr. Bane:

The GEORGIA TECH RESEARCH CORPORATION desires to submit for your consideration the subject proposal prepared by Dr. L.N. Sankar, School of Aerospace Engineering, Georgia Institute of Technology.

A description of the research program, the time required and estimated costs are included in the proposal. Should additional information be desired, please do not hesitate to contact Dr. Sankar at 404/894-3014 regarding technical matters or the undersigned at 404/894-4817 for administrative concerns.

In the event of an award, we propose that the work be authorized by a supplement to Grant No. NAG-3-768 drawn in the name of the GEORGIA TECH RESEARCH CORPORATION.

We appreciate the opportunity of submitting this proposal and look forward to working with you on this project.

Sincerely,

R. Dennis Farmer
Contracting Officer

RDF/pet
Addressee: Five (5) copies
Enclosure: Proposal - Five (5) copies
xc: Mr. Dennis L. Huff
Mail Stop 2770
NASA Lewis Research Center
Propeller Aerodynamics and Acoustics Technology

NUMERICAL STUDY OF EFFECTS OF SWEEP ON VISCOUS FLOW OVER WINGS

A Renewal Research Proposal
Submitted to

NASA LEWIS RESEARCH CENTER
CLEVELAND, OHIO

by

School of Aerospace Engineering
Georgia Institute of Technology
Atlanta, GA

September 1987

L. N. Sankar, Associate Professor
Principal Investigator
(404)-894-3014

W. M. Sangster, Dean
College of Engineering
(404)-894-3350

Robin B. Gray, Acting Director
School of Aerospace Engineering
(404)-894-3000

R. Dennis Farmer
Contracting Officer
(404)-894-4814

INTRODUCTION

During the period January 1- December 31, 1987, a research project titled "Studies of Unsteady Viscous Flows Using a Two-Equation Model of Turbulence" has been in progress at the School of Aerospace Engineering, Georgia Institute of Technology. This project is funded by NASA Lewis Research Center under the Grant NAG 3-768. The objective of the above research effort is to evaluate three popular turbulence models for their usefulness in predicting unsteady turbulent viscous flow past propfan and helicopter rotor blade sections, and steady/unsteady turbulent flow past airfoils with iced leading edge shape.

The first model studied is the Baldwin-Lomax two layer eddy viscosity model, patterned after the well-known Cebeci-Smith model [Ref. 1]. The second model is the Johnson-King model which requires the numerical solution of a first order ordinary differential equation for the mean turbulent kinetic energy levels within boundary layers and separated flows [Ref. 2]. Rather than coding the Johnson-King model independently, FORTRAN subroutines of the above model as implemented by Johnson and King was acquired from the above researchers and was modified for use in the Georgia Tech 2-D compressible Navier-Stokes solver(NSE2D) [Ref. 3], and the NASA Lewis version of the ARC2D code [Ref. 4].The third model considered is the k-ε model which requires the solution of two partial differential equations for the transport, production and depletion of turbulent kinetic energy k and turbulent energy dissipation rate ε. In the vicinity of the wall, a law of the wall formulation proposed by Gorski [Ref. 5] is used to avoid the need for very fine grid spacing in the inertial layer.This model was coded independently and was adapted into the NSE2D and ARC2D codes.

A number of calculations for clean and iced airfoil shapes have been carried out. Detailed surface pressure data and load data taken by McAlister et al [Ref. 6] for clean airfoils experiencing dynamic stall, and the experimental data obtained at the Ohio State University

by Bragg [Ref. 7] are being used to evaluate these models. The objective in this study is not to fine tune the parameters and empirical constants in these three models to improve correlation between the theory and experiments, but to evaluate how the above three models perform in their off-the-shelf form. A final report summarizing the findings of this research will be made available at the end of the current research period.

In this renewal proposal, it is proposed that the above research on unsteady and steady viscous flow past clean and iced airfoil configurations be extended to address three-dimensional flows. The separation and stall phenomena experienced by fixed and rotary wings at high angles of attack, or under leading edge icing conditions is strongly influenced by factors such as wing planform, airfoil camber, wing sweep, taper and twist. These parameters influence the spanwise pressure gradient and contribute to premature separation near wing tips. Even on fixed wings of rectangular planform, the stall pattern often does not resemble that predicted by 2-D analyses. There is a need for carefully designed experiments and 3-D analyses which will shed light on the stall characteristics of fixed and rotary wings with clean and iced leading edge shapes. The proposed research will address this need, at least in part, through 3-D Navier-Stokes calculations for a fixed wing with a simulated ice shape, for a wide range of Mach numbers and angles of attack.

Recently, Bragg [Ref. 8] has proposed a series of experiments featuring a fixed wing with a simulated leading edge ice shape. Configurations identical to those used in the experimental studies will be studied in the present research, for identical flow conditions, so that a well-coordinated theoretical and experimental approach will emerge for this interesting and important problem.

FEATURES OF THE SOLUTION PROCEDURE

A three-dimensional Navier-Stokes solver developed at Georgia Tech will be used to study the steady and unsteady, turbulent viscous

flow past wings with and without simulated ice shapes. This flow solver has in the past been used to study unsteady viscous and inviscid flow past a number of fixed and rotary wing configurations with success [Ref. 9-12]. Some of the special features of this solver are briefly listed here:

1) This solver can handle wings of arbitrary planform, taper, and twist. The airfoil coordinates may be arbitrary.

2) A hybrid implicit-explicit algorithm is used to advance the numerical solution in time. This solution procedure is highly stable, and may be used for a wide range of Reynolds number, Mach number and angle of attack conditions.

3) The calculations are done in a moving body-fitted coordinate system. A variety of configurations ranging from fixed wing to propfan blades may be solved using different versions of this solver.

4) This solution procedure has been vectorized for efficient solution on the CRAY XMP class of computers.

5) The Baldwin-Lomax turbulence model is presently available within the solver. However, because of the similarities between this solver and the 2-D Navier-Stokes solver, it should be a straightforward task to incorporate the Johnson-King model, or the k-ε model into this solver.

In Appendix A, a brief description of the governing equations, and the solution procedure are given. For the sake of simplicity, the appendix deals with numerical solution of the Euler equations. In Reference 12, modifications to this formulation to account for the viscous effects may be found.

PROPOSED RESEARCH

A one year research effort focusing on the performance characteristics of fixed wings with and without simulated ice shapes is proposed. Specifically, the following tasks will be carried out.

1) The 3-D Navier-Stokes solver, and the built-in grid generation scheme will be modified for analysis of the wing-alone configuration to be tested at the Ohio State University by Bragg and his co-workers [Ref. 8].

2) A series of calculations will be done for this wing at 0.15 freestream Mach number, at zero sweep for a wide range of angles of attack. The purpose of this series of calculations is to determine if the flow features over the wing (80% span and inboard) differs significantly from the 2-D flow characteristics.

3) Calculations will be carried out for the same wing-alone configuration, for two different sweep angles, for a range of angles of attack to be chosen in coordination with the researchers at NASA Lewis Research Center. The purpose of this phase of research is to study the effect of sweep angle on the stall characteristics of clean and iced wing configurations.

It is proposed that the above research work be carried out during the period January 1- December 31, 1988.

REFERENCES

1. Baldwin, B.S. and Lomax, H., "Thin Layer Approximation and Algebraic Model for Separated Turbulent Flows," AIAA Paper 78-257, January 1978.

2. Johnson, D.A. and King, L.S., "Transonic Separated Flow Predictions Based on a Mathematically Simple Nonequilibrium Turbulence Model," NASA TM 86826, October 1985.

3. Huff, D.L., Wu, Jiunn-chi and Sankar, L.N., "Analysis of Viscous Transonic Flow Over Airfoil Sections," AIAA Paper 87-0420.

4. Potapczuk, M.G. and Gerhart, P.M., "Progress in the Development of a Navier-Stokes Solver for Evaluation of Iced Airfoil Performance," AIAA Paper 85-0410.

5. Gorski, J.J. , "A New Near-Wall Formulation for the k-ε Equations of Turbulence," AIAA 24th Aerospace Sciences Meeting, Reno, Nevada, 1986.

6. McAlister, K., Pucci, S. L., McCroskey, W. J. and Carr, L. W., "An Experimental Study of Dynamic Stall of Advanced Airfoil Sections," NASA TM 84245, 1982.

7. Bragg, M. B., "An Experimental Study of the Aerodynamics of a NACA 0012 Airfoil With a Simulated Glaze Ice Accretion," NASA CR 179571, January 1987.

8. Bragg, M. B., "Two-Dimensional Experiments and Proposed Three-Dimensional Experiments," Airfoil Performance-in-Icing Workshop, NASA Lewis Research Center, August 12, 1987.

9. Sankar, L.N., Wake, B.E. and Lekoudis, S.G., "Solution of the Unsteady Euler Equations for Fixed and Rotary Wing Configurations," Journal of Aircraft, Vol. 23, April 1986, pp283-290.

10. Sankar, L.N., Malone, J.B. and Schuster, D., "Euler Solutions for Transonic Flow past a Fighter Wing," Journal of Aircraft, Vol. 24, No. 1, pp 10-16, January 1987.

11. Wake, B.E. and Sankar, L.N., "Solution of the Navier-Stokes Equations for Flow About a Rotor Blade," Proceedings of the American Helicopter Society National Specialists Meeting on Aerodynamics and Aeroacoustics, February 1987.

12. Wake, B.E., Sankar, L.N. and Ruo, S.Y., "An Efficient Procedure for the Numerical Solution of Three-Dimensional Viscous Flows," AIAA Paper 87-1159, Proceedings of the AIAA 8th Computational Fluid Dynamics Conference, June 1987.

NAG 3-768
Supplement #1

E-16-609
R6251-0AD/2

BUDGET
effective date: 1/1/87

SALARIES AND WAGES

Mr. Jiunn-Chi Wu, Graduate Research Assistant (January 1- March 31, 1988)	$3,000
Post-Doctoral Fellow (25% Time)	$6,250
FRINGE BENEFITS ON APPLICABLE SALARIES AND WAGES (27.6%)	$1,725
TRAVEL	$1,000
SUPPLIES	$ 500
TOTAL DIRECT COST	**$12,475**
OVERHEAD (60% OF DIRECT COST)	$ 7,485
TOTAL COST TO THE SPONSOR	**$19,960**

cc:

APPENDIX A

The three-dimensional unsteady Euler equations may be written in conservation form in the cartesian coordinate system as follows:

$$q_t + F_x + G_y + H_z = 0 \qquad (1)$$

where q is the flow properties vector {ρ, ρu, ρv, ρw, e}, and F, G, and H are the flux vectors along the x, y, and z directions respectively. For example, F is defined as

$$F = \begin{matrix} \rho u \\ \rho u^2 + p \\ \rho uv \\ \rho uw \\ u(e+p) \end{matrix} \qquad (2)$$

In the above equation set, ρ is the density; u, v, and w are the flow velocity components along the x, y, and z directions respectively. Also, e is the total energy per unit volume, and p is the pressure.

The Euler equations were solved in a body-fitted coordinate system (ξ, η, ζ, τ) obtained by first constructing a sheared parabolic coordinate system around the wing, and then clustering the C-lines at each span station so that the first C-line off the wing surface is at a constant distance of 0.01 chord from the surface. In this transformed plane, the governing equations become

$$q_\tau + F_\xi + G_\eta + H_\zeta = 0 \qquad (3)$$

The quantities q, F, G and H are related to the flow variables {q} and the flux vectors in the cartesian coordinate system through the metrics of transformation. For example,

$$\mathbf{q} = q/J$$

$$F = (\xi_t \, q + \xi_x \, F + \xi_y \, G + \xi_z \, H) \, / \, J \qquad (3a)$$

The quantity J is the Jacobian of transformation, and is given for the special case where y is only a function of η by

$$J = \eta_y \, (\xi_x \, \zeta_z - \xi_z \, \zeta_x) \qquad (3b)$$

The unknown in the above system of equations is the flow property vector q. The time derivative q was discretized using two point backward differences as $(\delta_\tau q)^{n+1}$. The spatial derivatives along the ξ- and the ζ- directions were discretized using the following formulas:

$$F_\xi = \delta_\xi \, F$$

$$H_\eta = \delta_\eta \, H \qquad (4)$$

where δ_ξ and δ_η are three-point central difference operators. The quantities F and H are nonlinear functions of **q** at the time level n+1. These functions were first linearized about the time level n. For example, F^{n+1} was written as follows:

$$F^{n+1} = F^n + [DF/Dq] \, (q^{n+1} - q^n) \qquad (5)$$

The spanwise derivative G_η was written as a combination of the n and n+1 time levels. During the odd time steps, calculations were done one span station at a time, from the wing root to the outboard span station, using the latest values of the flow vector at the (n+1) time level as soon as they are available. Thus, the quantity G_η was written at a typical node (i,j,k) as

$$(G_{j+1}{}^n - G_{j-1}{}^{n+1}) \, / \, 2$$

During the even time steps, the calculations started at the last span station outboard, and progressed till the root station was reached. Then, the term G_η was discretized as

$$(G_{j+1}{}^{n+1} - G_{j-1}{}^{n}) / 2$$

Since the above differencing uses a mixture of solution vectors at the n and the (n+1) time levels, the above procedure is called a hybrid scheme. It may show that the use of the values at the (n+1) time level as soon as they are available leads to a stable time marching scheme, from a von Neumann analysis. The reversal of the difference scheme in the spanwise direction from one time step to the next removes any dependence that the solution may have on the sweep direction.

The above approach has one disadvantage, however. The spanwise derivatives are no longer conservative with respect to time, although they are conservative with respect to space. This fact that the spanwise derivatives are non-conservative with respect to time is not expected to affect the solution accuracy since the streamwise and the normal derivatives are all conservatively differenced.

At each of the interior points in the above discretization, the following difference equation results for the quantity $(q^{n+1}-q^n)$:

$$[I+\Delta t\delta_\xi\{DF/Dq\}^n+\Delta t\delta_\zeta\{DH/Dq\}^n](q^{n+1}-q^n)=R \qquad (6)$$

where for the odd time steps, the residual R is given by

$$R = - \Delta t[\delta_\xi F^n+\delta_\zeta H^n+(G_{j+1}{}^n- G_{j-1}{}^{n+1})/2] \qquad (7)$$

and for the even even time steps, the residual is given by

$$R = -\Delta t [\delta_\xi F^n+\delta_\zeta H^n+(G_{j+1}{}^{n+1}- G_{j-1}{}^n)/2] \qquad (8)$$

If pure central differences are used to discretize the spatial derivatives, it may be shown that an odd-even decoupling of the solution will occur after only a few time steps. To prevent this, and in order to remove high frequency errors from the solution, the above finite difference equation was modified by adding a set of artificial dissipation terms to the residual R:

$$R_1 = -\Delta t \varepsilon_E [\delta_{\xi\xi\xi\xi} + \delta_{\eta\eta\eta\eta} + \delta_{\zeta\zeta\zeta\zeta}] J \mathbf{q}^n \qquad (9)$$

To the left-hand side operator of Eq. (6), the following implicit dissipation operators were added:

$$-\Delta t \varepsilon_I J^{-1} (\delta_{\xi\xi} + \delta_{\zeta\zeta}) J \qquad (10)$$

The constants ε_E and ε_I are user input coefficients. Typically these two coefficients were set equal to 1 and 3 respectively.

After the above dissipation terms were added, the left-hand side operator appearing in Eq. (6) was approximately factored into a product of two one-dimensional operators, resulting in the following equation:

$$[I + \Delta t \delta_\xi \{DF/D\mathbf{q}\}^n - \Delta t \varepsilon_I J^{-1} \delta_{\xi\xi} J] \times$$

$$[I + \Delta t \delta_\zeta \{DH/D\mathbf{q}\}^n - \Delta t \varepsilon_I J^{-1} \delta_{\zeta\zeta} J] (\mathbf{q}^{n+1} - \mathbf{q}^n) = R + R_1 \qquad (11)$$

This factored equation was solved using a series of block tridiagonal matrix inversions. The values of **q** at the computational boundaries were set to zero. The flow vector q at these boundaries was updated after the interior points were updated.

E-16-801

SIMULATION OF UNSTEADY ROTATIONAL FLOW OVER PROPFAN CONFIGURATION

NASA GRANT No. NAG 3-730

FINAL REPORT

for the period

JUNE 1986 - NOVEMBER 30, 1990

submitted to

NASA LEWIS RESEARCH CENTER

CLEVELAND, OHIO

Attn: Mr. G. L. Stefko

Project Monitor

Prepared by:

Rakesh Srivastava
Post Doctoral Fellow

L. N. Sankar
Associate Professor

School of Aerospace Engineering
Georgia Institute of Technology
Atlanta, Georgia 30332

INTRODUCTION

During the past decade, aircraft engine manufacturers and scientists at NASA have worked on extending the high propulsive efficiency of a classical propeller to higher cruise Mach numbers. The resulting configurations use highly swept twisted and very thin blades to delay the drag divergence Mach number. Unfortunately, these blades are also susceptible to aeroelastic instabilities. This was observed for some advanced propeller configurations in wind tunnel tests at NASA Lewis Research Center, where the blades fluttered at cruise speeds. To address this problem and to understand the flow phenomena and the solid fluid interaction involved, a research effort was initiated at Georgia Institute of Technology in 1986, under the support of the Structural Dynamics Branch of the NASA Lewis Research Center. The objectives of this study are:

a) Development of solution procedures and computer codes capable of predicting the aeroelastic characteristics of modern single and counter-rotation propellers,

b) Use of these solution procedures to understand physical phenomena such as stall flutter, transonic flutter and divergence

Towards this goal a two dimensional compressible Navier-Stokes solver and a three dimensional compressible Euler solver have been developed and documented in open literature.

The two dimensional unsteady, compressible Navier-Stokes solver developed at Georgia Institute of Technology has been used to study a two

dimensional propfan like airfoil operating in high speed transonic flow regime. A two degree of freedom structural model was coupled to study classical flutter and flutter dip phenomena observed at transonic Mach numbers. The Euler code solving three dimensional compressible Euler equations was used to predict the flow field around single and counter rotation advanced propellers. This solver has been applied for several flight conditions and both aerodynamic and aeroelastic analyses have been done.

These flow solvers have been validated through comparisons with measured data and documented in several publications (Refs. [1-5]), and have demonstrated the importance of accounting for the elastic characteristics of the structure while evaluating the aerodynamic characteristics of modern high speed propellers. Currently the solver is being modified to solve inviscid flow past ducted propellers.

SUMMARY OF PROGRESS

Two Dimensional Studies:

The two dimensional compressible Navier-Stokes solver has been used for numerical simulation of stall flutter and transonic flutter dip phenomena. For this purpose the aerodynamic solver was coupled to a two degree of freedom structural dynamics solver allowing the airfoil to rigidly pitch and plunge. The resulting solver was used to explore the stall flutter and classical flutter characteristics of several airfoils, through a simultaneous integration in time of the fluid solid dynamics equations. This solver has been shown to predict the onset of stall flutter. The results obtained have been summarized in Ref. [1]. The solver was also used to successfully predict the transonic flutter dip phenomena

and to study the effects of various parameters, such as thickness, shape and viscosity on the phenomena. These results have been summarized in Ref. [2] .

Three Dimensional Studies:

A three dimensional Euler solver developed at Georgia Institute of Technology for solving flow past isolated helicopter blades has been modified to solve the flowfield around advanced propeller configurations. The solver may be used to study steady or unsteady compressible flow past single and counter rotating propellers. In order to make the solver efficient, a hybrid scheme is used. The solver is second order accurate in space and first order accurate in time. The accuracy has been extended to fourth order using the compact (Pade) formulation along the streamwise direction.

The advanced propeller blades are somewhat flexible and under cruise conditions are highly loaded. This could lead to large structural deformations. These deformations could be critical to the performance of advanced propellers. In order to study the effect of deformation on the propeller aerodynamic performance characteristics, the solver was modified to be coupled in an open loop fashion with any structural solver.

The solver allows the flowfield to be divided into different relatively moving blocks. This considerably simplifies flow solutions around complex geometries, such as counter rotating propellers or ducted propellers. An effort is currently underway to update the solver for solving flow past ducted propellers. The formulation and results obtained for single and counter rotation propellers are documented in detail in the Ph. D. dissertation [3] of Dr. Rakesh Srivastava, which will be published as a NASA CR in 1991.

Single Rotation Propeller: The modified solver was applied for predicting the aerodynamic performance characteristics and blade loading of advanced geometries such as the SR-3 and the SR-7 propellers. To efficiently solve the flowfield around an advanced propeller, the solution domain was divided into several blocks. In the present study the number of blocks were kept the same as that of the number of blades. The Euler equations are solved in one block at a time, with the flow properties associated with the remaining blocks being stored in the solid state memory. The additional fluid block boundaries were updated by averaging the flow properties across the boundary. The boundary conditions also allow for axisymmetric and unsymmetric (unsteady) flight configurations. The results obtained show good comparison with experimental data [6,7] for spanwise and chordwise blade loading. It was also possible to properly and accurately capture the leading edge suction peaks. These results have been documented in detail in Ref. [3,4]. Because Ref.4 is not yet available in an archival form, a copy of Ref. [4] is included in the appendix.

Counter Rotation Propeller: As mentioned earlier the flow solver has been written in a fashion to treat a complex flowfield by dividing it into different possibly relatively moving blocks. This scheme was utilized here to obtain flow solutions around counter rotating propellers by dividing the solution domain into blocks associated with each of the blade rows. As the blades are rotating in opposite direction the grid blocks will also be rotating in opposite direction with one common interfacing surface. The Euler equations are solved in each of the blocks independently. The communication between the blocks is handled by averaging the flow properties across the interface boundary. Using the averaging procedure used in the present solver allows arbitrary time steps without requiring complex grid distortion techniques. The solver was used to

predict performance characteristics of a GE F7/A7 counter rotating propeller. The results obtained showed good comparison with experimental data [8]. The comparisons are not as good for lower advance ratio where the blades are loaded more heavily than higher advance ratios. Higher loading will lead to larger deformations under operating conditions. As the solver is purely aerodynamic, it was not possible to account for these deformations. The formulation of the solver and the results are documented in detail in Ref. [3].

Aeroelastic Effects: The solver has been also modified to allow the study of blade deflections and deformations under loading. However, the solver does not have the capability of solving structural equations. The effect of deformations on performance was studied by coupling the solver with NASTRAN in a loose open loop fashion. This requires interpolating the loads obtained from the aerodynamic solver grid onto the NASTRAN grid, and interpolating the deflections from the NASTRAN grid back onto the aerodynamic solver grid. First, a centrifugally deformed geometry was used to calculate aero loads on a SR-7 advanced propeller. These air loads were the used in NASTRAN to calculate a new deformed shape due to combined centrifugal and steady air loads. This deformed shape was then again used to obtain the updated air loads using the Euler solver. This study showed that as much as 40% change in performance can be expected once the blade deformations are taken into account. The formulation and the iteration process has been discussed in detail in Ref. [3] and has been documented in Ref. [5] and may be found in the appendix.

Ducted Propeller: Work is currently under way to modify the solver for solving the flowfield around ducted advanced propellers. Again the ability of the solver to divide the flow domain into different possibly relatively moving blocks is being used. In order to be able to resolve the suction peak of the cowl a wrap around C-O grid topology is being used. The grid topology around the blades is being retained as H-O. The grid block around the cowl will be stationary whereas the grid block around the blades will be rotating with the blades. The communication between the blocks would again be handled by averaging the flow properties across the block interface boundary. The coding modifications have been completed however, the code has not been applied and verified at the present time.

CONCLUDING REMARKS

A versatile two dimensional Navier-Stokes solver capable of carrying out stall flutter and classical flutter has been developed and verified. It has successfully predicted the onset of stall flutter and flutter dip phenomena for several airfoil cross sections operating in different speed regimes.

An efficient three dimensional Euler solver capable of obtaining flow solutions around advanced propeller geometries, such as single rotation counter rotation and ducted propellers, has been developed. The predicted spanwise and chordwise blade load distributions compare very well with experimental measurements. It has also been successfully coupled with the NASTRAN structural analysis program to study the effect of blade loading on the performance of advanced propellers.

REFERENCES

1. Wu, J. C., Kaza, K. R. V., and Sankar, L. N., "A Technique for Prediction of Airfoil Characteristics in Separated Flow," *Journal of Aircraft.* Vol. 26, No. 2, 1989, pp. 168-176.

2. Reddy, T. S. R., Srivastava R., Kaza, K. R. V., "The Effects of Rotational Flow, Viscosity, Thickness, and Shape on Transonic Flutter Dip Phenomena," AIAA Paper 88-2348, April 1988 (to appear in *Journal of Aircraft*).

3. Srivastava, R., "An Efficient Hybrid Scheme for the Solution of Rotational Flow Around Advanced Propellers," Ph. D. Dissertation, Georgia Institute of Technology, August 1990.

4. Srivastava, R., and Sankar, L. N., "An Efficient Hybrid Scheme for the Analysis of Counter Rotating Propellers," AIAA Paper 91-0703.

5. Srivastava, R., Sankar, L. N., Reddy, T. S. R., and Huff, D. L., "Application of an Efficient Hybrid Scheme for Aeroelastic Analysis of Advanced Propellers," AIAA Paper 90-0028, January 1990 (to appear in *Journal of Propulsion and Power*).

6. Roharbach, C., Metzger, F. B., Black, D. M., and Ladden, R. M., "Evaluation of Wind Tunnel Performance Testings of an Advanced 45^{o} Swept Eight-Bladed Propeller at Mach Numbers From 0.45 to 0.85," NASA CR-3505, 1982.

7. Bushnell, P., " Measurement of the Steady Pressure Distribution on a Single Rotation Large Scale Advanced Prop-Fan Blade at Mach Numbers From 0.03 to 0.78," NASA CR 182124, July 1988.

8. Jeraki, R. J., and Rose, G. E. "Effects of Mach Number, Loading, and Blade Angle on High-Speed Performance of the F7/A7 Highly Loaded Counterrotation Propeller," NASA TP 2927, 1991.

AIAA 91-0703
An Efficient Hybrid Scheme for the Analysis of Counter Rotating Propellers

R. Srivastava and L. N. Sankar
Georgia Institute of Technology
Atlanta, GA

29th Aerospace Sciences Meeting
January 7–10, 1991/Reno, Nevada

An Efficient Hybrid Scheme for the Analysis of Counter Rotating Propellers

R. Srivastava* Lakshmi N. Sankar†

Georgia Institute of Technology
Atlanta, Georgia 30332

Abstract

An efficient solution procedure has been developed for analyzing inviscid unsteady flow past counter rotating propellers. This scheme is first order accurate in time and second order accurate in space, and has been extended to fourth order accuracy in the axial direction. The solution procedure has been applied to a 2-bladed SR-7 single rotation propeller and to a GE F7/A7 counter rotation propeller. The pressure coefficients and the global quantities, power and thrust, show good comparison with experimental measurements.

Introduction

Modern high speed propellers are designed to delay the compressibility losses, and extend the high efficiency of a propeller to relatively high cruise Mach numbers. This is accomplished by sweeping the blade backwards and using thinner airfoils, on the outboard section of the blade. In addition low aspect ratio blades are used. This, combined with high tip Mach number, leads to high blade twist and high disk loading. The requirement of high disk loading further dictates a large number of blades per propeller. However, as the blades are very highly loaded, loss in efficiency due to swirl becomes important. By recovering the swirl losses, the efficiency can be further increased by 4% - 5%. This can be done either by using stationary guide vanes, as done in turbomachinery, or another set of blades rotating in opposite direction. The latter configuration of counter rotating blades is currently under study by industry.

Several numerical techniques varying in complexity from simple Goldstein type strip analysis to analyses that solve the Euler and Navier - Stokes equations references [1 - 10], have been applied to single-rotation propellers. Several researchers have extended these earlier works to counter rotation propellers. Celestina *et al.* [11] have solved the steady Euler equations around a counter rotating configuration by casting the equations in blade fixed coordinates, where the axisymmetric flow reduces to a steady flow problem. Whitfield *et al.* [9] solved the unsteady Euler equations around the counter rotating configuration using a finite volume scheme. The scheme was later modified in Ref. [12] to allow arbitrary time step. Kobayakawa and Nakao [13] have solved the flow field around a counter rotating propeller by recasting the unsteady Euler equations in a weak conservation form. These equations are discretized using finite difference formulas, then solved using an Alternating Direction Implicit (ADI) scheme.

Objectives

The primary objective of the present research is to develop a method for predicting the aeroelastic characteristics of a counter rotating propeller. The method developed has the capability to incorporate blade static deformation, rigid blade dynamics, and dynamic elastic deformations, as described in the first author's Ph. D. thesis [14]. As a first step towards using this solver to such aeroelastic applications, this method has been applied to the computation of the steady airloads and performance characteristics of the SR-3 and SR-7 single rotation propeller, and for the GE F7/A7 unducted counter rotating propeller.

Formulation

Solution Procedure:

The Euler equations, in conservation form, in a Cartesian coordinate system can be written as

$$(\hat{q})_t + (\hat{E})_x + (\hat{F})_y + (\hat{G})_z = 0 \qquad (1)$$

where $\hat{q}$ is the vector containing conserved flow properties. $\hat{E}$, $\hat{F}$ and $\hat{G}$ are the nonlinear flux vectors which

*Post-Doctoral Fellow, School of Aerospace Engineering. Member AIAA.

†Associate Professor, School of Aerospace Engineering. Member AIAA.

are functions of the vector $\hat{q}$, the subscripts denote the partial derivative of the vector. To simplify treatment of arbitrary geometries, the Euler equations in (1) are transformed and recast in a generalized coordinate system. The transformed equations are then solved using a semi-implicit hybrid algorithm similar to the scheme by Rizk and Chaussee [15]. In the present scheme, in order to decrease the computational time, flux terms in two directions (ξ, ζ), are treated implicitly while the radial direction (η) flux terms are treated semi-explicitly. The η derivative is obtained using the latest available values of the flow variables. This leads to a system of block pentadiagonal system of equations coupling the nonlinear fluxes $\hat{E}$ and $\hat{G}$. As in the Beam-Warming algorithm [16] these fluxes are linearized about their values at the previous time level, resulting in a block penta diagonal system of equations for the changes in the flow properties. This penta diagonal system is approximately factored into two block tridiagonal system of equations, and inverted using Thomas algorithm. Second or fourth order spatial accuracy in any one or more directions can be easily achieved.

This method requires only two inversions of the block tridiagonal matrix, in the two implicit directions. It also reduces the memory requirement as only two time levels of information needs to be stored at any given time, one of which needs to be only two dimensional. Using this technique the solver marches along the radial direction, solving the equations one radial plane at a time. The marching direction is reversed after every time step, in order to remove any dependency on the marching direction.

Because, two rows of blades in relative motion must be analyzed, the flow field is solved using multi block grid technique, with only one grid and its solution being in the core memory at any given time. The interface boundary points, and the adjoining nodes used to update them are always kept in the core memory. The interface boundaries are updated explicitly after all the interior points have been updated.

Initial and Boundary Conditions

The Euler equations are solved by marching in time. This requires an initial condition for the flow field. The initial conditions may be important to rate of convergence and, convergence itself. Hence, it is important to use a reasonable initial condition. An easily implemented initial condition used here is to set the whole flow field at its free stream value.

In the present analysis the flow variables at the boundaries are updated explicitly after the governing equations have been solved for the interior flow field. On the solid surfaces of blade and nacelle the no penetration condition is applied as:

$$\vec{V}_b . \vec{n} = 0 \tag{2}$$

Where $\vec{V}_b$ is the relative velocity vector between fluid and solid at the surface and $\vec{n}$ is the outward unit vector normal to the surface. The tangential velocity components are extrapolated from interior of the domain.

For steady state calculations all disturbances from the solid surface must propagate to infinity. On the subsonic inflow boundary, one characteristic should be allowed to escape. Hence, density is extrapolated and the three components of momentum, and energy are fixed at the free stream value. For a supersonic inflow boundary, all quantities are fixed to that of the free stream. At the subsonic outflow boundary, four characteristics should escape, thus four fluid properties are extrapolated from interior of the domain using the one dimensional characteristics approximation as discussed in Ref. [9]. The static pressure is obtained by solving the simple radial equilibrium equation [17].

$$\frac{\partial p}{\partial r} = \frac{\rho v_\theta^2}{r} \tag{3}$$

where, p is the pressure, ρ is the density, v_θ is the tangential velocity, and r is the radius.

For supersonic outflow, all characteristics should escape, hence all quantities are extrapolated from inside the flow domain.

Block Interface Boundary

It is neither efficient nor practical to solve all the blade passages simultaneously, hence, one blade passage is handled at a time. This introduces additional boundaries in the computation. Across these boundaries all the variables must be continuous, except on solid boundaries. The boundary condition, for these boundaries, depends on the type of flow being solved. Axisymmetry would require periodicity at the fluid block interface boundaries. Periodicity will require that the boundaries between the blade passages have the same fluid properties.

For an unsymmetric flow, the periodicity on these boundaries do not exist. Also in order to obtain the solution for such a problem, the flow field in all blade passages should be solved. This is done by advancing the solution of each block by one time step, one block at a time. In this case again the boundaries are updated explicitly, after the interior points have been updated. This is done by averaging the flow variables from the nodes on each side of the boundary from the adjoining blocks.

Row Interface Boundary

To simplify the solution procedure the domain of counter rotating blade is divided into two sets of blocks associated with each blade. This creates an additional fluid boundary. Proper handling of this boundary is critical as it is through this boundary each row of blades feels the presence of the other. As the rest of the boundaries, this boundary is also updated explicitly after the interior of the computational domain has been updated. The flow properties on this boundary is updated as the average of the values of adjacent constant axial planes. However as the two blocks are rotating in the opposite direction, the grid lines do not always align.

To carry out the averaging process the solution needs to be known for the 360° ring at the axial location adjacent to the row interface boundary. For an unsymmetric flow field (e. g. propeller at an angle of attack) this information is automatically available, as all the blade passages are solved. For an axial flight, where only one blade passage needs to be solved for each blade row, this information is obtained by imaging the block data to obtain flow properties for the 360° ring.

A schematic of the grid at the interface boundary for a constant η plane is shown in figure 1. The $I = IMAX$ plane for the front blade row, and $I = 1$ plane of the rear blade row form the interface boundary. The interface boundary of the rear blade row is updated first, one grid point at a time. In order to update the flow properties at the node B (refer to figure 1), the grid line AB is extended until it intersects the plane $I = IMAX - 1$ of the front row at point C. The flow properties are then obtained at point C by interpolating from the flow properties of the $IMAX - 1$ plane using a Lagrangian polynomial fit. The node B is then updated by taking the average of the values at node A and point C. This is repeated for all the nodes associated with $I = 1$ plane of the rear row.

Again, for an axisymmetric flow field this is done for only one block and the solution is imaged. For an unsymmetric flow field, the process is repeated for all the nodes for all the blade passages. The boundary $I = IMAX$ of the front row is then updated by simply interpolating flow variables from the boundary $I = 1$ of the rear row. The only requirement in this process, in order to minimize the error, is that the constant radial-surfaces from both the rows, at the interface boundary, be at the same radial distance.

Results and Discussion

Single-Rotation Propeller Studies

The hybrid numerical scheme discussed in the previous section was first applied to a single rotation propeller in [18] and has been validated for several flight conditions in [14]. In figure 2 the pressure coefficient for a two bladed SR7 propeller is compared with experimental data [19] for different span location, for free stream Mach number of 0.2, advance ratio of 0.883 and setting angle of 30.4°. These calculations were carried out using the fourth order scheme on a 100 x 22 x 35 grid, with 46 x 15 grid points on each of the blade surfaces. The effect of grid spacing in the normal direction is also shown in this figure. Three different normal spacings have been used, however, the number of grid points have been kept same. As can be seen, the smaller the normal spacing, the better is the comparison with experimental data, especially the suction peak. The comparison of pressure coefficients are good all along the span of the blade.

The error for larger normal spacing is greater for the inboard stations where the airfoil sections are thicker and the pressure suction peaks are higher. Using a second order accurate scheme leads to large wiggles near the leading edge [14]. This has been considerably reduced for the fourth order scheme. Increasing the accuracy to fourth order using the Pade approximation does not significantly increase the computer requirement. The only additional work required is to invert a tridiagonal matrix for each grid line in the direction of the higher accuracy, as discussed in Ref. [14].

A leading edge vortex exists for this flight condition, as can be observed from the plot of measured pressure coefficients. The vortex moves down the chord, and is near the midchord, near the tip region. As a leading edge vortex is a purely viscous phenomena, it may not be possible for an Euler analysis to properly capture it.

Counter Rotation Propeller Studies

The scheme has been applied here to a GE F7/A7 counter rotating propeller operating at a freestream Mach number of 0.71. This propeller has 8 blades in each blade row. Both the blade rows operate at the same advance ratio. The blade setting angles reported in experiments were 58.5° for the front blade row and 55.7° for the rear blade row. The setting angles were changed to 56.7° for the front row and 56.2° for the rear row, to match the power coefficient at the advance ratio of 3.0. These setting angles were then used for all other advance ratios. Again, as in the case of single rotation propeller, a body fitted H-O grid was used for calculating the flow field around the counter rotating

propeller. A wire frame gird is shown in figure 3. For the eight bladed GE F7/A7 propeller each blade row has 58 x 22 x 15 grid points for each blade passage with 25 x 15 grid points on each blade surface.

In general, in order to model the influence of adjacent blades (cascade effect) the entire propeller with all the blades (passages) need to be solved. However, for an axisymmetric flow field, with same number of blades in both the rows, considered here, all blade passages of one blade row can be assumed to be identical. Hence, only one blade passage, for each blade row, is solved enforcing the conditions of symmetry. Even though the flow field is axisymmetric, it is unsteady, being periodic through the blade passages for each row. Therefore, the power coefficient was monitored, rather than the residuals to determine the convergence of the solution. For the advance ratio of 3.0, the variation of power coefficient is plotted versus rotation angle of the front row of the blade in figure 4. As can be seen, after approximately two and a half revolutions the power coefficient has reached to a converged value.

The power coefficients and the thrust coefficients are compared with experimental data [20] in figures 5 through 7 and 8 through 10, respectively. The total power and thrust coefficients are overpredicted at the lower advance ratio, whereas they compare well with experiment for higher advance ratios. The individual blade row power coefficients, exhibit the same trend, whereas the thrust coefficient is consistently overpredicted for the front row. In figure 11 the variation of torque ratio, (aft rotor : front rotor), with advance ratio is compared. The torque ratio is well predicted for all advance ratios.

From these figures, it can be seen that the prediction of the global performance quantities compare well with experimental data. At the lower advance ratios, the blades are heavily loaded. This causes the blade to deflect more during operation. It is not possible to account for such deflections in a purely aerodynamic code. Also the Euler calculations tend to overpredict the shock strength, which will lead to higher wave drag. Furthermore, the present inviscid analysis cannot account for complex shock wave and boundary layer interaction, flow separation and leading edge vortices. Any or all of the above factors may have contributed to the overprediction of the performance parameters at the lower advance ratio.

In figures 12 through 15 the pressure and density are plotted at two constant radial locations, at the nacelle surface and near the midspan. The front rotor is rotating in a counter clockwise direction, and the aft rotor is rotating in the clockwise direction, as viewed from the front of the propeller (left side of the figure). The freestream is moving from left to right, with a relative Mach number of 0.71, and the advance ratio, for both the blade rows, is 3.0. The pressure and the density plots shown in these figures, show that the treatment of the interface boundary as discussed earlier does not introduce any significant error. In fact it is very difficult to locate the boundary from these figures. The interface boundary lies exactly halfway between the two blade rows. Furthermore, these figures also show that a strong shock exists on the suction surface of the front blade, at approximately midchord. This shock does not extend from blade to blade, and its strength reduces, away from the centerbody. The shock also moves downstream along the chord, and is almost at the trailing edge, near the midspan location. The aft blade does not have a strong shock. Our calculations also show that the total temperature rises in the rear row due to the work done by the front row on the fluid.

Concluding Remarks

A solution procedure for computing inviscid flow past single and counter rotation propellers has been developed. This procedure is computationally efficient, and may be used to study the aerodynamic performance characteristics of modern propellers.

The calculations also shows that a sufficiently fine grid must be used in the normal direction to capture the large suction peaks at the leading edge regions of propeller blades. The study of the counter rotation propeller showed that the present scheme of handling the row interface boundary allows arbitrary time step without requiring any complex interpolation or grid deformation technique. The error introduced does not seem to be significant. Furthermore, the global quantities, power and thrust, and their variation with advance ratio compares well with experimental measurement.

Computer Requirements:

All of the above computations were performed on the CRAY XMP24 computer available at NASA Lewis Research Center. For a grid size of 58 x 22 x 15, used for each block, the total memory and CPU time per time step required were 1.3 MW and 1.7 sec. respectively.

Acknowledgements

This work has been carried out under NASA grant NAG3-730 from NASA Lewis Research Center in Cleveland, Ohio. Mr. George L. Stefko is the grant monitor.

References

[1] Goldstein, S., "On the Vortex Theory of Screw Propellers," Royal Society Proceedings, Vol. 123, No. 792, Apr. 6, 1929, pp 440-465

[2] Sullivan, J. P., "The effect of Blade Sweep on Propeller Performance,"AIAA Paper 77-176, June 1977

[3] Egolf, T. A., Anderson, O. L., Edwards, D. E., and Landgrebe, A. J., "An Analysis for High Speed Propeller-Nacelle Aerodynamic Performance Prediction; Volume 1, Theory and Initial Application and Volume 2, User's Manual for the Computer Program," United Technologies Research Center, R79-912949-19, June 1979.

[4] Hanson, D. B., "Compressible Lifting Surface Theory for Propeller Performance Calculation," AIAA paper 82-0020.

[5] Williams, M. H., and Hwang, C., "Three Dimensional Unsteady Aerodynamics and Aeroelastic Response of Advanced Turboprops," AIAA Paper 86-0846.

[6] Jou, W. H., "Finite Volume Calculation of the Three - Dimensional Flow Around a Propeller," AIAA Paper 82-0957.

[7] Jameson, A., and Caughy, D. A., "A Finite Volume Method for Transonic Potential Flow Calculations," Proceedings Third AIAA Computational Fluid Dynamics Conference, Albuquerque, 1977.

[8] Chaussee, D. S., "Computation of Three-Dimensional Flow Through Prop Fans," Nielsen Engineering and Research Inc., NEAR TR-199, June 1979.

[9] Whitfield, D. L., Swafford, T. W., Janus, J. M., Mulac, R. A., Belk, D. M., "Three-Dimensional Unsteady Euler Solutions for Propfans and Counter-Rotating Propfans in Transonic Flow," AIAA Paper 87-1197, June 1987.

[10] Matsuo, Y., Arakawa, C., Saito, S., and Kobayashi, H., "Navier-Stokes Computations for Flowfield of an Advanced Turboprop," AIAA Paper 88-3094.

[11] Celestina, M. L., Mulac, R. A., Adamczyk, J. J., "A Numerical Simulation of the Inviscid Flow Through A Counter-Rotating Propeller", NASA TM-87200.

[12] Janus, J. M. and Whitfield, D. L., "Counterrotating Prop-Fan Simulations which Feature a Relative Multiblock Grid Decomposition Enabling Arbitrary Time Steps," AIAA Paper 90-0687, Jan. 1990.

[13] Kobayakawa, M. and Nakao, M., "Numerical Solutions for the Flowfield Around a Counter-Rotating Propeller," *Journal of Aircraft*, Vol. 26, No. 5, pp. 417-422, May 1989.

[14] Srivastava, R., "An Efficient Hybrid Scheme for the Solution of Rotational Flow Around Advanced Propellers," Ph. D. Thesis, Georgia Institute of Technology, 1990.

[15] Risk, Y. M. and Chaussee, D. S., "Three-Dimensional Viscous-Flow Computations Using a Directionally Hybrid Implicit-Explicit Procedure," AIAA paper 83-1910, 1983.

[16] Beam, R. M. and Warming, R. F., "An Implicit Factored Scheme for the Compressible Navier-Stokes Equations," *AIAA Journal*, Vol. 16 No. 4, 1978.

[17] Horlock, J. H., *Azial Flow Turbines - Fluid Mechanics and Thermodynamics*, Robert E. Krieger Publishing Company, Malabar, Florida, 1982, pp. 11-13, 148.

[18] Srivastava, R., Sankar, N. L., Reddy, T. S. R., Huff, D. L., "Application of an Efficient Hybrid Scheme for Aeroelastic Analysis of Advanced Propellers", AIAA Paper 90-0028, January 1990.

[19] Bushnell, P., "Measurement of the Steady Surface Pressure Distribution on a Single Rotation Large Scale Advanced Prop-Fan Blade at Mach Numbers from 0.03 to 0.78," NASA CR 182124, July 1988.

[20] Jeraki, R. J. and Rose, G. E., "Effects of Mach Number, Loading, and Blade Angle on High-Speed Performance of the F7/A7 Highly Loaded Counterrotation Propeller," NASA TP 2927, 1990.

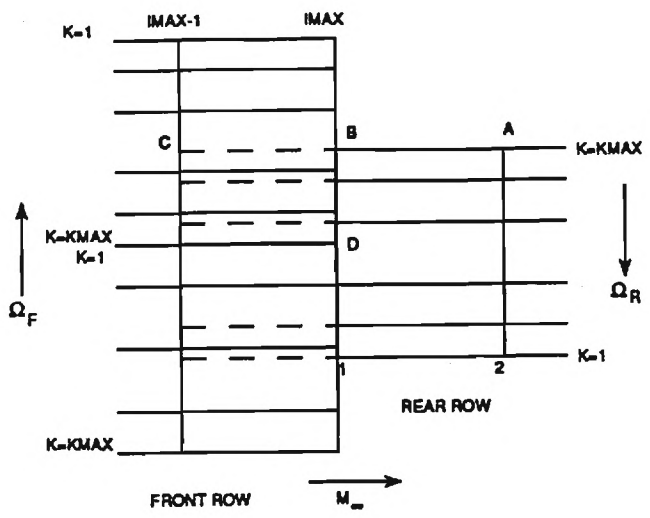

Figure 1: Row-Interface Boundary

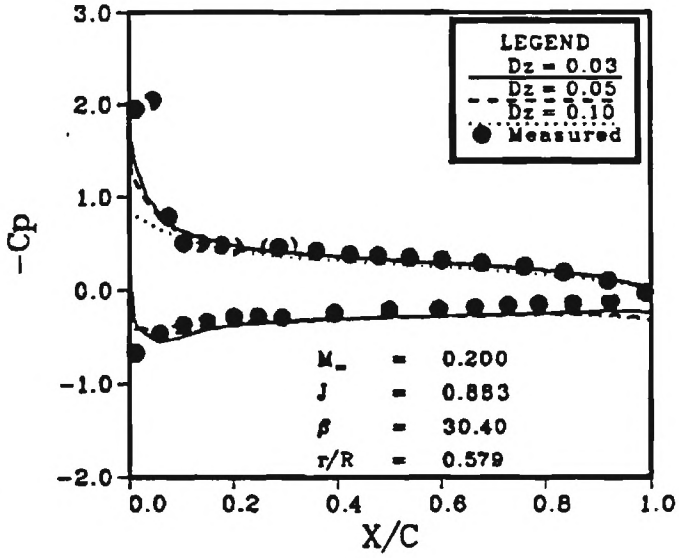

Figure 2: (Continued)

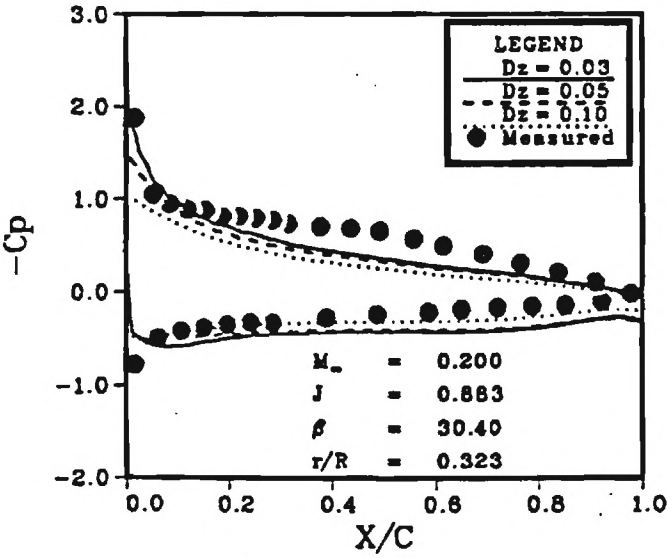

Figure 2: Comparison of Chordwise Variation of Pressure Coefficient at Constant Span Locations for SR7L 2-Bladed Propfan Operating at $M_\infty = 0.2$.

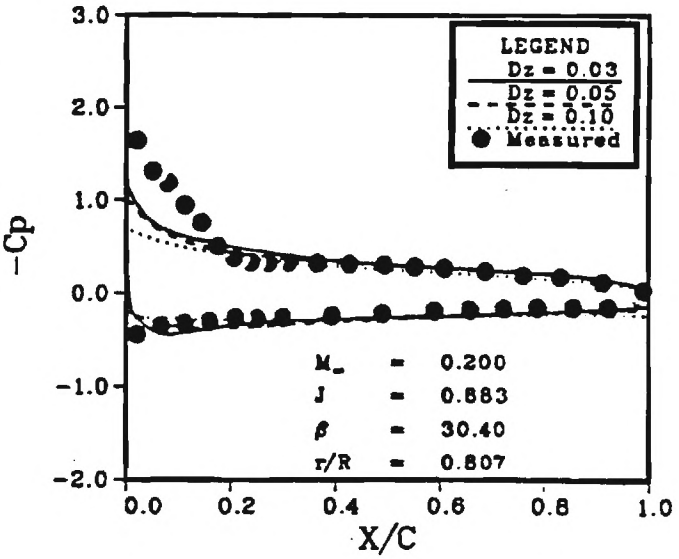

Figure 2: (Concluded)

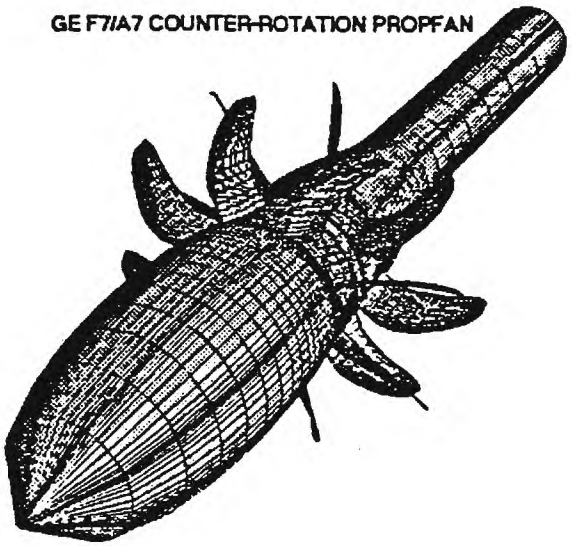

Figure 3: Wire Frame Grid

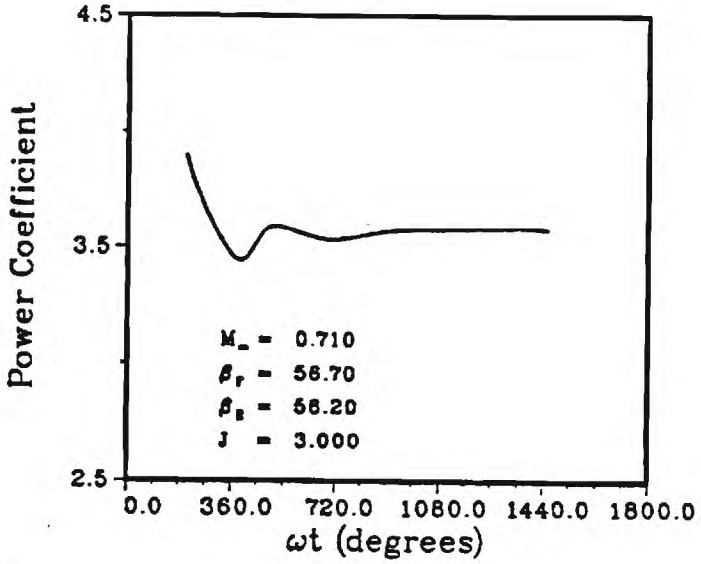

Figure 4: Power Coefficient Convergence Trend for GE F7/A7 Counter Rotation Propfan.

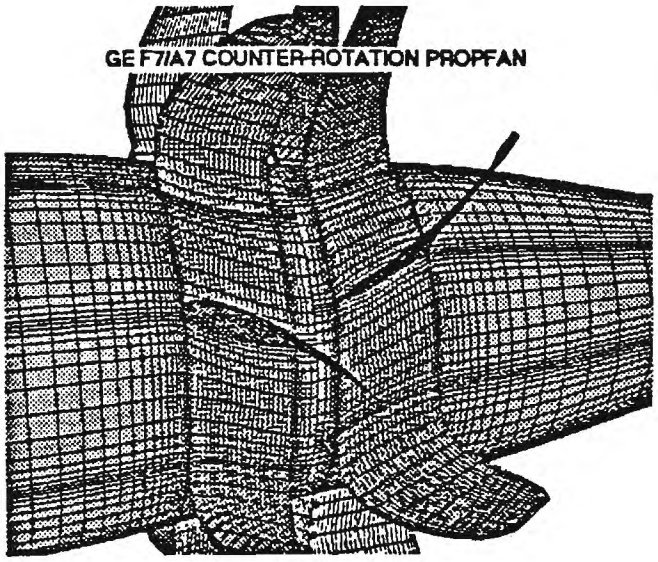

Figure 3: Concluded

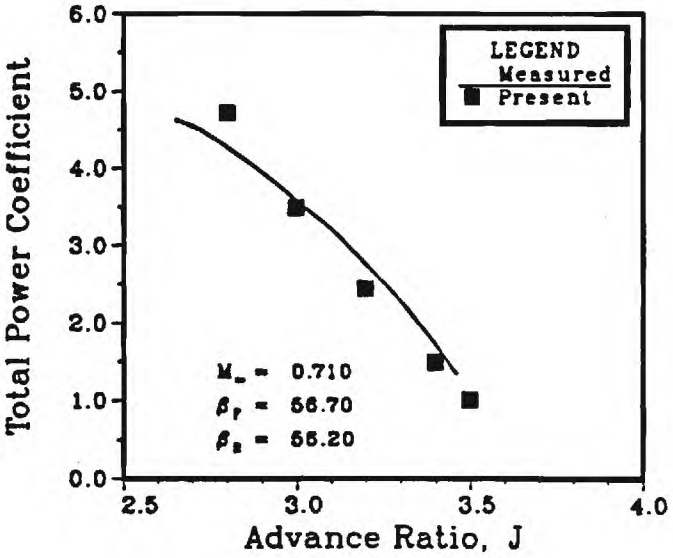

Figure 5: Comparison of Total Power Coefficient for GE F7/A7 Counter Rotation Propfan.

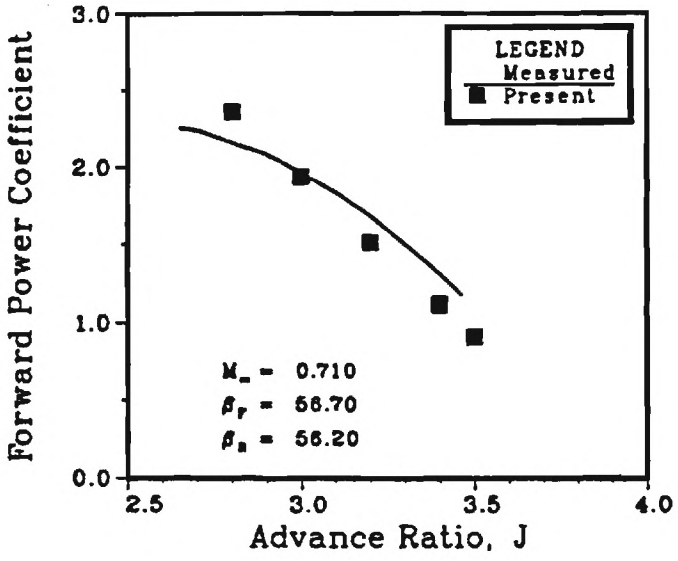

Figure 6: Comparison of Front Rotor Power Coefficient for GE F7/A7 Counter Rotation Propfan.

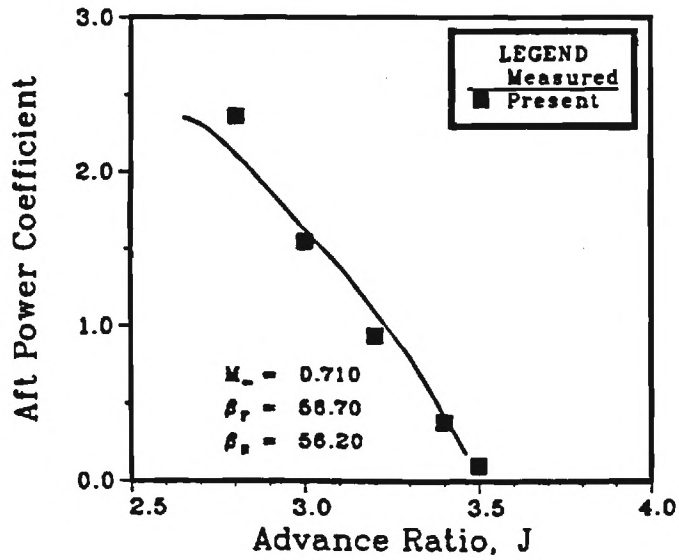

Figure 7: Comparison of Rear Rotor Power Coefficient for GE F7/A7 Counter Rotation Propfan.

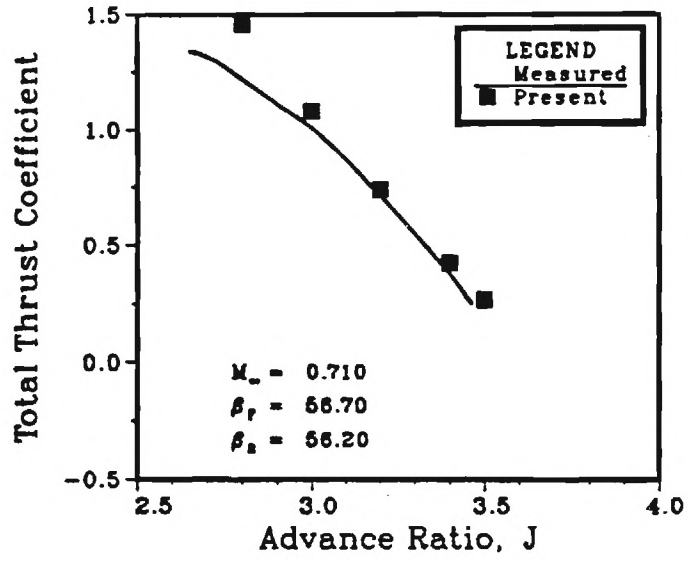

Figure 8: Comparison of Total Thrust Coefficient for GE F7/A7 Counter Rotation Propfan.

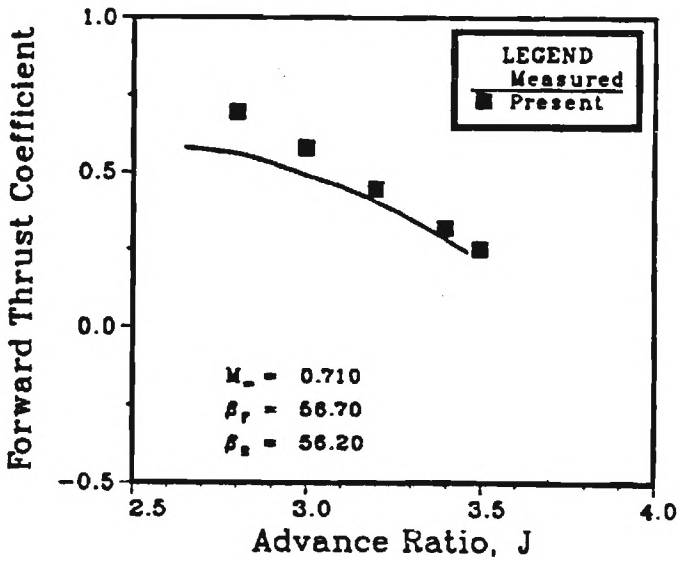

Figure 9: Comparison of Front Rotor Thrust Coefficient for GE F7/A7 Counter Rotation Propfan.

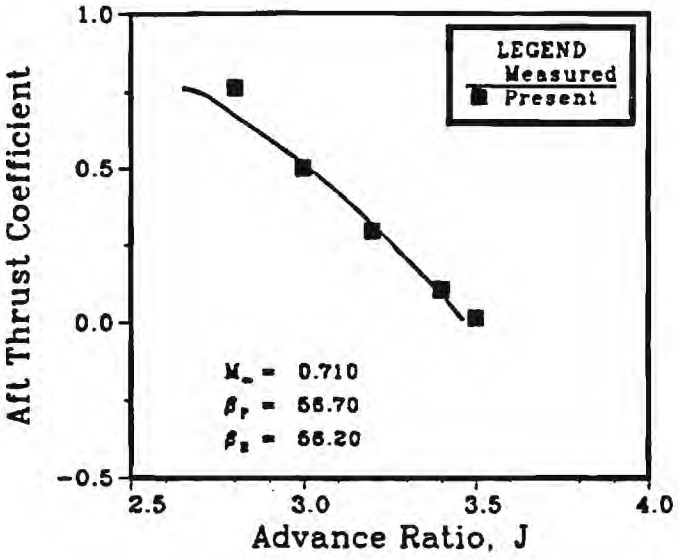

Figure 10: Comparison of Rear Rotor Thrust Coefficient for GE F7/A7 Counter Rotation Propfan.

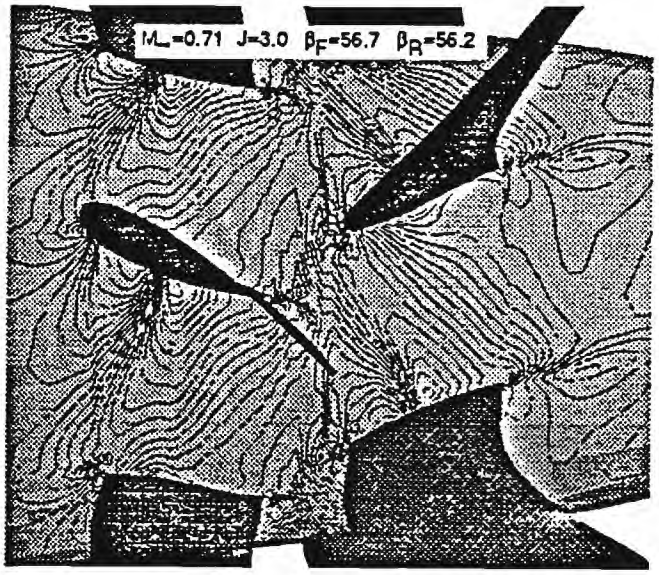

Figure 12: Density Contours at Constant η Plane on Nacelle for GE F7/A7 Counter Rotating Propfan.

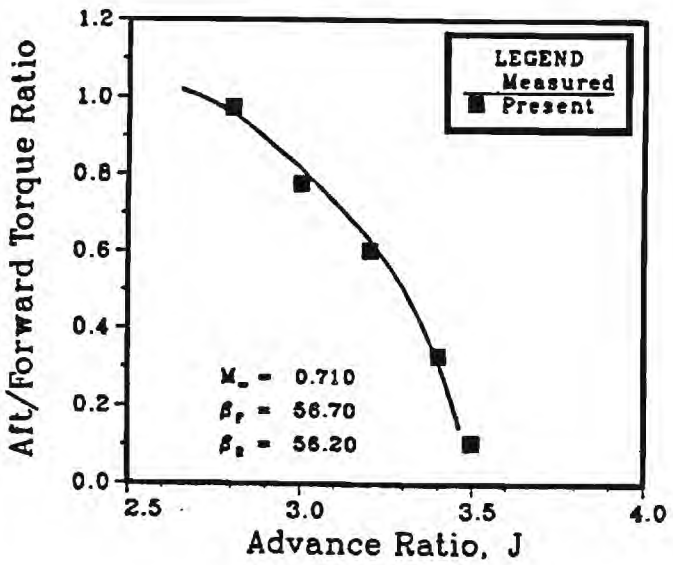

Figure 11: Comparison of Aft Rotor : Forward Rotor Torque Ratio for GE F7/A7 Counter Rotation Propfan.

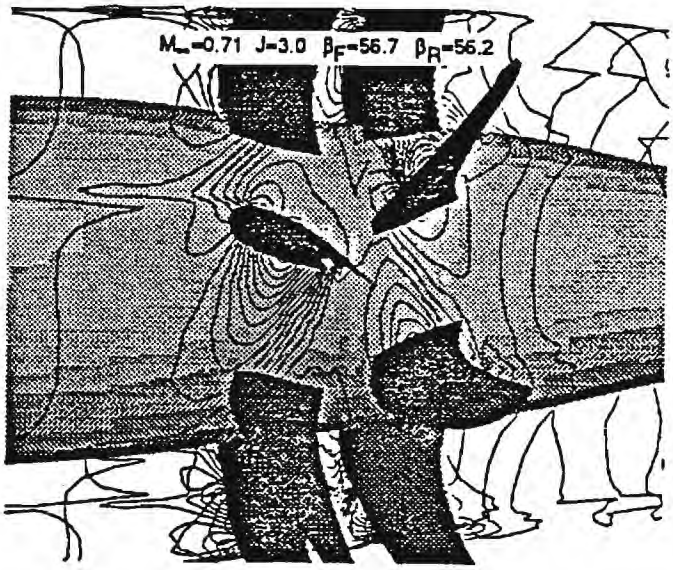

Figure 13: Density Contours at Constant η Plane Near Mid Span for GE F7/A7 Counter Rotating Propfan.

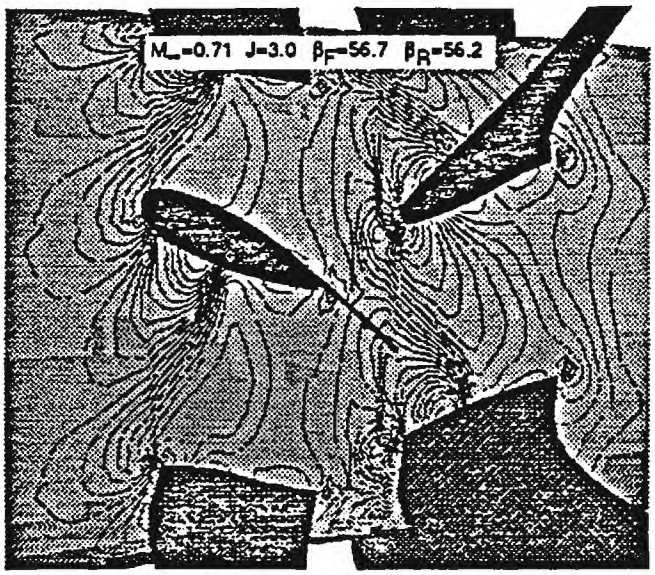

Figure 14: Pressure Contours at Constant η Plane on Nacelle for GE F7/A7 Counter Rotating Propfan.

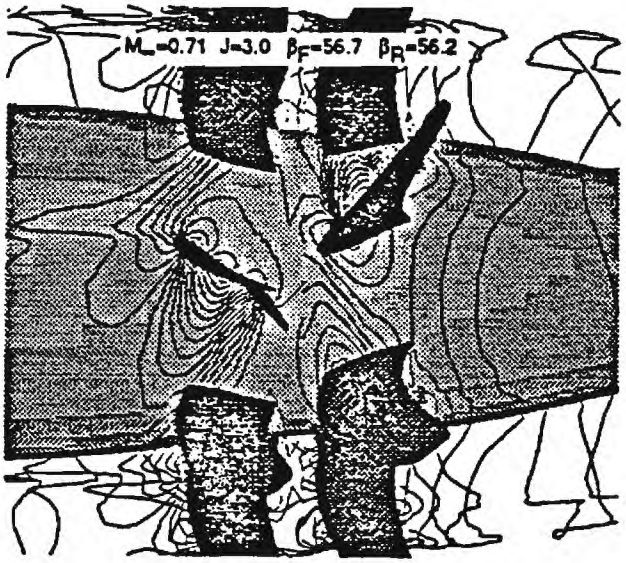

Figure 15: Pressure Contours at Constant η Plane Near Mid Span for GE F7/A7 Counter Rotating Propfan.

AIAA-90-0028

Application of an Efficient Hybrid Scheme for Aeroelastic Analysis of Advanced Propellers

R. Srivastava and N.L. Sankar, Georgia Institute of Technology, Atlanta, GA;
T.S.R. Reddy, The University of Toledo, Toledo, OH; and D.L. Huff, NASA Lewis Research Center, Cleveland, OH

28th Aerospace Sciences Meeting
January 8-11, 1990/Reno, Nevada

Application of an Efficient Hybrid Scheme for Aeroelastic Analysis of Advanced Propellers

R. Srivastava* and N.L. Sankar*
Georgia Institute of Technology
Atlanta, Georgia

T.S.R.Reddy†
The University of Toledo
Toledo, Ohio

and

D.L. Huff††
National Aeronautics and Space Administration
Lewis Research Center
Cleveland, Ohio

Abstract

An efficient three-dimensional hybrid scheme is applied for solving Euler equations to analyze advanced propellers. The scheme treats the spanwise direction semi explicitly and the other two directions implicitly, without affecting the accuracy, as compared to a fully implicit scheme. This leads to a reduction in computer time and memory requirement.

The calculated power coefficients for two advanced propellers, SR3 and SR7L, and various advance ratios showed good correlation with experiment. Spanwise distribution of elemental power coefficient and steady pressure coefficient differences also showed good agreement with experiment. A study of the effect of structural flexibility on the performance of the advanced propellers showed that structural deformation due to centrifugal and aero loading should be included for better correlation.

---

*Member AIAA and AHS.
†NASA Resident Research Associate at Lewis Research Center; member AIAA and AHS.
††Member AIAA.

Introduction

It has been known for some time now that the best propulsive efficiency is offered by propellers. However the efficiency drops off very rapidly as the cruise Mach number increases beyond 0.5, as high tip Mach numbers lead to high compressibility losses (due to wave drag). Currently an effort is underway to improve the propulsive efficiency of commercial and military aircraft. Newly designed high speed advanced propellers, also known as propfans, show a very high propulsive efficiency at cruise speeds upto Mach 0.8 [1].

The propfans are designed to delay the compressibility losses, thus extending the high efficiency of a propeller to relatively higher cruise Mach numbers. This is accomplished by sweeping the blade backwards and using thinner airfoils, on the outboard section of the blade. In addition low aspect ratio blades are used. This, combined with high tip Mach number, leads to high blade twist and high disk loading. The requirement of high disk loading further dictates a large number of blades per propeller, which must maintain structural integrity. However, these special features of the propfans lead to new problems.

One of the critical problems arises due to the fact that these blades are thin and hence moderately flexible. They are also highly swept near the tips, and hence are succeptible to transonic classical flutter or large amplitude oscillations. As concluded by Mehmed and Kaza [2], through wind tunnel tests of a propfan, there exists a strong aerodynamic coupling or cascade effect between blades. They also observed a classical bending - torsion unstalled flutter for a wide range of blade loading.

To understand and alleviate the problems associated with the propfan, the flow phenomena on the blades have to be accurately known. Also, in order to obtain the loads, an accurate prediction of pressure distribution on the blade is required. These could be obtained through experimental or numerical techniques. At the design stage experimental techniques are very expensive. Therefore, a need definitely exists to support the development of potentially high propulsive efficiency propfans through numerical techniques. With numerical techniques it is easier and cheaper to obtain pressure distribution, and flow details can easily be obtained at any point in the flow field.

The existing numerical methods vary in complexity from simple Goldstein type strip analysis to analyses that solve the Euler and Navier - Stokes equations. The strip theory based on Goldstein's work [3], assumes the flow to be inviscid and incompressible (hence irrotational). The propeller is modeled by a lifting line vortex and the wake is assumed to be composed of a rigid helical vortex sheet. In this analysis the propeller is restricted to having straight blades and no provision can be made for the nacelle, since the vortex wake extends to the axis. Sullivan [4] has improved on this method by using the curved lifting line concept to account for the sweep. In this approach the vortex wake is represented by a finite number of vortex filaments in place of the continuous sheet of vorticity as used in Goldstein's approach. The analysis has been further extended in reference [5] by placing the vortex filaments along the stream surfaces so that they conform to the shape of the axisymmetric nacelle.

Hanson [6] and Williams [7] applied the Kernel function approach to a propfan blade. They numerically solve a linear integral equation for upwash angle due to the blade pressure distribution by discretizing the load representation. The friction drag is obtained from the two- dimensional airfoil tables as a function of lift coefficient for the appropriate section camber, thickness and a Mach number adjusted for sweep and three-dimensional effects. The induced drag is obtained by determining the kinetic energy-per-unit-length of the far wake. The methods mentioned so far are based on linearized analyses. However, as the advanced propeller operates at or near transonic tip Mach number, flow nonlinearities may become important.

Jou [8] has applied the finite volume approach of Jameson [9] for the analysis of propfans using full potential equation. The formulation was not able to provide converged solutions for free stream Mach numbers greater than 0.6. It was concluded that strong rotational flow effects were present near the leading edge, which could not be modelled by the potential equation. In addition the potential flow equations at times, lead to non-unique solutions.

Chausee [10] and Whitfield *et al.* [11] have applied the unsteady, three dimensional Euler equations to the propfan geometry. Matsuo *et al.* [12] have recently solved the full Navier - Stokes equations around a propfan. Some of these methods have been reviewed in reference [13], with regards to performance prediction.

All the analyses mentioned so far, with the exception of Whitfield *et al.* [11] have been for axisymmetric flows. For a propfan in flight configuration, the flow is not axisymmetric. Even for cruise conditions the nacelle is at an angle of attack to the free stream, which destroys the axisymmetric nature of the flow. A true unsteady analysis would permit the analysis of the propfan in all flight configurations, including climb and descent. The propfan may also encounter off design conditions such as gusts or cross winds due to the disturbances in atmosphere. The cross winds could result in the propfan being exposed to the wake of the fuselage. The performance of the propfan due to gusts or fuselage wake may be very critical for the safety of the aircraft, and it should be possible to include them in the analysis.

The primary objective of the present research is to develop a method to solve unsteady Euler equations to predict flowfield around a propfan. The solution method should be able to solve the unsteady flow field around a propfan in non-axisymmetric flight condition, undergoing time dependent forcing function, unsteady blade vibratory motion etc. To accomplish this objective, a versatile body fitted grid is used. The blade motion is simulated by grid motion, allowing any time dependent blade motion. This will permit the calculation of both forced and free response due to any time dependent forcing function for a flexible blade. It also allows the governing equations to be cast in Cartesian coordinates, and yet be able to simulate a rotating blade. A Cartesian grid system simplifies the governing equations, as the Coriolis forces do not appear explicitly. This is true not only for a rotating blade but also for a blade undergoing time dependent arbitrary motion.

The governing equations in fully conservative form are discretized using second order accurate central differencing for the spatial derivatives and a first order upwind differencing for the temporal derivative, to obtain a set of algebraic equations. The Alternating Direction Implicit (ADI) scheme is used to solve the algebraic equations. The geometry of the propfan and the spanwise load distribution permits the grid to be at least an order of magnitude larger in the spanwise direction as compared to the other two directions. This allows the radial direction fluxes to be treated semi - explicitly, and the other two directions implicitly, without affecting the accuracy

significantly as compared to a fully implicit scheme. Treating one direction semi-explicitly requires only two costly inversions of block tridiagonal matrix, as opposed to three inversions for a fully implicit scheme, per time step. It also reduces the memory requirement as only two time levels of information needs to be stored at any given time, one of which needs to be only two dimensional. The use of such a hybrid scheme leading to reduction in computer time and memory requirement makes the scheme more efficient.

The specific objectives of the present paper are 1) to apply an efficient hybrid scheme to analyze advanced propellers, 2) to calculate steady performance, 3) to include structural deformation, due to centrifugal and steady aero loading in the analysis, 4) to study the effects of structural flexibility on the performance of advanced propellers. The governing equations and the numerical solution method are described first, followed by results and discussion. The methods developed here are expected to be helpful for future aeroelastic research.

Formulation

Aerodynamic Model:

The Euler equations, in conservation form and in Cartesian coordinates, can be written as:

$$(\hat{q})_t + (\hat{E})_x + (\hat{F})_y + (\hat{G})_z = 0 \tag{1}$$

where $\hat{q}$ is the vector containing conserved flow properties. $\hat{E}, \hat{F}$ and $\hat{G}$ are the nonlinear flux vectors which are functions of the vector $\hat{q}$. The subscripts denote the partial derivative of the vector. In the above equation

$$\hat{q} = \begin{pmatrix} \rho \\ \rho u \\ \rho v \\ \rho w \\ e \end{pmatrix} \qquad \hat{E} = \begin{pmatrix} \rho u \\ \rho u^2 + p \\ \rho uv \\ \rho uw \\ u(e + p) \end{pmatrix} \tag{2}$$

$$\hat{\mathbf{F}} = \begin{pmatrix} \rho v \\ \rho uv \\ \rho v^2 + p \\ \rho vw \\ v(e+p) \end{pmatrix} \qquad \hat{\mathbf{G}} = \begin{pmatrix} \rho w \\ \rho uw \\ \rho vw \\ \rho w^2 + p \\ w(e+p) \end{pmatrix}$$

where ρ is the fluid density, u, v, w are the inertial Cartesian components of the flow velocity, e is the total energy of the fluid per unit volume and p is the hydrodynamic pressure and may be expressed using the equation of state for perfect gas as:

$$p = (\gamma - 1)[e - \frac{1}{2}\rho(u^2 + v^2 + w^2)] \tag{3}$$

where γ is the ratio of specific heats. The advantage of using the conservation form is that it ensures the conservation of physical flux properties across discontinuities (e.g. shock) in the flow [14].

In order to analyze flow past an arbitrary geometry undergoing arbitrary motion, these equations need to be transformed and recast in a generalized coordinate system. The coordinates of the generalized system, have the following one to one relationship with the coordinates in the physical domain of interest :

$$\begin{aligned} \xi &= \xi(x, y, z, t) \\ \eta &= \eta(x, y, z, t) \\ \zeta &= \zeta(x, y, z, t) \\ \tau &= t \end{aligned} \tag{4}$$

These coordinates are non orthogonal and completely general. The equation (1) can be rewritten as:

$$\mathbf{q}_\tau + \mathbf{E}_\xi + \mathbf{F}_\eta + \mathbf{G}_\zeta = 0 \tag{5}$$

where

$$\mathbf{q} = J^{-1}\begin{pmatrix} \rho \\ \rho u \\ \rho v \\ \rho w \\ e \end{pmatrix} \qquad \mathbf{E} = J^{-1}\begin{pmatrix} \rho U \\ \rho u U + \xi_x p \\ \rho v U + \xi_y p \\ \rho w U + \xi_z p \\ (e+p)U - \xi_t p \end{pmatrix} \tag{6}$$

$$\mathbf{F} = J^{-1}\begin{pmatrix} \rho V \\ \rho u V + \eta_x p \\ \rho v V + \eta_y p \\ \rho w V + \eta_z p \\ (e+p)V - \eta_t p \end{pmatrix} \qquad \mathbf{G} = J^{-1}\begin{pmatrix} \rho W \\ \rho u W + \zeta_x p \\ \rho v W + \zeta_y p \\ \rho w W + \zeta_z p \\ (e+p)W - \zeta_t p \end{pmatrix}.$$

U, V, and W are the contravariant velocities, and J is the jacobian and ξ_x, η_x, ζ_x etc. are the metrics of transformation.

Initial and Boundary Conditions

A large number of problems can be described by the same set of governing equations. It is the proper application of the boundary condition that makes the solution unique to any given problem. Hence using proper and physically meaningful boundary conditions is as important as the correct governing equations.

The initial conditions may be critical to convergence of the numerical scheme. An intelligent guess of the initial conditions could help in achieving convergence faster. For these calculations the free stream conditions are used as the initial condition.

In the present analysis the flow variables at the boundaries are updated explicitly after the governing equations have been solved for the interior flow field. The following boundary conditions need to be addressed:

The blade and nacelle - surface boundary condition :

Physically, there can be no flow through or on a solid surface, hence the velocity on a solid surface must go to zero. The physical boundary condition of no slip can be ignored for the Euler equations. Thus the boundary condition on the blade and nacelle surfaces can be mathematically written as:

$$\vec{V_b}.\vec{n} = 0 \tag{7}$$

Where $\vec{V_b}$ is the velocity vector at the surface and $\vec{n}$ is the unit vector normal to the surface. The velocity vector $\vec{V_b}$,at any point (x, y, z) in the blade fixed coordinate can be given as

$$\vec{V_b} = (u - x_\tau)\hat{i} + (v - y_\tau)\hat{j} + (w - z_\tau)\hat{k} \tag{8}$$

Far-field conditions :

Since the propfan is operating in free air, the far field conditions should be the same as that of the free air. For steady state calculations all disturbances from the solid surface must propagate to infinity. On the subsonic inflow boundary, one characteristic should be allowed to escape hence ρ is extrapolated and the remaining variables $\rho u, \rho v, \rho w$ and e are fixed at the free stream value. For a supersonic inflow boundary, all quantities are fixed to that of the free stream,as disturbances cannot travel upstream in a supersonic flow. At the subsonic outflow boundary, four characteristics should escape, thus the four quantities $\rho, \rho u, \rho v, \rho w$ are extrapolated from inside while the pressure is fixed to that of the free stream. For supersonic outflow, all characteristics should escape, hence all quantities are extrapolated from inside the flow domain.

The block interface boundary :

It is neither efficient nor practical to solve all the blades at the same time, hence, one blade passage is handled at a time. This introduces additional boundaries for computation. Across these boundaries all the variables must be continuous, except on solid boundaries and boundaries downstream of the blade. The boundary condition, for these boundaries, depends on the type of flow being solved. An axisymmetric flow would require periodicity on the fluid interface boundaries. Periodicity will require that the two boundaries have same fluid properties. As shown in figure (1a), the fluid properties at the boundaries K=1 and K=KMAX are updated as the average of fluid properties at K=2 and K=KMAX-1 for a symmetric flow field.

For an unsymmetric flow, the periodicity on these boundaries does not exist. Therefore, in order to obtain the solution for such a case, the whole propfan should be solved. This is done by advancing the solution of each block one time step, one block at a time. In this case again the boundaries are updated explicitly, after the interior points have been updated.This is done by averaging the flow variables from the nodes on each side of the boundary from the adjoining blocks. Referring to figure (1b), (the subscripts refer to the corresponding block) the quantities at boundary K=KMAX of block N (which is also the boundary K=1 for block N+1) would be the average of flow quantities at K=KMAX-1 of block N and K=2 of block N+1. In doing so the latest available values at any given time are used.

Solution Procedure:

The descretized forms of the governing equations described earlier, are solved using a hybrid scheme, described in next section. The algebraic equations are approximately factorized and solved using the ADI scheme. An implicit method is more demanding as far as coding is concerned. However it allows larger time steps to be taken as opposed to the explicit schemes.

Time integration is carried out using the first order accurate Euler implicit rule

$$q^{n+1} = q^n + \Delta\tau \frac{\partial q^{n+1}}{\partial \tau} \tag{9}$$

where the superscript n denotes the current time level, at which the flow variables are known, and $n+1$ the next or unknown time level. Even though this is a first order accurate scheme, satisfactory time accuracy is obtained because a relatively small time step is required to maintain numerical stability.

Substituting the Euler equations (5) in (9) we get

$$q^{n+1} = q^n - \Delta\tau \left(E_\xi + F_\eta + G_\zeta\right)^{n+1} \tag{10}$$

The partial derivatives E_ξ, F_η, G_ζ are obtained using the standard second order accurate central differences.

The hybrid scheme:

In order to decrease the computational time, flux terms in two directions (ξ, ζ), are treated implicitly while the radial direction (η) flux terms are treated semi-explicitly. The η derivative is obtained using the latest available values of the flow variables. This method requires only two costly inversions of the block tridiagonal matrix, in the two implicit directions. Rizk and Chausee [15] first used this hybrid scheme with the Beam and Warming algorithm. Using this technique the solver marches along the η direction, solving the equations one η plane at a time. The marching direction is reversed after every sweep, in order to remove any dependency on the marching direction. Equation (10) can then be rewritten as :

$$q^{n+1} = q^n - \Delta\tau \left(E_\xi^{n+1} + F_\eta^{n,n+1} + G_\zeta^{n+1}\right) \tag{11}$$

Since the η marching direction is changed every iteration, the $F_\eta^{n,n+1}$ alternates between

$$\frac{F^n_{i,j+1,k} - F^{n+1}_{i,j-1,k}}{2\Delta\eta}$$

during the odd time steps, and

$$\frac{\mathbf{F}^{n+1}_{i,j+1,k} - \mathbf{F}^{n}_{i,j-1,k}}{2\Delta\eta}$$

during the even time steps.

The above discretization leads to a set of algebraic equations for $\mathbf{q}$. These equations are costly to solve since the flux vectors $\mathbf{E}$ and $\mathbf{G}$ are highly nonlinear. The nonlinearity is removed by linearising the fluxes about the previous time step value, resulting in the following linear equation :

$$\left[I + \Delta\tau\left(\delta_\xi A^n + \delta_\zeta B^n\right)\right]\mathbf{q}^{n+1} = \left[I + \Delta\tau\left(\delta_\xi A^n + \delta_\zeta B^n\right)\right]\mathbf{q}^{n} + \mathbf{R}^{n,n+1} \tag{12}$$

where

$$\mathbf{R}^{n,n+1} = -\Delta\tau\left(\delta_\xi \mathbf{E}^n + \delta_\eta \mathbf{F}^{n,n+1} + \delta_\zeta \mathbf{G}^n\right) \tag{13}$$

and the operator notation $\delta_\xi(A\mathbf{q}) = [\delta_\xi A]\mathbf{q}$ and $\delta_\zeta(B\mathbf{q}) = [\delta_\zeta B]\mathbf{q}$ is used.

This Euler equation formulation can be very easily extended to solve the Navier-Stokes equations by simply adding the viscous terms to the right hand side. This does not alter the numerical formulation.

Now defining $\Delta\mathbf{q}^{n+1} = \mathbf{q}^{n+1} - \mathbf{q}^n$, we can rewrite the equation (12) as

$$\left[I + \Delta\tau\left(\delta_\xi A^n + \delta_\zeta B^n\right)\right]\Delta\mathbf{q}^{n+1} = \mathbf{R}^{n,n+1} \tag{14}$$

Only two levels of storage, $\mathbf{q}$ and $\Delta\mathbf{q}$, are required, and since one direction is treated explicitly, the $\Delta\mathbf{q}$ array and the residual array $\mathbf{R}^{n,n+1}$ need to be only two dimensional. It is also possible to store $\Delta\mathbf{q}$ and $\mathbf{R}^{n,n+1}$ in the same memory locations, further reducing the memory requirements.

Even though the governing equation has been linearized, equation (14) is still very difficult to solve, as the matrix operator on the left hand side is very large and very sparse. However the matrix operator can be approximately factorized as

$$[I + \Delta\tau\,(\delta_\xi A + \delta_\zeta B)] = [I + \Delta\tau\delta_\xi A]\,[I + \Delta\tau\delta_\zeta B] + \bigcirc\left(\Delta\tau^2\right) \tag{15}$$

This factorization does not affect the temporal accuracy. Equation (14) can then be written as

$$[I + \Delta\tau\delta_\xi A^n]\,[I + \Delta\tau\delta_\zeta B^n]\left\{\Delta\mathbf{q}^{n+1}\right\} = \mathbf{R}^{n,n+1} \tag{16}$$

or defining

$$\Delta\mathbf{q}^{*n+1} = [I + \Delta\tau\delta_\zeta B^n]\,\Delta\mathbf{q}^{n+1} \tag{17}$$

we get the following system of equation:

$$[I + \Delta\tau\delta_\xi A^n]\,\Delta\mathbf{q}^{*n+1} = \mathbf{R}^{n,n+1} \tag{18}$$

$$[I + \Delta\tau\delta_\zeta B^n]\,\Delta\mathbf{q}^{n+1} = \Delta\mathbf{q}^{*n+1} \tag{19}$$

These equations can be easily solved for $\Delta\hat{\mathbf{q}}^{n+1}$ by performing two successive block tridiagonal inversions. Since the ξ and ζ directions are uncoupled, the two inversions are performed first with a ξ sweep and then with a ζ-sweep, thus the name 'Alternating Direction'. These inversions are performed at each spanwise station, marching along the spanwise direction. As mentioned earlier, the marching direction is reversed every iteration. Each element of the block tridiagonal matrix has 5×5 elements.

Artificial Dissipation:

The use of central difference, makes the scheme mildly unstable, and also introduces odd even decoupling. This is remedied by adding artificial dissipation. The implementation of artificial dissipation, in the present work is based on the formulation of Jameson et al. [16]. This scheme has a second order implicit dissipation and a blend of second/ fourth difference explicit dissipation terms. A scaling factor for both

implicit and explicit dissipation is employed to control the amount of dissipation in the scheme. Adding the dissipation terms, equations (18) and (19) can be written as:

$$\left[I + \Delta\tau\left(\delta_\xi A^n + \epsilon_I D_{I_\xi}\right)\right]\Delta\mathbf{q}^{*n+1} = \mathbf{R}^{n,n+1} - \epsilon_E D_E \Delta\tau \tag{20}$$

$$\left[I + \Delta\tau\left(\delta_\zeta B^n + \epsilon_I D_{I_\zeta}\right)\right]\Delta\mathbf{q}^{n+1} = \Delta\mathbf{q}^{*n+1} \tag{21}$$

where D_{I_ξ} and D_{I_ζ} are second order implicit dissipation terms and D_E is the explicit dissipation term, given in reference [22]. ϵ_I and ϵ_E are user supplied constants, which depend on grid spacing. At the boundaries the fourth order differences are repalced by second order differences.

Aeroelastic Model:

As mentioned earlier, the propfan has thin, swept, and twisted blades. Since the blades are thin and flexible, deflections due to centrifugal and steady aero loads are large. Hence, the aeroelastic problem is inherently nonlinear, requiring geometric nonlinear theory of elasticity [17].

The blades have large sweep and twist, which couples blade bending and torsional motions. They behave like plate-like structures because of the low aspect ratio. These factors require a finite element structural model which accounts for centrifugal softening and stiffening effects and, possibly, Coriolis effects. It has been found that the Coriolis effects are negligible for thin blades [18]. The centrifugal terms are important because of large blade sweep and flexibility. By assuming a rigid hub, the blades are structurally decoupled from one another. Consequently, it is sufficient to structurally model just one blade. Then, the governing aeroelastic equation can be written as

$$\{[\mathrm{K}(\Omega)_s] + [\mathrm{K}(u)]\}\{u\} = \{\mathrm{P}(u)\} \tag{22}$$

where $[\mathrm{K}(\Omega)_s]$ is the centrifugal softening matrix, which is a function of the rotational speed, Ω, $[\mathrm{K}(u)]$ is the nonlinear stiffness matrix which is a function of the

nodal displacements, $\{u\}$ represents the blade deflections at the finite element nodes, and $\{P(u)\}$ is the equivalent aerodynamic force vector.

In the present paper, the geometric nonlinear analysis was perfomed using the MSC/NASTRAN [19], in which the geometric nonlinear analysis is identified by " solution 64". The Solution 64 uses a modified Newton-Raphson algorithm, along with load updating to simulate the correct displacement-load relationship. It has the capability to update the displacement dependent centrifuga forces. The solution sequence is controlled through "subcases" or iterations with a minimum of two being required. The first subcase computes the initial, linear deflected shape. Subsequent subcases, then use the previously deflected shape to compute the differential stiffness matrix along with the new set of displacements [20].

The iterative method of solving equation (23) is shown in figure (2). Basically, a centrifugally deformed geometry is used to calculate steady aero loads with the Euler solver described in the previous section. These aero loads are then used to calculate a new deformed shape due to combined centrifugal and steady aero loads. The process, steps 4-6, is repeated until a converged, deformed geometry is obtained i.e., until the change in deflection from the $(i+1)^{th}$ iteration is equal to that from the i^{th} iteration.

Results and Discussion

The hybrid numerical scheme discussed in the previous section, was first applied to an isolated aircraft wing in reference [21] and to a helicopter rotor blade in reference [22]. Typical results showing blade loading, are reproduced in figures (3) and (4). As can be seen from both these figures, the hybrid scheme is able to predict flow phenomena of varying complexity with fairly good degree of accuracy.

The propfan blade has a much more complex shape than the aircraft wing or the helicopter blade. The high twist, large sweep, low aspect ratio, close proximity of other blades, presence of nacelle and thinner blades near the tip, make the flow field around it very complex. In the following, the flow solutions obtained for two advanced propellers, namely SR3 and SR7L, are presented. The calculations have been

performed on a 'hot shape', obtained by including the deflections due to centrifugal loading in the undeflected blade shape ('cold shape').

A body fitted H-O grid was used for these calculations. A typical grid used in the calculation is shown in figure (5). The domain of calculation was taken to be the region between two blades with upper surface of one blade and lower surface of the adjoining blade as the boundaries of the domain. This region is referred to as blade passage. In general, in order to model the influence of adjacent blades (cascade effect) the entire propfan with all the blades (passages) are solved. However, for an axisymmetric flow field, considered here, all blade passages can be assumed to be identical, and only one blade passage is solved enforcing the conditions of symmetry.

SR3 Propfan

The hybrid scheme, described earlier, was used to solve the flow field around an 8-bladed SR3 propfan. The SR3 propfan was designed to operate at a free stream Mach number of 0.8, advance ratio of of 3.06, at an altitude of 30,000 feet. Experimental data has been reported in [23], and the results obtained from the present analysis are compared in figures (6) and (7).

Figure (6) shows a comparison of the power coefficient of the propfan as a function of the advance ratio, with experimental [23] data. It also shows the comparison with other published numerical results [11, 12]. As can be seen the comparison with experiment is good, however the power coefficients are consistently overpredicted. The results compare well with other published results, as well. As shown in reference [23] the power coefficients are quite sensitive to the blade setting angle, however an accurate measure of the blade setting angle, β, is difficult. Also, since the blades are thin and somewhat flexible, they are susceptible to deformations under loading during operation. These deformations result in a modified twist distribution on the blade. Also, the viscous effects are not included in the present analysis. Any or all of these phenomena could contribute to the overprediction of the power coefficient.

The variation of elemental power coefficient with radial location is plotted and compared with experimental results in figure (7). In order to obtain a more meaningful comparison, the flight conditions were modified slightly in the numerical calculation, so as to match the experimental power coefficient. The power coefficient measured in experiment was 1.385 for a free stream Mach number of 0.8, β setting angle of 60.7 deg and the advance ratio of 3.002. The calculations were carried out with the free stream Mach number of 0.8, the setting angle of 58.5 deg and the advance ratio of 3.002 to obtain the same power coefficient. As can be seen a fairly good correlation is obtained, however, the elemental power is underpredicted for the inboard stations and overpredicted for the outboard stations. This is because the effect of the tip vortex is not properly accounted for. In these calculations no wake modelling is included, also the grid is not fine enough to properly capture the strength of the tip vortex. Capturing a weaker tip vortex results in smaller downwash velocity near the tip region, thus resulting in an over prediction ob blade loading near the tip. As the total power is matched with the experiment, an overprediction in the tip region results in an under prediction on the inboard region.

SR7L Propfan

The SR7L propfan has been designed for an operating free stream Mach number of 0.8, rotational speed of 1700 rpm, at an altitude of 35,000 feet. In this section calculations for a two bladed SR7L propfan are presented. The aerodynamic calculations are first performed on the 'hot shape'. The effect of blade flexibility is then included in the calculations.

In figure (8) the elemental pressure coefficient difference is compared with experiment for a 2-bladed SR7L propfan. The blade was operating at a free stream Mach number of 0.775 and advance ratio of 3.088. The 75% span setting angle was adjusted to match the power coefficient by a rigid body rotation of the blade about the pitch change axis. The pressure coefficient difference ΔC_p ($C_{p_l} - C_{p_u}$) is plotted and compared against experimental data [27] at various span locations. The comparison is good, except near the leading edge on the outboard stations.

The effect of blade flexibility on performance was studied next for the SR7L propfan blade. The effect of flexibility is included by the aeroelastic iteration process, described earlier and shown in figure (2).

It is important that the blade finite element model accurately reflects its structural characteristics, since the entire analysis process is centered around the stiffness matrix. The NASTRAN finite element model used in this study is based on the final blade design [24]. The SR7L blade has an aluminum spar, nickel sheath, and fiber glass shell with foam fill. The shell, adhesive, spar, and shell filler material were combined using the Composite Blade Structural Analysis (COBSTRAN) program to produce equivalent, monolithic shell elements [25]. The finite element model of the SR7L blade is shown in figure (9a). The model has 261 nodes and 449 triangular shell elements. Bar elements are used to model the shank. Multipoint constraint grid chords are used to define the shank/blade interface [26].

The validity of the above finite element blade model has been shown in reference [20]. Frequencies and corresponding mode shapes were calculated over a range of speeds for a blade setting angle of 58 degrees and compared with those of Ref.[24]. For the sake of completeness, the calculated frequencies and the experimental values are reproduced in figure (9b). The model showed good agreement at the first, third and fourth modes. The calculated second mode is much stiffer. This is a edgewise mode, which is the most sensitive mode to the support stiffness used in the finite element model. This mode is very difficult to model accurately [20], over a range of speeds because of nonlinear rotational effects. However, generally good agreement with the other modes implies an accurate determination of the blade's stiffness matrix, validating its use to calculate steady state deflections.

The aero loads obtained from the Euler solver are transferred to the NASTRAN grid for structural deformation calculations. The loads required as inputs to NASTRAN are the pressure differences at the centroids of the triangular element. As the

two grids are not identical, an interpolation of the data was required. A spline interpolation was used to obtain the loads at the centroids of the elements. The deflections obtained from NASTRAN, under these loads, are then used to define the new blade shape. The loads are then recalculated for this new blade shape, and the process is repeated till convergence. The effect of the aeroelastic iteration on the calculation is shown in figures (10) through (14).

Figure (10) shows the 75% span twist or blade setting angle versus the iteration. The effect of centrifugal loads is seen as a change in the blade setting angle from iteration 0 to iteration 1. It shows that the centrifugal loads reduce the blade setting angle. This seems to be the largest effect on blade shape. Adding the deflections from centrifugal loads, to the blade shape gives the blade shape known as 'hot shape'. The loads obtained from this shape are then again used to obtain the new deflected shape. This iteration has been continued till the change in power coefficient is minimal. It shows that four iterations are sufficient for convergence to the final blade shape.

In figure (11) the thrust coefficient is plotted against the power coefficient for subsequent iterations. The setting angle used in the calculations has been obtained by rigid body rotation of the hot shape so as to match the power coefficient obtained by experiments. The experimental point is also plotted. The power coefficient obtained from the hot shape (marked 1), compares well with the experiment. However, the power coefficient changes considerably (marked 2 to 4), as the blade is allowed to deform under this load. It can be seen from figures (10) and (11), that the initial change in shape, lead to large change in power coefficient. For this particular case, under which the blades are loaded heavily almost 40% change in power coefficient is observed when the effect of aerodynamic loading is included in the blade shape. The subsequent changes are not as large. Hence, in order to obtain a better comparison with experimental power coefficient and load distribution on blade, the blade setting angle should be chosen such that the converged shape power coefficient is compared against the experimental data. This requires some trial and error in selecting the 'cold' or 'hot' shape from which the aeroelastic iteration should be started. Arriving

at the final blade shape might be critical for vibration and flutter calculations, as well.

In figure(12) the relative change in twist angle over the span is plotted. This shows that the largest deflection occurs near the tip, with practically no deflection on the root sections. Also it should be noted that the variation in the blade twist is nonlinear and is largest near the tip. A rigid body rotation of the blade to account for the change in twist, would result in a linear variation along the span. This clearly shows that better performance calculations structural flexibility should be included in the analysis.

Figure (13) shows the in-plane deflection of the blade planform and figure (14) shows the out of plane deflection of the blade at constant chord. Again, the largest deflection is towards the tip, with practically no deflection towards the root. Figure (12) through (14) show clearly, that rigidly rotating the blade to match the power coefficient, does not simulate the correct blade shape. Also, as seen from figure (11) for highly loaded blades, these small differences might change the loading considerably.

Computer Requirements:

All of the above computations were performed on the CRAY XMP24 computer available at NASA Lewis Research Center. For a grid size of 70 x 35 x 27, the total memory and CPU time per time step required were 1.8 MW and 2.4 sec. respectively. The NASTRAN run required 100 cpu sec for 261 nodes, for each structural integration.

Concluding Remarks

This study showed that the hybrid scheme can be applied successfully to a propfan configuration (low aspect ratio, highly swept and very thin blades). In the numerical scheme described, the unsteady, time averaged Euler equations are solved in a fully conservative form. In the hybrid scheme two directions are treated implicitly and the spanwise direction is treated semi-explicitly. This reduces the computer time as only two costly inversions of the block tridiagonal matrix are required, corresponding to

the two directions that are treated implicitly. It also reduces the computer memory requirement, as only one level of information need to be stored at any given time, thus making it a more efficient scheme.

From the present study following conclusions are drawn:

1. The calculated power coefficient for SR3 showed good correlation with experiment

2. The elemental power coefficient variation with radius compared well with experiment

3. The pressure coefficient difference for SR7L agreed well with measured values

4. The effect of aero loads was to compensate for the untwisting due to centrifugal loads

Acknowledgements

The authors wish to acknowledge Dr. Richard August of Sverdrup Technology Inc., Cleveland, OH, for many helpful suggestions. This work has been carried out under NASA grant NAG3-730 from NASA Lewis Research Center in Cleveland, Ohio, Mr. George L. Stefko, grant monitor.

References

[1] Whitlow, J. B., Jr. and Sievers, G. K.," Fuel Savings Potential of the NASA ATP," NASA TM 83736, 1984.

[2] Mehmed, O. and Kaza, K. R. V., " Experimental Classical Flutter Results of a Composite Advanced Turboprop Model," NASA TM-88792

[3] Goldstein, S.," On the Vortex Theory of Screw Propellers," Royal Society Proceedings, Vol. 123, No. 792, Apr. 6, 1929, pp 440-465

[4] Sullivan, J. P.," The effect of Blade Sweep on Propeller Performance,"AIAA Paper 77-176, June 1977

[5] Egolf, T. A., Anderson, O. L., Edwards, D. E., and Landgrebe, A. J.," An Analysis for High Speed Propeller-Nacelle Aerodynamic Performance Prediction; Volume 1, Theory and Initial Application and Volume 2, User's Manual for the Computer Program," United Technologies Research Center, R79-912949-19, June 1979.

[6] Hanson, D. B.," Compressible Lifting Surface Theory for Propeller Performance Calculation," AIAA paper 82-0020.

[7] Williams, M. H., and Hwang, C.," Three Dimensional Unsteady Aerodynamics and Aeroelastic Response of Advanced Turboprops," AIAA Paper 86-0846.

[8] Jou, W. H.," Finite Volume Calculation of the Three - Dimensional Flow Around a Propeller," AIAA Paper 82-0957.

[9] Jameson, A., and Caughy, D. A., " A Finite Volume Method for Transonic Potential Flow Calculations," Proceedings Third AIAA Computational Fluid Dynamics Conference, Albuquerque, 1977.

[10] Chausee, D. S.," Computation of Three-Dimensional Flow Through Prop Fans," Nielsen Engineering and Research Inc., NEAR TR-199, June 1979.

[11] Whitfeild, D. L., Swafford, T. W., Janus, J. M., Mulac, R. A., Belk, D. M., "Three-Dimensional Unsteady Euler Solutions for Propfans and Counter-Rotating Propfans in Transonic Flow," AIAA Paper 87-1197, June 1987.

[12] Matsuo, Y., Arakawa, C., Saito, S., and Kobayashi, H., "Navier-Stokes Computations for Flowfield of an Advanced Turboprop," AIAA Paper 88-3094.

[13] Bober, L. A., Mitchell, G. A.," Summary of Advanced Methods for Predicting High Speed Propeller Performance," NASA TM 81409, 1980.

[14] Lax, P. D., "Weak Solutions of Nonlinear Hyperbolic Equations and their Numerical Computation," *Communications in Pure and Applied Mathematics*, Vol. 7, pp. 159-193.

[15] Rizk, Y. M. and Chaussee, D. S., "Three-Dimensional Viscous-Flow Computations Using a Directionally Hybrid Implicit-Explicit Procedure," AIAA paper 83-1910, 1983.

[16] Jameson, A., Schimdt, W. and Turkel, E., "Numerical Solutions of the Euler Equations by Finite Volume Methods Using Runge-Kutta Time-Stepping Schemes," AIAA Paper 81-1259, 1981.

[17] Kaza, K. R. V., et al.,"Analytical Flutter Investigation of a Composite Propfan Model," Journal of Aircraft, Vol. 26, No. 8, pp 772-780, August 1989.

[18] Subrahmanyan, K. B., Kaza, K. R. V., Brown, G. V., and Lawrence, C.," Nonlinear Bending-Torsional Vibration and Stability of Rotating, Pretwisted, Preconed Blades Including Coriolis Effects," NASA TM 87207, 1986.

[19] "The NASTRAN Theoretical Manual," NASA SP 221(06), 1981.

[20] August, R., and Kaza, K. R. V.," Vibration, Performance and Flutter Response Characteristics of a Large-Scale Propfan and its Aeroelastic Model," AIAA Paper 88-3155, 24^{th} Joint Propulsion Conference, Boston, Massachusetts, July 11-13, 1988.

[21] Ruo, S. Y., and Sankar, L. N., "Euler Calculations for Wing-Alone Configuration," *Journal of Aircraft*, Vol. 25, No. 5, pp 436-441, May 1988.

[22] Wake, B. E., and Sankar, L. N., "Solutions of the Navier-Stokes Equations for the Flow about a Rotor Blade," *Journal of the American Helicopter Society*, Vol. 34, No. 2, pp 13-23, April 1989.

[23] Rohrbach, C., Metzger, F. B., Black, D. M., and Ladden, R. M., "Evaluation of Wind Tunnel Performance Testings of an Advanced 45° Swept Eight-Bladed Propeller at Mach Numbers From 0.45 to 0.85," NASA CR-3505, 1982.

[24] Sullivan, W. E., Turnberg, J. E., and Violette, J. A.," Large Scale Advanced Propfan (LAP) Blade Design," NASA CR 174790.

[25] Aiello, R. A., and Chi, S.," Advanced Composite Turboprops: Modeling, Structural and Dynamic Analyses," ASME Paper 87-GT-78, 1987.

[26] Chou, S., "SR7L Turboprop Blade Finite Element Model," Sverdrup Topical Report, March 1986.

[27] Bushnell, P.," Measurement of the Steady Surface Pressure Distribution on a Single Rotation Large Scale Advanced Numbers from 0.03 to 0.78," NASA CR 182124, July 1988.

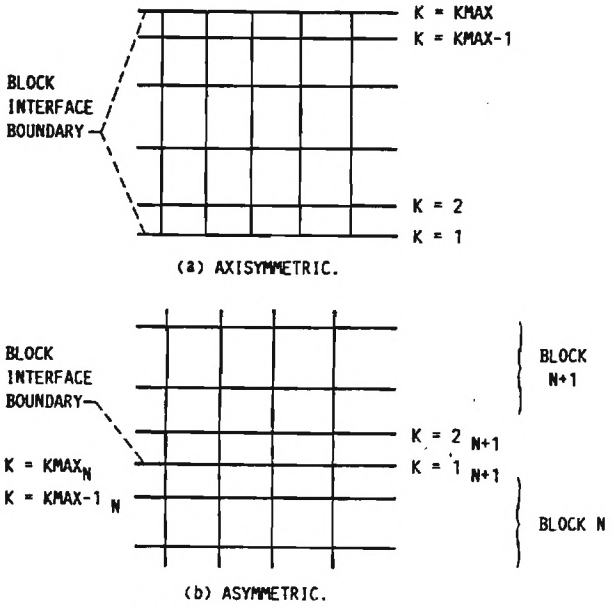

FIG. 1. BLOCK-INTERFACE BOUNDARIES.

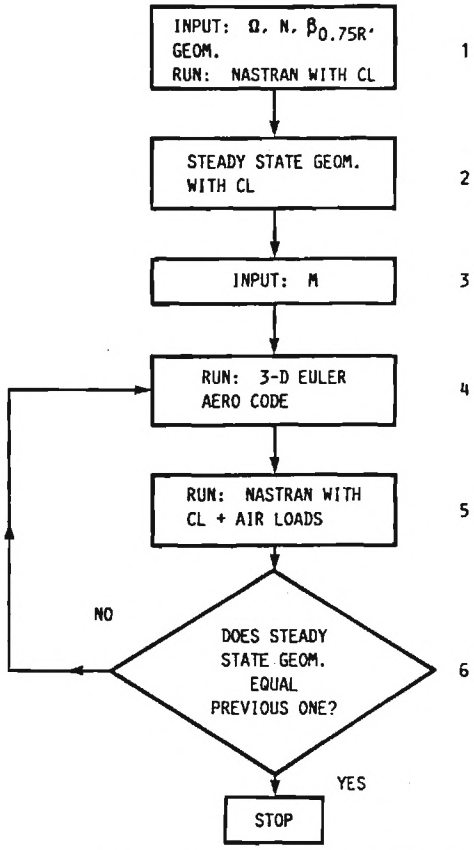

FIG. 2. FLOW CHART OF THE AEROELASTIC ANALYSIS.

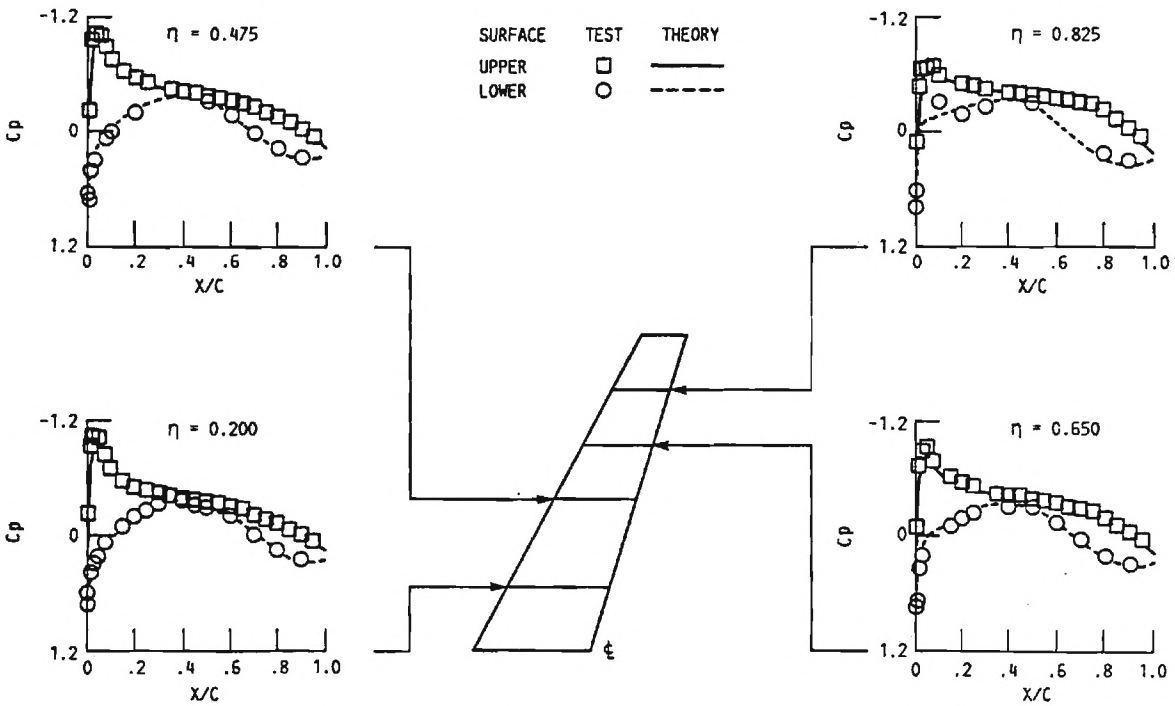

FIG. 3. EULER CALCULATIONS FOR A WING (REF. 20), $M_\infty = 0.62$; $\alpha_0 = 0.58^\circ$.

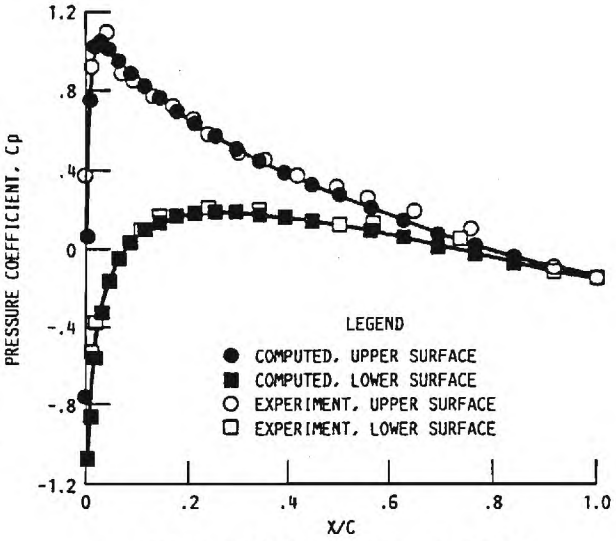

(a) PRESSURE DISTRIBUTION. y/R = 0.800.

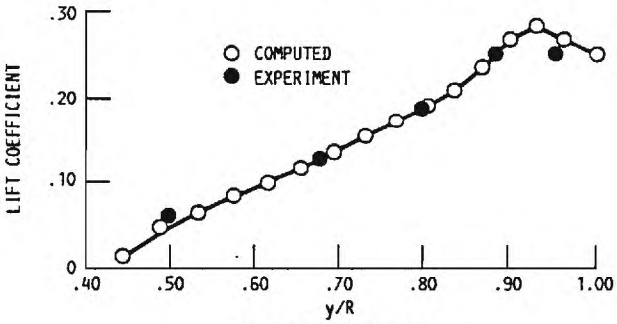

(b) LIFT DISTRIBUTION.

FIG. 4. DISTRIBUTION COEFFICIENTS FOR NACA 0012 ROTOR BLADE (FROM REF. 21).

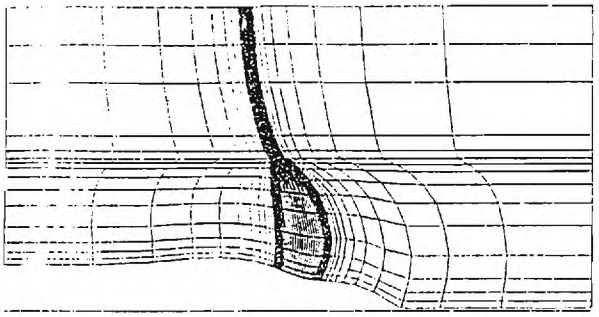

(a) H-GRID IN STREAMWISE PLANE. I = 1 TO 60; J = 1 TO 16; K = 1 TO 1.

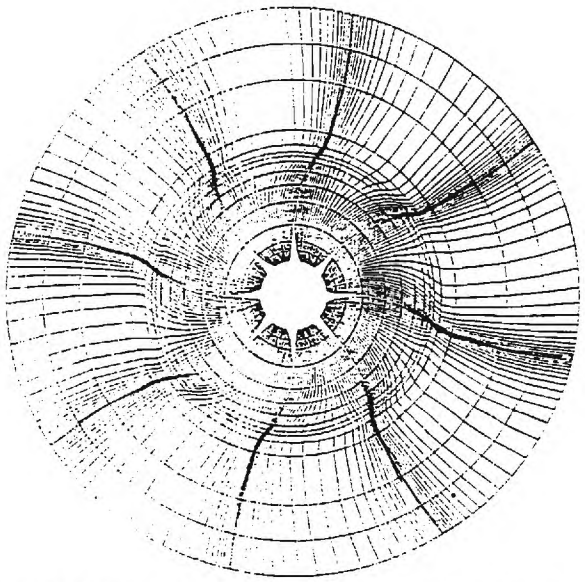

(b) O-GRID IN AZIMUTHAL PLANE. I = 30 TO 30; J = 1 TO 16; K = 1 TO 29.

FIG. 5. GRIDS.

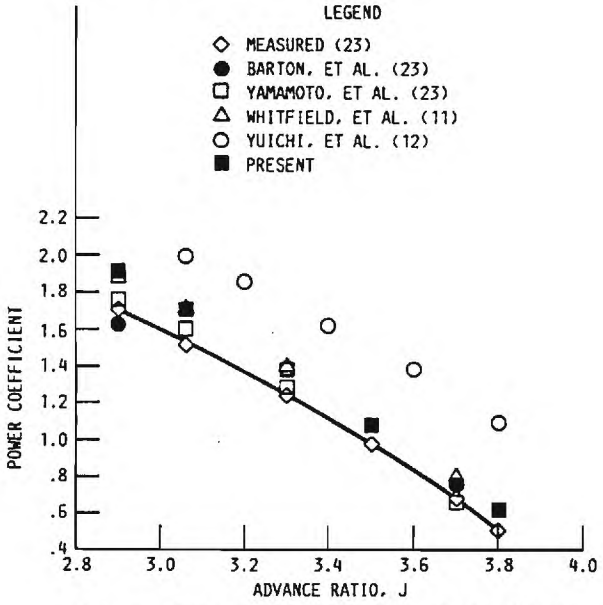

FIG. 6. POWER COEFFICIENT VERSUS ADVANCE RATIO FOR SR-3, 8-BLADED PROPFAN. M_∞ = 0.8.

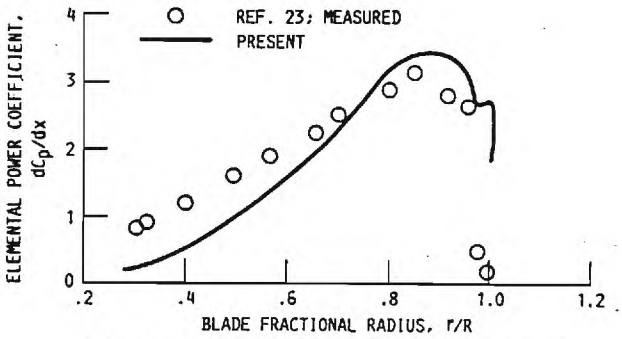

FIG. 7. ELEMENTAL POWER COEFFICIENT VERSUS RADIUS FOR SR-3, 8-BLADED PROPFAN. J = 3.002; M_∞ = 0.8; β = 60.5.

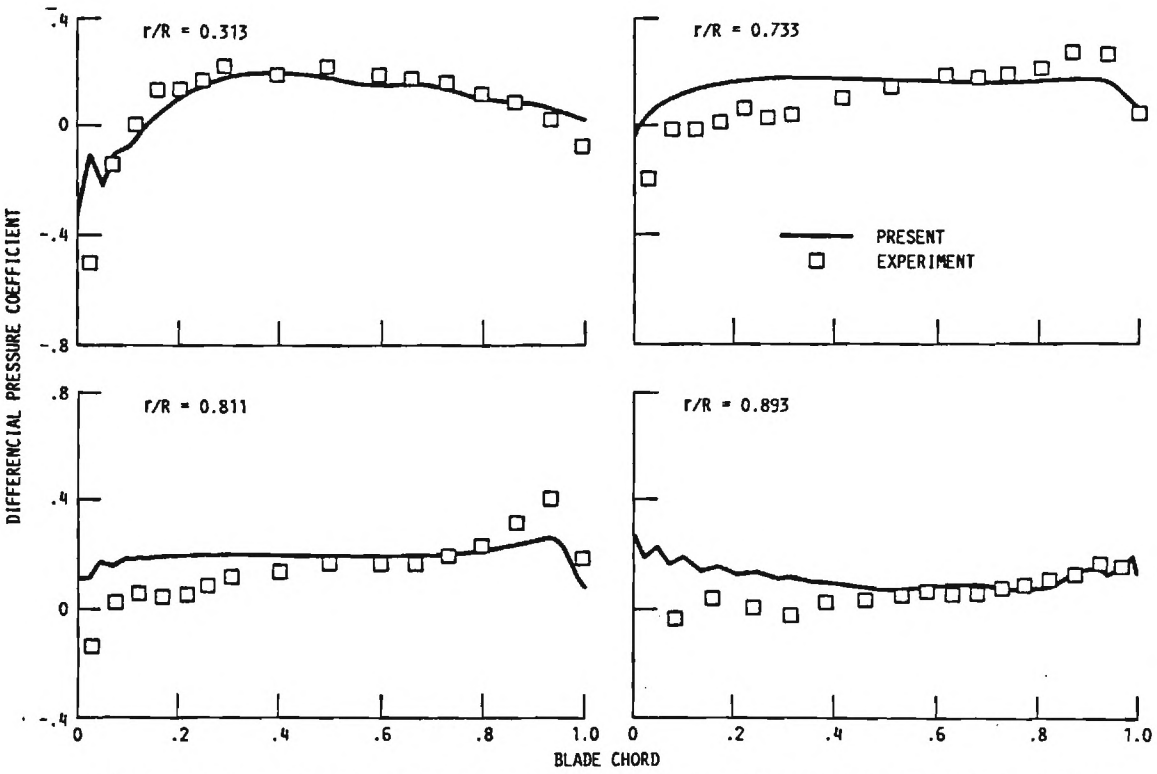

FIG. 8. PRESSURE COEFFICIENT DIFFERENCE AT VARIOUS RADIAL LOCATIONS FOR 2 BLADED SR-7L PROPFAN. M = 0.775; J = 3.088; $\beta = 54.6^{o}$.

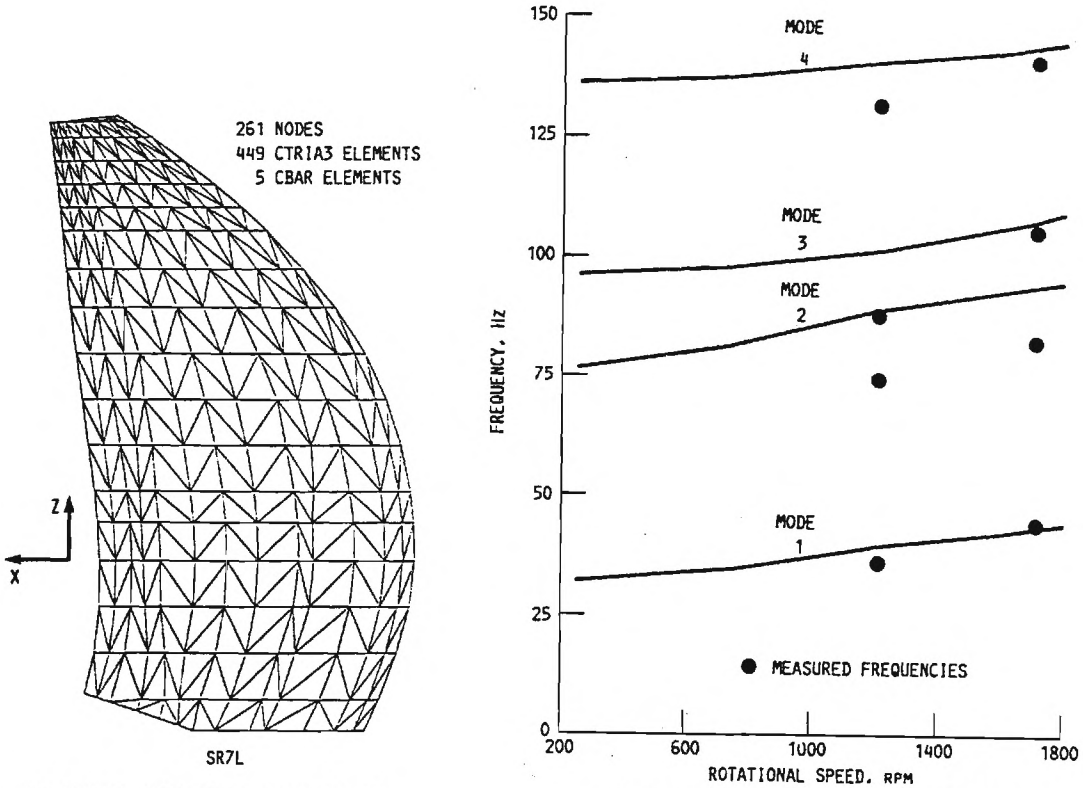

(a) PROPFAN BLADE FINITE-ELEMENT MODEL (REF. 19).

(b) SR-7L FREQUENCIES VERSUS RPM (REF. 19).

FIG. 9. SR-7L MODAL ANALYSIS.

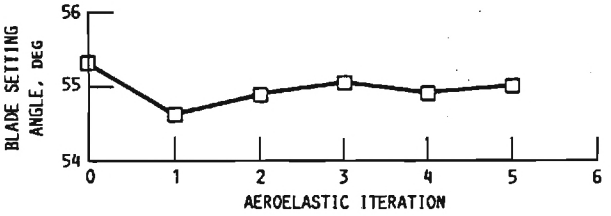

FIG. 10. BLADE SETTING ANGLE AT 75 PERCENT SPAN VERSUS AEROELASTIC ITERATION FOR SR-7L PROPFAN. J = 3.088; M = 0.775.

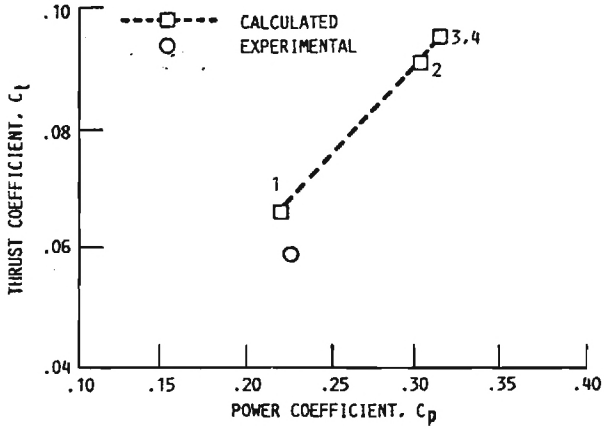

FIG. 11. CALCULATED THRUST COEFFICIENT VERSUS POWER COEFFICIENT FOR EACH AEROELASTIC ITERATION SR-7, 2-BLADED PROPFAN; J = 3.088; M = 0.775.

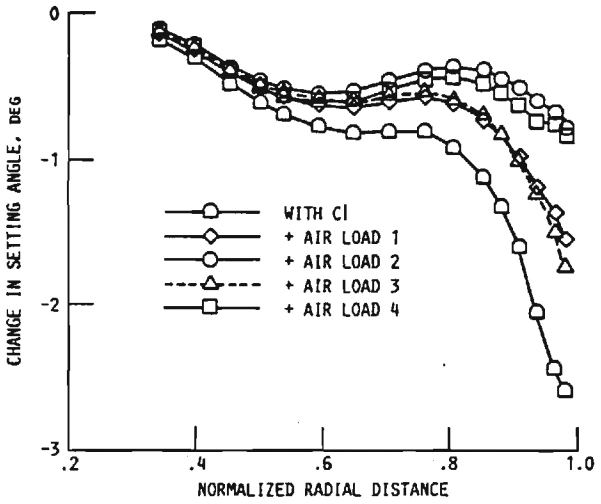

FIG. 12. CHANGE IN BLADE SETTING ANGLE VERSUS BLADE SPAN FOR SR-7L PROPFAN. M = 0.775; J = 3.088.

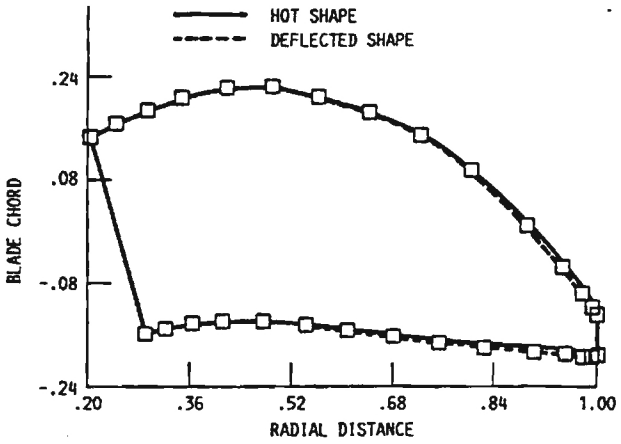

FIG. 13. IN PLANE DEFLECTION OF BLADE PLANFORM FOR SR-7L, 2 BLADED PROPFAN. M = 0.775; J = 3.088; $\beta = 54.6^{o}$.

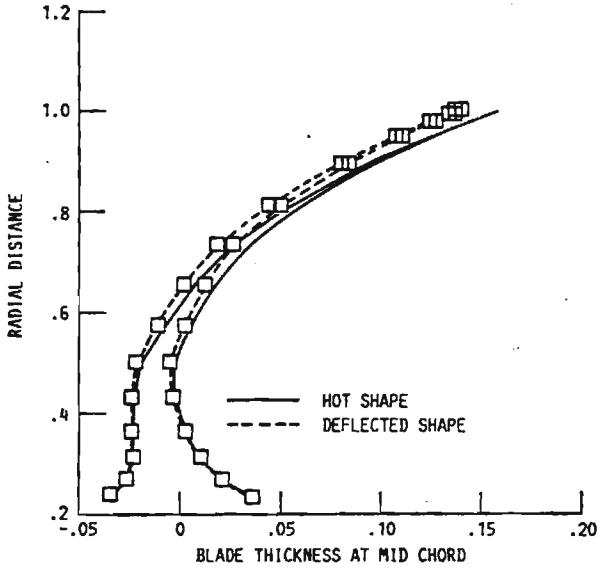

FIG. 14. OUT-OF-PLANE DEFLECTION AT MID CHORD FOR SR-7L, 2-BLADED PROPFAN. M = 0.775; J = 3.088; $\beta = 54.6^{o}$.